Reaction Kinetics and Structural Evolution of Pyrolysis and Gasification Chars

Kagiso Bikane

Department of Chemical Engineering

Imperial College London

A thesis submitted in fulfilment of the requirements for the degree of

Doctor of Philosophy of Imperial College London

September 2020

Declaration of Originality

I hereby declare that this thesis is the result of my own work, and that any ideas or quotations from the work of other people are appropriately referenced.

Kagiso Bikane, 2020.

Copyright Declaration

Abstract

Gasification is a versatile technology used to convert coal into synthesis gas for use in cleaner power generation and production of high-value products. This work investigates the pyrolysis and gasification behaviour of a relatively unknown Morupule coal, from Botswana, using a wire-mesh reactor. Morupule coal was pyrolysed in a helium atmosphere and gasified in CO_2 at temperatures of 400 – 1050 ºC and heating rates of 1 – 1000 ºC s^{-1} under pressures of up to 30 bar_a and holding times of up to 400 s at peak temperature.

Elevated pressures induced a suppression of the volatile release during the temperature ramp up. However, ultimate yields at 1000 ºC prove insensitive to pressure. A novel direct gasification approach with *in-situ* coal pyrolysis, as opposed to decoupling the pyrolysis and gasification experiments, was used to study the intrinsic CO_2 gasification kinetics as would be observed in a gasifier. An activation energy of 320 kJ mol^{-1}, higher than published data, is reported. Enhanced gasification rates were obtained at pressures of up to 20 bar_a, with reduced gasification lag periods previously observed under atmospheric pressure conditions. Morupule coal gasification propagated through the consumption of C-C/C=C bonds, without preference for smaller aromatics. Char morphology was characterised by a developing external surface porosity as gasification proceeded.

A distributed activation energy model, assuming a Gaussian distribution, accurately represented the pyrolysis behaviour of Morupule coal. The shrinking core, volumetric and random pore models adequately represented the early-stage atmospheric pressure gasification kinetics. The Langmuir – Hinshelwood rate expression described the high-pressure gasification kinetics fairly well but could not account for the initial gasification lag. In studying the effect of particle size on pyrolysis, larger particles exhibited lower product yields during the heating up period. However, identical yields were obtained under prolonged holding at 1000 ºC at both atmospheric and elevated pressures.

Dedication

To my brother, *Kabo Badisa Bikane*. You are always in my thoughts.

Acknowledgements

My deepest gratitude to my supervisor Dr. Marcos Millan-Agorio for affording me the opportunity to undertake this research. I am thankful for the guidance, patience, support and encouragement he has shown me during my stay at Imperial College London and the times to come. I have also thoroughly enjoyed the football battles (and basketball even though my lack of talent in this sport was on full display), mainly the fact that my supervisor could not get past my defending over three full seasons.

I would also like to thank Dr. Ronny Pini for the support and motivation he has afforded me as my academic mentor, and introducing me to the application of X-Ray computed tomography. I am grateful to Dr. Saurabh Shah for carrying out the characterisation of my samples using X-Ray computed tomography.

Special thanks are also extended to Dr. Nigel Paterson for his continued advice, support and the constructive discussions we have had during this study.

I gratefully acknowledge the role played by Dr. Jie Yu in training me on the use of the wire-mesh reactor and the fruitful discussions we have had over the years. My sincere thanks to members of the FuelGroup, past and present: Dr. Jose Bermudez Menendez, Dr. Pedro Arcelus Arrillaga, Dr. Aderlanio Cardoso, Dr. Xiangyi Long, Dr. Ziyin Chen, Jonathan Ball, Arifa Sembiring, Hualun Zhu, Xudong Yuan, Tarek Lahoud and Abdullah Baubaid. I would also like to express my deepest gratitude to Ravi Shankar for his help with X-Ray photoelectron spectroscopy measurements and friendship from the moment we found ourselves in the same pairing for our very first laboratory coursework in 2012 and the journey throughout our undergraduate and postgraduate studies. Many thanks to Bala, Latha and Ajay for the support they have shown me. I also thank Dr. Diana Iruretagoyena for her support and mentorship.

Publications

1. **Bikane, K**.; Yu, J.; Long, X.; Paterson, N.; Millan, M., Linking Char Reactivity to Structural and Morphological Evolution during High Pressure Pyrolysis of Morupule Coal. Chemical Engineering Science: X 2020, 100072.

2. **Bikane, K**.; Yu, J.; Shankar, R.; Long, X.; Paterson, N.; Millan, M., Early-Stage Kinetics and Char Structural Evolution during Atmospheric Pressure Gasification of Morupule Coal in CO_2. *Submitted, under review*.

3. **Bikane, K**.; Yu, J.; Shankar, R.; Long, X.; Paterson, N.; Millan, M., High Pressure Gasification of Morupule Coal in CO_2: Intrinsic Kinetics and Char Structural Evolution. *In preparation*.

4. **Bikane, K**.; Yu, J.; Long, X.; Paterson, N.; Millan., Modelling of Single Particle Pyrolysis Behaviour using Model-Based and Model-Free Methods. *In preparation*.

Table of Contents

List of Figures

17

List of Tables

Nomenclature

A	Pre-exponential factor (s^{-1})
C	Unreacted coal fraction (-)
c_p	Specific heat capacity (J kg^{-1} K^{-1})
C_t	Total number of active sites (-)
C_f	Free active site (-)
E_a	Activation energy (kJ mol^{-1})
E_0	Gaussian distribution mean activation energy (kJ mol^{-1})
$f(E_a)$	Gaussian distribution (-)
$f(\alpha)$	Factor accounting for the reaction model in Friedman equation (-)
$g(\alpha)$	Factor accounting for the integrated reaction model in the KAS and Ozawa-Flynn-Wall methods (-)
ΔH_i	Enthalpy of reaction i (kJ mol^{-1})
h_T	Total convective heat transfer coefficient
k	Reaction rate in the nth power global equation (s^{-1})
k_1, k_2, k_3	Rate constants in the Langmuir – Hinshelwood rate expression (s^{-1})
k_{RPM}	Random pore model rate constant (s^{-1})
k_{SCM}	Shrinking core model rate constant (s^{-1})
k_{VM}	Volumetric model rate constant (s^{-1})
L_0	Length of pores per volume (m^{-2})
m	Dimensionless ratio during the heating or cooling of a spherical particle (-)
n	Reaction order (-)
P_{CO_2}	Partial Pressure of CO_2 (bar$_a$)
P_{CO}	Partial pressure of CO (bar$_a$)
R	Universal gas constant (J mol^{-1} K^{-1})

R_{in}	Reaction rate in the Langmuir – Hinshelwood rate expression (s^{-1})
$R_{50\%}$	Combustion reactivity at 50 % conversion (% min^{-1})
r_p	Particle radius (m)
S_0	Pore surface area per volume (m^{-1})
t	Time (s)
T	Temperature (K)
T_0	Initial temperature (K)
T_b	Particle body temperature (K)
T'	Particle surface temperature (K)
V	Volatile yield (wt.%, daf)
V^*	Ultimate volatile yield (wt.%, daf)
W_0	Initial weight of the char (kg)
W	Weight of char (kg)
X	Gasification conversion (-)
Y	Dimensionless ratio for temperature during the heating or cooling of a spherical particle (-)
ρ	Density of coal
λ	Thermal conductivity of coal (W m^{-1} K^{-1})
β	Heating rate (K s^{-1})
α	Conversion during non-isothermal pyrolysis (-)
σ	Gaussian distribution standard deviation (kJ mol^{-1})
ε_0	Char porosity (-)
Ψ	Random pore model structural parameter (-)
θ	Dimensionless ratio for time during the heating or cooling of a spherical particle (-)
χ^2	Chi-squared (-)

Abbreviations

AAEMs	Alkali and Alkaline Earth Metals
ATR	Attenuated Total Reflectance
CFD	Computational Fluid Dynamics
CPD	Chemical Percolation Devolatilisation
DAE	Distributed Activation Energy
FBDB	Fixed Bed Dry Bottom
FTIR	Fourier-Transform Infrared
HPWMR	High Pressure Wire-Mesh Reactor
IGCC	Integrated Gasification Combined Cycle
KAS	Kissinger-Akahira-Sunose
L – H	Langmuir – Hinshelwood
MCM	Morupule Coal Mine
NMP	N-Methyl-2-Pyrrolidone
RPM	Random Pore Model
SEC	Size Exclusion Chromatography
SEM	Scanning Electron Microscopy
SCM	Shrinking Core Model
TGA	Thermogravimetric Analyser
UV	Ultraviolet
VM	Volumetric Model
WMR	Wire-Mesh Reactor
X-Ray CT	X-Ray Computed Tomography
XRF	X-Ray Fluorescence
XPS	X-Ray Photoelectron Spectroscopy

Chapter 1

Introduction

1.1 Background and Research Motivation

Coal has been utilised as a low-cost source of reliable energy by combustion in the thermal production of power for years. In 2018, coal accounted for 27 % of the world energy supply at a consumption of 5500 Mtce [1]. However, its use is greatly associated with environmental and health concerns pertaining to the undesirable release of SOx, NOx, ash and slag, particulates and greenhouse gas emissions, including CO_2 [2]. Stringent legislation continues to be put in place to combat the excessive release of these anthropogenic emissions and potentially minimise their adverse impacts. The abundance of natural gas and increased environmental concerns relating to coal utilisation has seen several European coal plants being closed [3], with ambitions to transition to cleaner, more sustainable sources of energy. However, the projected increase in the energy demand will see a continued use of coal in the energy mix, particularly in developing countries where it is affordable, abundant and provides reliable electricity supply.

The economy of Botswana is heavily dependent on revenues from diamond mining, which contributed about 84 % of the exports in 2014 [4]. However, diamond revenues are expected to dwindle when the Jwaneng diamond mine, dubbed the richest diamond mine in the world, will be converted from open pit to shaft in 2026 as the reserves become difficult to exploit. Furthermore, a luxury commodity such as diamonds is susceptible to economic downturns as evidenced by substantially reduced sales post the 2008 recession and more recently, during the COVID-19 pandemic. To develop a robust economy, efforts have been placed on natural resources beneficiation. With an estimated 208 billion tonnes of coal reserves [4], Botswana has abundant reserves to develop a coal-based industrialisation and export sector. 2.8 million tonnes of bituminous coal, mainly used for thermal power production and as exports to the seaborne market, are mined at the Morupule Coal Mine (MCM) per annum. Extraction of coal-based high-value products is therefore at the forefront of the Botswana national strategy to develop a diversified economy. There is therefore an immediate necessity to understand the thermochemical behaviour of Morupule coal for the development and enhancement of sustainable cleaner coal technologies with high fuel efficiencies and reduced environmental impacts.

Gasification is increasingly receiving significant attention as an attractive and cleaner pathway of converting coal into the highly flexible synthesis gas (syngas). It is, however, not a particularly new technology, and was first demonstrated in the 1700s when coal syngas was used for house lighting applications. In conjunction with the prosperity that resulted from the industrial revolution in some countries, the application of gasification technologies broadened around the world with a recorded 1200 industrial gasification plants in the United States of America around the 1920s [5]. The steady growth in gasification has seen the production of syngas with over 200 GW_{th} capacity in 2020, with projections of 425 GW_{th} in 2022 [6]. The energy rich syngas from gasification can be used to drive an integrated gasification combined cycle (IGCC) for power generation and reduced emissions associated with improved downstream fuel gas cleaning operations. Such a process can potentially produce a high

concentration CO_2 stream suitable for subsequent sequestration when adapted to include carbon capture and storage technologies [7,8]. Syngas also serves as a building block in chemical industries. This includes the use of H_2 in electrochemical fuel cells, methanol synthesis, production of speciality chemicals and liquid hydrocarbon fuels *via* Fischer-Tropsch synthesis. In Southern Africa, coal gasification is demonstrated by the 7 million tonnes per annum of synthetic liquid fuels produced at the SASOL Secunda plant in South Africa [9]. Although plant gasifier design is achieved through a heuristic process [10], laboratory scale kinetic investigations are critical in the design, optimisation and troubleshooting of gasification systems. They are also used to develop predictive models, as well as allowing studies of aggregated phenomena present in industrial gasifiers to be investigated [9].

The vast literature reported on coal char gasification reactivity and the influence of char structure on gasification are a testament to the importance of understanding coal conversion kinetics and char physicochemical structural evolution [11,12,13,14]. Gasification is a two-step process which involves pyrolysis (devolatilisation) and actual gasification of the residual carbon matrix [15]. While the gasification step limits the rate of the overall process, the Boudouard reaction, between char and CO_2, is among the slowest gasification reactions. This reaction converts CO_2 into CO, a primary constituent of syngas, and can be a route for CO_2 utilisation as it opens the vast possibilities associated to syngas chemistry [16]. In addition, the char – CO_2 reaction can lessen the reliance on the energy intensive steam generation process [17]. The Boudouard reaction is also of interest in oxyfuel combustion technologies, where CO_2 is used to replace N_2 with aim to limit the adiabatic flame temperature and maintain fluidisation [14,18]. Oxyfuel combustion is particularly useful in conjunction with carbon capture technologies as it eliminates the complexity brought upon by the CO_2/N_2 flue gas separation in air combustion technologies. A thorough knowledge of the char – CO_2 reaction kinetics and the influence of CO_2 on char structural evolution is necessary for the design of commercial gasifiers and combustion technologies. Although atmospheric pressure pyrolysis and gasification have been comprehensively investigated, there is limited literature on high

pressure characterisation of the thermochemical behaviour of coals (even more so of Morupule coal), quintessential of industrial gasification processes.

Long-standing research in coal gasification is typically undertaken through isolation of gasification from pyrolysis in an indirect experimental methodology. The coal is usually pyrolysed at high temperatures for extended periods and thereafter gasified in a different reactor system [19]. The pyrolysis preparative step is known to compromise the subsequent reactivity of the char due to exacerbated thermal annealing [20,21], misrepresenting the overall intrinsic kinetics. This also limits the understanding of the char structural development since excessive heat treatment produces chars that do not resemble the structural properties of the parent coal. There is a research gap pertaining to gasification kinetic determinations using a direct gasification approach, without separating pyrolysis and gasification. While the available research provides valuable information on gasification behaviour, most reported bench-scale studies are not representative of the fundamental thermochemical behaviour of coals. Such studies relate to the use of thermogravimetric analysers (TGA) to investigate coal conversion kinetics [19,22,23,24]. Despite their ability to record weight loss continuously, TGA instruments are not truly absent of transport phenomena limitations [25], have lower heating rates and allow for particle stacking. This results in tar secondary reactions on particle surfaces and forms relatively unreactive residues [12]. In order to provide a better understanding of the gasification process, intrinsic pyrolysis and gasification kinetics for heterogeneous reactions in oxidising atmospheres should be studied under process conditions free of both technology-specific influences and transport phenomena limitations.

An ideal bench-scale reactor for investigating coal pyrolysis and intrinsic gasification kinetics should be able to study the independent behaviour of samples at particle size fractions small enough to minimise intra – as well as inter – particle reactions involving tar precursors. The reactor should be able to uniformly heat the sample particles at a well-defined heating rate typical of commercial-scale gasifiers. Minimisation of secondary reactions is key to prevent tar repolymerisation when in contact with heated surfaces. A wire-mesh reactor

(WMR), developed at Imperial College London, has the operating capability to accurately represent performance in commercial gasifiers with its high pressure (up to 150 bar$_a$), heating rate (up to 10,000 °C s^{-1}) and temperature ranges (up to 2000 °C) [11,12,26]. The continuous removal of evolving volatiles from the reaction zone using a sweep gas limits potential secondary reactions and enables the characterisation of primary products, giving valuable insights into the coal structure. Independent particle behaviour is achieved through a monolayer distribution of the sample on the wire-mesh, allowing for particle segregation. This reactor allows for direct gasification which mimics the time-temperature history in commercial fluidised bed and entrained flow gasifiers, preserving the structural properties of the parent coal. Therefore, there is scope to obtain fundamental gasification data of a coal from Botswana using a novel direct gasification approach representative of the thermal history of coal in a gasifier.

1.2 Research Objectives

This work aims to study the thermochemical behaviour of a Morupule bituminous coal under various conditions ranging from atmosphere, pressure, temperature and exposure time at peak temperature. In a first of its nature, this work provides gasification kinetic parameters of Morupule coal determined from direct gasification (*in-situ*) in the WMR. Coal char reactivity is intrinsically linked with the char chemical structure and morphological development. In this context, a comprehensive characterisation of the early-stage char structural and morphological evolution is relevant. The influence of particle size on Morupule pyrolysis and gasification is also extensively studied to understand the influence of heat and mass transfer limitations. With the data obtained during the elucidation of both pyrolysis and gasification, model development is then undertaken. The research objectives of this work are presented as follows:

- To characterise Morupule coal and determine its chemical composition and thermochemical behaviour to provide, for the first time, valuable empirical data on the utilisation of coals from Botswana for the development of coal conversion technologies.

- Determine the influence of pressure on the pyrolysis of Morupule coal and assess changes in the chemical structure, morphology and subsequent reactivity of the residual char.

- Develop a novel analytical method based on non-destructive X-Ray computed tomography to characterise the internal porous structure of chars produced from WMRs.

- Provide fundamental atmospheric pressure direct gasification kinetics data for Morupule coal in a CO_2 atmosphere under conditions relevant for intrinsic kinetic determinations. An in-depth comparison of kinetic parameters obtained using this experimental approach and those from published literature (using an indirect gasification approach) is carried out. The influence of CO_2 on char structural and morphological development is also sought to be comprehensively understood.

- Investigate the influence of pressure on the direct CO_2 gasification of Morupule coal and associated changes in the char chemical and morphological structure.

- Model the intrinsic single-particle behaviour of Morupule coal to describe its intrinsic pyrolysis and direct CO_2 gasification thermochemical conversion. The applicability of model-free methods for describing non-isothermal pyrolysis kinetics is investigated using data from the WMR and compared to the widely published literature based on TGA.

- Assess the influence of particle size on the thermochemical conversion of Morupule coal during pyrolysis and gasification in CO_2, both at atmospheric and elevated pressures.

1.3 Thesis Structure

Nine chapters, including this introduction (*Chapter 1*), are presented in this thesis. An extensive literature review on the structure of the coal, bench-scale reactor setups, fundamental data on pyrolysis and gasification, and relevant research findings are scrutinised and presented in *Chapter 2*. A comprehensive description of the WMR reactor setup, used to carry out both the pyrolysis and gasification experimentation, is provided in *Chapter 3*. Analytical techniques used to characterise the coal char and tar physicochemical properties and reactivity are also described, together with the chemical properties and composition of Morupule raw coal. *Chapter 4* describes an extensive investigation of the influence of pressure on the pyrolysis of Morupule coal and subsequent characterisation of the residual char chemical structure and morphology. The relative combustion and gasification reactivities of the residual char are determined. Kinetic information on the atmospheric pressure gasification of Morupule coal in a CO_2 atmosphere and elucidation of the influence of atmosphere on the char structural, morphological and reactivity evolution are provided in *Chapter 5*. High pressure gasification of Morupule coal in CO_2 and a comprehensive study on the early-stage char structural, morphological and reactivity development are presented in *Chapter 6*. *Chapter 7* describes the modelling of single-particle Morupule coal thermochemical behaviour under pyrolysis and gasification conditions using data obtained from Chapters 4, 5 and 6. In *Chapter 8*, the influence of particle size on the thermochemical behaviour of Morupule coal under conditions consistent with those presented in Chapters 4, 5 and 6 is addressed. The overall conclusions of this thesis and recommendations for further research works are presented in *Chapter 9*.

References

1.   IEA, World Energy Outlook 2019. **2019**; pp https://www.iea.org/reports/world-energy-outlook-2019.

2.   Munawer, M. E., Human health and environmental impacts of coal combustion and post-combustion wastes. *Journal of Sustainable Mining* **2018,** *17* (2), 87-96.

3.   Maamoun, N.; Kennedy, R.; Jin, X.; Urpelainen, J., Identifying coal-fired power plants for early retirement. *Renewable and Sustainable Energy Reviews* **2020,** *126*, 109833.

4.   Harvey, R. G., From diamonds to coal? Critical reflections on Botswana's economic future. *The Extractive Industries and Society* **2015,** *2* (4), 827-839.

5.   Mahinpey, N.; Gomez, A., Review of gasification fundamentals and new findings: Reactors, feedstock, and kinetic studies. *Chemical Engineering Science* **2016,** *148*, 14-31.

6.   Lutyński, A.; Lutyński, M., Review of technologies for low-quality solid fuel gasification. *IOP Conference Series: Materials Science and Engineering* **2019,** *545*, 012012.

7.   Hecht, E. S.; Shaddix, C. R.; Geier, M.; Molina, A.; Haynes, B. S., Effect of CO_2 and steam gasification reactions on the oxy-combustion of pulverized coal char. *Combustion and Flame* **2012,** *159* (11), 3437-3447.

8.   Spiegl, N.; Berrueco, C.; Long, X.; Paterson, N.; Millan, M., Production of a fuel gas by fluidised bed coal gasification compatible with CO_2 capture. *Fuel* **2020,** *259*, 116242.

9.   Morgan, T. J.; Kandiyoti, R., Pyrolysis of Coals and Biomass: Analysis of Thermal Breakdown and Its Products. *Chemical Reviews* **2014,** *114* (3), 1547-1607.

10.   Bell, D. A.; Towler, B. F.; Fan, M., Chapter 3 - Gasification Fundamentals. In *Coal Gasification and Its Applications*, Bell, D. A.; Towler, B. F.; Fan, M., Eds. William Andrew Publishing: Boston, **2011**; pp 35-71.

11.   Peralta, D.; Paterson, N.; Dugwell, D.; Kandiyoti, R., Pyrolysis and CO_2 Gasification of Chinese Coals in a High-Pressure Wire-Mesh Reactor under Conditions Relevant to Entrained-Flow Gasification. *Energy & Fuels* **2005,** *19* (2), 532-537.

12.   Messenböck, R. C.; Dugwell, D. R.; Kandiyoti, R., CO_2 and steam-gasification in a high-pressure wire-mesh reactor: the reactivity of Daw Mill coal and combustion reactivity of its chars. *Fuel* **1999,** *78* (7), 781-793.

13.   Roberts, D. G.; Harris, D. J., A Kinetic Analysis of Coal Char Gasification Reactions at High Pressures. *Energy & Fuels* **2006,** *20* (6), 2314-2320.

14.   Irfan, M. F.; Usman, M. R.; Kusakabe, K., Coal gasification in CO_2 atmosphere and its kinetics since 1948: A brief review. *Energy* **2011,** *36* (1), 12-40.

15.   Higman, C.; Tam, S., Advances in Coal Gasification, Hydrogenation, and Gas Treating for the Production of Chemicals and Fuels. *Chemical Reviews* **2014,** *114* (3), 1673-1708.

16.   Wang, T., 1 - An overview of IGCC systems. In *Integrated Gasification Combined Cycle (IGCC) Technologies*, Wang, T.; Stiegel, G., Eds. Woodhead Publishing: **2017**; pp 1-80.

17.   Liu, L.; Cao, Y.; Liu, Q.; Yang, J., Experimental and kinetic studies of coal–CO_2 gasification in isothermal and pressurized conditions. *RSC Advances* **2017,** *7* (4), 2193-2201.

18.   Spiegl, N.; Sivena, A.; Lorente, E.; Paterson, N.; Millan, M., Investigation of the Oxy-fuel Gasification of Coal in a Laboratory-Scale Spouted-Bed Reactor: Reactor Modifications and Initial Results. *Energy & Fuels* **2010,** *24* (9), 5281-5288.

19.   Roberts, D. G.; Harris, D. J., Char Gasification with O_2, CO_2, and H_2O: Effects of Pressure on Intrinsic Reaction Kinetics. *Energy & Fuels* **2000,** *14* (2), 483-489.

20.   Cai, H. Y.; Güell, A. J.; Chatzakis, I. N.; Lim, J. Y.; Dugwell, D. R.; Kandiyoti, R., Combustion reactivity and morphological change in coal chars: Effect of pyrolysis temperature, heating rate and pressure. *Fuel* **1996,** *75* (1), 15-24.

21.   Laurendeau, N. M., Heterogeneous kinetics of coal char gasification and combustion. *Progress in Energy and Combustion Science* **1978,** *4* (4), 221-270.

22.   Aranda, G.; Grootjes, A. J.; van der Meijden, C. M.; van der Drift, A.; Gupta, D. F.; Sonde, R. R.; Poojari, S.; Mitra, C. B., Conversion of high-ash coal under steam and CO_2 gasification conditions. *Fuel Processing Technology* **2016,** *141*, 16-30.

23.   Huang, Z.; Zhang, J.; Zhao, Y.; Zhang, H.; Yue, G.; Suda, T.; Narukawa, M., Kinetic studies of char gasification by steam and CO_2 in the presence of H_2 and CO. *Fuel Processing Technology* **2010,** *91* (8), 843-847.

24.   Gomez, A.; Mahinpey, N., Kinetic study of coal steam and CO_2 gasification: A new method to reduce interparticle diffusion. *Fuel* **2015,** *148*, 160-167.

25.   Babinski, P.; Sciazko, M.; Ksepko, E., Limitation of thermogravimetry for oxy-combustion analysis of coal chars. *Journal of Thermal Analysis and Calorimetry* **2018,** *133* (1), 713-725.

26.   Kandiyoti, R.; Herod, A.; Bartle, K. D.; Morgan, T. J., *Solid fuels and heavy hydrocarbon liquids: thermal characterization and analysis*. Elsevier: **2016**.

Chapter 2

Literature Review

2.1 Introduction

This chapter surveys the extensive literature in the field of coal pyrolysis and gasification. Section 2.2 introduces Morupule coal and its petrographic properties. A brief overview of the gasification process, commercial gasifiers and lab-scale apparatus used to study the thermochemical conversion of coal is provided in Section 2.3. Factors affecting coal pyrolysis are discussed in Section 2.4 while Section 2.5 evaluates the literature pertaining to coal gasification in CO_2, both at atmospheric and high pressures, and the structural evolution of the char. Modelling of both pyrolysis and gasification processes is discussed in Section 2.6. Lastly, a brief summary is provided on the comprehensive literature review and explicitly presents avenues for potential study (Section 2.7).

2.2 Morupule Coal and Maceral Distribution

Morupule bituminous coal, the subject feedstock of study in this thesis, is found in Palapye, about 260 km from Gaborone, the capital of Botswana. A detailed history of coal mining and utilisation in Botswana is provided by Machete [1]. This coal is mainly used for the generation of thermal power at the Morupule Power Station. As with other Southern African coals, this coal is situated in the Karoo (*Permian, 220 – 275 million years ago*) sedimentary rocks [2]. These coals are thought to have been deposited from broad-leafed flora of the *Glossopteridae* group [3]. To gain insights on the structure of coal, petrographic analyses are typically used to quantitatively determine the composition of organic constituents (macerals). The primary maceral groups are vitrinites, inertinites and liptinites. These groups can be further divided into their respective sub-groups (selected maceral sub-groups dominant in Morupule coal are shown in Tables 2.1 – 2.3). Karoo basin Botswana coals are believed to exhibit a domination of inertinite macerals over liptinite and vitrinite macerals [2]. Hower, *et al.* [4] carried out a comprehensive study on the maceral composition of 11 Morupule coal samples. Their findings are summarised in Tables 2.1 – 2.3.

Table 2. 1 Vitrinite maceral sub-groups in Morupule coal and the vitrinite reflectance (R_{max}) [4].

Telovitrinite	Detrovitrinite	Gelovitrinite	*Total Vitrinite*	R_{max}
2.0 - 8.0 %	0.4 - 2.2 %	0.0 - 0.7 %	*2.8 – 8.8 %*	0.75 - 0.85 %

Table 2. 2 Liptinite maceral sub-groups found in Morupule coal [4].

Sporinite	Cutinite	Resinite	Liptodetrinite	*Total liptinite*
2.0 - 6.1%	0.2 - 1.9 %	0.2 - 0.5 %	0.0 - 0.5 %	*2.4 - 8.0 %*

Table 2. 3 Inertinite maceral sub-groups found in Morupule coal [4].

Fusinite	Semifusinite	Micrinite	Macrinite	Secretinite	*Total inertinite*
5.5 - 13.7 %	54.6 - 75.0 %	0.4 - 1.6%	0.8 - 3.5 %	6.0 - 12.4 %	*75.4 - 91.5 %*

The maceral distribution in coal is particularly important in understanding its botanical origins and thermochemical behaviour [3]. The maximum vitrinite reflectance of 0.75 – 0.85 %, shown in Table 2.1, confirms that Morupule coal is indeed of bituminous rank [5]. Basing on the work carried out by Hower, *et al*. [4], summarised in Tables 2.1 – 2.3, in agreement with other researchers [2], Morupule coal petrographic analyses indicate an inertinite rich coal, with vitrinite and liptinite macerals accounting for a total of up to 17 % of the maceral composition. Amongst the inertinite maceral sub-groups, semifusinite dominates, followed by fusinite and secretinite. Fusinite and semifusinite-rich coals are derived from 'carbonised' woody tissues and are characterised by a high aromatic carbon content [3]. Such properties have a significant impact on the pyrolysis behaviour of the coal. The liptinite maceral is characterised by the highest volatile matter release, followed by vitrinite and lastly, inertinite [6]. Semifusinites in the coals formed in the paleocontinent of *Gondwana* (the Karoo sedimentary rocks were formed in this continent) are known to have a high degree of aromaticity, which may inhibit reactivity [3]. However, they are more reactive than their Northern Hemisphere counterparts, especially at high temperatures [3]. Despite the lower volatile release associated with inertinite-rich coals, which may affect the flame stability during combustion [3,7], their higher reactivity, at high temperatures in particular, presents potential avenues for utilisation in coal char conversion processes.

With an urgent need to diversify its economy, Botswana, with its abundant bituminous coal reserves, has considerable scope to venture into advanced coal utilisation technologies, such as gasification, to produce high-value products. This thesis presents the first fundamental characterisation of Morupule coal in terms of its thermal breakdown and early-stage gasification behaviour, free from char deactivation and secondary reactions due to reactor design effects. A novel direct gasification approach, representative of behaviour in commercial gasifiers, is used in this work, unlike the many studies in literature which investigate the kinetics of gasification *via* a decoupling of pyrolysis and gasification. Such a separation of the two processes is known to alter the chemical structure of the coal char and reduce its reactivity.

2.3 Fundamentals of Coal Gasification

2.3.1 Overview

Gasification is a two-step coal conversion process which involves pyrolysis (devolatilisation) and coal char gasification, *via* char – gas heterogeneous reactions. During pyrolysis, the coal undergoes thermal breakdown, resulting in volatile matter release and irreversible chemical structure and morphological changes [8]. The pyrolysis step is faster than the gasification step, and therefore has an insignificant bearing on the overall kinetics of the coal gasification process. However, as previously mentioned, the amount of volatiles generated during pyrolysis affect the flame stability during combustion [3], gasifier bed stability [9] and provide heat for the endothermic char – gas reactions [10]. The structural and physical changes occurring in the char during pyrolysis inherently affect subsequent gasification kinetics. The slower gasification step, however, is considered to be the overall rate-limiting step and has been the subject of extensive research with aim to understand the conversion process to produce carbon monoxide (CO) and hydrogen (H_2). Heterogeneous gas-solid reactions mainly considered for gasification involve CO_2 (Boudouard reaction) and steam (H_2O) as the reactive species (Equation 2.1 and 2.2, respectively). In practical gasification systems, water – gas shift reactions between steam and the product gas, CO, take place (Equation 2.3). Additionally, steam – methane (CH_4) reforming (Equation 2.4) and methanation (Equation 2.5) reactions occur in a gasifier. Combustion, involving the char and pyrolysis products, also takes place in the gasifier and provides energy for the endothermic reactions [11].

$$C + CO_2 \leftrightarrow 2CO \qquad\qquad \Delta H_{R1} = 172.5 \; kJ \; mol^{-1} \qquad (2.1)$$

$$C + H_2O \rightarrow CO + H_2 \qquad\qquad \Delta H_{R2} = 131.3 \; kJ \; mol^{-1} \qquad (2.2)$$

$$CO + H_2O \leftrightarrow CO_2 + H_2 \qquad\qquad \Delta H_{R3} = -42.2 \; kJ \; mol^{-1} \qquad (2.3)$$

$$CH_4 + H_2O \leftrightarrow CO + 3H_2 \qquad\qquad \Delta H_{R4} = 205.8 \; kJ \; mol^{-1} \qquad (2.4)$$

$$C + 2H_2 \leftrightarrow CH_4 \qquad\qquad \Delta H_{R5} = -74.5 \; kJ \; mol^{-1} \qquad (2.5)$$

2.3.2 Process Gasification Reactors

Various gasifiers have been employed for the gasification of coal at a commercial scale. These gasifiers are typically distinguished by their bed type as moving bed (confusingly also called fixed bed), fluidised bed and entrained flow [11]. Operation temperature is also of critical importance in consideration of whether the conversion technology is slagging or non-slagging. In a slagging operation, gasification takes place at higher temperatures (> 1600 ºC) to ensure that the slag, composed of the inorganic matter in coal, is removed as liquid. For non-slagging applications, ash sintering and agglomeration must be minimised by using a temperature low enough to avoid ash softening [11]. In moving beds, lump coal (particle size of less than 70 mm [12]) traverses downwards under gravitational forces while the reactive gas usually moves countercurrent to the falling feedstock [11,13]. The syngas produced provides heat for pyrolysis as the coal enters the reactor. One such reactor is the Lurgi Fixed Bed Dry Bottom (FBDB) used at Sasol Synfuels III in South Africa [14]. This reactor operates in a temperature range of 1100 – 1350 ºC [15]. In fluidised bed gasifiers, 0.5 – 8 mm coal particles are reacted with the gaseous species at 800 – 1000 ºC [12, 16]. Such low temperatures allow for a non-slagging operation, which may adversely affect the bed fluidisation if not accounted for. Particle size is particularly important in ensuring that the coal particles remain fluidised in the reactor and are not too small to be entrained by the product gas [11]. The SES U-Gas gasifier used at the Hai Hua gasification plant in China employs the fluidised bed gasification technology [16]. Entrained flow gasification involves feeding coal of a 200 µm particle size and reactive gases concurrently at high speeds to entrain the particles [17]. The smaller particle size minimises mass and heat transport limitations [11]. This reactor usually operates at high temperatures of 1500 – 1800 ºC [15], allowing for faster carbon conversion rates and slagging operation. The ConocoPhillips E-gas gasifier is a technology based on entrained flow gasification [16]. The aforementioned gasifier technologies typically operate at pressures of 25 – 35 bar_a [16].

2.3.3 Lab-Scale Pyrolysis and Gasification

As briefly mentioned in Chapter 1, the design of commercial gasifiers is typically a heuristic process. However, knowledge of coal properties and char reactivity is essential in the design, implementation and troubleshooting of the gasifier. Moreover, lab-scale experiments investigating both pyrolysis and gasification enable an in-depth understanding and disentanglement of complex thermal breakdown and conversion behaviour [8]. Over the years, thermogravimetric analysers, fluidised bed gasifiers, entrained flow gasifiers and wire-mesh reactors have been used to study the lab-scale pyrolysis and gasification behaviour of coals [3].

2.3.3.1 Thermogravimetric Analysis (TGA)

TGA is one of the most practical systems that can provide insights into the reaction kinetics of coal gasification. It measures the continuous weight changes of the sample coal or chars as a function of temperature and time. Numerous studies have been carried to study pyrolysis and intrinsic coal gasification kinetics using TGA [18,19,20,21,22]. Whilst the weight temporal resolution is advantageous, TGA systems do have drawbacks that rather limit the application of the measured kinetic data to large scale plants. They normally operate at extremely low heating rates (less than 100 °C min^{-1}) far less than the temperature ramp up in commercial gasifiers (up to 20,000 °C s^{-1} [3]). Excessive exposure of the feedstock to high temperatures, due to the low heating rate, results in the thermal annealing of the char and a subsequent reduction in its reactivity [23]. Furthermore, particles tend to stack in the TGA sample holder, promoting transport phenomena limitations and secondary reactions between evolving volatiles and heated char surfaces. This may result in tar repolymerisation which can produce relatively unreactive residues [24], inhibiting char reactivity and distorting the measure of volatiles. Most TGA systems operate at atmospheric pressure and therefore do not provide kinetic data relevant to high pressure gasification applications. Although advances have been made to develop pressurised TGA systems, these techniques tend to have buoyancy

variations and heat transport limitations [25], misrepresenting the kinetics that are relevant to real systems.

2.3.3.2 Fluidised Bed Gasifiers

Lab scale fluidised bed gasifiers have also been used to study the pyrolysis and gasification of coal [26,27,28,29]. This configuration is favoured because of its fuel flexibility and better distribution, which minimises heat and mass transfer limitations [17], and ability to simulate gasifier behaviour. However, significant tar losses, attributed to charring and cracking reactions, have been reported when using fluidised bed gasifiers as the pyrolysis products circulate in the reaction zone [3]. This limits the ability to characterise the coal structure and primary thermochemical behaviour. Additionally, there are suggestions that the volatile-char interactions in this reactor can inhibit gasification reactions by promoting the volatilisation of the catalytic alkali and alkaline earth metals [27].

2.3.3.3 Entrained Flow Gasifiers

In a laboratory setting, drop tube reactors are used to represent the entrained flow gasifier behaviour in studying the thermal breakdown of coal [3]. Tar volatiles suffer the same fate as those in fluidised beds *via* secondary charring and cracking reactions, making the elucidation of primary pyrolysis behaviour rather difficult. It must be noted that this reactor configuration is designed to operate at relatively high temperatures (1500 – 1800 ºC [15]). Char conversion kinetic investigations have thus been carried using this configuration to gain insights on high temperature gasification behaviour [30,31]. While these kinetic determinations provide valuable experimental data, fundamental intrinsic gasification kinetics, required in the present work, should be isolated from the influence of mass transport limitations (prevalent at temperatures used in entrained flow gasifiers) [22]. Moreover, the use of entrained flow gasifiers is associated

with difficulties in estimating the particle temperature history, resulting in less accurate pyrolysis and gasification reactivity measurements [3].

2.3.3.4 Wire-Mesh Reactors (WMRs)

The above discussion highlights the various shortcomings of different reactor configurations used to investigate fundamental pyrolysis and gasification behaviour. Given the need to bridge the research gap on the pyrolysis and gasification of Morupule coal, the objective of the present work is to characterise its fundamental independent thermochemical conversion behaviour (see Section 1.2). To successfully execute this objective, reactor configuration effects on the thermal breakdown of the coal must be sufficiently suppressed [8].

The WMR, described in detail in Chapter 3, can be used to the study single particle pyrolysis and gasification behaviour of coals and biomass with minimal reactor design effects. This reactor can operate over wide heating rate (0.1 – 10,000 ºC s^{-1}), pressures (up to 150 bar$_a$) and temperature (25 – 2000 ºC) ranges [3]. The basic principle is that a monolayer distribution of coal sample is held between a folded wire-mesh, which acts as a resistance heater when electric current is passed through it. The wire-mesh then heats the particles to the desired experimental temperature at a controlled heating rate. This reactor configuration was first conceptualised in 1964 by Loison and Chauvin [32] to study the rapid pyrolysis of coal held between two electrodes. Anthony and co-workers [33,34] thereafter used a similar setup to study the hydrogasification of coal with the sample held between a stainless-steel screen. Large brass electrodes were used to electrically heat the sample under rapid heating rates of 65 – 10,000 ºC s^{-1}. Further work using the same WMR configuration was carried out by Suuberg, *et al*. [35,36]. However, it is argued that pyrolysis results were distorted in this reactor setup as thermocouples were placed between the mesh layers, instead of a direct attachment to the mesh, in order to prevent electrical interference with the direct current [9]. Subsequent works in the development of the WMR saw the incorporation of a feedback temperature

controller with thermocouples directly tied through the wire-mesh [37,38] and a sweep gas system to carry volatiles away from the reaction zone and avoid secondary reactions [39,40].

At Imperial College London, Gibbins and Kandiyoti [41] developed an atmospheric pressure WMR (Figure 2.1) equipped with a continuous sweep flow gas system and an excellent temperature control at high heating rates. With the sweep flow gas system in place, a tar trap was built by Li, *et al.* [6], enabling a quantitative measurement of condensable volatiles and their chemical structure characterisation [42]. An electrode water cooling system was also implemented to enable studies at slower heating rates and extended holding times at high temperatures. This reactor served as basis for the development of a high-pressure WMR facility, with an operation capability of up to 150 bar$_a$ [43]. Subsequent works extended the use of this facility to temperatures of up to 2000 ºC by switching from K-type to S-type thermocouple wires and the use of a molybdenum mesh [44]. Initial tests with a steam injection unit led to condensation in the pipes leading to the reactor, resulting in varied steam flowrates [24]. Furthermore, the facility could only operate at atmospheric pressure. To overcome the operation pressure limitation and the variable steam flowrates due to condensation, Messenböck [9] preheated the gas and steam inlet path to the reactor. The heater temperature was maintained at 300 ºC, above the steam condensation temperature of 212.4 ºC at 20 bar$_a$ [24].
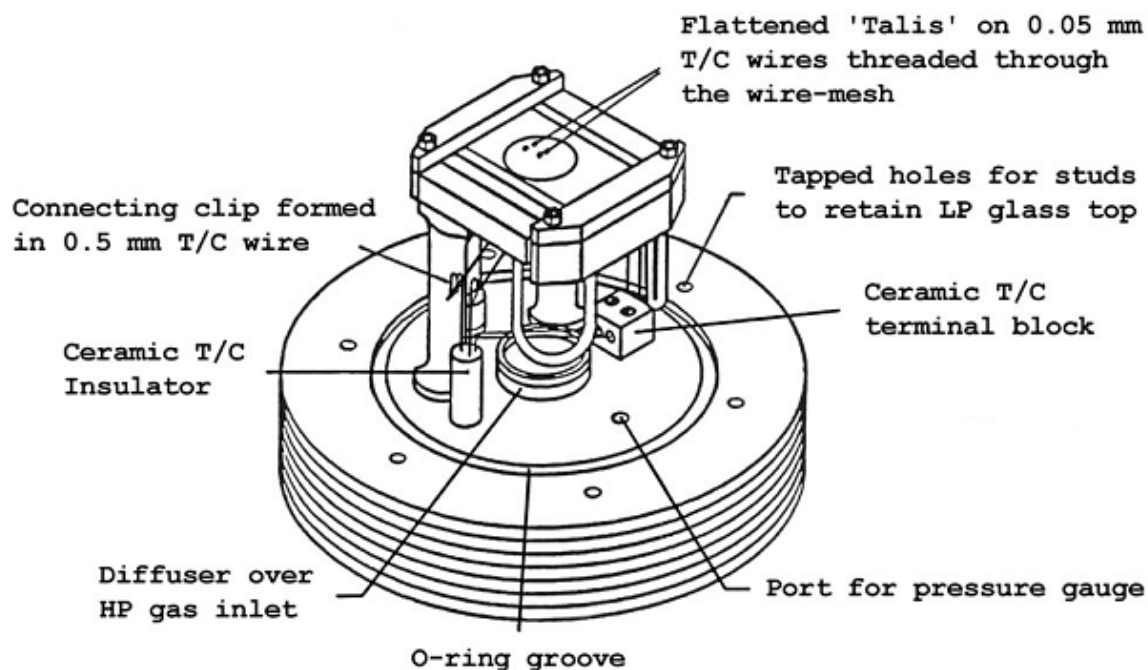
Figure 2. 1 A schematic of the atmospheric pressure wire-mesh reactor. Reproduced from Gibbins (1988)[45].

A comparison of the WMR and fluidised bed configurations reveals a suppression of tar cracking reactions in the WMR, particularly at high temperatures where such reactions typically occur [3]. The WMR appears to have a better consistency than entrained flow reactors which are rather unreliable in studying pyrolysis due to problems in char retrieval after experiments [3]. Given its advantageous characteristics, the WMR is used to study the primary pyrolysis and gasification behaviour of Morupule coal in the present work. It must be highlighted that possible slower kinetics and heat transfer limitations at temperatures below 500 ºC have been shown to result in lower volatiles than expected in the WMR [3]. The observed differences may be due to the different holding times in these two reactor systems, with particles staying at high temperatures for longer periods in the fluidised bed gasifier. Nonetheless, this effect will be limited in the present work given the high temperatures necessary for complete devolatilisation and endothermic heterogeneous char – gas reactions.

Perhaps the main drawback of the WMR is the inability to accrue enough residual char for characterisation using micropore surface area analyses due to the small sample weight used in experimental tests (5 – 6 mg). Semi-quantitative analytical techniques such as scanning electron microscopy and X-Ray computed tomography, presented in Chapter 3, although restricted to macropore properties, are used to study the morphological evolution of Morupule coal chars. Despite the many reactivity studies on coal/char kinetics utilising the WMR, there is no literature on the determination of coal gasification kinetic parameters using this reactor configuration.

2.4 Coal Pyrolysis

Section 2.3.3 has introduced the influence of reactor configuration on the thermochemical conversion of coal. There are additional factors such as coal properties, temperature, pressure, heating rate and particle size, which play a significant role in the volatile matter release and structural changes in the coal, and subsequently, char reactivity in presence of oxidising gases.

2.4.1 Influence of Coal Properties

The pyrolysis of coals of different rank and macerals has previously been investigated to understand their inherent devolatilisation behaviour. Xu and Tomita [46] studied the rapid pyrolysis of 17 coals, with their rank ranging from lignite to anthracite. It was found that coals with higher carbon contents tend to have lower total volatile and tar yields. Similarly, Cai, *et al.* [47], using the WMR, observed a decrease in the tar and total volatile yields with an increase in coal rank. However, it is argued that for bituminous coals, a category in which Morupule coal falls, volatile matter release is not only dependent on the coal properties, with operating pressure and heating rate having significant influence of its pyrolysis behaviour [9]. The effect of these factors on pyrolysis are extensively reviewed in the succeeding sections. Further work

by Cai, *et al.* [48] investigated the effect of varying inertinite concentration on volatile yields and char reactivity using two South African coals. A decrease in both the tar and total volatile yields was observed for coals with higher inertinite concentrations. This is unsurprising since it is well established that inertinite macerals tend to have a lower volatile release owing to higher aromaticity and lower hydrogen/carbon ratio (liptinite has the highest) [3,49]. This order is also followed when it comes to reactivity as it is reported that liptinite macerals derived from a Northern Hemisphere coal are the most reactive, followed by vitrinites and lastly, inertinites [3]. These findings must be treated with caution as the coals are of different origin/age to Morupule coal and the pyrolysis, of which these results are based, was carried out at 700 ºC. In contrast, the treatment of inertinite-rich Southern Hemisphere coals at 1500 ºC has shown significantly higher reactivity than their Northern Hemisphere counterparts [3]. Furthermore, combustion reactivity analyses on the effect of inertinite concentration in two South African coals did not yield conclusive results, with one coal showing a higher sensitivity to inertinite concentration while the other was less sensitive [48].

2.4.2 Effect of Temperature

Volatile matter release is dependent on the temperature at which the thermal breakdown of coal is studied. Typically, a rapid increase in the total volatile yield is observed between 300 – 700 ºC, with an asymptotic release of tars being reached at 600 ºC. Sathe, *et al.* [50] suggest that the aromatic ring system constituents of tar only require high temperatures at short holding times or lower temperatures at longer holding times to be completely released from the coal. Similar behaviour has been observed during the pyrolysis of bituminous coal macerals [6]. Further increases in temperature, beyond 700 ºC, result in gentle increases in the total volatile yield, mainly from the release of permanent/light gases and light aliphatics. The released primary volatiles may undergo subsequent thermal cracking depending on operation conditions and reactor configuration as previously discussed. It has been suggested that an asymptotic yield is reached at 1000 ºC during the pyrolysis of coal with few studies reporting

additional volatile releases at temperatures higher than 1000 ºC [9]. Structural characterisation of coal chars has revealed a gradual loss of oxygen-containing species and a greater degree of aromaticity when the pyrolysis temperature is increased [51]. This condensation of the char carbon matrix is linked to the subsequent loss of reactivity observed when pyrolysis temperature is increased [23]. Morphological evaluations indicate a significant impact of temperature on the thermoplasticity of resulting chars. Some coal chars have been observed to retain their parent particle shape, while others have exhibited cenospheric structures, attributable to coal fluidity during pyrolysis, at different temperatures [52]. The temperature dependence of Morupule coal pyrolysis must be investigated and well-understood as it precedes subsequent reactions in reactive atmospheres. Although this section provides a comprehensive overview of the pyrolysis behaviour of coal as a function of temperature, the heating rate at which the peak temperature is reached can influence char chemical structure, morphology and reactivity.

2.4.3 Effect of Heating Rate

There is a consensus that high heating rates result in a higher volatile matter release. Low heating rates are associated with the char matrix rearrangement, lowering potential yields [45]. However, for 0 s holding time experiments at low temperatures (< 500 ºC), there have been reports of lower heating rates leading to higher total volatile yields as pyrolysis reactions have sufficient time to take place, more especially in the thermal breakdown of biomass [53]. It is suggested that this phenomenon could be an artefact of intraparticle heat transfer limitations incurred in fast heating rates and short holding times [3]. It is therefore essential that the influences of transport phenomena limitations on intrinsic pyrolysis are minimised. Cai, *et al*. [52] studied the effect of heating rate, between 1 ºC s^{-1} and 5000 ºC s^{-1}, on the pyrolysis of various coals. An increase in both product yields, total volatiles and tar, and char reactivity was observed when the heating rate was increased. This effect appeared to level off at 1000 ºC s^{-1}, eliminating the need for using heating rates of up to 10,000 ºC s^{-1} in lab-scale studies to

accurately predict commercial gasifier performance. Heating rate can also affect the morphological development of chars. Some chars, produced under low heating rates, were found to retain the parent particle shape while exhibiting notable melting under high heating rates [52]. However, it appears that this behaviour is also linked to the rank of the studied coal. Coals with 80 – 85 % carbon are reported to not exhibit any melting characteristics during rapid pyrolysis [9]. Heating rate also influences the volatile release transport mechanism, with high heating rates associated with an explosive release of volatiles induced by the intraparticle pressure build-up while slow non-explosive volatile release characterises transport behaviour at low heating rates [9]. Inertinite-rich coals, such as Morupule coal, and inertinite maceral concentrates have been shown to be less affected by heating rate [6,54]. The thermochemical behaviour of Morupule coal will be investigated at a heating rate of 1000 ºC s^{-1} only. However, a brief discussion on the effect of heating rate on the total volatile yields is presented in Chapter 7.

2.4.4 Effect of Pressure

As stated in Section 2.3.2, commercial gasifiers typically operate at pressures of up to 35 bar$_a$ to attain high conversions and drive gas turbines in power generation applications. Despite useful information being obtained under atmospheric pressure conditions, representative pyrolysis behaviour must also be investigated at high pressures. The influence of pressure has therefore been a subject of interest in coal pyrolysis. An increase in pressure typically results in lower total volatile and tar yields, especially for lignites and bituminous coals, when pyrolysis is carried out at high temperatures [9,55]. This behaviour is commonly attributed to tar repolymerisation and cracking reactions that occur in the particle under increased residence times as the external pressure restricts volatile transport. Alternatively, it has been suggested that the pressure alters the vapour-liquid equilibrium properties of the volatile matter, increasing their boiling point [56,57]. The effect of pressure is prominent up to 20 bar$_a$, with further increases showing no further changes in the total volatile yields [55]. It is also suggested that

pressure influences are dependent on the coal type and its petrographic properties. Messenböck [9], using a WMR, studied the effect of pressure on the pyrolysis of various maceral concentrates. While liptinite and vitrinite maceral concentrates exhibited a decrease in the total volatile yields, inertinite maceral concentrates were insensitive to changes in pressure. This result suggested that pressure plays a significant role during the pyrolysis of softening coals, typical of liptinite and vitrinite, and its effect is closely linked to the inherent volatile matter content.

Pressure has also been observed to affect residual char morphology and reactivity. Some coals have been shown to swell when pyrolysed at elevated pressures, a characteristic previously not observed under atmospheric pressure conditions [55,58]. This thermoplastic behaviour is closely linked to the petrographic properties of the coal, with the vitrinite maceral thought to be the most likely to contribute to the swelling of the particle. In a study by Messenböck [9], vitrinite maceral concentrates were observed to undergo substantial swelling and a propensity to agglomerate. Liptinite maceral concentrates underwent melting but did not agglomerate. Inertinite macerals, however, did not exhibit melting properties but were characterised by large blowholes suggesting a bubble volatile transport mechanism. Zeng and Fletcher [57] observed blowholes on coal chars produced from the high-pressure pyrolysis of various American bituminous coals. The particle internal morphology was characterised by a homogeneous spread of thin-walled bubbles. Surface area measurements generally demonstrate a reduction in the internal surface area of char produced during high pressure pyrolysis [55]. However, other researchers have reported an increase in the surface area at high pressures, possibly due to the thermoplastic behaviour of the coal based on its inherent properties [59].

Generally, chars produced under high-pressure pyrolysis in the WMR tend to be less reactive than their atmospheric pressure counterparts due to the presence of a relatively unreactive secondary char layer formed during tar repolymerisation [9,52,60]. Zeng and Fletcher [57], in agreement with the above statement, suggest that the intrinsic reactivity of chars

produced during high-pressure pyrolysis tends to be lower than their atmospheric pressure counterparts. In contrast, Roberts, *et al.* [61] reported that the intrinsic reaction rate of Australian bituminous coal chars is less affected by pressure. In other cases, identical reaction rates, normalised to the specific surface area, with pressure have been observed, but faster burn-off rates for high-pressure chars owing to pore structural changes have been reported [30], highlighting the effect of pressure on the morphological evolution of the char. In studying the combustion reactivity of maceral concentrates pyrolysed at high pressures, Messenböck [9] reported that vitrinites and liptinites exhibited a decrease in reactivity with increasing pressure, while that of the inertinite maceral concentrate was insensitive to increases in pressure. This behaviour in vitrinites and liptinites was attributed to the formation of a rather unreactive secondary char layer formed during tar repolymerisation. Lee, *et al.* [62] suggested that the reduced gasification reactivity of chars produced under high pressures was due to enhanced structural graphitisation. These findings suggest an influence of pressure on the chemical structure of the char and its impact on subsequent combustion and gasification reactions. Yang, *et al.* [63] studied the influence of pressure on the physicochemical structure of chars produced during the pyrolysis of a Shenfu bituminous coal using a pressurised TGA. The aromatic $C - H$, aliphatic $C - C$, and $C–O–C$ organic functional groups were observed to decrease with an increase in pressure due to secondary cracking reactions. More ordered chars were also recovered at high pressure. However, it should be kept in mind that a TGA reactor set-up promotes secondary reactions due to particle stacking, more so given that a mass of 1000 mg was used in the study. There are limited studies aiming to elucidate the links between the structural evolution of char under elevated pressures, through comprehensive chemical structure characterisation, and its reactivity. This thesis therefore aims to provide an in-depth characterisation of the char structural evolution of Morupule coal chars obtained from pyrolysis under high pressures and provide links to combustion and gasification reactivities.

2.4.5 Effect of Particle Size

Particle size also affects the product distribution during coal pyrolysis due to the onset of intraparticle transport phenomena limitations. Lower volatile and tar yields have generally been reported as the particle size is progressively increased [64]. This behaviour is ascribed to the intraparticle reactions between tar precursors and heated internal char surfaces under increased residence times, resulting in secondary charring [64,65]. This effect of particle size on pyrolysis is therefore similar to that of pressure [9]. In biomass, recent reports suggest a possible pathway that involves cracking of tar precursors to produce lighter gases [66]. Structural changes in larger particle sizes have profound effects on the subsequent reactivity of the char. Zhu, *et al.* [64] demonstrated a decrease in char reactivity due to the formed secondary char layer. For coals with total volatile and tar yields that are insensitive to changes in particle size (no formation of secondary char layer), the intrinsic reactivity of their chars was independent of particle size [55,67]. This contradiction in char reactivity suggests that the effect of particle size on coal pyrolysis may be unique to the coal type. Therefore, the present work will study the effect of Morupule coal particle size on its pyrolysis behaviour and product distribution.

2.5 Gasification

Following pyrolysis, gasification is the succeeding step in coal char conversion processes. This section reviews the fundamental principles of gasification, kinetics regimes, reaction kinetics and mechanisms, and the structural evolution of the char during both low-pressure and high-pressure gasification.

2.5.1 Kinetic Regimes

Gasification is governed by a series of chemical reactions and diffusion steps [68]. Initially, the reactant gas molecule must make its way from the bulk gas to the outer surface of the char (bulk diffusion). The gas molecule can then permeate the char through its porosity. Thereafter,

it adsorbs on the surface of the char. A chemical reaction then takes place between the reactant gas molecule and the carbon in the char matrix. Product gas molecules then desorb from the char surface and are transported within the char porosity to the outer surface where they then diffuse into the bulk gas.

In a process gasifier, one or more of these steps can be rate controlling. For sufficiently small particle sizes with minimal heat transfer limitations, whether the overall reaction is controlled by the chemical reaction or diffusion processes, the limitation is mainly dependent on the reaction temperature [69] (changes in other operating parameters such as pressure, particle size *etc.,* have also been observed to result in slight changes in the kinetic regime [68]). At lower temperatures, less than 1000 ºC [22,69], the chemical reaction rate is the controlling step, and this kinetic regime is termed Regime I. In this regime, there are no diffusional limitations and the reactant gas concentration is constant within the particle and same as the bulk gas phase. Given the temperatures at which the chemical reaction kinetics are determined, intrinsic kinetics from this region are suitable for fluidised bed applications as previously stated that the operation temperature for this type of gasifier is in the 800 – 1000 ºC range. At slightly higher temperatures (1100 – 1600 ºC [70]), the kinetics transition to Regime II, where the overall rate of reaction is limited by a mixture of pore diffusion and the chemical reaction. The reactant gas concentration at the outer surface of the particle is equal to that of the bulk gas phase. However, within the particle, there exists a reactant gas concentration gradient. Entrained flow gasification takes place in Regime II [68]. Under Regime III conditions (suitable for pulverised coal combustion applications) at even higher temperatures of over 1600 ºC, the chemical reaction rate is rapid and takes place on the outer surface of the char particle due to external mass transfer limitations [68,71]. In this case, the reactant gas diffusion from the bulk gas phase to the outer surface of the char is the overall rate controlling step. A reactant gas concentration gradient occurs outside the particle, reaching zero at the particle surface. Figure 2.2 shows a schematic of the different kinetic regimes.
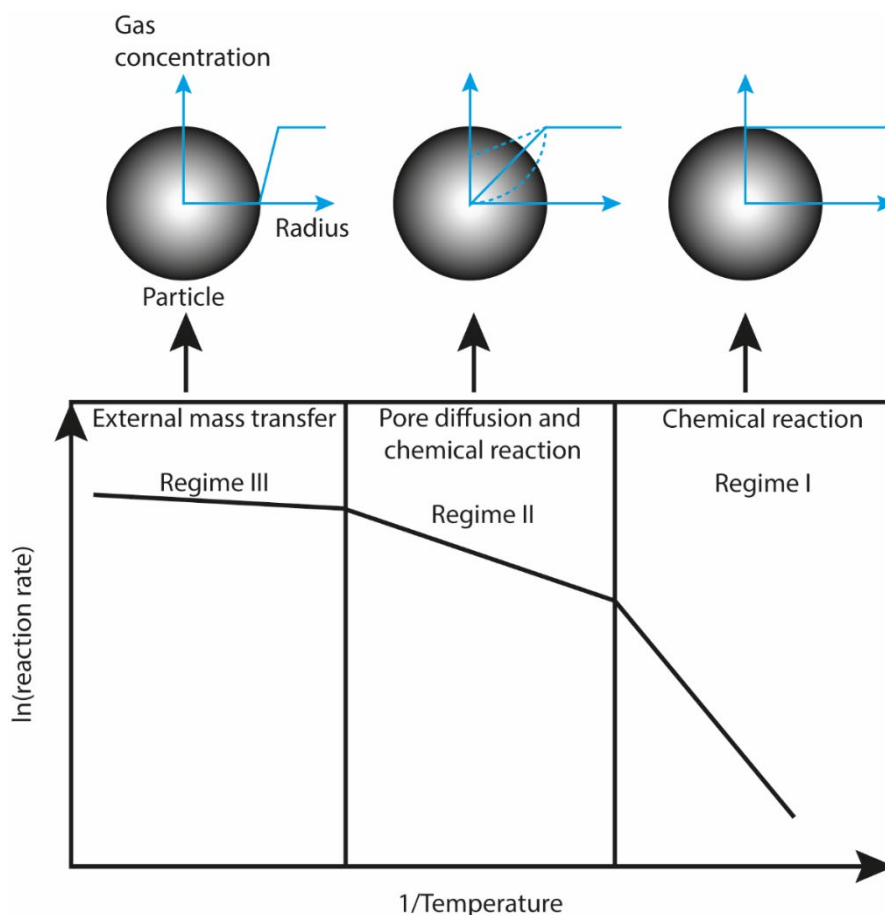
Figure 2. 2 Arrhenius plot showing the dependence of the gasification rate on temperature and how the gas concentration changes within a particle. Adapted from Tremel [68].

The development of char conversion models necessitates the determination of gasification kinetic parameters under conditions where the chemical reaction dominates the overall reaction rate, isolated from diffusional contributions [22,25]. Furthermore, an independent study of the intrinsic gasification kinetics allows the determination of the kinetic regime transition temperature [22]. At present, there is no available literature detailing the gasification kinetics of Morupule coal. This thesis therefore aims to provide, for the first time, the direct gasification kinetics data of Morupule coal, coupling both pyrolysis and gasification, under conditions deemed suitable for determining the '*true*' kinetic parameters. A maximum temperature of 1050 ºC will be used in the present work. In addition, most of the literature pertaining to the use of the WMR in gasification of coals and maceral concentrates has been carried out at 1000 ºC [24,65]. As such, this will provide a direct comparison of the gasification

reactivity of Morupule coal with other coals which have been extensively studied in this reactor setup and allow for a comprehensive understanding of its thermochemical behaviour within the sets of data available in the literature for a range of coals.

2.5.2 Char – Gas Heterogeneous Reactions

As discussed in Section 2.3.1, char – gas heterogeneous reactions are particularly important in evaluating the gasification process due to their relatively slow kinetics. Consequently, char – steam and char – CO_2 reactions have been an intense subject of research in understanding their kinetic behaviour [22,25,69]. It is generally accepted that the char – steam reaction has a faster overall gasification rate than the char – CO_2 reaction [22,25]. Being the slowest reaction, it is essential to gain further understanding of the char – CO_2 reaction kinetics. This reaction is also of interest in new generation technologies such as oxy-fuel gasification with the aim to enhance power generation efficiencies in an IGCC process, whilst minimising greenhouse gas emissions [28]. In technologies looking into the integration of carbon capture and storage facilities, the separation of the CO_2/N_2 gas mixture from air blown gasifiers is rather complex and capital intensive [28,72]. In oxy-fuel gasification, an O_2/CO_2 gas mixture is used in a fluidised bed gasifier, with CO_2 moderating the temperature and maintaining the fluidisation [69,72]. The presence of CO_2, in place of N_2, brings about changes in the coal char structural development and affects char consumption [28], presenting a requirement to gain data on the char – CO_2 reaction kinetics.

2.5.3 Fundamentals of Gasification in CO_2

The Boudouard reaction, between char and CO_2, is represented as a reaction between carbon and CO_2 with CO being the product gas (Equation 2.1). A simple, and generally accepted, reversible carbon – CO_2 reaction mechanism was proposed by Ergun [73]. This mechanism suggests an oxygen atom exchange between CO_2 and a free reactive site (C_f), forming CO

and a C(O) complex (Equation 2.6). k_1 and k_2 are the forward and backward reaction rate constants, respectively. Equation 2.7 represents the desorption of the previously formed C(O) complex, unveiling a new unreacted active site C_f [9], where k_3 is the desorption reaction rate constant. As indicated in Equation 2.6, the produced CO inhibits the gasification reaction rate [74]. The reaction rate (R_{in}), based on this carbon – CO_2 reaction mechanism, is presented in Equation 2.8 (Langmuir – Hinshelwood (L – H) rate expression) where P_{CO_2} is the CO_2 partial pressure and P_{CO} represents the CO partial pressure. C_t is the total number of available active sites.

$$C_f + CO_2 \leftrightarrow C(O) + CO \qquad\qquad k_1, k_2 \qquad\qquad (2.6)$$

$$C(O) \rightarrow CO + C_f \qquad\qquad k_3 \qquad\qquad (2.7)$$

$$R_{in} = \frac{k_1[C_t]P_{CO_2}}{1 + (k_1/k_2)P_{CO} + (k_1/k_3)P_{CO_2}} \qquad\qquad (2.8)$$

Other researchers have proposed additional reaction mechanism steps, especially during high-pressure gasification studies. Blackwood and Ingeme [75] proposed a further interaction between CO_2 and the adsorbed complex producing an adsorbed oxygen, as their experimental investigations revealed greater amounts of CO produced than expected. Several other mechanisms, proposing modified L – H rate expressions, have been suggested by other researchers [76,77]. An excellent review of these mechanisms is provided by Irfan, *et al.* [69].

While the L – H form rate expressions allow for the incorporation of various mechanistic steps and are deemed suitable for high-pressure gasification, the nth order global equation (Equation 2.9) is typically used in low pressure gasification investigations [21,69]. This rate law is based on an Arrhenius representation where k is the reaction rate, E_a is the activation energy,

A is the pre-exponential factor, R is the universal gas constant, n is the reaction order and P_{co_2} is the partial pressure of CO_2. A accounts for factors such as alkali and alkaline earth metals catalysis, active sites, molecular collision frequency, surface area and other rate-influencing parameters [22]. E_a and A are estimated from the gradient and the y-intercept, respectively, of the Arrhenius plot for the natural logarithmic of the reaction rate versus the inverse of reaction temperature. To determine the reaction order, the influence of reactant partial pressure on reactivity must be examined at various partial pressures. An estimation of the reaction rate from the experimental data is typically made by fitting the shrinking core, volumetric and random pore models to the gasification data. These models are comprehensively discussed in Section 2.6.2.1 of this chapter.

$$k = Ae^{-\frac{E_a}{RT}}P_{co_2}{}^n \qquad (2.9)$$

2.5.4 Atmospheric Pressure Reaction Kinetics

Atmospheric pressure gasification of coal chars in CO_2 has been extensively studied to determine the reaction kinetic parameters. Liu, *et al.* [78] studied the gasification of a Kentucky bituminous coal in CO_2. Their work suggested that the gasification rate increases slowly for conversions below 50 %, followed by a rapid increase at 60 % until a maximum gasification rate is attained at 90 %. This zonal behaviour was attributed to the presence of rate limiting factors such as pore diffusion as the experiment was carried out at 950 – 1150 ºC, characteristic of Regime II conditions [68,71]. The CO_2 gasification kinetics of Argentinian bituminous coals were investigated at temperatures between 900 – 1160 ºC by Ochoa, *et al.* [79] using a TGA. The authors found that the gasification reaction was dominated by the chemical reaction control at temperatures below 1060 ºC, with higher temperatures indicating the onset of diffusional limitations. Activation energies were found to be in the 148 – 184 kJ mol^{-1} range. Some authors have reported a kinetic regime transition temperature of 1000 ºC between Regime I and Regime II [22] while others suggest it could be up to 1100 ºC [80,81]. This further

supports a maximum temperature of 1050 ºC selected for investigations pertaining to intrinsic kinetic determinations in this thesis. Jayaraman, *et al.* [82] studied the kinetics of the gasification of high-ash coal chars obtained under various heating rates in CO_2 between 900 ºC and 1000 ºC. It was observed, in agreement with other researchers [83], that chars produced at low heating rates had a lower gasification rate owing to poorer porosity. Table 2.4 presents a summary of the kinetic parameters obtained by various authors during the gasification of coal chars in CO_2.

Table 2. 4 Intrinsic kinetic parameters of coal char gasification in CO_2 at atmospheric pressure.

Author (Year)	Feedstock	Reactor	Temperature (ºC)	Activation Energy (kJ mol^{-1})	Pre-Exponential factor (s^{-1})	Reaction Order
Tanner and Bhattacharya [22]	Victorian brown coal chars	TGA	650 - 1100	164 - 176	10^4 - 10^5	0.39 - 0.48
Ochoa, *et al.* [79]	Argentinian bituminous coal chars	TGA	900 - 1060	148 - 182	-	0.50 - 0.58
Jayaraman, *et al.* [82]	High ash Indian coal chars	TGA	900 - 1000	130 - 214	10^5 - 10^8	-
Everson, *et al.* [84]	High ash South African coal chars	TGA	850 - 900	247	10^8	0.46 - 0.54
Chen, *et al.* [85]	Xinjiang bituminous coal char	Quartz reactor	900 - 1100	47.81	44.34	-
Osafune and Marsh [86]	Various coal chars of different rank	TGA	870 - 1286	165 - 195	10^2 - 10^4	-
Liu, *et al.* [87]	Tri - High coal chars	TGA	950 - 1200	235 - 260	10^5 – 10^7	-
Kim, *et al.* [88]	Berau coal char	Wire – heating reactor	700 - 1100	152	10^{-3}	0.5 (assumed)
Gomez and Mahinpey [89]	Canadian coals	TGA	800 - 900	82 - 185	-	-

The above discussion on the impact of heating rate on gasification highlights the underlying influence of char preparation methods on the overall kinetics. Investigations on the kinetics of CO_2 coal gasification have largely been carried out in a two-step indirect gasification process [22,25,85]. The coal is typically held in an inert atmosphere at high temperatures for prolonged periods of up to 3 hours prior to gasification, decoupling the pyrolysis and gasification steps. The indirect gasification method is perhaps necessary when considering that most of the kinetic studies are carried out using the TGA, well known for the previously discussed shortcomings of particle stacking and the promotion of secondary reactions between evolving tars and the heated char surfaces [24]. However, coal char reactivity is highly sensitive to the pyrolysis conditions, particularly the prolonged holding under extreme thermal histories associated with the loss of microporosity and active sites [23,52,90]. This exacerbates char deactivation, thus distorting and possibly underestimating the gasification reactivity.

An alternative approach of pyrolysing coal in an inert atmosphere during heating up and switching to a reactive gas when the isothermal temperature is reached has been investigated by Gomez, *et al.* [91]. However, it was found that switching the gas induces an artificial maximum reaction rate due to an initially uneven concentration of the reactive gas in the reaction zone. In addition, the authors studied a direct gasification method where both the heating up and the isothermal steps were carried out in a reactive gas medium. The authors reported an increased gasification reactivity using the direct gasification method, suggesting that it might be the appropriate method in studying the kinetics of coal gasification. Despite these promising results, a maximum heating rate of 200 K min^{-1} (3.3 K s^{-1}) was used in their study. Studies using the WMR have shown that such low heating rates profoundly reduce the reactivity of the resultant char [52]. Therefore, there is scope to investigate the direct gasification approach under rapid heating rates typical in WMRs (1000 ºC s^{-1}). Messenböck, *et al.* [24] previously studied the direct gasification of Daw Mill coal using the WMR. However, this study was carried out at only one temperature (1000 ºC), limiting the determination of kinetic parameters suitable for describing the gasification process.

2.5.5 High Pressure Reaction Kinetics

Although extensive work has been carried out to study the kinetics of coal char gasification in CO_2 at atmospheric pressure, there are limited studies investigating high pressure gasification of coals in CO_2. Zhou, *et al.* [92] observed that higher pressures led to higher reaction rates during the gasification of Rhenish brown coal char. The authors attributed this behaviour to increased collision frequency between the reactant gas and the active carbon. Roberts and Harris [25] studied the high-pressure gasification of Australian bituminous coal chars in CO_2 in a chemically controlled kinetic regime. While the reaction order changed over the pressure range studied, the activation energy was found to be independent of pressure. The constant activation energy as a function of pressure was echoed by Malekshahian and Hill [93] during the gasification of petroleum coke, suggesting an unchanged gasification reaction mechanism at low and high pressures. However, changes in the reaction order might be linked to the char surface saturation, with low pressures yielding a lower concentration of CO_2 surface complexes, while high pressures promote surface saturation wherein the reaction order becomes zero [25,94]. As discussed in Section 2.5.3 of this chapter, most kinetic studies at high pressure have employed various forms of the L – H rate expression [21,76]. Other authors have simplified the L – H rate expression by assuming a negligible concentration of CO in the reaction zone, while some studies have opted for the use of additional terms to describe the reaction mechanism. In a study carried out by Roberts and Harris [21], it was found that the chemisorption step limited the overall gasification reaction. However, using a similar rate expression, Liu, *et al.* [95] deduced a desorption-controlled gasification reaction rate. It is therefore clear that there is a lack of agreement in the research community regarding high pressure gasification and necessitates further investigation at elevated pressures.

As has been done under atmospheric pressure conditions, most high-pressure gasification studies are carried out using the indirect gasification approach with chars prepared separately (*ex-situ*). However, as previously discussed, high pressures result in significant consequences during pyrolysis by promoting tar repolymerisation and affecting the

morphological development of the char, impacting its subsequent reactivity [9,52]. It is therefore essential to simulate the thermal history of coal in commercial gasifiers by studying the combined effects of pressure on pyrolysis and gasification using a direct gasification method. Messenböck, *et al.* [24] studied the direct gasification of a Daw Mill coal in CO_2 at 1000 ºC and pressures up to 30 bar$_a$ using a high-pressure WMR. The repolymerisation of the tar, producing a relatively unreactive secondary char layer, led to an observed minimum in the total volatile yield at 10 bar$_a$ when short holding times (less than 10 s) were applied. After the consumption of the secondary char layer, the total volatile yield increased as the gasification of the main char residue had commenced. Zhuo, *et al.* [65] also showed that the combustion reactivity of chars produced from high pressure CO_2 gasification was lower than those from atmospheric pressure investigations owing to the formation of a secondary char layer under pressurised conditions. These findings showcase the importance of studying the coupled pyrolysis and gasification behaviour under elevated pressures to accurately simulate performance in a commercial gasifier.

2.5.6 Influence of Particle Size

One of the factors known to affect the gasification of coal chars in CO_2 is the particle size. Although intrinsic kinetics are typically obtained under conditions free from diffusional limitations, including the minimisation of particle size induced effects, the temperature at which the intrinsic kinetics are usually obtained is directly suitable for fluidised bed applications [68]. Section 2.3.2 of this chapter has already established that particle sizes of 0.5 – 8 mm are used in fluidised bed gasifiers [16], necessitating investigations of particle size on gasification kinetics. It has been reported that the char – CO_2 reaction rate tends to decrease with an increase in particle size [64]. This behaviour was attributed to the secondary charring reactions, between tars and char surfaces, resulting from increased intraparticle residence times during pyrolysis. Jayaraman, *et al.* [82] discerned a reduced CO_2 gasification rate of a high-ash Indian coal when the particle size was increased due to the lower surface area available for reaction. In contrast,

other researchers postulate a dependence of the effect of particle size on the conditions at which char reactivity is studied. It is suggested that char reactivity is independent from the effects of particle size under conditions where chemical reactions alone control the overall gasification reaction [76]. However, when gasification is influenced by diffusional limitations, larger particle sizes result in a lower reactivity. It has also been suggested that the inherent coal properties also have an impact on the particle size dependence of reactivity [69]. A study on the effect of particle size on Morupule coal gasification in CO_2 is therefore interesting to elucidate its thermochemical behaviour.

2.5.7 Influence of Mineral Matter

Amongst other factors affecting char reactivity, the inherent mineral matter (alkali and alkaline earth metals (AAEMs)) is known to catalytically influence gasification reaction rates. Its effect is particularly important in assessing the feasibility of low-temperature gasification in CO_2 [69]. Mi, *et al.* [96] studied the catalytic effects of AAEMs during the steam gasification of a raw Shengli brown coal, coal washed with different concentrations of hydrochloric acid (to remove the inherent AAEMs) and an Na-doped coal prepared by impregnating the hydrochloric acid washed coal with NaCl. The raw coal had the lowest char yields of all the coals, indicating enhanced gasification rates. Despite having similar contents of Na, the authors observed that the Na-doped coal had higher char yields than the raw coal, thereby suggesting that other AAEMs such as Mg and Ca enhanced the gasification of raw coal. Loading iron-based catalysts on carbons has been reported to significantly enhance gasification rates in CO_2 [69,97]. Literature on catalytic coal gasification has also been extended to decipher the mechanistic roles of both inherent and extrinsic catalysts [98,99,100,101]. AAEMs can facilitate the creation of oxygen complexes in the char matrix as they are considered bonding sites for oxygen containing structures [100]. The authors also postulate that the AAEMs speed up the gasification reactions by being involved in the char – radicals and char – steam/CO_2 reactions rather than promoting the dissociation and adsorption of gaseous reactants. Contrastingly, other

researchers suggest that Ca accelerates the desorption of both CO_2 and CO during the gasification of coal chars [102]. Zhang, *et al.* [101] investigated the catalytic gasification mechanism between potassium carbonate (K_2CO_3) and the char. They suggest a formation of a K-char intermediate by electron transfer from the aromatic ring to the K metal ion, thereby weakening the delocalised pi bonds, hence generating faster gasification rates.

The above review highlights the importance of understanding the catalytic effect of AAEMs and the contrasting views presented in literature. One stumbling block in the study of the influence of AAEMs is the necessity to remove inherent mineral matter using acids. This is known to change the chemical structure and morphology of the coal. The alternative method of loading the metals onto the coal does not necessarily reproduce the natural metal distribution in coals [9], making the study of the influence of AAEMs a rather complicated task. Kandiyoti, *et al.* [3] also discuss that the ash in Southern African coals is finely dispersed in the coal, further complicating the washing process. For these reasons, this thesis focuses on the gasification kinetics and structural evolution of Morupule raw coal only without any attempt to remove the ash.

2.5.8 Char Structural Evolution

Understanding the evolution of the chemical structure and morphological properties of char, which are inherently intertwined with the kinetics, during gasification is crucial in assessing its reactivity. However, there are limited studies investigating the structural development of coal chars produced under gasification conditions. The available literature suggest a dependence of the intrinsic reactivity of coals on the concentration of smaller aromatic ring structures [103,104]. The researchers report a preferential consumption of smaller aromatic ring systems of three to five fused benzene rings instead of those with six or more fused benzene rings during gasification in CO_2. However, these findings are highly likely to be an artefact of the prolonged exposure of the coal to heat treatment during char preparation, inducing ring ordering and condensation. This would make it rather difficult to consume the larger aromatic ring systems

as other studies have already shown than excessive heat treatment results in thermal annealing and reduced reactivity [23]. Therefore, there is scope to investigate changes in the chemical structure of the char under conditions that suppress the influence of char preparation methods and preserve the resemblance to the parent coal structure. As far as the author of this thesis is aware, there are currently no studies investigating the structural evolution of chars produced during high pressure gasification in CO_2. Roberts and Harris [25] argue that pressure has an influence on the physical properties, rather than the chemical properties, of the char. This assertion was made after observing that the intrinsic rates of gasification obtained by normalising the apparent rate using the specific surface area showed negligible sensitivity to the effects of pressure. An in-depth characterisation of the chemical structure and morphological properties of the char is necessary to validate this assertion and provide links to the reaction kinetics. Additionally, Roberts, *et al.* [80] state that for reliable application of WMR findings to commercial gasifier development, the data should be accompanied by an exhaustive detailed analysis of the char structure and morphology. At present, there is limited information on the physicochemical properties of chars produced from WMRs.

2.6 Process Modelling and Kinetics

Having described the thermochemical behaviour of Morupule coal experimentally, there is scope to develop predictive kinetic models that can simulate the pyrolysis and gasification behaviour applicable in computational fluid dynamics (CFD) modelling.

2.6.1 Pyrolysis Modelling

2.6.1.1 Overview

Various methods have been employed to predict the kinetics of non-isothermal processes at a constant heating rate. These methods can be divided into structural and empirical models. In structural models, an exhaustive knowledge of the coal-specific structural properties is used

to predict the product distribution during pyrolysis. One such model is a 'chemical model' presented by Solomon, *et al.* [105] to characterise the evolution and distribution of char, tar, gas and other molecules. Structural models can also be used to model the surface area and pore structure of the char. Yang, *et al.* [106] used a chemical percolation devolatilisation (CPD) model in conjunction with a thorough knowledge of the coal ash, molten metaplast and cross-linking reactions to predict the porosity evolution of the char. Zeng and Fletcher [57] also used a CPD model to describe the influence of pressure on pyrolysis. However, the development of a comprehensive structural model to describe coal pyrolysis requires detailed knowledge of the coal structure, primary product distribution and textural properties [107], which are somewhat beyond the scope of the work presented in this thesis. In addition, these models are rather computationally complex and require prolonged periods of computational simulations [108].

2.6.1.2 Empirical Methods for Non-Isothermal Coal Pyrolysis

Other works have focused on the development of empirical non-isothermal coal pyrolysis methods capable of describing the global kinetics without an extensive knowledge of the coal properties. These methods involve the use of the traditional Arrhenius based equations to estimate the process activation energy and pre-exponential factor. Amongst these methods, there are those which are model-free and those which are model-based.

2.6.1.2.1 Model-Free Methods

In model-free methods, the activation energy is determined at constant conversion for experiments carried out at three or more different heating rates without employing a kinetic model [109,110]. Such methods have been proposed by Friedman [111], Kissinger [112] together with Akahira and Sunose [109] (KAS method) and Ozawa [113] in conjunction with Flynn and Wall [114] (Ozawa-Flynn-Wall method). In the iso-conversional method proposed by Friedman (Equation 2.10), $ln(d\alpha/dt)$ is plotted against $1/T$ for several heating rates, where α is the conversion

during the non-isothermal pyrolysis and $f(\alpha)$ accounts for the reaction model. $ln(\beta/T^2)$ is plotted against $1/T$ for different heating rates and identical conversions when using the KAS method (Equation 2.11), where β is the heating rate and $g(\alpha)$ accounts for the integrated reaction model [110]. In the Ozawa-Flynn-Wall method (Equation 2.12), $ln(\beta)$ is plotted against $1/T$. The activation energy is thereafter estimated from the slopes of the iso-conversional plots [110,115].

$$ln\left(\frac{d\alpha}{dt}\right) = ln[A\,f(\alpha)] - \frac{E_a}{RT} \tag{2.10}$$

$$ln\left(\frac{\beta}{T^2}\right) = ln\left(\frac{AR}{E_a g(\alpha)}\right) - \frac{E_a}{RT} \tag{2.11}$$

$$ln(\beta) = ln\left(\frac{AE_a}{R\,g(\alpha)}\right) - 5.331 - 1.052\frac{E_a}{RT} \tag{2.12}$$

These methods have gained increasing recognition in the kinetic analysis of data produced from TGAs for the pyrolysis of polymers, plastics, biomass and coal [109,110,116,117,118]. It is apparent from this review that the underlying principle for the suitable application of these methods is a change in the volatile yield with heating rate. In studies that employ these methods, a decrease in the heating rate results in higher conversions at the same temperature (*i.e.* the same conversion is achieved at a lower temperature for a lower heating rate compared to a higher heating rate). Higher coal pyrolysis conversions at lower heating rates would therefore be a consequence of overcoming intraparticle and/or interparticle heat transfer limitations or a factor of the slower pyrolysis kinetics. Higher heating rates shorten the time particles are exposed to temperature, and consequently result in lower conversions for pyrolysis reactions with slower reactions. The WMR aims to study the pyrolysis of solid fuels in the absence of both intraparticle and interparticle heat transfer limitations by using sufficiently small particle sizes and allowing for a monolayer distribution of the particles

entrapped by the wire-mesh, the resistance heater. Furthermore, previous studies using the WMR have shown that coal pyrolysis is virtually completed during the heating up period [9,45], highlighting the extremely fast kinetics of this process. While volatile matter evolution may be independent of heating rate at low temperatures in the WMR, rearrangement and thermal annealing reactions take place under extended exposure of the feedstock to high temperatures when using low heating rates [52]. Consequently, the application of model-free kinetic methods, such as those presented above, using WMR data would yield near infinite activation energies at low temperatures as the iso-conversion temperature would be insensitive to heating rate. Since higher pyrolysis conversions are obtained under rapid heating due to the explosive release of volatiles, negative activation energies would be deduced at high temperatures. Furthermore, unlike the TGA, the WMR uses pre-set time-temperature conditions and does not employ a continuous weight-loss measurement system, limiting the accuracy of iso-conversion kinetic determinations. The application of model-free methods on data obtained from the WMR will be briefly investigated in Chapter 7 of this thesis.

2.6.1.2.2 Model-Based Methods

Kinetic analyses using model-based methods employ a simplified reaction model fitted to the experimental data based on regression analysis to estimate the kinetic parameters [110]. First order models, generally of the form presented in Equation 2.13, are typically used to study the kinetics of solid fuel pyrolysis (where V is the volatile yield and V^* is the asymptotic ultimate volatile yield). Single activation energy one-step first order models have previously been reported for the non-isothermal kinetics of coal pyrolysis [119]. However, these models have a limited applicability, failing to predict the salient features of the non-isothermal pyrolysis plots, particularly over broader operating conditions.

$$\frac{dV}{dt} = Ae^{-\frac{E_a}{RT}}(V^* - V) \qquad (2.13)$$

To ensure applications over wider operating ranges, a modified one-step model which uses a distribution of activation energies, the distributed activation energy (DAE) model, was proposed (this model is provided in Chapter 7) [120,121]. This model assumes an infinite number of irreversible parallel reactions, with a range of activation energies. A Gaussian distribution is typically used to describe the distribution of activation energies in the DAE model [33]. However, other forms of distributions such as the double Gaussian [122] and Weibull [123] have also been studied. The DAE model has been shown to validly describe the pyrolysis behaviour of different coals, indicating a near representation of the breaking of aliphatic bridges and other bonds [108]. However, as discussed by Maki, *et al.* [124], an arbitrary pre-exponential factor, used for all parallel reactions, must be assumed to solve the model equation. The high linear correlation between the pre-exponential factor and the mean activation energy therefore suggests that there is no unique solution. Miura and Maki [125] sought to resolve this by developing a new method that can describe the activation energy distribution without assuming a pre-exponential factor. Their method relies on the different devolatilisation rates obtained under different heating rates, akin to the model-free methods. As previously noted, the WMR, used in this thesis, will possibly yield a near complete temperature dependence of pyrolysis due to fast kinetics and the absence of heat transfer limitations. Therefore, the method proposed by Miura and Maki [125] would prove to be redundant in the present work. Alternatively, researchers have sought to assign the pre-exponential factor value using those extracted from literature to allow for direct comparison with other coals [122].

The applicability of the DAE model depends on prior knowledge of the ultimate volatile yields at the conditions studied. Without these, a simple prediction using the DAE model fails to accurately represent ultimate volatile yields obtained at different heating rates [108]. To overcome this limitation, two-step models, of the form presented in Equation 2.14, have been proposed to describe the devolatilisation behaviour of solid fuels [126], where C is the unreacted coal fraction. In this method, there are two competing steps, with one prevailing at low temperatures and one accounting for high temperature pyrolysis. Several variations of this

model have been proposed to improve its accuracy by using a corrective factor and a distribution of activation energies [127,128]. Although the modified model accurately represents the data at different heating rates, it requires a high number of coefficients (with at least 8 and a reported 18 in some cases [108]).

$$\frac{dC}{dt} = -\left(A_1 e^{-\frac{E_{a1}}{RT}} + A_2 e^{-\frac{E_{a2}}{RT}}\right) \tag{2.14}$$

2.6.2 Gasification Modelling

2.6.2.1 Atmospheric Pressure Gasification

It was previously stated that atmospheric pressure gasification of coal chars in CO_2 is often described using an Arrhenius global equation (Equation 2.9). The reaction rate constants are typically determined by fitting kinetic gas-solid models to the measured gasification data. The volumetric, shrinking core and random pore models (RPM) are commonly used to fit the data by linear regression. These models account for structural and morphological changes in the coal char as gasification proceeds and are therefore distinguished by their respective assumptions. The volumetric model, shown in Equation 2.15, assumes a uniform gasification reaction throughout the particle volume [129]. X is the conversion and k_{VM} is the volumetric model intrinsic surface reaction rate constant. The shrinking core model (Equation 2.16, k_{SCM} is the shrinking core model intrinsic surface reaction rate constant) postulates that the reaction takes place on the exterior surface of the particle, resulting in a progressive reduction of the particle diameter until the reaction is complete [129]. It assumes that the reaction is neither chemical reaction controlled nor limited by the rate of pore diffusion at high temperatures, rather it is dominated by the external mass transfer rate from the bulk gas to the particle surface [17]. The random pore model accounts for the morphological changes in the coal char by assuming pore growth in the early stages of gasification [130]. However, at higher gasification conversions, the pores are assumed to coalesce, leading to a loss of the available surface area and a reduced chemical reaction rate. This model is presented in Equation 2.17, where

k_{RPM} is the RPM intrinsic surface reaction rate constant. Ψ is a dimensionless structural property parameter (Equation 2.18), with L_0 being the length of the pores per volume, S_0 as the pore surface area per volume and ε_0 being the porosity. Recent studies have presented modified forms of the RPM to enhance its applicability in describing the gasification process [87].

$$\frac{dX}{dt} = k_{VM}(1-X) \tag{2.15}$$

$$\frac{dX}{dt} = k_{SCM}(1-X)^{\frac{2}{3}} \tag{2.16}$$

$$\frac{dX}{dt} = k_{RPM}(1-X)\sqrt{1 - \Psi ln(1-X)} \tag{2.17}$$

$$\Psi = \frac{4\pi L_0(1-\varepsilon_0)}{S_0{}^2} \tag{2.18}$$

2.6.2.2 High Pressure Gasification

The application of the global reaction model (Equation 2.9) in describing coal char gasification is reportedly limited to the atmospheric pressure gasification conditions as the reaction order, n, and the pre-exponential factor, A, change with pressure as it impacts the evolution of the surface area [21]. Consequently, analyses of high-pressure coal char gasification kinetics have largely utilised the Langmuir – Hinshelwood (L – H) rate model (Equation 2.8) based on the Ergun mechanism for CO_2 gasification (Equation 2.6 and 2.7). As discussed in Section 2.5.3, other researchers have introduced additional steps to the Ergun mechanism, resulting in a slightly different C – CO_2 mechanism [75,76]. One such mechanism was proposed by Liu, *et al.* [131] to account for the CO inhibition of the gasification reaction at high pressures and is given in Equations 2.19 – 2.23. The resulting L – H type reaction is presented in Equation 2.24, where R_{in} is the intrinsic reaction rate and k_i are the reaction rate constants. In the context of the capability of the WMR to carry evolving volatiles, including CO, away from the reaction zone,

such complex mechanisms encompassing the inhibition of gasification by CO will be assumed to be negligible.

$$C_f + CO_2 \leftrightarrow C(O) + CO \qquad (2.19)$$

$$C(O) \rightarrow CO \qquad (2.20)$$

$$CO + C_f \rightarrow C(CO) \qquad (2.21)$$

$$CO_2 + C(CO) \rightarrow 2CO + C_f \qquad (2.22)$$

$$CO + C(CO) \rightarrow CO_2 + 2C_f \qquad (2.23)$$
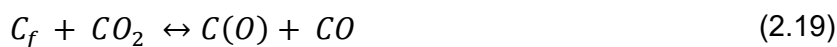
$$R_{in} = \frac{k_1 P_{CO_2} + k_2 P_{CO_2}^2}{1 + k_2 P_{CO_2} + k_3 P_{CO}} \qquad (2.24)$$

2.7 Summary

This review discusses the petrographic properties of a relatively unknown Morupule coal, lab-scale apparatus, coal thermal breakdown during pyrolysis, coal char gasification kinetics under atmospheric and high-pressure conditions, and lastly process modelling to describe chemical interactions. The review has indicated areas where there are research gaps in the application of Morupule coal to gasification. The petrographic properties of Morupule coal are dominated by the inertinite maceral of a semi-fusinite maceral sub-group made from 'carbonised' wood tissues. Such coals typically have a low hydrogen/carbon ratio and are characterised by high aromaticity and low volatile release. This will have an impact on the pyrolysis and gasification behaviour of the coal.

Existing research has largely investigated coal pyrolysis and gasification using thermogravimetric analysers. This reactor configuration is characterised by low heating rates and particle stacking which promotes transport phenomena limitations and secondary

reactions between evolving volatiles and chars. Fluidised bed and entrained flow gasifiers induce secondary charring and cracking reactions as the volatiles circulate in the reaction zone. These factors rather limit the understanding of the primary pyrolysis behaviour and an accurate characterisation of the coal structure. This necessitates the use of an experimental setup, such as the WMR, capable of minimising reactor design effects with its high heating rates, segregation of particles and the use of a continuous sweep flow gas to limit secondary interactions. Despite the limitations associated with the TGA, the literature is awash with informative findings pertaining to the study of coal pyrolysis. Investigations reveal a dependence of coal pyrolysis on pressure, reporting reduced yields and a general reduction in char reactivity attributed to the formation of a secondary char layer during tar repolymerisation. However, little has been done to characterise the structural evolution of the char during high pressure pyrolysis, especially during the dynamic temperature ramp up.

Studies pertaining to the determination of the kinetics of coal gasification are typically carried out using chars that have undergone excessive heat treatment, decoupling pyrolysis and gasification. However, prolonged holding under extreme thermal histories is associated with aromatic ring condensation and loss of microporosity. These factors distort and underestimate the reactivity of coal chars and the obtained kinetic parameters. There is a considerable scope for extensive lab-scale investigations on the early-stage direct gasification of coals under conditions which simultaneously preserve the structural properties of the parent coal and mimic commercial gasifier thermal histories. While there is an abundance of gasification studies carried out at atmospheric pressure, few studies have sought to investigate the coupled behaviour of pyrolysis and gasification under high pressure conditions, with none characterising the structural evolution of the char.

Particle size has been identified as one of the factors affecting pyrolysis and gasification rates. During pyrolysis, it is reported that increases in particle size tend to result in reduced total volatile and tar yields due to intraparticle secondary charring reactions. Other researchers report that pyrolysis and gasification are insensitive to particle size, indicating a clear

disagreement of views in the research field and suggesting that the inherent coal properties may influence its sensitivity to changes in particle size. In the interest of characterising Morupule coal, it is essential to investigate the effect of particle size on its thermochemical conversion behaviour.

Lastly, model-free methods, used in describing the non-isothermal pyrolysis kinetics, were reviewed. Their use may prove challenging for coals with an insensitive dependence on heating rate. The distributed activation energy model is reported to accurately represent the non-isothermal behaviour of coals. The volumetric, shrinking core, random pore and Langmuir – Hinshelwood rate models are discussed to describe gasification reactions. There is a potential area of study in testing the applicability of these well-known models to describe single particle thermochemical behaviour in the WMR in the absence of product interactions and heat transfer limitations.

References

1.   Machete, M., A History of Coal and the Morupule Colliery, 1973-2005. *Botswana Notes and Records* **2012,** *44*, 45-59.

2.   Cairncross, B., An overview of the Permian (Karoo) coal deposits of southern Africa. *Journal of African Earth Sciences* **2001,** *33* (3), 529-562.

3.   Kandiyoti, R.; Herod, A.; Bartle, K. D.; Morgan, T. J., *Solid fuels and heavy hydrocarbon liquids: thermal characterization and analysis*. Elsevier: **2016**.

4.   Hower, J. C.; Wagner, N. J.; O'Keefe, J. M. K.; Drew, J. W.; Stucker, J. D.; Richardson, A. R., Maceral types in some Permian southern African coals. *International Journal of Coal Geology* **2012,** *100*, 93-107.

5.   Kim, A. G., Chapter 1 - Coal Formation and the Origin of Coal Fires. In *Coal and Peat Fires: A Global Perspective*, Stracher, G. B.; Prakash, A.; Sokol, E. V., Eds. Elsevier: Amsterdam, **2011**; pp 1-28.

6.   Li, C.-Z.; Bartle, K. D.; Kandiyoti, R., Characterization of tars from variable heating rate pyrolysis of maceral concentrates. *Fuel* **1993,** *72* (1), 3-11.

7.   Miller, B., 3 - Fuel considerations and burner design for ultra-supercritical power plants. In *Ultra-Supercritical Coal Power Plants*, Zhang, D., Ed. Woodhead Publishing: **2013**; pp 57-80.

8.   Morgan, T. J.; Kandiyoti, R., Pyrolysis of Coals and Biomass: Analysis of Thermal Breakdown and Its Products. *Chemical Reviews* **2014,** *114* (3), 1547-1607.

9.   Messenböck, R. C. Rapid Pyrolysis and Gasification of Coal in a High Pressure Wire-Mesh Reactor. PhD Thesis, University of London, **1998**.

10.   Roberts, D. G. Intrinsic Reaction Kinetics of Coal Chars with Oxygen, Carbon Dioxide and Steam at Elevated Pressures. PhD Thesis, University of Newcastle, **2000**.

11.   Higman, C.; Tam, S., Advances in Coal Gasification, Hydrogenation, and Gas Treating for the Production of Chemicals and Fuels. *Chemical Reviews* **2014,** *114* (3), 1673-1708.

12.   Everson, R. C.; Neomagus, H. W. J. P.; van der Merwe, G. W.; Koekemoer, A.; Bunt, J. R., The properties of large coal particles and reaction kinetics of corresponding chars. *Fuel* **2015,** *140*, 17-26.

13.   Cheremisinoff, N. P.; Haddadin, M. B., 1 - Refining Operations and the Sources of Pollution. In *Beyond Compliance*, Cheremisinoff, N. P.; Haddadin, M. B., Eds. Gulf Publishing Company: **2006**; pp 1-77.

14.   Skhonde, M. P.; Matjie, R. H.; Bunt, J. R.; Strydom, A. C.; Schobert, H., Sulfur Behavior in the Sasol−Lurgi Fixed-Bed Dry-Bottom Gasification Process. *Energy & Fuels* **2009,** *23* (1), 229-235.

15.   Hower, J. C.; Henke, K. R.; Dai, S.; Ward, C. R.; French, D.; Liu, S.; Graham, U. M., 2 - Generation and nature of coal fly ash and bottom ash. In *Coal Combustion Products (CCP's)*, Robl, T.; Oberlink, A.; Jones, R., Eds. Woodhead Publishing: **2017**; pp 21-65.

16.   Bell, D. A.; Towler, B. F.; Fan, M., Chapter 4 - Gasifiers. In *Coal Gasification and Its Applications*, Bell, D. A.; Towler, B. F.; Fan, M., Eds. William Andrew Publishing: Boston, **2011**; pp 73-100.

17.   Mahinpey, N.; Gomez, A., Review of gasification fundamentals and new findings: Reactors, feedstock, and kinetic studies. *Chemical Engineering Science* **2016,** *148*, 14-31.

18.   Yun, Y.; Lee, G.-B., Effects of pressure in coal pyrolysis observed by high pressure TGA. *Korean Journal of Chemical Engineering* **1999,** *16* (6), 798-803.

19.   Shi, L.; Liu, Q.; Guo, X.; Wu, W.; Liu, Z., Pyrolysis behavior and bonding information of coal — A TGA study. *Fuel Processing Technology* **2013,** *108*, 125-132.

20.   Dwivedi, K. K.; Chatterjee, P. K.; Karmakar, M. K.; Pramanick, A. K., Pyrolysis characteristics and kinetics of Indian low rank coal using thermogravimetric analysis. *International Journal of Coal Science & Technology* **2019,** *6* (1), 102-112.

21.   Roberts, D. G.; Harris, D. J., A Kinetic Analysis of Coal Char Gasification Reactions at High Pressures. *Energy & Fuels* **2006,** *20* (6), 2314-2320.

22.   Tanner, J.; Bhattacharya, S., Kinetics of CO_2 and steam gasification of Victorian brown coal chars. *Chemical Engineering Journal* **2016,** *285*, 331-340.

23.   Laurendeau, N. M., Heterogeneous kinetics of coal char gasification and combustion. *Progress in Energy and Combustion Science* **1978,** *4* (4), 221-270.

24.   Messenböck, R. C.; Dugwell, D. R.; Kandiyoti, R., CO_2 and steam-gasification in a high-pressure wire-mesh reactor: the reactivity of Daw Mill coal and combustion reactivity of its chars. *Fuel* **1999,** *78* (7), 781-793.

25.   Roberts, D. G.; Harris, D. J., Char Gasification with O_2, CO_2, and H_2O: Effects of Pressure on Intrinsic Reaction Kinetics. *Energy & Fuels* **2000,** *14* (2), 483-489.

26.   Zhang, X.; Dong, L.; Zhang, J.; Tian, Y.; Xu, G., Coal pyrolysis in a fluidized bed reactor simulating the process conditions of coal topping in CFB boiler. *Journal of Analytical and Applied Pyrolysis* **2011,** *91* (1), 241-250.

27.   Kajitani, S.; Tay, H.-L.; Zhang, S.; Li, C.-Z., Mechanisms and kinetic modelling of steam gasification of brown coal in the presence of volatile–char interactions. *Fuel* **2013,** *103*, 7-13.

28.   Spiegl, N.; Sivena, A.; Lorente, E.; Paterson, N.; Millan, M., Investigation of the Oxy-fuel Gasification of Coal in a Laboratory-Scale Spouted-Bed Reactor: Reactor Modifications and Initial Results. *Energy & Fuels* **2010,** *24* (9), 5281-5288.

29.   Long, X.; Spiegl, N.; Berrueco, C.; Paterson, N.; Millan, M., Fluidised bed oxy-fuel gasification of coal: Interactions between volatiles and char at varying pressures and fuel feed rates. *Chemical Engineering Science: X* **2020,** *8*, 100068.

30.   Tremel, A.; Haselsteiner, T.; Kunze, C.; Spliethoff, H., Experimental investigation of high temperature and high pressure coal gasification. *Applied Energy* **2012,** *92*, 279-285.

31.   Steibel, M.; Halama, S.; Geißler, A.; Spliethoff, H., Gasification kinetics of a bituminous coal at elevated pressures: Entrained flow experiments and numerical simulations. *Fuel* **2017,** *196*, 210-216.

32.   Loison; Chauvin, Chim. Ind. (Paris). *Chim. Ind. (Paris)* **1964,** *91*, 269.

33.   Anthony, D. B.; Howard, J. B., Coal devolatilization and hydrogastification. *AIChE Journal* **1976,** *22* (4), 625-656.

34.   Anthony, D. B.; Howard, J. B.; Hottel, H. C.; Meissner, H. P., Rapid devolatilization and hydrogasification of bituminous coal. *Fuel* **1976,** *55* (2), 121-128.

35.   Suuberg, E. M.; Peters, W. A.; Howard, J. B., Product Composition and Kinetics of Lignite Pyrolysis. *Industrial & Engineering Chemistry Process Design and Development* **1978,** *17* (1), 37-46.

36.   Suuberg, E. M.; Peters, W. A.; Howard, J. B., Product compositions in rapid hydropyrolysis of coal. *Fuel* **1980,** *59* (6), 405-412.

37.   Hamilton, L. H.; Ayling, A. B.; Shibaoka, M., A new experimental device for pyrolysing coal particles under controlled conditions over a wide range of heating rates. *Fuel* **1979,** *58* (12), 873-876.

38.   Hamilton, L. H., A preliminary account of char structures produced from Liddell vitrinite pyrolysed at various heating rates. *Fuel* **1980,** *59* (2), 112-116.

39.   Stangeby, P. C.; Sears, P. L., Rapid pyrolysis and hydropyrolysis of Canadian coals. *Fuel* **1981,** *60* (2), 131-135.

40.   Niksa, S. J.; Russel, W. B.; Saville, D. A., Captive sample reactor for kinetic studies of coal pyrolysis and hydropyrolysis on short time scales. *Fuel* **1982,** *61* (12), 1207-1212.

41.   Gibbins-Matham, J.; Kandiyoti, R., Coal pyrolysis yields from fast and slow heating in a wire-mesh apparatus with a gas sweep. *Energy & Fuels* **1988,** *2* (4), 505-511.

42.   Madrali, E. S.; Wu, F.; Rahman, M.; Kinghorn, R. R. F.; Herod, A. A.; Kandiyoti, R., Structural relationships between kerogens and their pyrolysis products determined with a wire-mesh reactor. *Fuel* **1994,** *73* (12), 1829-1835.

43.   Gibbins, J.; Kandiyoti, R., Experimental study of coal pyrolysis and hydropyrolysis at elevated pressures using a variable heating rate wire-mesh apparatus. *Energy & Fuels* **1989,** *3* (6), 670-677.

44.   Peralta, D.; Paterson, N.; Dugwell, D.; Kandiyoti, R., Pyrolysis and CO_2 Gasification of Chinese Coals in a High-Pressure Wire-Mesh Reactor under Conditions Relevant to Entrained-Flow Gasification. *Energy & Fuels* **2005,** *19* (2), 532-537.

45.   Gibbins, J. R. Investigation of Primary Coal Pyrolysis Processes using a Variable Heating Wire-Mesh Apparatus. PhD Thesis, University of London, **1988**.

46.   Xu, W.-C.; Tomita, A., Effect of coal type on the flash pyrolysis of various coals. *Fuel* **1987,** *66* (5), 627-631.

47.   Cai, H. Y.; Chatzakis, I. N.; Dugwell, D. R.; Kandiyoti, R., Correlations of pyrolysis yields with coal properties: Characterisation using a wire-mesh reactor and FT-ir spectroscopy. ELSEVIER SCIENCE PUBL B V: **1995**; pp 841-844.

48.   Cai, H. Y.; Megaritis, A.; Messenböck, R.; Dix, M.; Dugwell, D. R.; Kandiyoti, R., Pyrolysis of coal maceral concentrates under pf-combustion conditions (I): changes in volatile release and char combustibility as a function of rank. *Fuel* **1998,** *77* (12), 1273-1282.

49.   Li, C.-Z.; Bartle, K. D.; Kandiyoti, R., Vacuum pyrolysis of maceral concentrates in a wire-mesh reactor. *Fuel* **1993,** *72* (11), 1459-1468.

50.   Sathe, C.; Pang, Y.; Li, C.-Z., Effects of Heating Rate and Ion-Exchangeable Cations on the Pyrolysis Yields from a Victorian Brown Coal. *Energy & Fuels* **1999,** *13* (3), 748-755.

51.   Li, Q.; Wang, Z.; He, Y.; Sun, Q.; Zhang, Y.; Kumar, S.; Zhang, K.; Cen, K., Pyrolysis Characteristics and Evolution of Char Structure during Pulverized Coal Pyrolysis in Drop Tube Furnace: Influence of Temperature. *Energy & Fuels* **2017,** *31* (5), 4799-4807.

52.   Cai, H. Y.; Güell, A. J.; Chatzakis, I. N.; Lim, J. Y.; Dugwell, D. R.; Kandiyoti, R., Combustion reactivity and morphological change in coal chars: Effect of pyrolysis temperature, heating rate and pressure. *Fuel* **1996,** *75* (1), 15-24.

53.   Barr, M. R.; Volpe, R.; Kandiyoti, R., Influence of Reactor Design on Product Distributions from Biomass Pyrolysis. *ACS Sustainable Chemistry & Engineering* **2019,** *7* (16), 13734-13745.

54.   Megaritis, A.; Messenböck, R. C.; Chatzakis, I. N.; Dugwell, D. R.; Kandiyoti, R., High-pressure pyrolysis and CO_2-gasification of coal maceral concentrates: conversions and char combustion reactivities. *Fuel* **1999,** *78* (8), 871-882.

55.   Wall, T. F.; Liu, G.-s.; Wu, H.-w.; Roberts, D. G.; Benfell, K. E.; Gupta, S.; Lucas, J. A.; Harris, D. J., The effects of pressure on coal reactions during pulverised coal combustion and gasification. *Progress in Energy and Combustion Science* **2002,** *28* (5), 405-433.

56.   Solomon, P. R.; Fletcher, T. H., Impact of coal pyrolysis on combustion. *Symposium (International) on Combustion* **1994,** *25* (1), 463-474.

57.   Zeng, D.; Fletcher, T. H., Effects of Pressure on Coal Pyrolysis and Char Morphology. *Energy & Fuels* **2005,** *19* (5), 1828-1838.

58.   Oh, M. S.; Peters, W. A.; Howard, J. B., An experimental and modeling study of softening coal pyrolysis. *AIChE Journal* **1989,** *35* (5), 775-792.

59.   Howaniec, N., The effects of pressure on coal chars porous structure development. *Fuel* **2016,** *172*, 118-123.

60.   Güell, A. J.; Cai, H. Y.; Dugwell, D. R.; Kandiyoti, R., Combustion and gasification reactivities of hydropyrolysis chars: Effect of pressure and heating rate. *Fuel Processing Technology* **1993,** *36* (1), 259-265.

61.   Roberts, D. G.; Harris, D. J.; Wall, T. F., On the Effects of High Pressure and Heating Rate during Coal Pyrolysis on Char Gasification Reactivity. *Energy & Fuels* **2003,** *17* (4), 887-895.

62.   Lee, C. W.; Jenkins, R. G.; Schobert, H. H., Structure and reactivity of char from elevated pressure pyrolysis of Illinois No. 6 bituminous coal. *Energy & Fuels* **1992,** *6* (1), 40-47.

63.   Yang, H.; Chen, H.; Ju, F.; Yan, R.; Zhang, S., Influence of Pressure on Coal Pyrolysis and Char Gasification. *Energy & Fuels* **2007,** *21* (6), 3165-3170.

64.   Zhu, W.; Song, W.; Lin, W., Effect of the Coal Particle Size on Pyrolysis and Char Reactivity for Two Types of Coal and Demineralized Coal. *Energy & Fuels* **2008,** *22* (4), 2482-2487.

65.   Zhuo, Y.; Messenböck, R.; Collot, A. G.; Megaritis, A.; Paterson, N.; Dugwell, D. R.; Kandiyoti, R., Conversion of coal particles in pyrolysis and gasification: comparison of

conversions in a pilot-scale gasifier and bench-scale test equipment. *Fuel* **2000,** *79* (7), 793-802.

66.   Yu, J.; Sun, L.; Berrueco, C.; Fidalgo, B.; Paterson, N.; Millan, M., Influence of temperature and particle size on structural characteristics of chars from Beechwood pyrolysis. *Journal of Analytical and Applied Pyrolysis* **2018,** *130*, 127-134.

67.   Hanson, S.; Patrick, J. W.; Walker, A., The effect of coal particle size on pyrolysis and steam gasification. *Fuel* **2002,** *81* (5), 531-537.

68.   Tremel, A. Reaction Kinetics of Solid Fuels during Entrained Flow Gasification. PhD Thesis, Technical University of Munich, **2012**.

69.   Irfan, M. F.; Usman, M. R.; Kusakabe, K., Coal gasification in CO_2 atmosphere and its kinetics since 1948: A brief review. *Energy* **2011,** *36* (1), 12-40.

70.   Hodge, E. M.; Roberts, D. G.; Harris, D. J.; Stubington, J. F., The Significance of Char Morphology to the Analysis of High-Temperature Char−CO_2 Reaction Rates. *Energy & Fuels* **2010,** *24* (1), 100-107.

71.   Walker, P. L.; Rusinko, F.; Austin, L. G., Gas Reactions of Carbon. In *Advances in Catalysis*, Eley, D. D.; Selwood, P. W.; Weisz, P. B., Eds. Academic Press: **1959**; Vol. 11, pp 133-221.

72.   Spiegl, N.; Berrueco, C.; Long, X.; Paterson, N.; Millan, M., Production of a fuel gas by fluidised bed coal gasification compatible with CO_2 capture. *Fuel* **2020,** *259*, 116242.

73.   Ergun, S., Kinetics of the Reaction of Carbon with Carbon Dioxide. *The Journal of Physical Chemistry* **1956,** *60* (4), 480-485.

74.   Roberts, D. G.; Harris, D. J., High-Pressure Char Gasification Kinetics: CO Inhibition of the C–CO_2 Reaction. *Energy & Fuels* **2012,** *26* (1), 176-184.

75.   Blackwood, J. D.; Ingeme, A. J., The Reaction of Carbon with Carbon Dioxide at High Pressure. *Australian Journal of Chemistry* **1960,** *13* (2), 194-209.

76.   Kajitani, S.; Suzuki, N.; Ashizawa, M.; Hara, S., CO_2 gasification rate analysis of coal char in entrained flow coal gasifier. *Fuel* **2006,** *85* (2), 163-169.

77.   Dutta, S.; Wen, C. Y.; Belt, R. J., Reactivity of Coal and Char. 1. In Carbon Dioxide Atmosphere. *Industrial & Engineering Chemistry Process Design and Development* **1977,** *16* (1), 20-30.

78.   Liu, L.; Cao, Y.; Liu, Q., Kinetics studies and structure characteristics of coal char under pressurized CO_2 gasification conditions. *Fuel* **2015,** *146*, 103-110.

79.   Ochoa, J.; Cassanello, M. C.; Bonelli, P. R.; Cukierman, A. L., CO_2 gasification of Argentinean coal chars: a kinetic characterization. *Fuel Processing Technology* **2001,** *74* (3), 161-176.

80.   Roberts, D. G.; Hodge, E. M.; Harris, D. J.; Stubington, J. F., Kinetics of Char Gasification with CO_2 under Regime II Conditions: Effects of Temperature, Reactant, and Total Pressure. *Energy & Fuels* **2010,** *24* (10), 5300-5308.

81.   Ahn, D. H.; Gibbs, B. M.; Ko, K. H.; Kim, J. J., Gasification kinetics of an Indonesian sub-bituminous coal-char with CO_2 at elevated pressure. *Fuel* **2001,** *80* (11), 1651-1658.

82.   Jayaraman, K.; Gokalp, I.; Bonifaci, E.; Merlo, N., Kinetics of steam and CO_2 gasification of high ash coal–char produced under various heating rates. *Fuel* **2015,** *154*, 370-379.

83.   Guizani, C.; Escudero Sanz, F. J.; Salvador, S., The gasification reactivity of high-heating-rate chars in single and mixed atmospheres of H_2O and CO_2. *Fuel* **2013,** *108*, 812-823.

84.   Everson, R. C.; Neomagus, H. W. J. P.; Kaitano, R.; Falcon, R.; du Cann, V. M., Properties of high ash coal-char particles derived from inertinite-rich coal: II. Gasification kinetics with carbon dioxide. *Fuel* **2008,** *87* (15), 3403-3408.

85.   Chen, J.; Chen, W.; Ji, R.; Jiao, Y.; Wang, X., Kinetic studies on bituminous coal char gasification using CO_2 and H_2O mixtures. *International Journal of Green Energy* **2019,** *16* (14), 1144-1151.

86.   Osafune, K.; Marsh, H., Gasification kinetics of coal chars in carbon dioxide. *Fuel* **1988,** *67* (3), 384-388.

87.   Liu, L.; Kong, B.; Jiao, Q.; Yang, J.; Liu, Q.; Liu, X., Structure Characterization and CO_2 Gasification Kinetics of Tri-High Coal-Chars Derived from High-Temperature Pyrolysis. *ACS Omega* **2019,** *4* (21), 19030-19036.

88.   Kim, R.-G.; Hwang, C.-W.; Jeon, C.-H., Kinetics of coal char gasification with CO_2: Impact of internal/external diffusion at high temperature and elevated pressure. *Applied Energy* **2014,** *129*, 299-307.

89.   Gomez, A.; Mahinpey, N., Kinetic study of coal steam and CO_2 gasification: A new method to reduce interparticle diffusion. *Fuel* **2015,** *148*, 160-167.

90.   Senneca, O.; Russo, P.; Salatino, P.; Masi, S., The relevance of thermal annealing to the evolution of coal char gasification reactivity. *Carbon* **1997,** *35* (1), 141-151.

91.   Gomez, A.; Silbermann, R.; Mahinpey, N., A comprehensive experimental procedure for CO_2 coal gasification: Is there really a maximum reaction rate? *Applied Energy* **2014,** *124*, 73-81.

92.   Zhou, L.; Zhang, G.; Schurz, M.; Steffen, K.; Meyer, B., Kinetic study on CO_2 gasification of brown coal and biomass chars: reaction order. *Fuel* **2016,** *173*, 311-319.

93.   Malekshahian, M.; Hill, J. M., Kinetic Analysis of CO_2 Gasification of Petroleum Coke at High Pressures. *Energy & Fuels* **2011,** *25* (9), 4043-4048.

94.   Hüttinger, K. J.; Nill, J. S., A method for the determination of active sites and true activation energies in carbon gasification: (II) Experimental results. *Carbon* **1990,** *28* (4), 457-465.

95.   Liu, L.; Cao, Y.; Liu, Q.; Yang, J., Experimental and kinetic studies of coal–CO_2 gasification in isothermal and pressurized conditions. *RSC Advances* **2017,** *7* (4), 2193-2201.

96.   Mi, J.; Wang, N.; Wang, M.; Huo, P.; Liu, D., Investigation on the catalytic effects of AAEM during steam gasification and the resultant char reactivity in oxygen using Shengli lignite at different forms. *International Journal of Coal Science & Technology* **2015,** *2* (3), 223-231.

97.   Ohme, H.; Suzuki, T., Mechanisms of CO_2 Gasification of Carbon Catalyzed with Group VIII Metals. 1. Iron-Catalyzed CO_2 Gasification. *Energy & Fuels* **1996,** *10* (4), 980-987.

98.   Wang, J.; Yao, Y.; Cao, J.; Jiang, M., Enhanced catalysis of K_2CO_3 for steam gasification of coal char by using $Ca(OH)_2$ in char preparation. *Fuel* **2010,** *89* (2), 310-317.

99.   Popa, T.; Fan, M.; Argyle, M. D.; Slimane, R. B.; Bell, D. A.; Towler, B. F., Catalytic gasification of a Powder River Basin coal. *Fuel* **2013,** *103*, 161-170.

100.   Tay, H.-L.; Kajitani, S.; Wang, S.; Li, C.-Z., A preliminary Raman spectroscopic perspective for the roles of catalysts during char gasification. *Fuel* **2014,** *121*, 165-172.

101.   Zhang, J.; Zhang, R.; Bi, J., Effect of catalyst on coal char structure and its role in catalytic coal gasification. *Catalysis Communications* **2016,** *79*, 1-5.

102.   Zhang, Z. G.; Kyotani, T.; Tomita, A., Dynamic behavior of surface oxygen complexes during oxygen-chemisorption and subsequent temperature-programmed desorption of calcium-loaded coal chars. *Energy & Fuels* **1989,** *3* (5), 566-571.

103.   Wang, M.; Roberts, D. G.; Kochanek, M. A.; Harris, D. J.; Chang, L.; Li, C.-Z., Raman Spectroscopic Investigations into Links between Intrinsic Reactivity and Char Chemical Structure. *Energy & Fuels* **2014,** *28* (1), 285-290.

104.   Li, X.; Hayashi, J.-i.; Li, C.-Z., Volatilisation and catalytic effects of alkali and alkaline earth metallic species during the pyrolysis and gasification of Victorian brown coal. Part VII. Raman spectroscopic study on the changes in char structure during the catalytic gasification in air. *Fuel* **2006,** *85* (10), 1509-1517.

105.   Solomon, P. R.; Hamblen, D. G.; Carangelo, R. M.; Serio, M. A.; Deshpande, G. V., General model of coal devolatilization. *Energy & Fuels* **1988,** *2* (4), 405-422.

106.   Yang, H.; Fletcher, T. H.; Li, S.; Hu, H.; Jin, L.; Li, Y., Model for the Evolution of Pore Structure in a Lignite Particle during Pyrolysis. 2. Influence of Cross-Linking Reactions, Molten Metaplast, and Molten Ash on Particle Surface Area. *Energy & Fuels* **2017,** *31* (8), 8036-8044.

107.   Solomon, P. R.; Hamblen, D. G.; Serio, M. A.; Yu, Z.-Z.; Charpenay, S., A characterization method and model for predicting coal conversion behaviour. *Fuel* **1993,** *72* (4), 469-488.

108.   Richards, A. P.; Fletcher, T. H., A comparison of simple global kinetic models for coal devolatilization with the CPD model. *Fuel* **2016,** *185*, 171-180.

109.   Mishra, G.; Bhaskar, T., Non isothermal model free kinetics for pyrolysis of rice straw. *Bioresource Technology* **2014,** *169*, 614-621.

110.   Liu, S.; Yu, J.; Bikane, K.; Chen, T.; Ma, C.; Wang, B.; Sun, L., Rubber pyrolysis: Kinetic modeling and vulcanization effects. *Energy* **2018,** *155*, 215-225.

111.   Friedman, H. L., Kinetics of thermal degradation of char-forming plastics from thermogravimetry. Application to a phenolic plastic. *J. Polym. Sci. Polym. Symp.* **1964,** *6* (1), 183-195.

112.   Kissinger, H. E., Reaction Kinetics in Differential Thermal Analysis. *Analytical Chemistry* **1957,** *29* (11), 1702-1706.

113.   Ozawa, T., A New Method of Analyzing Thermogravimetric Data. *Bulletin of the Chemical Society of Japan* **1965,** *38* (11), 1881-1886.

114.   Flynn, J. H.; Wall, L. A., A quick, direct method for the determination of activation energy from thermogravimetric data. *Journal of Polymer Science Part B: Polymer Letters* **1966,** *4* (5), 323-328.

115.   Opfermann, J. R.; Kaisersberger, E.; Flammersheim, H. J., Model-free analysis of thermoanalytical data-advantages and limitations. *Thermochimica Acta* **2002,** *391* (1), 119-127.

116.   Bhagavatula, A.; Shah, N.; Honaker, R., Estimating the Pyrolysis Kinetic Parameters of Coal, Biomass, and Their Blends: A Comparative Study. *Energy & Fuels* **2016,** *30* (12), 10045-10054.

117.   Zhang, Q.; Luo, M.; Yan, L.; Yang, A.; Hui, X., Kinetic Analysis of Low-Rank Coal Pyrolysis by Model-Free and Model-Fitting Methods. *Journal of Chemistry* **2019,** *2019*, 9075862.

118.   Yan, J.; Jiao, H.; Li, Z.; Lei, Z.; Wang, Z.; Ren, S.; Shui, H.; Kang, S.; Yan, H.; Pan, C., Kinetic analysis and modeling of coal pyrolysis with model-free methods. *Fuel* **2019,** *241*, 382-391.

119.   Anthony, D. B.; Howard, J. B.; Hottel, H. C.; Meissner, H. P., Rapid devolatilization of pulverized coal. *Symposium (International) on Combustion* **1975,** *15* (1), 1303-1317.

120.   Vand, V., A theory of the irreversible electrical resistance changes of metallic films evaporated in vacuum. *Proceedings of the Physical Society* **1943,** *55* (3), 222-246.

121.   Pitt, G. J., The kinetics of the evolution of volatile products from coal. *Fuel* **1962,** *41* (3), 267-274.

122.   de Caprariis, B.; De Filippis, P.; Herce, C.; Verdone, N., Double-Gaussian Distributed Activation Energy Model for Coal Devolatilization. *Energy & Fuels* **2012,** *26* (10), 6153-6159.

123.   Cai, J.; Liu, R., Weibull Mixture Model for Modeling Nonisothermal Kinetics of Thermally Stimulated Solid-State Reactions: Application to Simulated and Real Kinetic Conversion Data. *The Journal of Physical Chemistry B* **2007,** *111* (36), 10681-10686.

124.   Maki, T.; Takatsuno, A.; Miura, K., Analysis of Pyrolysis Reactions of Various Coals Including Argonne Premium Coals Using a New Distributed Activation Energy Model. *Energy & Fuels* **1997,** *11* (5), 972-977.

125.   Miura, K.; Maki, T., A Simple Method for Estimating f(E) and k_0(E) in the Distributed Activation Energy Model. *Energy & Fuels* **1998,** *12* (5), 864-869.

126.   Kobayashi, H.;   Howard, J. B.; Sarofim, A. F., Coal devolatilization at high temperatures. *Symposium (International) on Combustion* **1977,** *16* (1), 411-425.

127.   Fletcher, T. H.; Kerstein, A. R.; Pugmire, R. J.; Solum, M. S.; Grant, D. M., Chemical percolation model for devolatilization. 3. Direct use of carbon-13 NMR data to predict effects of coal type. *Energy & Fuels* **1992,** *6* (4), 414-431.

128.   Yamamoto, K.; Murota, T.; Okazaki, T.; Taniguchi, M., Large eddy simulation of a pulverized coal jet flame ignited by a preheated gas flow. *Proceedings of the Combustion Institute* **2011,** *33* (2), 1771-1778.

129.   Bell, D. A.; Towler, B. F.; Fan, M., Chapter 3 - Gasification Fundamentals. In *Coal Gasification and Its Applications*, Bell, D. A.; Towler, B. F.; Fan, M., Eds. William Andrew Publishing: Boston, **2011**; pp 35-71.

130.   Bhatia, S. K.; Perlmutter, D. D., A random pore model for fluid-solid reactions: I. Isothermal, kinetic control. *AIChE Journal* **1980,** *26* (3), 379-386.

131.   Liu, G.-s.; Tate, A. G.; Bryant, G. W.; Wall, T. F., Mathematical modeling of coal char reactivity with CO_2 at high pressures and temperatures. *Fuel* **2000,** *79* (10), 1145-1154.

Chapter 3

Experimental Methods

3.1 Introduction

This chapter extensively describes both the atmospheric pressure and high-pressure wire-mesh reactor setups, used for the pyrolysis and gasification of Morupule coal, equipped with gas and heating control systems. Section 3.2 describes the WMR reactor setup developed at Imperial College London, and the standard procedures for running wire-mesh reactor experimental tests coupled with product quantification. Section 3.3 details the analytical techniques used for the characterisation of the chemical structure and morphology of coal chars obtained from pyrolysis and gasification. The use of size exclusion chromatography to characterise liquid products (tars) is also described in this section. In addition, the chemical properties of Morupule raw coal are provided together with the relevant analytical techniques.

3.2 Wire-Mesh Reactor (WMR)

3.2.1 Wire-Mesh Reactor Configuration

The WMR reactor configuration was used to study the single particle behaviour of Morupule coal, providing valuable insights into its fundamental pyrolysis and gasification behaviour. The historical development of this reactor system is discussed in Section 2.3.3.4. The basic principle is that a monolayer distribution of coal particles is produced between a folded wire-mesh, which acts as a resistance heater when electric current is passed through it, heating the particles to the desired experimental temperature at a controlled heating rate. Contact between the particles is avoided, owing to the monolayer segregation, allowing each particle to behave independently. This provides insight into the single particle behaviour of the coal. Small particle sizes, typically within the 105 – 150 μm range, are used in order to minimise the effects of transport phenomena limitations which may result in the undesired intraparticle reactions. A continuous sweep flow gas is used to carry volatiles away from the reaction zone, avoiding secondary reactions between volatiles and chars, and allowing for the capture of condensable products by means of a tar trap.

Schematics of the atmospheric pressure and high pressure WMRs used in this work are presented in Figures 3.1 and 3.2, respectively. Figure 3.3 shows the images of the WMR. Both reactors have a brass support plate insulated by mica to avoid short circuiting. Additionally, a 2 mm thick layer of alumina ceramic sheet with a 30 mm hole, purchased from Goodfellow Cambridge Ltd, was used to provide further insulation. The brass support plate has a 30 mm (diameter) hole at the centre to allow for the passage of the gas. During experiments, the mesh retained its size and shape owing to the use of a spring-loaded electrode. Cooling water, circulated through the hollow brass pillars, was used to prevent the electrodes from overheating [1]. Tar traps filled with liquid nitrogen were used to capture the tar (defined as condensable volatiles with a boiling point higher than 50 ⁰C[1]) during atmospheric pressure operation as shown in Figure 3.1. In the high-pressure WMR, a 30 mm glass sintered filter disc was used to smooth the gas flow and avoid gas turbulence under high pressures.

Furthermore, a thick steel pressure bell was used to sustain operation at elevated pressures as shown in Figure 3.2 (a glass bell was used in the atmospheric pressure WMR).
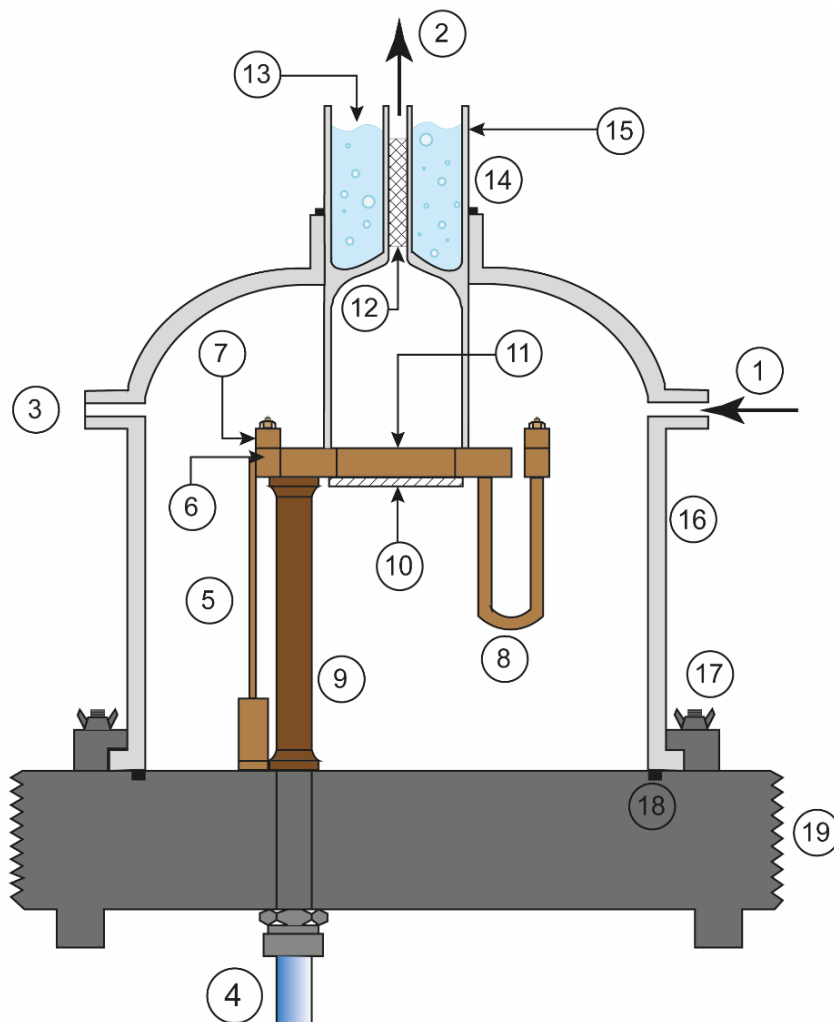
Figure 3. 1 Schematic of the atmospheric pressure WMR adapted from Gibbins [2]. (1) Gas inlet (2) gas outlet (3) outlet to vacuum pump (4) cooling water (5) electric current supply (6) electrode (7) electrode clamp (8) hollow spring (9) hollow brass pillars (10) glass sintered disc (11) sample holder support plate (12) wire-mesh packing (13) liquid nitrogen (14) O-ring (15) tar trap (16) glass bell (17) glass bell clamp (18) base O-ring seal (19) base plate.
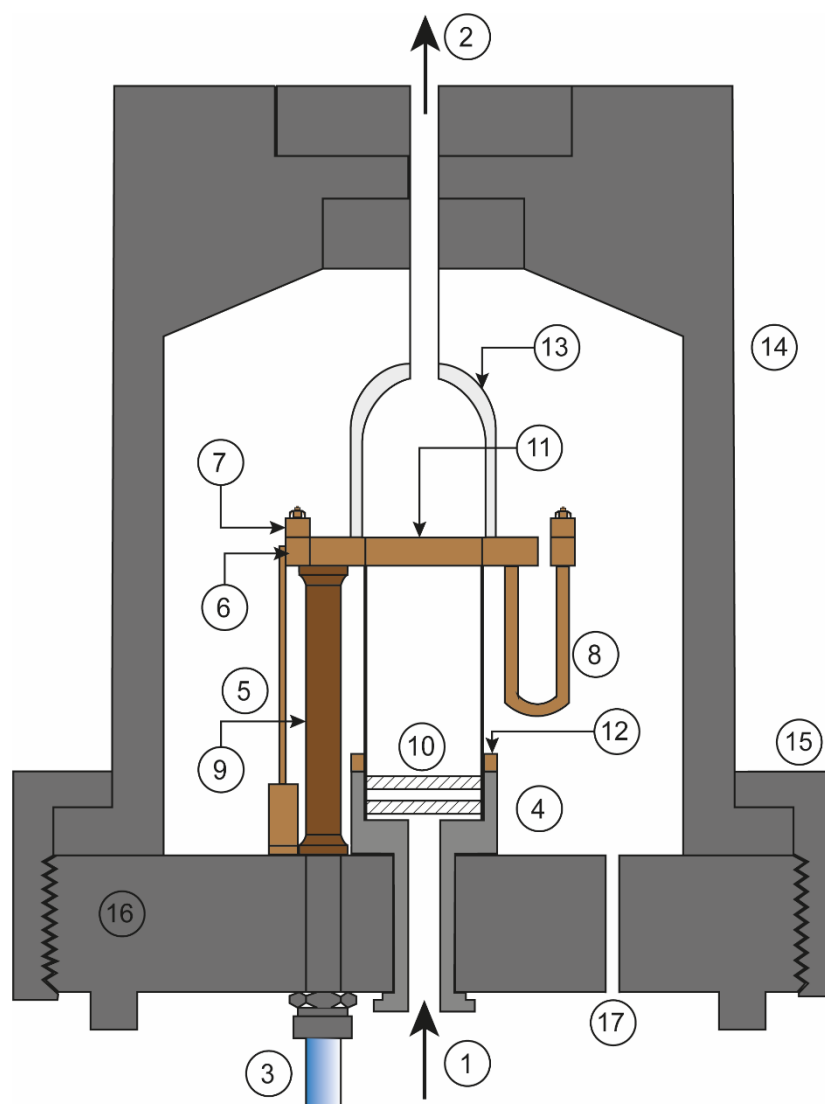
Figure 3. 2 Schematic of the high-pressure WMR adapted from Messenböck [1]. (1) Gas inlet (2) gas outlet (3) cooling water (4) smoothing cell (5) electric current supply (6) electrode (7) electrode clamp (8) hollow spring (9) hollow brass pillars (10) glass sintered disc (11) sample holder support plate (12) copper seals (13) quartz bell (14) stainless steel pressure bell (15) pressure bell clamp (16) base plate (17) pressure gauge inlet.
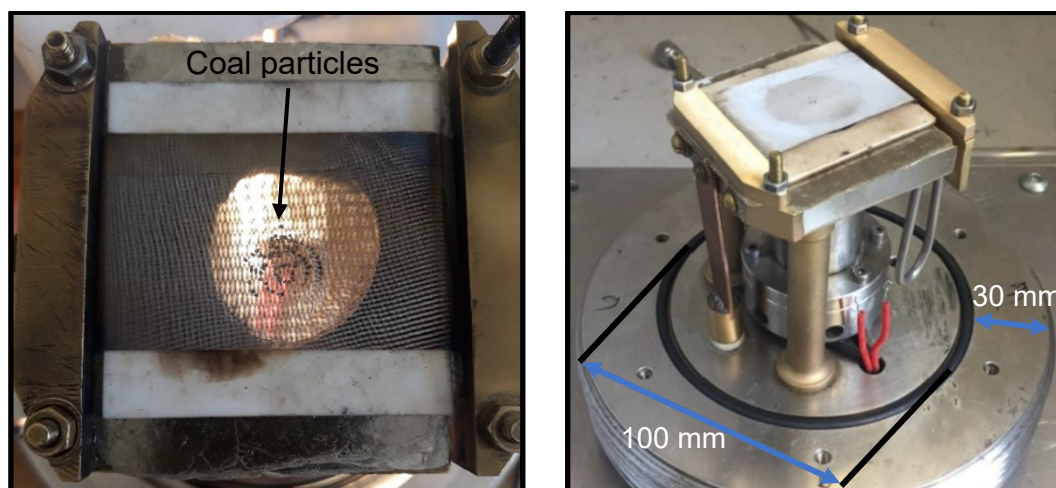
Figure 3. 3 Images of the atmospheric (left) and high (right) pressure wire-mesh reactor (top and side view).

3.2.2 Gas and Heating Control Systems

Figure 3.4 shows a schematic of the experimental rig used for carrying out WMR experiments. The rig is divided into 5 sections: WMR, continuous cooling water flow, gas supply control system, power supply and feedback temperature control system (paired together). A helium CP grade (99.999 % purity) gas cylinder and a CO_2 gas cylinder (99.8 % purity) were used as gas supply for pyrolysis and gasification studies, respectively. Thermal mass flow controllers from IGI Systems Ltd, connected to an interface box and a computer IGI Systems LAB interface software, were used to control the flowrate of helium and CO_2. Feedback temperature was measured using two thermocouples attached to the wire-mesh. K-type thermocouples, Ni90/Cr10 thermocouple alloy (positive thermocouple wire) and Ni95/(Al + Mn + Si)5 thermocouple alloy (negative thermocouple wire) were used for pyrolysis and atmospheric pressure gasification experiments. In high-pressure gasification, S-type thermocouples were used (Pt90/Rh10 as a positive thermocouple wire and a 100 % platinum wire as a negative thermocouple wire). These thermocouple wires were purchased from Goodfellow Cambridge Ltd. Temperature measurement using thermocouple wires allowed comparison with the pre-set experimental temperature, and subsequent power adjustment using a proportional–integral–derivative control system. Within 5 ms, a voltage signal (0 – 5 V) is sent from the control system to the thyristor bridge which then provides an adjusted

alternating current (current is stopped during temperature measurement, alternating current avoids the disturbance in the thermocouple output) of 0 – 120 A at 50 Hz frequency that is passed through variable transformers to the wire-mesh *via* the two electrodes. The feedback temperature control system is well-described by Messenböck [1].
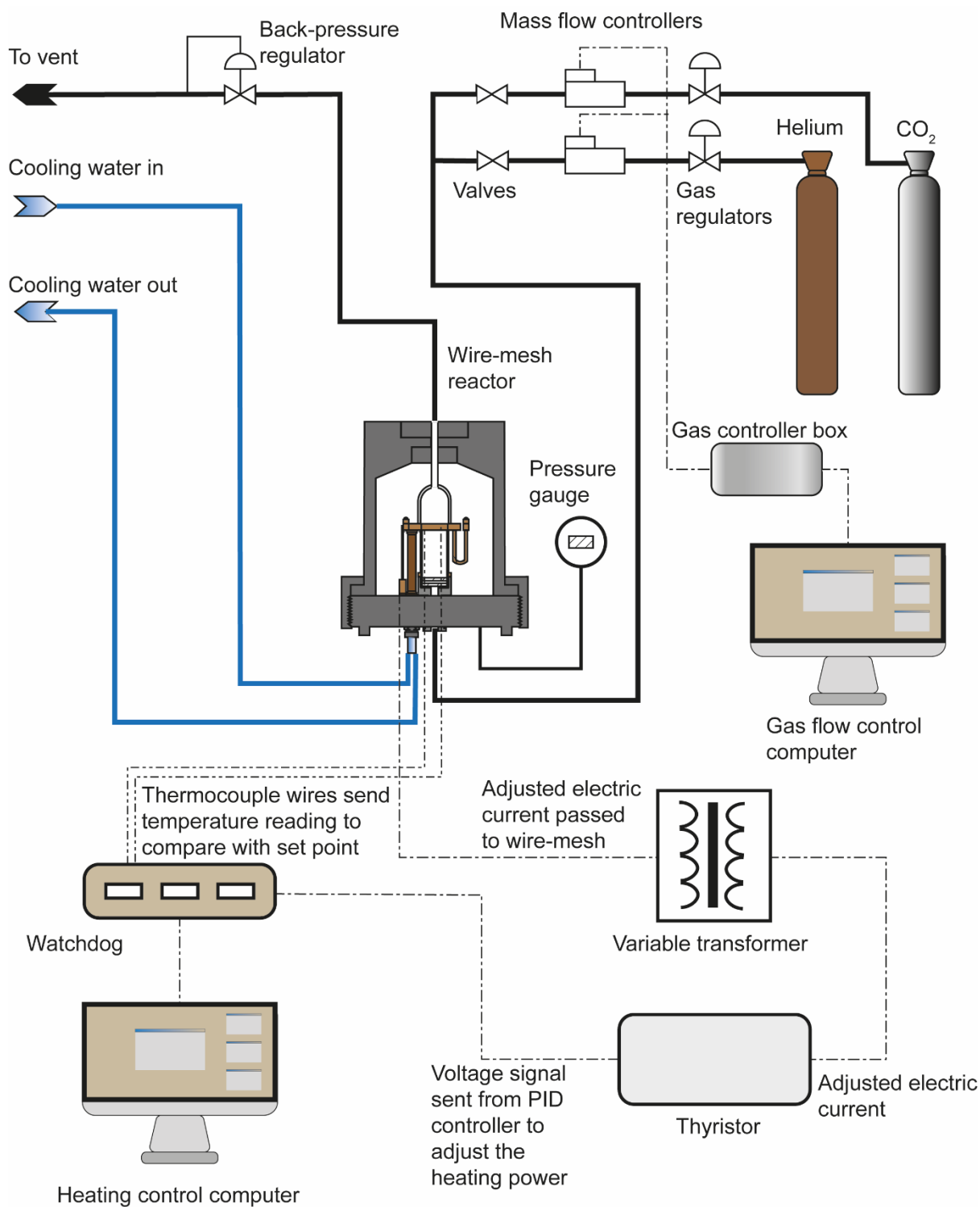
Figure 3. 4 A schematic of the wire-mesh reactor experimental rig.

3.2.3 Experimental Procedure

3.2.3.1 Wire-Mesh Preparation

A Type 304 stainless-steel wire-mesh, with a 63 µm aperture and a wire diameter of 40 µm, purchased from G.Bopp & Co. Ltd, was used for pyrolysis experiments in the present work. Gasification entailed the use of a 106 µm twilled weave molybdenum gauze of 50.9 µm wire diameter purchased from VWR. The mesh was cut using scissors and folded to make the sample holder. Prior to experimentation, the prepared wire-mesh sample holders were washed in N-Methyl-2-pyrrolidone (NMP) for 15 min in an ultra-sonic bath. The NMP-washed sample holders were rinsed using water in an ultra-sonic bath for 15 min and dried overnight in a vacuum oven at 50 ºC. The dried wire-mesh was then washed in a 4:1 mixture of chloroform and methanol in an ultra-sonic bath for 15 min. Thereafter, the washed sample holders were rinsed using water in an ultra-sonic bath for 15 min and dried overnight in the vacuum oven at 50 ºC. The washed stainless-steel wire-mesh were subjected to thermal annealing at 1000 ºC for 30 s in the WMR to ensure complete removal of any present trace impurities [1]. Molybdenum mesh sample holders were ready for experimental tests after the second drying without subsequent annealing.

3.2.3.2 Wire-Mesh Reactor Experimental Tests

Prior to experiments, Morupule coal sample was dried overnight at 105 ºC in a vacuum oven and stored in a desiccator. During experiments, 5 – 6 mg of Morupule coal sample, dispersed to achieve a monolayer distribution (see Figure 3.3), was folded between a stainless-steel or molybdenum wire-mesh, which was then stretched between two electrodes. Depending on the experiment, appropriate thermocouples (K-type or S-type) were installed on the stretched wire-mesh. The closed system was then purged with helium gas to ensure complete removal of air. For tar collection experiments, the tar trap was filled with liquid nitrogen to collect condensable volatiles. To reach a pre-set temperature at a controlled heating rate, an electrical current was applied through the mesh and adjusted accordingly using the feedback

temperature control system. The wire-mesh acts as a resistance heater, enabling the thermal breakdown of Morupule coal. The electrodes were cooled using a water circulation system as shown in Figure 3.4. A continuous stream of helium or CO_2 gas (0.1 m s^{-1}) was passed to carry the evolving volatiles away from the reaction zone to minimise secondary reactions between the evolved volatiles and the heated char. At least three experimental runs were performed and averaged to obtain a data point at each condition. Figure 3.5 presents a fully assembled atmospheric pressure WMR, with liquid nitrogen for tar capture, during an experimental test.
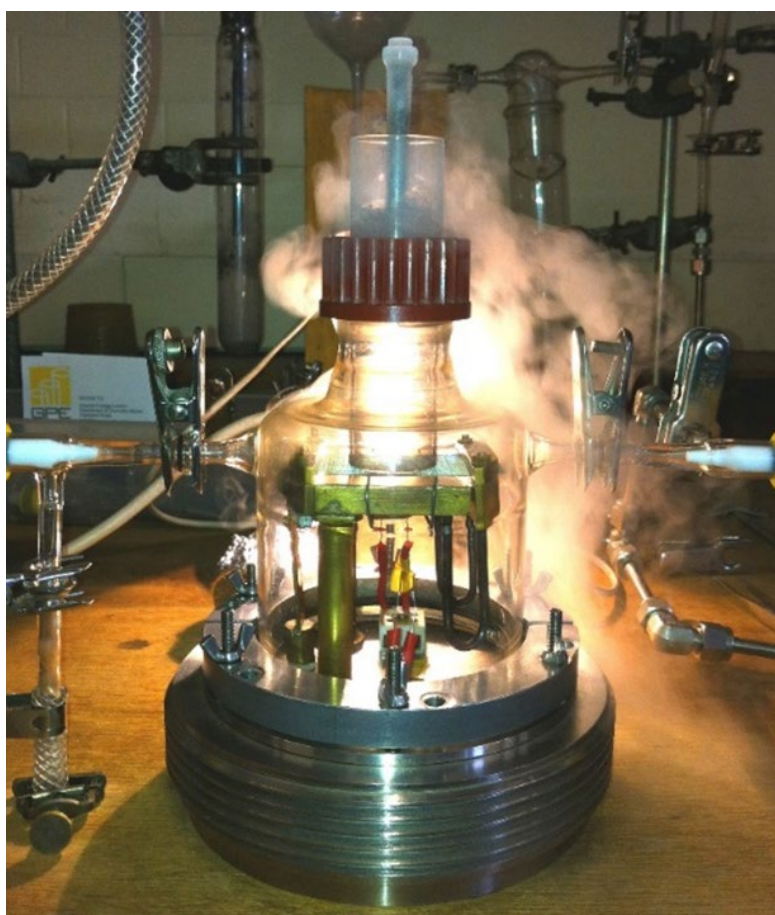
Figure 3. 5 An assembled atmospheric pressure wire-mesh reactor.

3.2.3.3 Product Yields

The key measurement in this work is the weight of the wire-meshes and tar traps before and after experimental tests. A Sartorius balance of model number ME2358, with a precision of 0.01 mg, was used to measure the weight of the wire-meshes and tar traps. This balance was

calibrated and certified yearly by a service engineer from Balance Technology using a set of national standard 10 mg, 20 mg and 200 mg weights. Before each measurement, the weight of the national standard weights was recorded to ensure reliability of the measurements made.

3.2.3.3.1 Total Volatile Yield

The empty and loaded wire-meshes were weighed to determine the weight of the sample before pyrolysis or gasification. After each experimental run, the mesh containing the char was weighed to measure the amount of char. Two weight measurements were carried out and were recorded if they were within 0.02 mg of each other. The total volatile yield was obtained as a percentage difference between the original weight of the sample and the weight of the recovered char on a dry basis (Equation 3.1). The yield was then corrected for the ash content of the coal to obtain it on a dry ash free basis (Equation 3.2). The char was thereafter collected in 5 mL vials for subsequent characterisation of its structural and morphological properties.

$$Total\ volatile\ yield = \frac{Original\ sample\ weight - Char\ weight}{Original\ sample\ weight} \times 100\ (wt.\%, db) \tag{3.1}$$

$$Total\ volatile\ yield = \frac{Original\ sample\ weight - Char\ weight}{Original\ sample\ weight(1 - \frac{ash(wt.\%)}{100})} \times 100\ (wt.\%, daf) \tag{3.2}$$

3.2.3.3.2 Tar Yield

Before each experimental run, the weight of the empty tar trap was measured and recorded. Following an experimental test, the tar trap was placed in a vacuum oven at 50 ºC for 40 min to remove water that had condensed on the outer surface of the tar trap. The tar trap was thereafter left to cool at room temperature for 1 h. It was then weighed to quantify the amount of condensed volatiles. Similarly, each measurement was repeated and recorded if the two measurements were within 0.02 mg of each other. The tar yield was calculated as a percentage of the measured tar weight to the original weight of the sample on a dry basis

(Equation 3.3). The tar yield was then corrected for the ash content of the coal (Equation 3.4). Tar was collected from the tar trap using a 4:1 mixture of chloroform and methanol. The mixture was dried in a nitrogen flow at atmospheric pressure, and the dried tar was stored in a freezer awaiting characterisation.

$$Tar\ yield = \frac{Tar\ trap\ weight - Empty\ tar\ trap\ weight}{Original\ sample\ weight} \times 100\ (wt.\%, db) \quad (3.3)$$

$$Tar\ yield = \frac{Tar\ trap\ weight - Empty\ tar\ trap\ weight}{Original\ sample\ weight(1 - \frac{ash(wt.\%)}{100})} \times 100\ (wt.\%, daf) \quad (3.4)$$

3.2.3.3.3 Gas Yield

The gas yield was estimated by subtracting the tar yield from the total volatile yield corrected for the ash content of the coal (Equation 3.5).

$$Gas\ yield = (total\ volatile\ yield - tar\ yield)\ wt.\%, daf \quad (3.5)$$

3.3 Coal Char and Tar Characterisation

3.3.1 Thermogravimetric Analysis (TGA)

A PerkinElmer Pyris 1 thermogravimetric analyser equipped with inert (N_2 of 99.998 % BOC purity) and oxidising (air of 19.9 - 21.9 % oxygen concentration - BOC) gases was used to study the thermal decomposition and reactivity of Morupule coal and its residual chars, providing further insights into their structural properties. A TGA gives a continuous measure of the time or temperature dependence of the sample weight loss [3].

3.3.1.1 Proximate Analysis

A standard proximate analysis methodology [4] was used to characterise the moisture, volatile matter, fixed carbon and ash contents of Morupule coal used in this work. 10 mg of Morupule

raw coal sample was held at 50 ºC for 10 min in nitrogen gas flowing at 40 mL min^{-1}. The sample was then heated to 110 ºC at 10 ºC min^{-1} and held at the final temperature for 30 min. Weight-loss in this region corresponds to the moisture content. Thereafter, it was heated to 900 ºC at a heating rate of 10 ºC min^{-1} and held for 30 min (volatile matter). The sample was then cooled to 800 ºC at 10 ºC min^{-1}. Upon reaching 800 ºC, the gas was switched to air immediately. This step was carried out for 40 min to determine the fixed carbon content of the coal. Once the 40 min elapsed, the TGA was cooled down. The remaining weight corresponded to the ash content of the coal. This experimental procedure is summarised in Figure 3.6. The proximate analysis of Morupule coal, averaged from three experimental runs, is given in Table 3.1.

Table 3. 1 Proximate analysis of Morupule raw coal as received.

Proximate Analysis (wt.%)	
Moisture	1.5
Volatile matter	22.6
Fixed carbon	56.6
Ash	19.3
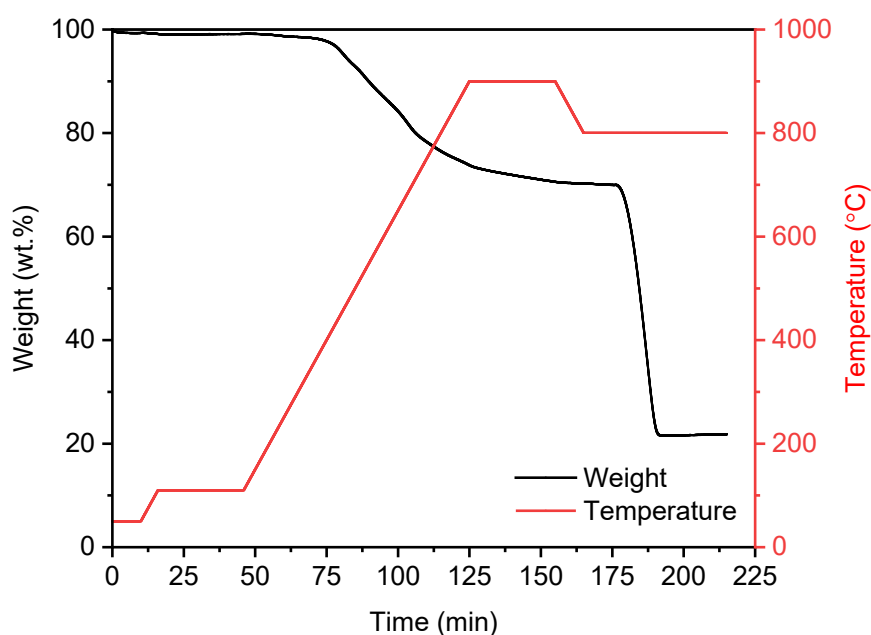
Figure 3. 6 Experimental method for characterising the proximate analysis of Morupule raw coal.

3.3.1.2 Combustion Reactivity

To characterise the combustion reactivity of chars, an isothermal or a non-isothermal method can be employed [1]. In a non-isothermal method, the reactivity is measured as a function of temperature over a constant heating rate. While the reaction time may be reduced, the increase in temperature results in an inconsistent kinetic regime, as diffusional limitations dominate the overall reactivity at high temperatures [5]. Moreover, the devolatilisation step may be incomplete during low temperature pyrolysis. Therefore, a continuous temperature increase in the non-isothermal method may fail to distinguish the influences of thermal degradation and oxidative reactions on char reactivity. An isothermal method fixes a reaction temperature, allowing for separation of chemical reaction and diffusional contributions in determining intrinsic reactivity. Furthermore, since isothermal combustion reactivity is typically carried out at low temperatures of about 500 ºC [1,5], mass losses and annealing processes due to thermal degradation are minimised.

The isothermal combustion method was therefore used to analyse the relative reactivity of Morupule coal chars. 2 – 2.5 mg of sample was heated to 500 ºC at a heating rate of 25 ºC min^{-1} in N_2 flowing at 40 mL min^{-1}. The sample was held at 500 ºC for 5 min. The N_2 sweep gas was switched to air flowing at 40 mL min^{-1} to initiate combustion under conditions believed to be in the chemical reaction controlled regime [6]. The above steps are summarised in the weight-loss profile presented in Figure 3.7. The relative combustion reactivity of chars (Equation 3.6.), $R_{50\%}$, was evaluated for a time required to combust 50 % of the combustible material [7], where W_0 is the dry ash-free weight of the char.
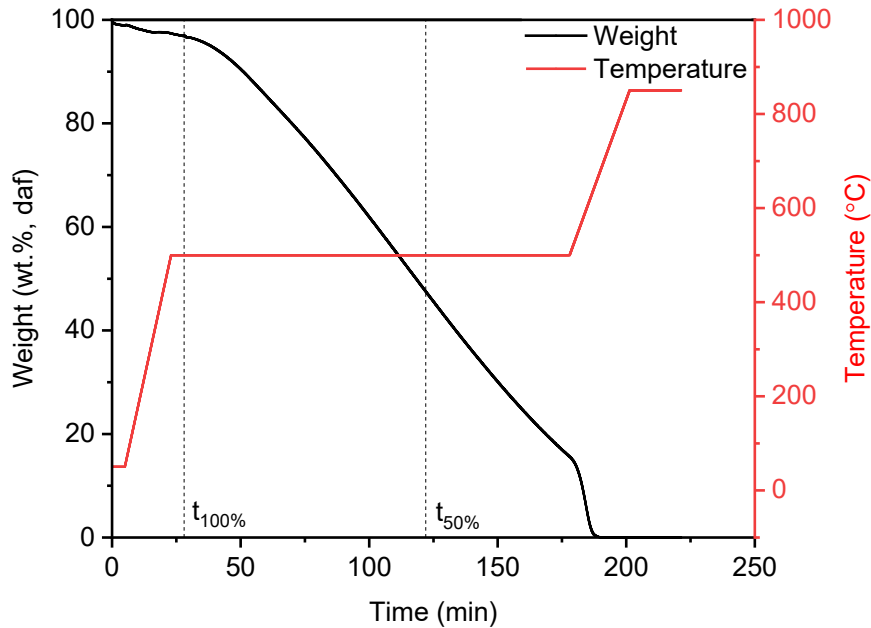
Figure 3. 7 Typical weight-loss profile during a study of combustion reactivity in a thermogravimetric analyser.

$$R_{50\%} = -\frac{1}{W_0}\left(\frac{dW}{dt}\right)_{W=0.5\,W_0} \tag{3.6}$$

3.3.2 Elemental Analysis

The determination of the relative proportions of carbon, hydrogen, nitrogen, sulphur and oxygen is critical in characterising the parent coal and evaluating char chemical structural changes. An Elementar Americas CHNS vario MICRO cube analyser was used to determine the elemental composition of Morupule coal and its chars. The premise of this analytical technique is established on the conversion of the elements to their respective gases, being CO_2, H_2O, NO_x and SO_2, during combustion. These gases are then detected, by means of thermal conductivity after purification in separation trap columns, and the respective elements quantified. The amount of oxygen is estimated by difference. The elemental composition of Morupule raw coal is shown in Table 3.2.

Table 3. 2 Elemental analysis of Morupule raw coal on a dry ash-free basis. b – estimated by difference.

Elemental Analysis (wt.%, daf)	
Carbon	80.7
Hydrogen	4.1
Nitrogen	2.0
Sulphur	1.0
Oxygen[b]	12.2

3.3.3 X-Ray Fluorescence (XRF) Spectroscopy

Morupule coal ash elemental composition was estimated using an X-Ray Fluorescence (XRF) Epsilon 3XLE spectrometer. The application of this analytical technique is predicated on the distinct fluorescent X-Rays emitted by the respective elements. The coal was irradiated with an X-Ray beam and the emerging fluorescent X-Ray was measured using a detector. The main constituents of Morupule coal ash are given in Table 3.3. There are traces of MgO, V_2O_5, Cr_2O_3, MnO, Fe_2O_3, NiO, CuO, ZnO, Ga_2O_3, As_2O_3, Rb_2O, SrO, Y_2O_3, ZrO_2, SnO_2, BaO, Eu_2O_3, Yb_2O_3, PbO and ThO_2 which make up the remaining 1.5 %. Each of these compounds accounts for less than 1000 ppm.

Table 3. 3 Main constituents of Morupule coal ash (%).

Na_2O	Al_2O_3	SiO_2	P_2O_5	SO_3	K_2O	CaO	TiO_2	Fe_2O_3
0.5	28.5	38.6	0.4	7.2	0.9	5.2	3.9	13.3

3.3.4 Fourier Transform Infrared (FTIR) Spectroscopy

The evolution of functional groups present in the coal and coal chars during thermal breakdown was assessed using FTIR spectroscopy. A Spectrum 100 spectrometer coupled with an attenuated total reflectance (ATR) accessory, from Perkin Elmer, was used to obtain the FTIR spectra of the char at a resolution of 4 cm^{-1} between a 4000 – 600 cm^{-1} spectral

range with 16 scans. This technique is based on the distinguished vibrational energies of molecular bonds. Specific infrared radiation frequencies, corresponding to the bond vibrational frequencies, are absorbed if the bond exhibits a change in the dipole moment while the unabsorbed radiation is transmitted and detected.

3.3.5 Raman Spectroscopy

Raman spectroscopy was used to study the bulk chemical structure of residual chars from both pyrolysis and gasification experiments. A confocal Raman microscope SENTERRA II, with a 532 nm laser beam operating at a laser power of 12.5 mW and a spectral resolution of 4 cm^{-1} was used to carry out Raman measurements in an 1800 – 800 cm^{-1} spectral range. Raman measurements are made based on the interactions between the molecular vibrations of the chemical microstructure and the incident light. A small fraction of the scattered light has a different frequency to the incident light as a result of the interactions with the char chemical structure. Such frequency changes correspond to different molecular vibrations and therefore produce a spectrum that characterises the different bonds in the sample of interest [5]. The intensity of the Raman spectrum is dependent on both the light absorptivity and Raman scattering ability of the char [8,9]. As a result of the resonance effect between the oxygen and the oxygen-containing aromatic ring systems, oxygen-containing groups have a high Raman scattering ability, which translates to high Raman intensities [10]. An increase in the concentration of aromatic ring systems leads to increased light absorptivity, and therefore reduces the Raman intensity [11].

In the measured 1800 – 800 cm^{-1} spectral range, there is a D (defect) band between 1327 – 1284 cm^{-1}, that is representative of aromatic ring systems with six or more fused benzene rings [8], and a G (graphite) band around 1590 cm^{-1} related to the inner graphitic plane of the coal/char [12]. The valley between the D and G bands is referred to as the V band (1460 cm^{-1}). It is characteristic of amorphous carbon with three to five fused benzene rings [11,13]. These distinct bands are shown in Figure 3.8.
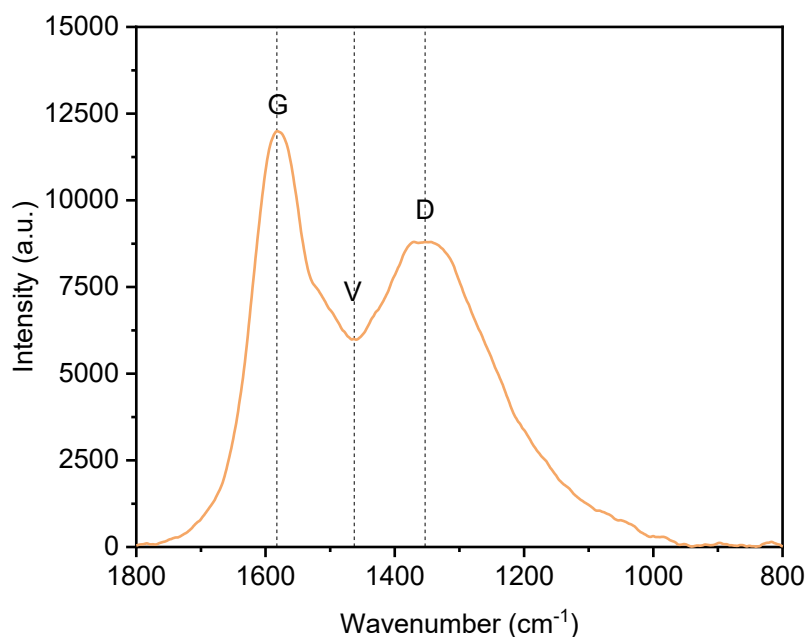
Figure 3. 8 Typical Raman spectra of Morupule coal chars

3.3.6 X-Ray Photoelectron Spectroscopy

The surface chemistry of Morupule coal chars was studied using a Thermo Scientific K-Alpha⁺ X-Ray photoelectron spectrometer with an Al Kα monochromatic X-Ray source of 1486.6 eV. The chars were placed on a conductive tape attached to a sample holder. A 200 eV pass energy at a step size of 0.5 eV was used to obtain survey scans while the C 1*s* high resolution spectra were acquired using a pass energy of 20 eV and a step size of 0.1 eV. The X-Ray irradiated surface emits photoelectrons corresponding to the elements present on the surface of the char. Further insights on the chemical states of the surface present carbon were acquired using a Thermo Avantage program used to deconvolute the C 1*s* peaks.

3.3.7 Scanning Electron Microscopy (SEM)

The morphological and topographical evolution of Morupule coal residual chars was characterised using a JEOL JSM-6010 scanning electron microscope (SEM) operating at a voltage of 20 kV. Prior to characterisation, the chars were coated using gold to enhance the conductivity of the char surface and allow better interactions with the focused electron beam [1].

This analytical technique maps out the morphology and topography using focused high-speed electrons rastered on the sample surface. Scattered electrons are thereafter measured by a detector.

3.3.8 X-Ray Computed Tomography (X-ray CT)

The small sample amount used in WMR experimentation (5 – 6 mg) limits the determination of the textural properties of the char using micropore analyses equipment. However, understanding char morphology is essential in characterising the thermochemical behaviour of coal. In this work, the development of the internal porosity of Morupule coal chars was studied using X-Ray CT 3D imaging, as a novel tool for chars produced from WMRs (it is typically used in medical applications [14] and geosciences [15]) to supplement observations made using SEM. An Xradia Versa XRM-500 microscope with a voxel resolution of 1 μm × 1 μm × 1 μm operating at a voltage and power of 80 kV and 7 W, respectively, was used to obtain a library of Morupule coal char scans. A rotating sample is penetrated by the X-Ray beam which is then detected opposite the X-Ray source. Once the rotation is complete, the X-Ray beam is shifted incrementally to produce another scan for a different slice, resulting in a stack of slices.

3.3.9 Size Exclusion Chromatography (SEC)

Size exclusion chromatography was used to characterise the molecular weight distribution of pyrolysis tar products [16]. SEC, operating at 80 °C with a mobile phase of NMP (0.5 mL min^{-1}), was carried out using a polystyrene/polydivinylbenzene-packed mixed-D column (Polymer Labs, UK) of 300 mm length and 7.5 mm internal diameter. A Knauer Smartline diode array UV-absorbance detector was used. Before experiments, polymer standard compounds were used to calibrate the mixed-D column. This analytical technique characterises the molecular weight distribution of tars based on their distinct molecular diffusion in the column packing. Smaller molecules permeate through the column packing and have longer retention times

while larger molecules cannot permeate the porosity of the column packing, and therefore have shorter retention times. The resulting chromatogram of coal tar samples is typically characterised by a bimodal distribution, with the early eluting peak representing compounds that could not permeate the column packing and is referred to as the excluded material.

References

1.   Messenböck, R. C. Rapid Pyrolysis and Gasification of Coal in a High Pressure Wire-Mesh Reactor. PhD Thesis, University of London, **1998**.

2.   Gibbins, J. R. Investigation of Primary Coal Pyrolysis Processes using a Variable Heating Wire-Mesh Apparatus. PhD Thesis, University of London, **1988**.

3.   Ebnesajjad, S., Chapter 4 - Surface and Material Characterization Techniques. In *Surface Treatment of Materials for Adhesive Bonding (Second Edition)*, Ebnesajjad, S., Ed. William Andrew Publishing: Oxford, **2014**; pp 39-75.

4.   Yu, J.; Sun, L.; Berrueco, C.; Fidalgo, B.; Paterson, N.; Millan, M., Influence of temperature and particle size on structural characteristics of chars from Beechwood pyrolysis. *Journal of Analytical and Applied Pyrolysis* **2018,** *130*, 127-134.

5.   Dong, S. Development of Analytical Methods for Characterizing Metallurgical Coke and the Injectant Coal Chars, Tars and Soots Formed during Blast Furnace Operation. PhD Thesis, Imperial College London of Science, Technology and Medicine, **2008**.

6.   Zhuo, Y.; Messenböck, R.; Collot, A. G.; Megaritis, A.; Paterson, N.; Dugwell, D. R.; Kandiyoti, R., Conversion of coal particles in pyrolysis and gasification: comparison of conversions in a pilot-scale gasifier and bench-scale test equipment. *Fuel* **2000,** *79* (7), 793-802.

7.   Tsai, C.-Y.; Scaroni, A. W., Reactivity of bituminous coal chars during the initial stage of pulverized-coal combustion. *Fuel* **1987,** *66* (10), 1400-1406.

8.   Li, X.; Hayashi, J.-i.; Li, C.-Z., Volatilisation and catalytic effects of alkali and alkaline earth metallic species during the pyrolysis and gasification of Victorian brown coal. Part VII. Raman spectroscopic study on the changes in char structure during the catalytic gasification in air. *Fuel* **2006,** *85* (10), 1509-1517.

9.   Zhang, S.; Min, Z.; Tay, H.-L.; Asadullah, M.; Li, C.-Z., Effects of volatile–char interactions on the evolution of char structure during the gasification of Victorian brown coal in steam. *Fuel* **2011,** *90* (4), 1529-1535.

10.   Keown, D. M.; Li, X.; Hayashi, J.-i.; Li, C.-Z., Characterization of the Structural Features of Char from the Pyrolysis of Cane Trash Using Fourier Transform−Raman Spectroscopy. *Energy & Fuels* **2007,** *21* (3), 1816-1821.

11.   Li, X.; Hayashi, J.-i.; Li, C.-Z., FT-Raman spectroscopic study of the evolution of char structure during the pyrolysis of a Victorian brown coal. *Fuel* **2006,** *85* (12), 1700-1707.

12.   Dong, S.; Alvarez, P.; Paterson, N.; Dugwell, D. R.; Kandiyoti, R., Study on the Effect of Heat Treatment and Gasification on the Carbon Structure of Coal Chars and Metallurgical Cokes using Fourier Transform Raman Spectroscopy. *Energy & Fuels* **2009,** *23* (3), 1651-1661.

13.   Dong, S.; Paterson, N.; Kazarian, S. G.; Dugwell, D. R.; Kandiyoti, R., Characterization of Tuyere-Level Core-Drill Coke Samples from Blast Furnace Operation. *Energy & Fuels* **2007,** *21* (6), 3446-3454.

14.   Boughton, O. R.; Ma, S.; Cai, X.; Yan, L.; Peralta, L.; Laugier, P.; Marrow, J.; Giuliani, F.; Hansen, U.; Abel, R. L.; Grimal, Q.; Cobb, J. P., Computed tomography porosity and spherical indentation for determining cortical bone millimetre-scale mechanical properties. *Scientific Reports* **2019,** *9* (1), 7416.

15.   Cnudde, V.; Boone, M. N., High-resolution X-ray computed tomography in geosciences: A review of the current technology and applications. *Earth-Science Reviews* **2013,** *123*, 1-17.

16.   Berrueco, C.; Venditti, S.; Morgan, T. J.; Álvarez, P.; Millan, M.; Herod, A. A.; Kandiyoti, R., Calibration of Size-Exclusion Chromatography Columns with 1-Methyl-2-pyrrolidinone (NMP)/Chloroform Mixtures as Eluent: Applications to Petroleum-Derived Samples. *Energy & Fuels* **2008,** *22* (5), 3265-3274.

Chapter 4

Characterisation of Morupule Coal Pyrolysis Behaviour at Elevated Pressures

4.1 Introduction

Chapter 1 discussed the need for the characterisation of the primary thermal breakdown behaviour of Morupule coal with view to develop advanced coal utilisation technologies to harness the available large coal reserves in Botswana. Pyrolysis, as the first stage of gasification, governs the residual char chemical and morphological structure, and consequently affects char conversion processes [1]. Current gasification technologies typically operate at high pressures of up to 35 bar$_a$ [2,3]. This necessitates the detailed unravelling of the influence of pressure on coal pyrolysis to optimise reactor design. The effect of pressure on pyrolysis was extensively discussed in Chapter 2. Typically, elevated pressures tend to lead to lower total volatile yields due to tar repolymerisation reactions and changes in

thermodynamic properties of the vapour – liquid equilibrium of tars [1,4,5,6,7,8,9]. This secondary char layer is known to reduce the reactivity of the char [10,11]. However, the characterisation of the structural and morphological evolution of chars produced under rapid pyrolysis and elevated pressures has not been adequately studied, especially during the temperature ramp up to describe early-stage pyrolysis behaviour.

The present work aims to elucidate links between char structural and morphological development of a relatively unknown Morupule coal from Botswana, during early-stage high pressure pyrolysis, and its combustion and gasification reactivities. The combined effects of temperature, pressure and holding time at peak temperature are extensively studied using a high-pressure wire-mesh reactor (HPWMR). This reactor setup studies the primary thermochemical behaviour of independent particles at high heating rates representative of entrained flow and fluidised bed gasifiers. Some of the results and discussion presented in this chapter have previously been published under a creative commons license [§], providing one of the first published literature on Morupule coal pyrolysis.

4.2 Materials and Methods

4.2.1 Feedstock and WMR

Morupule raw coal was ground and sieved to a particle size fraction of 125 – 150 μm. Prior to experiments, the sample was dried overnight at 105 ºC in a vacuum oven and stored in a desiccator. The primary pyrolysis experiments were carried using a WMR setup described in Chapter 3, using helium gas flowing at a velocity of 0.1 m s^{-1} as the continuous sweep gas. Liquid nitrogen was used to capture the condensable pyrolysis products in the tar trap.

[§] Bikane, K.; Yu, J.; Long, X.; Paterson, N.; Millan, M., Linking Char Reactivity to Structural and Morphological Evolution during High Pressure Pyrolysis of Morupule Coal. Chemical Engineering Science: X 2020, 100072.

4.2.2 Experimental Conditions

During the heating up period where samples were held at peak temperature for 0 s (electric current was cut immediately upon reaching the desired temperature), experiments were carried out in a 400 – 1000 ºC temperature range at a heating rate of 1000 ºC s^{-1}. Experiments studying the influence of hold time (0 – 60 s) were performed at 1000 ºC. This experimental methodology was carried out at pressures of 1, 10 and 30 bar$_a$. The error bars presented in this work correspond to a 95 % confidence interval using data from three experimental repeats.

4.2.3 Char and Tar Characterisation

4.2.3.1 Char Structure

FTIR spectroscopy was run on pellets made of Morupule coal chars to determine the present organic functional groups using a Spectrum 100 spectrometer coupled with an attenuated total reflectance accessory. Raman spectroscopy was performed using a Confocal Raman Senterra II microscope to study the evolution of the char chemical structure. The morphological development of Morupule coal chars was investigated using scanning electron microscopy (SEM) and X-Ray computed tomography (CT). Morupule coal tars were characterised using size exclusion chromatography (SEC).

4.2.3.2 Char Reactivity

The isothermal relative residual char combustion reactivity was analysed using a PerkinElmer Pyris 1 thermogravimetric analyser (TGA) using the method detailed in Section 3.3.1.2. To study the gasification reactivity, 5 – 6 mg of Morupule coal char sample was held at 1000 ºC for 30 s under CO_2 at atmospheric pressure using the HPWMR. To eliminate the effects of pyrolysis, identical experiments were carried under helium at atmospheric pressure [12]. The amount reacted due to pyrolysis or gasification was calculated using the weight difference between the initial char weight and the final char weight. The extent of gasification was

determined by subtracting the mass loss under pyrolysis from the mass loss under gasification (Equation 4.1) [12, 13]. Conversion due to gasification in CO_2 was calculated as a ratio of the extent of gasification to the char yield obtained under otherwise identical pyrolysis conditions (Equation 4.2).

$$Extent\ of\ Gasification\ (wt.\%, daf) = Total\ Volatiles_{CO_2}\ (wt.\%, daf) - Total\ Volatiles_{He}\ (wt.\%, daf) \quad (4.1)$$

$$Gasification\ Conversion\ (\%) = \frac{Extent\ of\ Gasification\ (wt.\%, daf)}{Char\ Yield\ (wt.\%, daf)_{He}} \times 100\ \% \quad (4.2)$$

4.3 Results and Discussion

4.3.1 Atmospheric Pressure Pyrolysis

4.3.1.1 Product Yields

Morupule coal was pyrolysed in an inert atmosphere (helium) at temperatures between 400 ºC and 1000 ºC for 0 s holding time at each peak temperature. The total volatile and tar yields were quantified as shown in Figure 4.1a. It is shown that the total volatile yield increases with temperature, with the most rapid increase taking place in the 400 – 700 ºC temperature range. Consistent with the literature [14], the tar yield appears to reach an asymptotic value at 600 ºC. Final total volatile and tar yields of 34 wt.%, daf and 11 wt.%, daf, respectively, were obtained at 1000 ºC. In comparison with the Linby and Daw Mill coals, which have been extensively studied using the WMR, both the total volatile and tar yields are on the lower end of the spectrum. A total volatile yield of about 50 wt.%, daf was obtained during the pyrolysis of Daw Mill coal at 1000 ºC and 0 s holding time [15]. Gibbins [16] reported a total volatile yield of about 45 wt.%, daf for the pyrolysis of Linby coal under identical conditions. This behaviour is expected as these two coals are characterised by low inertinite maceral contents of less than 21 vol.% [15,16] whilst Morupule coal records inertinite concentrations of over 75 vol.% [17]. As discussed in Chapter 2, the total volatile yield follows a general trend of liptinites > vitrinites >

inertinites in terms of maceral concentration [13]. The Morupule coal total volatile yield is insensitive to prolonged holding at peak temperature as shown for studies carried out at 600 ºC and 1000 ºC (Figure 4.1b), highlighting the fast kinetics of the pyrolysis reactions. This agrees with previous studies that suggested that devolatilisation is virtually completed well within 2 s of holding at peak temperature [13,16]. It also showcases the capability of the WMR to sufficiently minimise heat and mass transfer limitations in the 125 – 150 µm particle size fraction. The total volatile yield obtained from the WMR at 900 ºC (32 wt.%, daf) slightly exceeds the proximate analysis volatile matter content (28 wt.%, daf – Table 3.1) also determined at a peak temperature of 900 ºC. This is likely due to the low heating rates and particle stacking nature of the TGA which induce thermal annealing and secondary reactions, respectively [18].
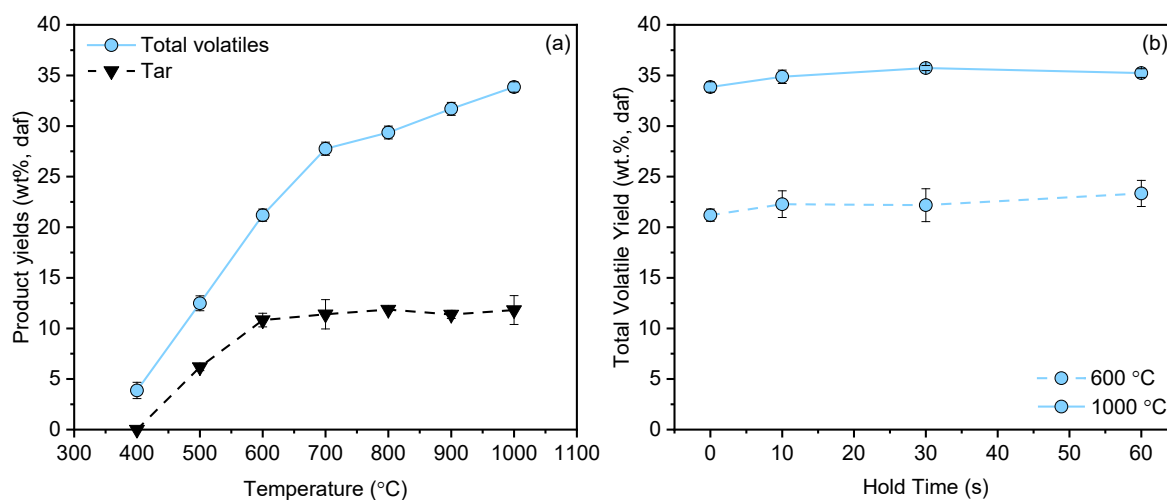
Figure 4. 1 (a) Total volatile and tar yields from the atmospheric pressure pyrolysis of Morupule coal at different temperatures (400 – 1000 °C), at a heating of 1000 °C s^{-1} and 0 s holding time at peak temperature in a helium atmosphere. (b) Total volatile yields from the atmospheric pressure pyrolysis of Morupule coal as a function of hold time at 600 °C and 1000 °C in a helium atmosphere.

4.3.1.2 Tar Characterisation

Figure 4.2 shows an SEC chromatogram for tar products produced at 1000 ºC and 0 s holding time. The first eluting peak shows the amount of compounds that could not penetrate through the column packing porosity. This peak occurs at 12 min for the studied Morupule coal tar. The last eluting peak represents the compounds that permeated through the column porosity, and has a maximum at 19 min. Most of the tar compounds from Morupule coal do penetrate through the column porosity as shown by the far larger late eluting peak, a characteristic of smaller aromatic hydrocarbon molecules [15]. A similar chromatogram profile was reported by Fidalgo, *et al.* [19] for tars produced from the pyrolysis of an inertinite-rich South African coal, possibly suggesting a dependence on the petrographic properties of the parent coal. An SEC study by Messenböck [15] on tars from maceral concentrates showed that inertinite maceral tars were lighter than those from vitrinites and liptinites, which were largely characterised by heavier molecules. Based on the calibration presented by Berrueco, *et al.* [20], Morupule coal tar maximum peak at 19 min corresponds to a polystyrene polymer molecular weight of 643 u.
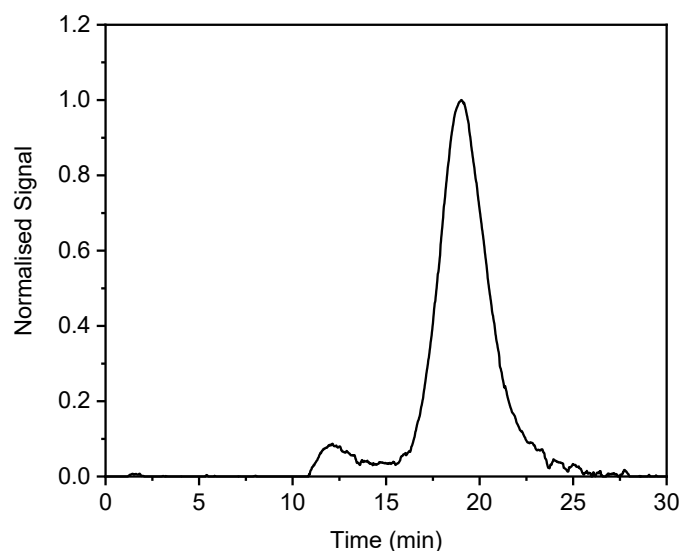
Figure 4. 2 SEC chromatogram of Morupule coal tar obtained from the wire-mesh reactor during pyrolysis at 1000 °C at a heating of 1000 °C s^{-1} and 0 s holding time at peak temperature in a helium atmosphere.

4.3.2 High Pressure Pyrolysis

4.3.2.1 Effect of Pressure during Heating Period

Figure 4.3a shows the effect of both temperature and pressure on the total volatile yields from the pyrolysis of Morupule coal. Similar total volatile yields are obtained at 400 ºC for all pressures studied owing to low tar devolatilisation rates, akin to torrefaction, since tar release commences at higher temperatures (Figure 4.1a). While a general increase with temperature is observed, total volatile yields at 600 ºC and 800 ºC from 30 bar$_a$ experiments are slightly lower than their 1 bar$_a$ counterparts by 4 wt.%, daf. Previous studies have linked the effect of pressure on the suppression of volatile release to the repolymerisation of tars that occurs during the plastic phase of pyrolysis, leading to the formation of larger stable hydrocarbon molecules within the char [6, 21]. Alternatively, some researchers argue that high pressures can alter the vapour-liquid thermodynamic properties of tars, resulting in the tars being retained in the char [1].

To gain insights on the pathway applicable to the pyrolysis of Morupule coal at high pressures, a set of cycling experiments were implemented, and the data is presented in Figure 4.3b. Initially, a primary pyrolysis experiment was carried out as described in Section 4.2.2 at two different pressures, 1 bar$_a$ and 30 bar$_a$, in the HPWMR (Run 1). The reaction was subsequently quenched and cooled to room temperature. With the sample still in place, this step was followed by a second pyrolysis run under identical conditions except pressure, in this case at 1 bar$_a$ (Run 2) (e.g. an initial primary pyrolysis of Morupule coal at 30 bar$_a$ and 1000 ºC followed by cooling to room temperature, and a second pyrolysis at 1 bar$_a$ and 1000 ºC). Total volatile yields from the cycling experiments reported in Figure 4.3b are given as additive yields of both Run 1 and Run 2 since the sample weight loss measurement was made after the completion of Run 2. If the vapour-liquid equilibrium properties of tars are the main factor explaining the tar yield dependence on pressure, then cycling experiments of chars produced at high pressure should give the same total volatile yields as those produced at 1 bar$_a$.

For each temperature, cycling experiments at 1 bar$_a$ did not lead to a larger volatile yield than the single run at 1 bar$_a$. This shows that there was no additional volatile release during the second cycle. For high pressure cycling experiments (30 bar$_a$ followed by 1 bar$_a$), marginal increases in the total volatile yields, within the experimental error of the original experiment, are observed (Figure 4.3b). However, their total volatile yields are significantly lower than their 1 bar$_a$ counterparts. High pressure pyrolysis therefore does not affect the thermodynamic properties of Morupule coal tars. Instead, the decrease in volatile release at high pressures seems due to a greater extent of tar repolymerisation during the heating up period, forming compounds which solidify in the particle when pyrolysis is quenched. Interestingly, the extent of suppression of the volatiles is almost identical at 600 ºC and 800 ºC, highlighting the thermal stability, at these temperatures, of the structures formed at elevated pressures. This finding suggests that the repolymerisation structures are much larger and more stable than their precursors which would otherwise evolve at 800 ºC and during cycling experiments. The influence of pressure is less pronounced at 1000 ºC where the differences in the yields for all pressures are within 2 wt.%, daf of each other, possibly due to the thermal cracking of the repolymerisation structures. Characterisation of Morupule coal tars from atmospheric pressure pyrolysis at 1000 ºC using SEC revealed a significant proportion of tar molecules with relatively lower molecular weights, which may produce repolymerisation structures of lower thermal stability at 1000 ºC (Figure 4.2). The total volatile yields for pyrolysis experiments carried out at 10 bar$_a$ and 30 bar$_a$ are similar and within experimental error at all temperatures, showing a diminishing effect with pressure.
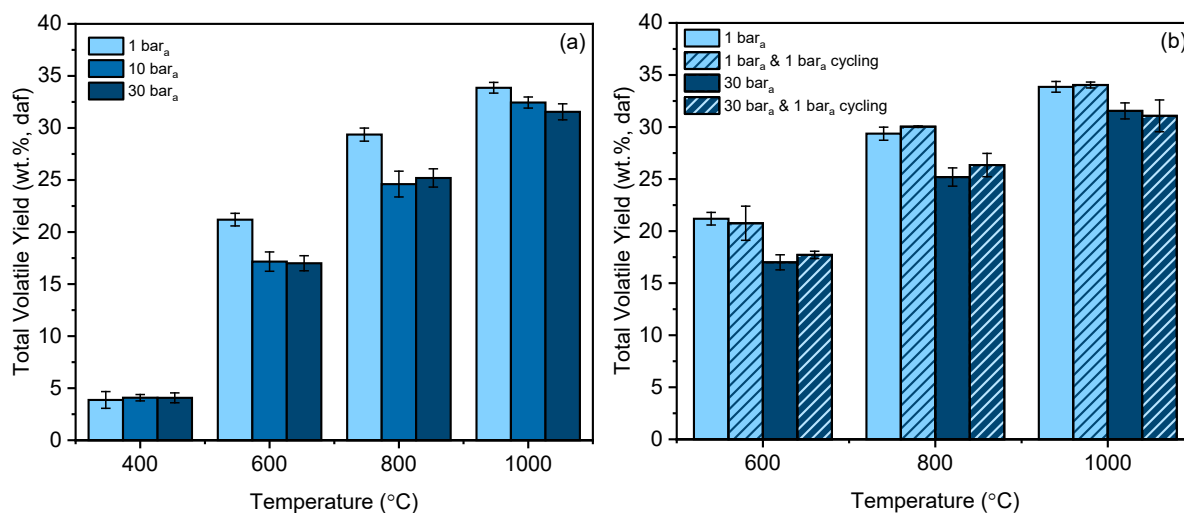
Figure 4. 3 (a) Total volatile yields from the pyrolysis of Morupule coal at different temperatures (400 – 1000 °C) and pressures (1 – 30 bar$_a$), at a heating of 1000 °C s^{-1} and 0 s holding time at peak temperature in a helium atmosphere. (b) Cycling pyrolysis of Morupule coal at various temperatures and pressures (1 bar$_a$ and 30 bar$_a$), heating rate of 1000 °C s^{-1} at 0 s hold time at peak temperature in a helium atmosphere.

4.3.2.2 Effect of Pressure during Holding at 1000 ºC

Upon reaching a peak temperature of 1000 ºC, the effect of holding time and pressure on the total volatile yields was investigated and the results are illustrated in Figure 4.4. For all the pressures and holding times studied, the total volatile yields obtained are within experimental error, indicating that the bulk of the devolatilisation reactions took place during the heating up period. This is consistent with the literature which has shown that pyrolysis is complete within 2 s of holding at peak temperature [13]. The 1 bar$_a$ pyrolysis yields remain slightly higher than high pressure total volatile yields. Perhaps not all repolymerisation structures were thermally cracked during heating up to 1000 ºC and therefore remain in the char.
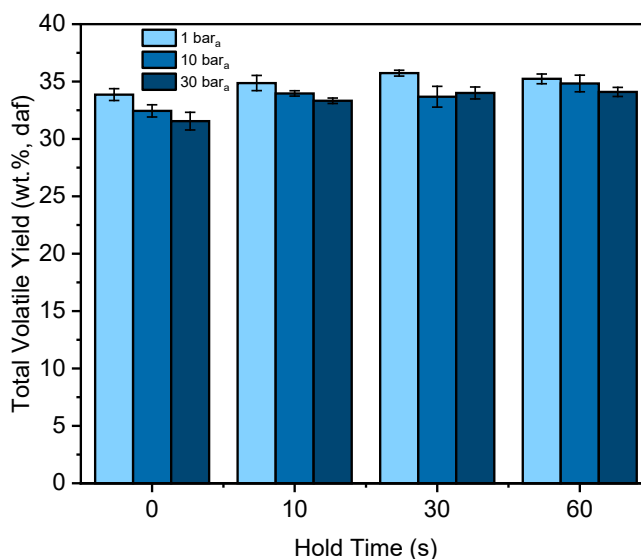
Figure 4. 4 Total volatile yields from the pyrolysis of Morupule coal at 1000 °C at a heating rate of 1000 °C s^{-1} in a helium atmosphere under different pressures (1 – 30 bar$_a$) and holding times (0 – 60 s).

4.3.3 Char Chemical Structure

4.3.3.1 Elemental Analysis

Elemental analysis of the recovered chars was carried out to determine the C, H and O distributions as a function of pyrolysis pressure and temperature (Table 4.1). Since hydrogen and oxygen are largely present in the volatile matter, a decrease in the H and O contents is observed when temperature is increased, producing carbon-rich chars as expected. At 600 ºC and 800 ºC, the O content, synonymous with a greater presence of alcohol, carbonyl and/or carboxyl groups [22], is slightly higher for chars produced at a pyrolysis pressure of 30 bar$_a$ than those from 1 bar$_a$. Chars of similar elemental composition are obtained at 1000 ºC and pressures of 1 bar$_a$ and 30 bar$_a$. Other research works have shown that the suppressed evolution of tars during the pyrolysis of bituminous coals tends to form a secondary char layer [18]. However, in the case of Morupule coal, it appears that the repolymerisation structures

are ultimately devolatilised at 1000 ºC, indicating that while they are stable at lower temperatures, they can be thermally cracked at higher temperatures.

Table 4. 1 Elemental analysis of Morupule coal chars from pyrolysis at various temperatures and 0 s hold time at pressures of 1 bar_a and 30 bar_a.

Pyrolysis	C (wt.% daf)		H (wt.% daf)		O (wt.% daf)	
Temperature (ºC)	1 bar_a	30 bar_a	1 bar_a	30 bar_a	1 bar_a	30 bar_a
400	82.4	83.7	4.0	3.9	10.7	10.0
600	88.6	84.2	3.2	3.2	4.4	6.6
800	93.7	91.4	2.6	2.7	0.9	2.5
1000	94.9	94.9	1.6	1.8	0.0	0.4

4.3.3.2 FTIR Spectroscopy

The chemical structure of chars recovered from the pyrolysis of Morupule coal in a temperature range of 400 – 1000 ºC under two different pressures (1 bar_a and 30 bar_a) was analysed using FTIR spectroscopy. Figures 4.5a and b show the absorption spectra of 1 bar_a and 30 bar_a chars, respectively, in the temperature range of interest. Table 4.2 presents the band assignment of the functional groups observed in the chars as per the literature.

Marked changes are observed as a function of pyrolysis temperature for Morupule coal chars recovered from low- and high-pressure experiments. While largely preserved at a pyrolysis temperature of 400 ºC, hydroxyl (O-H) groups evolve at 600 ºC, possibly in a dehydration mechanism, as indicated by the disappearance of the 3700 – 3600 cm^{-1} band. However, this band is slightly more pronounced for chars produced at 30 bar_a, suggesting that hydroxyl groups constitute a part of the repolymerisation structures. This finding is consistent with the elemental analyses which showed that high pressure chars have a higher oxygen content at 600 ºC than their low-pressure counterpart. The C=O and C-H groups observed at 1850 – 1590 and 3090 – 2850 cm^{-1}, respectively, also disappeared at 600 ºC for chars

obtained at both 1 bar$_a$ and 30 bar$_a$. Their loss corresponds to the release of quinones and aliphatic side chains, such as methyl groups, as part of the volatile matter [22]. Consistent with the loss of methyl groups, a band assigned to the vibration mode of aliphatic C-H bond (1460 – 1380 cm^{-1}) also disappears at 600 ºC along with the C-O- bond (1300 – 1000 cm^{-1}) assigned to the vibration of ethers. A higher intensity is observed for the aromatic C-H vibration mode at 925 – 785 cm^{-1} for chars produced at 30 bar$_a$, possibly indicating that aromatic ring systems tend to undergo repolymerisation and remain in the char at 600 ºC.

Further increases in temperature to 800 ºC indicate an erosion of most bands previously observed at 600 ºC, with noticeable vibrations of the C-O bonds (1300 – 1000 cm^{-1}) due to ether linkages in the char matrix and aromatic C-C bonds (1600 – 1540 cm^{-1}) still present. At 1000 ºC, only the C-O bond is noticeable, indicating that the sample has become quite dark and poorly transparent, without any significant differences between low- and high-pressure chars. Raman spectroscopy was then used to gain further insights on the chemical structure of these chars, particularly those from high pyrolysis temperatures.
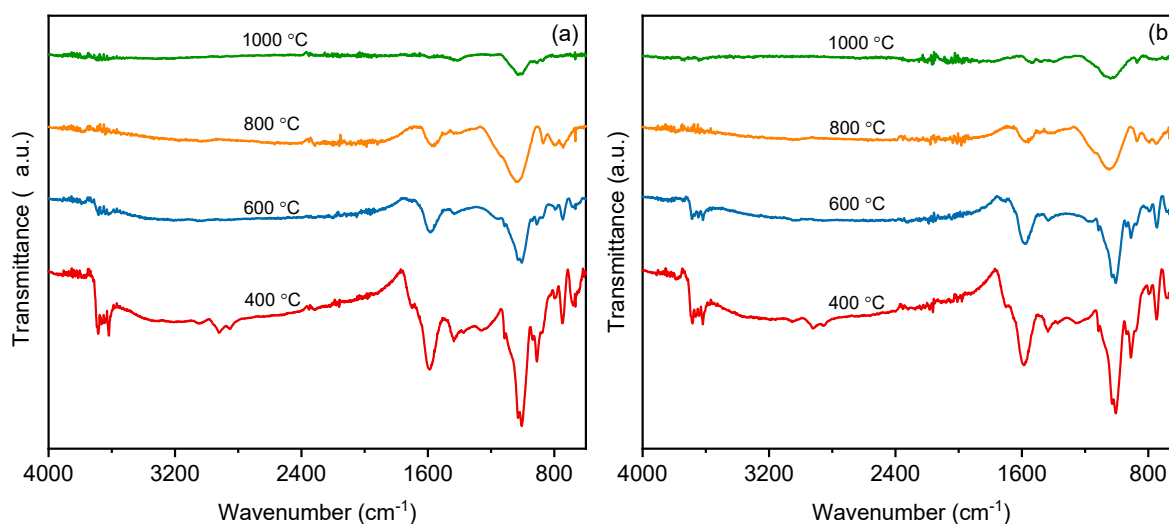
Figure 4. 5 FTIR spectra of Morupule coal chars produced at different pyrolysis temperatures. Pressures of (a) 1 bar$_a$ and (b) 30 bar$_a$.

Table 4. 2 FTIR band assignment of the different functional groups present in coal chars based on the literature [22, 23].

Band Wavenumber (cm^{-1})	Assignment of Functional Groups
3700 - 3600	O-H stretching vibration
3090 - 3030	C-H stretching vibration, aromatic ring
3000 - 2880	C-H stretching vibration, asymmetric aliphatic
2870 - 2850	C-H stretching vibration, symmetric aliphatic
1850 - 1590	C=O stretching vibration, aromatic ring (carbonyl)
1600 - 1540	C=C stretching vibration, skeletal and aromatic ring
1460 - 1380	C-H bending vibration, aliphatic
1300 - 1000	C-O vibrations, alcohols and aliphatic ethers
925 - 785	C-H bending vibration, aromatic ring
~ 750	Ortho-substituted aromatic rings
~ 650	C-OH bending

4.3.3.3 Raman Spectroscopy

4.3.3.3.1 Effect of Temperature and Pressure during Heating Period

4.3.3.3.1.1 Total Raman Peak Areas

Figures 4.6a and b show the Raman spectra of Morupule coal chars produced during pyrolysis at different temperatures, between 400 – 1000 ºC, and pressures of 1 bar$_a$ and 30 bar$_a$, respectively. For both pressures, an increase in pyrolysis temperature results in a notable decrease in Raman intensity. This observation is quantitatively represented in Figure 4.7, showing the total Raman peak areas at different pyrolysis temperatures and pressures of interest. Raman intensity is governed by the Raman scattering ability and light absorptivity of the char [24, 25]. O-containing groups have a high Raman scattering ability which translates to high Raman intensities as a result of the resonance effect between the oxygen and the aromatic ring [26]. In contrast, an increase in the concentration of the aromatic ring systems tends to increase the light absorptivity of the char, thereby reducing its Raman intensity [27]. In

113

agreement with the loss of O-containing groups, mainly present in the volatile matter shown by a decrease in the O content in Table 4.1, it is unsurprising that the total Raman peak area decreases as a function of pyrolysis temperature. In addition, ring condensation tends to be promoted at higher temperatures, enhancing the light absorptivity of the char. Similar observations have been made in both biomass and coal pyrolysis studies, attributing the decrease in the total Raman peak area as a function of pyrolysis temperature to the loss of O-containing groups during devolatilisation and increased light absorptivity [22,27,28]. Consistent with the elemental analysis and total volatiles yields data, the total Raman peak area is higher for chars produced at 30 bar$_a$ at 600 ºC and 800 ºC as a result of the suppressed release of tars through repolymerisation reactions. Similar total Raman peak areas are observed at 1000 ºC for both pressures, in agreement with the postulation that repolymerisation structures are thermally cracked and released at higher temperatures, producing chars of similar chemical structure.
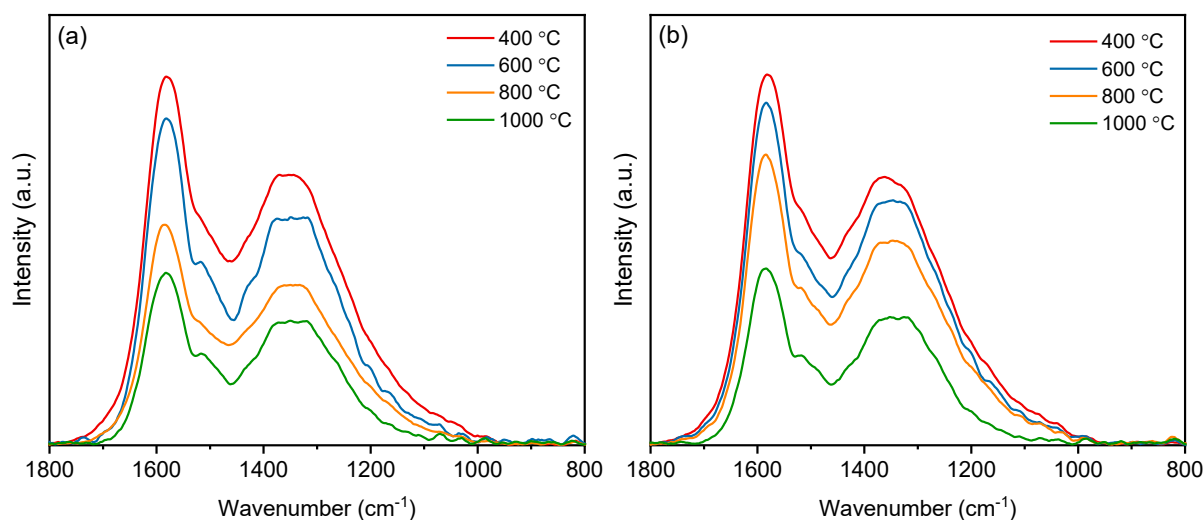
Figure 4. 6 Raman spectra of Morupule coal chars produced at different pyrolysis temperatures (0 s hold time). Pressures of (a) 1 bar$_a$ and (b) 30 bar$_a$.
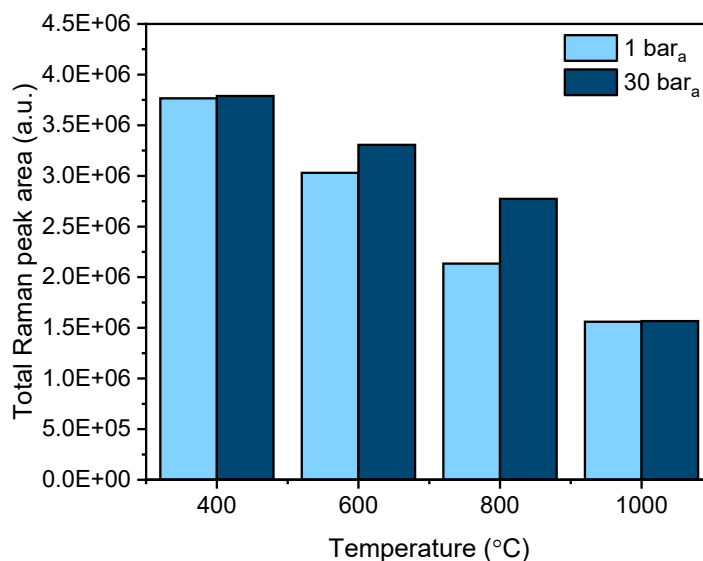
Figure 4. 7 Total Raman peak areas of chars produced at 1 bar$_a$ and 30 bar$_a$ as a function of pyrolysis temperature (0 s hold time).

4.3.3.3.1.2 Intensity Ratios

The extent of the graphitisation of Morupule coal char during pyrolysis at 1 bar$_a$ and 30 bar$_a$ was studied using the I_D/I_G intensity ratios shown in Figure 4.8a. Intense char ordering is typically denoted by an increase in the I_D/I_G intensity ratio [29]. In the case of Morupule coal chars produced during pyrolysis at both pressures, the I_D/I_G intensity ratio is constant with increasing temperature, suggesting that the relative concentration of aromatic ring systems with six or more benzene rings was unaltered. This finding contradicts numerous observations that have been made in literature where a general increase of the I_D/I_G ratio has been observed during the pyrolysis of carbonaceous materials due to the conversion of amorphous carbon to aromatic rings that give rise to the D band [27]. However, it is important to note that experiments reported in literature were carried out under conditions where the extent of ordering was rather promoted by the reactor specific effects. Chars were produced under relatively low heating rates (5 – 50 ºC min^{-1}) and held at each pyrolysis temperature for 15 min in reactor systems where the secondary reactions between the evolving volatiles and the heated particles were not minimised [22,27]. This promotes the rearrangement of the char matrix, producing more

115

ordered structures, since the char spends prolonged periods at high temperatures. Conversely, samples were pyrolysed at a heating rate of 1000 °C s^{-1} and held at peak temperature for 0 s in the present work. Moreover, secondary reactions were minimised by continuously flowing a sweep gas to carry the evolving volatiles away from the reaction zone. Such conditions minimised the extent of aromatic ring system condensation of Morupule coal chars. These findings highlight the significance of isolating the influence of the reactor design from the primary reactions that occur during pyrolysis.

The I_D/I_V intensity ratios were quantified to further characterise Morupule coal chars, focusing on the evolution of aromatic ring systems with six or more fused benzene rings in proportion to the structures normally found in amorphous carbon containing three to five fused benzene rings [27, 29] (Figure 4.8b). Since it has been established that the concentration of larger aromatic ring systems was unchanged, the increase in the I_D/I_V intensity ratio for chars produced at both 1 bar$_a$ and 30 bar$_a$ can be attributed to the release of O-containing structures in the V band during pyrolysis, lowering the intensity at the valley of the spectrum.
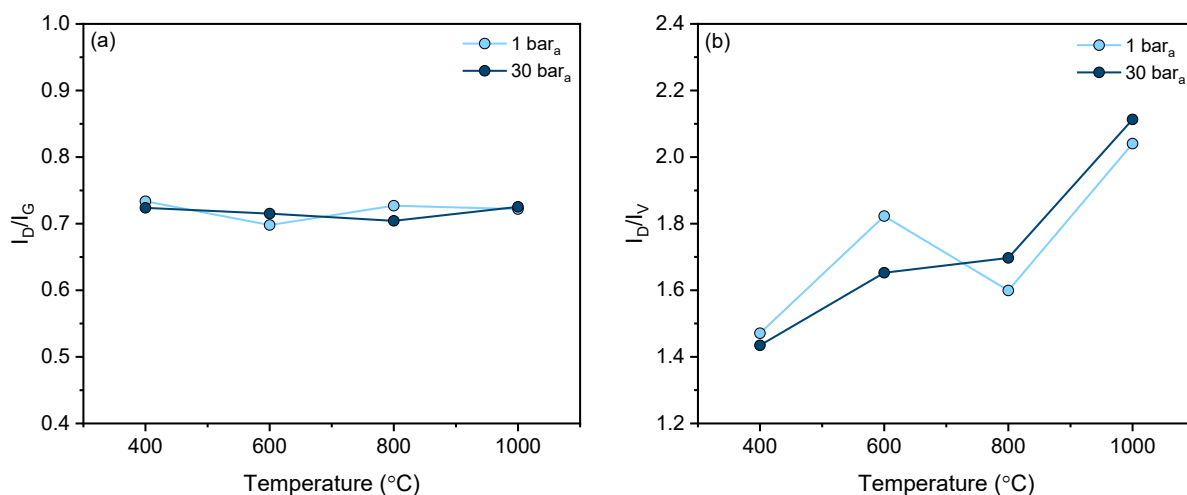
Figure 4. 8 (a) I_D/I_G and (b) I_D/I_V intensity ratios of Morupule coal chars as a function of pyrolysis temperature (0 s hold time).

4.3.3.3.2 Effect of Pressure during Holding at 1000 ºC

4.3.3.3.2.1 Total Raman Peak Areas

Prolonged holding of Morupule coal at 1000 ºC led to a decrease in the Raman intensities for both the D and G bands due to the release of O-containing permanent gases that typically evolve at such temperatures, resulting in the lower Raman scattering ability of the char (Figures 4.9a and b). Additionally, the release of these gases may result in the rearrangement of the char matrix to form larger aromatic ring systems with a higher light absorptivity. A combination of these factors led to a decrease in the observed Raman intensity. A slight decrease in the total Raman peak area as a function of hold time at 1000 ºC is shown in Figure 4.10, with the greatest structural changes taking place in the first 10 s of holding at peak temperature. This is consistent with the total volatile yield data and literature that suggests that devolatilisation is virtually completed within 2 s of holding at peak temperature [13]. The identical total Raman peak areas for chars produced at 1 bar$_a$ and 30 bar$_a$ suggests that the effect of pressure on the chemical structure of Morupule coal chars is insignificant under these conditions.
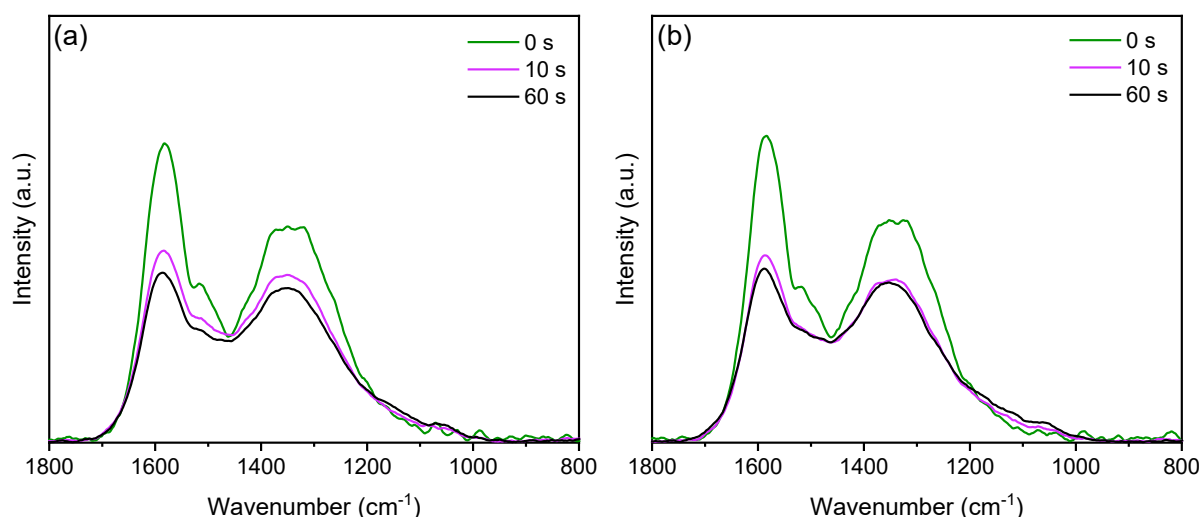
Figure 4. 9 Raman spectra of Morupule coal chars from different holding times at a peak temperature of 1000 ºC. Pressures of (a) 1 bar$_a$ and (b) 30 bar$_a$.
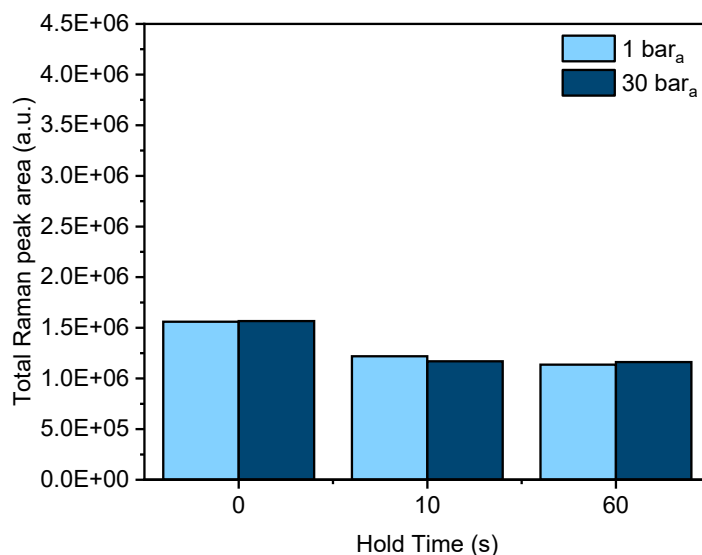
Figure 4. 10 Total Raman peak areas of Morupule coal chars produced at 1 bar$_a$ and 30 bar$_a$ as a function of hold time at 1000 ºC.

4.3.3.3.2.2 Intensity Ratios

An increase in the I_D/I_G intensity ratio is observed for chars held for prolonged periods at 1000 ºC, with the greatest rise occurring in the first 10 s as shown in Figure 4.11a. This indicates the formation of larger and ordered aromatic ring systems during the release of permanent gases. Further increases in hold time to 60 s reveal a comparatively stable I_D/I_G intensity ratio, suggesting that there are no significant changes in the char structure beyond 10 s and up to 60 s. It has previously been reported that the I_D/I_G ratio tends to be relatively stable at high temperatures due to the opposing effects of ring enlargement, which lower Raman intensity, and the greater presence of the defect structures which are Raman active at the D band position [27]. While there is a clear decrease in the intensity of D and G bands at longer holding times, the intensity of the V band remains relatively unchanged (Figures 4.9a and b). Consequently, the I_D/I_V intensity ratio for chars held for longer holding times at 1000 ºC decreased as illustrated in Figure 4.11b. Contrary to the expectation, it is postulated that the amorphous carbon structures, representing small aromatic rings, are not converted to larger aromatic rings systems. Instead, the larger aromatic ring systems that give rise to the D band undergo ring condensation. As a result, the Raman intensity of the D band decreases due to

118

the higher light absorptivity of the char without the competing effect of the Raman active aromatic ring systems which would otherwise occur if amorphous carbon structures were converted to the 'defect' structures. In agreement with the total volatile yields (Figure 4.4), the I_D/I_G and I_D/I_V intensity ratio values are near identical for chars produced at different pressures, rendering the influence of pressure negligible at longer holding times.
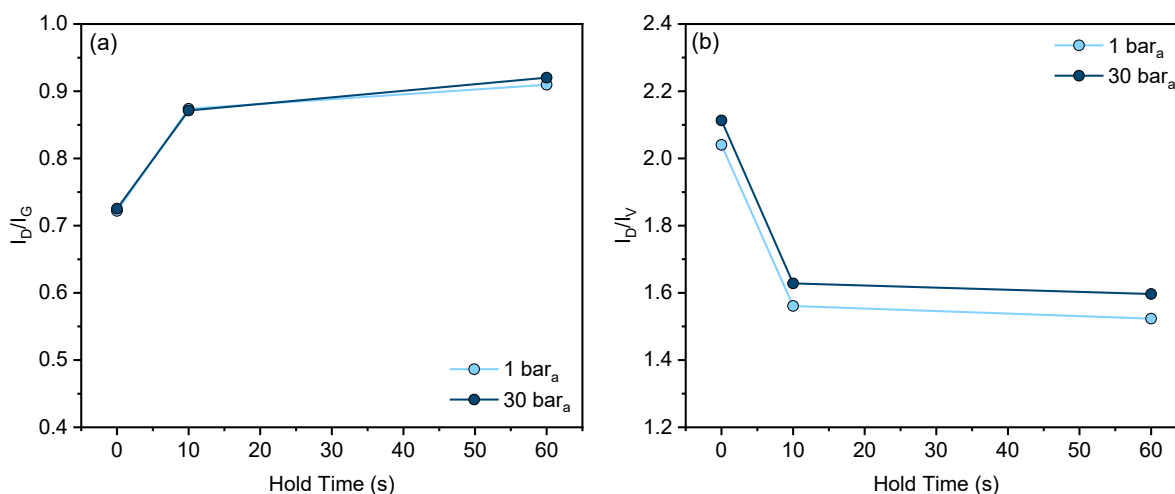
Figure 4. 11 (a) I_D/I_G and (b) I_D/I_V intensity ratios of Morupule coal chars produced at 1 bar$_a$ and 30 bar$_a$ as a function of hold time at 1000 ºC.

4.3.4 Char Morphology

4.3.4.1 Scanning Electron Microscopy

SEM images were captured to study the effects of temperature and pressure on the morphological evolution of Morupule coal during pyrolysis (Figures 4.13 and 4.14). Compared to the parent coal (Figure 4.12), differences in particle size are not sufficiently distinguished for the four chars studied. This is particularly unsurprising since the maximum total volatile yields at 1000 ºC constitute only 35 wt.%, daf, of the parent sample, leaving the particle size relatively unaltered after pyrolysis. Highly volatile coals are known to melt, swell and agglomerate during high pressure pyrolysis [21, 30], characteristics which are in contrast with the performance of Morupule coal. Extensive thermoplasticity of coal during pyrolysis is typical of

high liptinite and vitrinite maceral contents [31]. In addition to the substantial evidence that Southern African coals are inertinite rich [32,33], it can be inferred that the inertinite maceral constitutes a significant proportion of Morupule coal used in this work since its presence tends to preserve the particle size after pyrolysis [15]. This discussion is supported by an extensive study by Hower, *et al.* [17] which shows that for 11 samples of Morupule coal, the total inertinite content was in a 76.6 – 91.5 vol.% range while liptinite and vitrinite macerals accounted for less than 8 vol.% and 10 vol.%, respectively (Tables 2.1 – 2.3).

Residual chars from pyrolysis at 600 ºC reveal localised blowholes resulting from the explosive release of volatiles, particularly tars, typical of high heating rates as those used in the present work. These blowholes indicate a bubble transport phenomenon wherein the volatile bubbles travel to the external surface of the particle and subsequently burst [15]. It is evident that there is a significant number of bubbles, previously identified as liquid bitumen composed of condensed tars [34], which are still intact on the char surface, particularly for chars produced at 600 ºC and 30 bar_a. These bubbles solidified before they could burst when the reaction was quenched due to the increased residence time under high external pressures. The prevalence of these bubbles possibly results in the lower total volatile yields observed under high pressure as their weight makes up part of the primary char. Other volatiles may condense within the porous network leading to the enclosed bubbles, thereby further reducing the total volatile yields in combination with tar repolymerisation at high pyrolysis pressures [34].

Increases in temperature to 1000 ºC allows the previously enclosed bubbles to burst as shown in Figure 4.14b, enabling a further release of volatiles. However, it can be observed that some bubbles remain intact, contributing to a slightly lower total volatile yield. Apart from a greater number of bubbles on the surface of chars produced at high pressure, the differences between Morupule coal chars produced at 1 bar_a and 30 bar_a are not adequately clear. Both chars are characterised by smooth surfaces around the blowholes, which are of similar sizes (10 µm). This is indicative of a similar volatile transport phenomenon characterised by an explosive release of volatiles. The localisation of the blowholes indicates a preferential

pathway for the volatiles promoted by the internal pressure build-up during the heating up period.
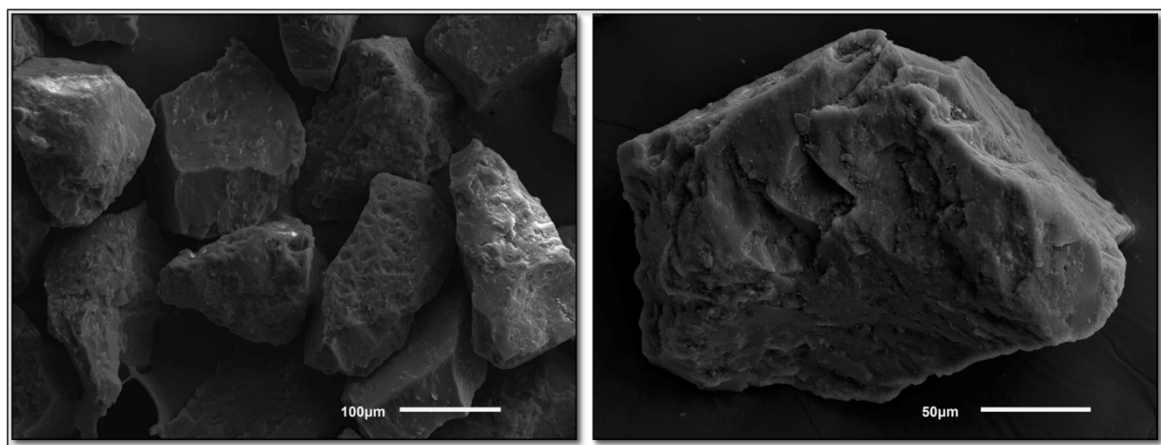
Figure 4. 12 SEM images of Morupule raw coal.
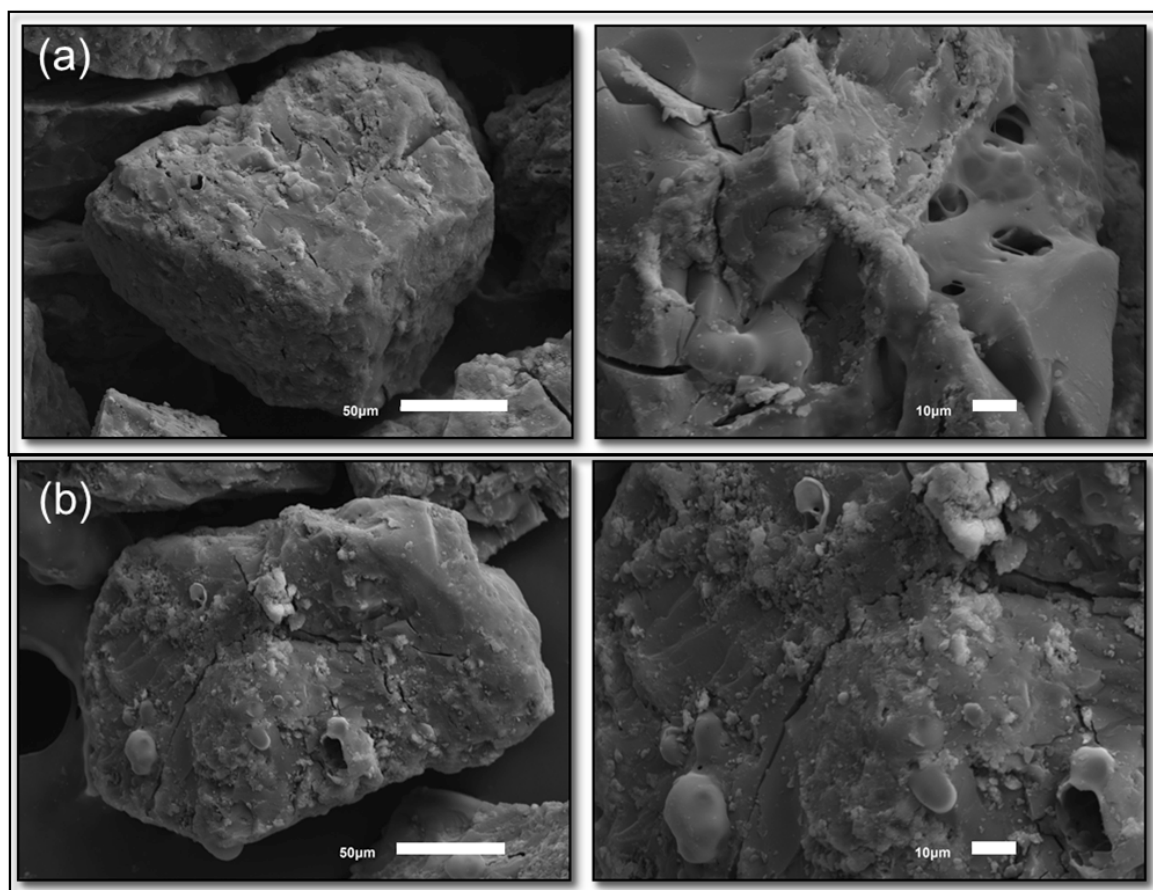
Figure 4. 13 SEM images of Morupule coal chars from pyrolysis at 600 ºC and holding for 0 s in a helium atmosphere. Pressures of (a) 1 bar$_a$ and (b) 30 bar$_a$.

121
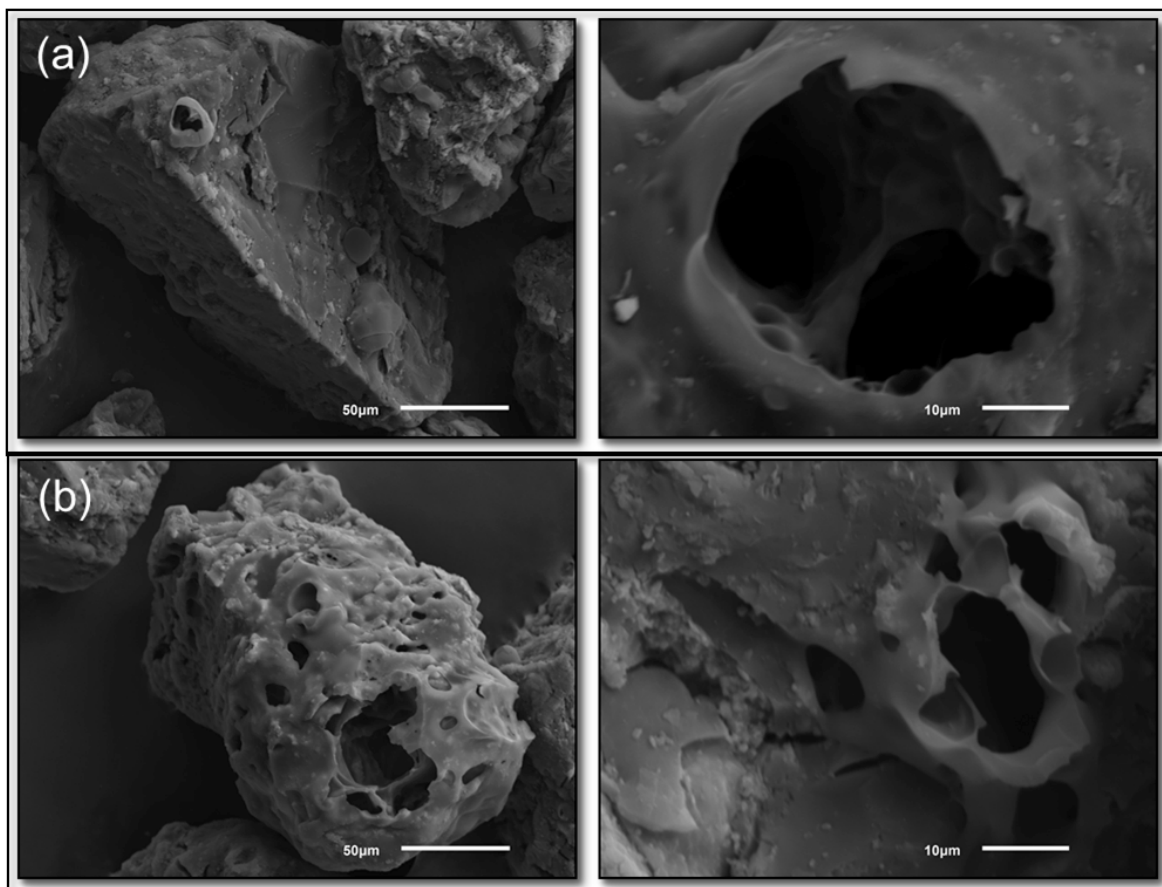
Figure 4. 14 SEM images of Morupule coal chars from pyrolysis at 1000 ºC and holding for 0 s in a helium atmosphere. Pressures of (a) 1 bar$_a$ and (b) 30 bar$_a$.

4.3.4.2 X-Ray Computed Tomography (CT)

As discussed in Chapter 2, the use of the WMR has limitations in relation to characterising the morphological development of residual chars due to small sample amounts used in this reactor (5 – 6 mg). As a first of its kind in WMRs, imaging of the internal porosity was carried out using the non-destructive X-Ray CT analytical technique to gain further insights on the morphological evolution of chars produced at 600 ºC (Figure 4.15) and 1000 ºC (Figure 4.16) for the two pressures (1 bar$_a$ and 30 bar$_a$). Although SEM images fail to sufficiently distinguish differences in surface char morphology, X-Ray CT imaging can discern the differences in the internal porosity of chars produced at different pressures. While SEM images presented above show localised blowholes on the external surface of the char, X-Ray CT images exhibit a well-developed internal macroporosity, throughout the particle, with rectangular shaped chars [35].

This confirms a preferential volatile transport pathway, releasing volatiles at localised points on the external surface of the char. Figure 4.15a, for pyrolysis at 600 ºC under atmospheric pressure, shows particles with thin and small pores. However, at the same temperature and at elevated pressures, there appears to be a mixture of char porosity, with some resembling those from atmospheric pressure pyrolysis and some showing thin-walled char particles with larger voidages. It is known that elevated pressures tend to enhance the plasticity and fluidity of the coal during rapid pyrolysis due to the suppression of tar release [36], as is the case at 600 ºC. Similar morphologies are observed for chars produced at 1000 ºC. This suggests that the development of the macroporosity of the char is largely influenced by tar release.

Using the ImageJ software and applying an Otsu threshold (Appendix B), the porosity of the char particles was estimated using 100 image slices of representative particles for each condition (Table 4.3). In agreement with the qualitative discussion above, chars produced under high pressures have a higher porosity than their atmospheric pressure counterparts due to increased coal fluidity which enhanced bubble formation of volatiles. The external pressure entraps these bubbles in the coal, forming the thin walls, before the explosive volatile release as temperature is increased [1]. Given the porosity range of 40 – 60 %, Morupule coal chars can be classified as a mixture of mesosphere and inertoid, typical of inertinite-rich coals [35]. A similar observation was made by Fermoso, *et al.* [36] for chars derived from the inertinite-rich South African coals. The X-Ray CT, with its qualitative and quantitative capabilities, presents opportunities for an in-depth characterisation of chars from the WMR, as well as those from other reactor systems, to provide further information on the thermochemical conversion of solid fuels.
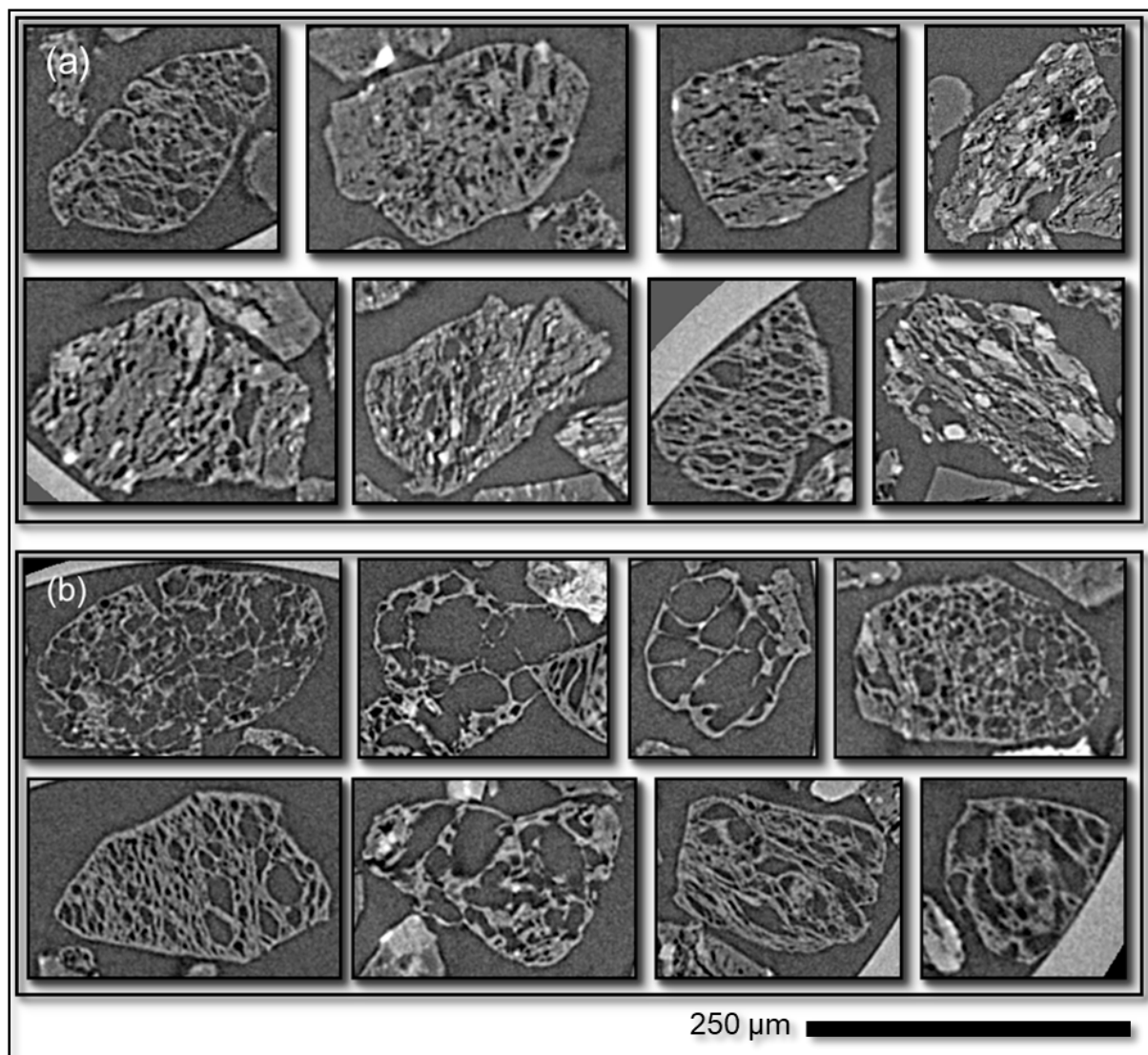
Figure 4. 15 X-Ray CT imaging of Morupule coal chars from pyrolysis at 600 ºC and holding for 0 s in a helium atmosphere. Pressures of (a) 1 bar$_a$ and (b) 30 bar$_a$.
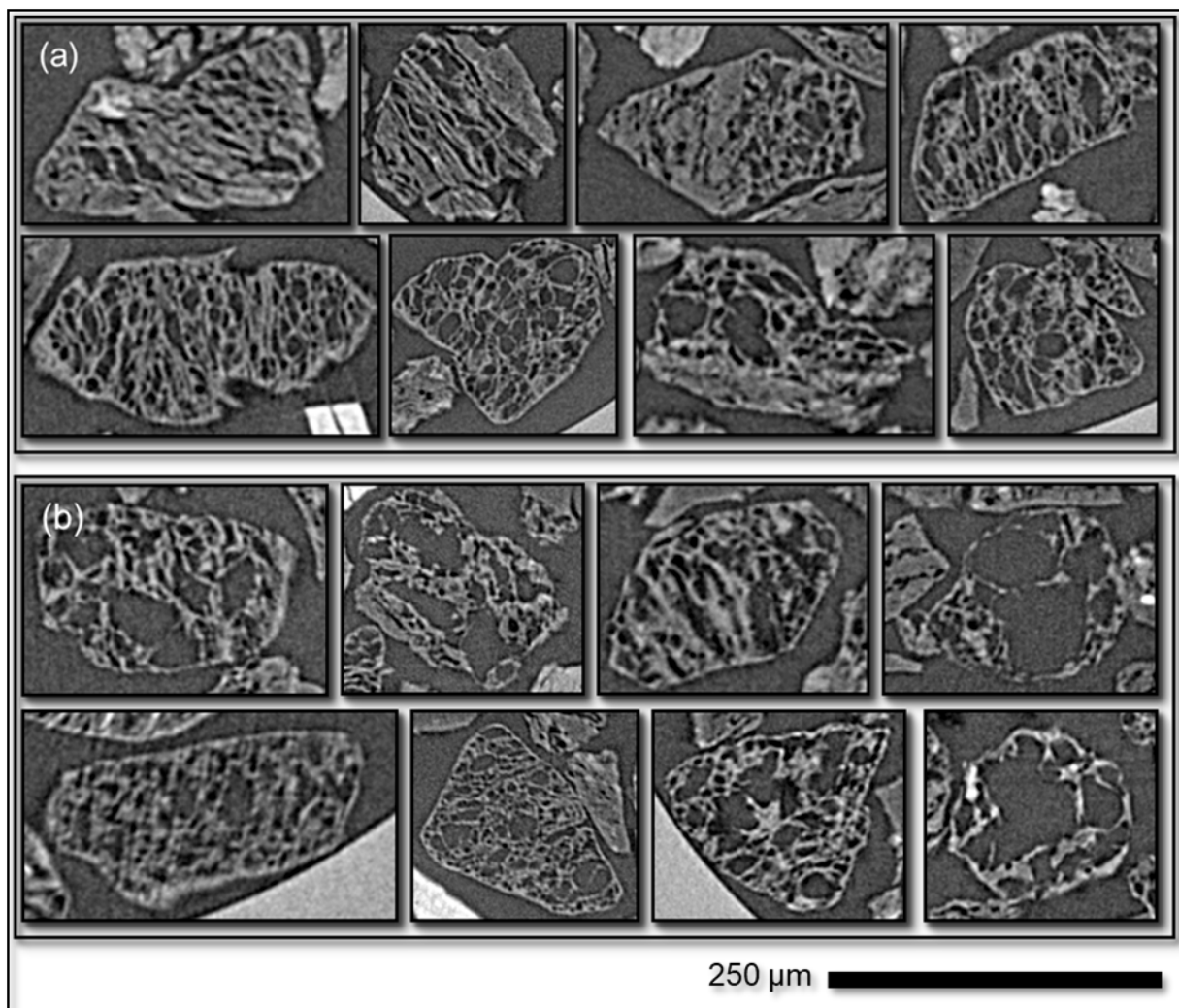
Figure 4. 16 X-Ray CT imaging of Morupule coal chars from pyrolysis at 1000 ºC and holding for 0 s in a helium atmosphere. Pressures of (a) 1 bar$_a$ and (b) 30 bar$_a$.

Table 4. 3 Morupule coal char porosity as a function of temperature and pressure.

Temperature	Porosity (%)	
(ºC)	1 bar$_a$	30 bar$_a$
600	40.8	56.3
1000	48.8	57.8

4.3.5 Char Reactivity

4.3.5.1 Char Combustion Reactivity

The effect of pyrolysis temperature and holding time at 1000 ºC on the isothermal combustion reactivity of chars produced at 1 bar$_a$ and 30 bar$_a$ is shown in Figures 4.17a and b, respectively.

In agreement with previous literature, a decrease in the combustion reactivity for chars produced at both pressures is observed with increasing temperature. This is attributed to the loss of O-containing functional and aliphatic groups, resulting in a reduction in the available active sites [22]. High pressure chars have markedly higher combustion reactivities at 0 s holding time than those produced at atmospheric pressure. This is consistent with their total volatile yields, Raman and elemental analyses, which have shown that Morupule coal chars produced at 30 bar$_a$ have a higher oxygen content. Moreover, Tremel, *et al.* [37] established that high pressure chars produced at short residence times tend to have higher surface areas than their low-pressure counterparts, allowing for a greater availability of active sites. However, other research works indicate that chars produced at high pressure have a lower combustion reactivity than those from atmospheric pressure pyrolysis due to the presence of the relatively unreactive secondary char layer formed during tar repolymerisation [38]. This layer has been shown to result in slower reaction rates in early-stage high pressure gasification [18]. Although Morupule coal tars undergo repolymerisation under high pressures at 600 ºC, the resultant structures are not highly stable as shown that increases in temperature possibly induce the release of the previously repolymerised tars (Figure 4.3a). The differences in porosity, as shown by X-Ray CT imaging, are not expected to have an influence in reactivity given the low temperature (500 ºC) used for combustion reactivity, suitable for a chemical reaction controlled regime [11].

Morupule coal chars exhibit a reduction in the combustion reactivity when held at 1000 ºC for a prolonged period, with the major decrease occurring in the first 10 s (Figure 4.17b). It is well known that thermal annealing results in the ordering of the char matrix, leading to loss of active sites and subsequent reactivity [39, 40]. Further holding to 60 s does not show a significant change in the combustion reactivity. This observation is consistent with Raman analyses wherein the I_D/I_G intensity ratio increased in the first 10 s due to the increased ordering of the char, and thereafter remained stable. Therefore, there are minimal char structural and morphological changes in the 10 – 60 s hold time range. Although high

pressure chars have a higher combustion reactivity at 0 s, similar reactivities are observed for chars produced under both pressures at longer holding times as graphitisation ensues, resulting in a loss of surface area, and consequently microporosity [37, 38].
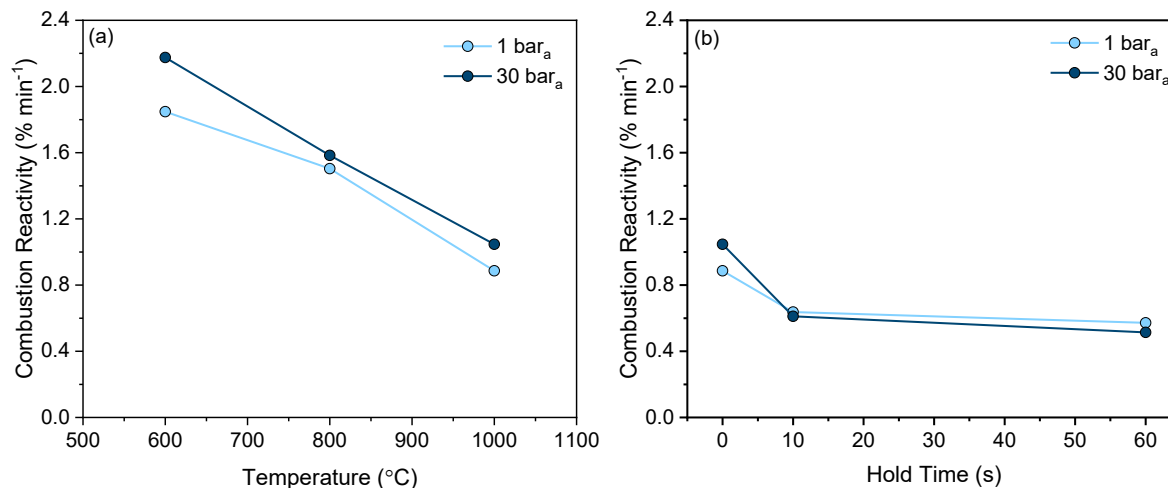
Figure 4. 17 (a) Combustion reactivities of Morupule coal chars produced at 0 s hold time as a function of temperature at pressures of 1 bar$_a$ and 30 bar$_a$. (b) Combustion reactivities of Morupule coal chars as a function of hold time at 1000 °C and pressures of 1 bar$_a$ and 30 bar$_a$.

4.3.5.2 WMR Gasification Reactivity

In the interest of char conversion processes, the CO_2 gasification reactivity of the low- and high-pressure chars produced at 1000 °C and different holding times, 0 and 60 s, was studied (Table 4.4). Both the extent of gasification and conversion values are in a limited range of 4.2 – 4.9 wt%, daf and 7.0 – 7.7 %, respectively, with the differences between the two pressures being well within the experimental error of the HPWMR experiments. As such, the differences in the apparent gasification reactivity of the investigated samples are insignificant. This corroborates the TGA combustion reactivities which showed similar performance for chars produced under these conditions. In contrast, Roberts, *et al.* [41] observed an increase in the apparent CO_2 gasification reaction rate with increasing pyrolysis pressure. However, normalising the apparent reaction rate to the surface area of the char indicated that the

pyrolysis pressure does not influence the reaction rate. In a study by Fermoso, *et al.* [36], higher apparent reactivities in H_2O for high pressure chars, which would otherwise remain independent of pyrolysis pressure if normalised by the measured surface area, were observed. These findings, including those from the present work, indicate that char chemistry as a function of pyrolysis pressure in the 1 – 30 bar_a range does not affect char gasification reactivity. Although a marked difference was observed in the TGA analyses of chars produced at 0 s, holding at 1000 ºC for 30 s during gasification promotes graphitisation and the loss of microporosity, producing structurally similar chars.

Table 4. 4 Influence of pressure and hold time on the CO_2 gasification reactivity of chars produced at 1000 ºC.

Pyrolysis Pressure (bar_a)	Extent of Gasification (wt%, daf) Pyrolysis Hold Time (s)		Conversion (%) Pyrolysis Hold Time (s)	
	0	60	0	60
1	4.7	4.2	7.7	7.0
30	4.5	4.9	7.2	7.7

4.4 Conclusions

The links between reactivity and char structural and morphological changes during high pressure pyrolysis of Morupule coal in a temperature range of 400 – 1000 ºC and holding for 0 – 60 s at 1000 ºC were investigated at a heating rate of 1000 ºC s^{-1}. Total volatile yields increased with temperature but remained unchanged under prolonged holding at peak temperature. Pyrolysis at high pressure resulted in lower total volatile yields at 600 ºC and 800 ºC due to tar repolymerisation. The repolymerisation structures were thermally cracked at 1000 ºC resulting in a reduced difference between the total volatile yields from low- and high-pressure pyrolysis.

Loss of O-containing functional groups takes place during the heating up period, resulting in a lower Raman scattering ability of the char. The extent of graphitisation, if any, of the chars was limited during the heating up period to 1000 ºC and became more pronounced under extended holding. The bulk graphitisation reactions took place during the first 10 s of holding at peak temperature. Due to its medium volatile content, the particle size of Morupule coal chars remained unchanged in comparison to the parent coal. Bubble transport is the main transport phenomenon for the release of volatiles at both 1 bar$_a$ and 30 bar$_a$, characterised by large blowholes due to an explosive release of the volatiles. The prevalence of intact bubbles on the surface of high-pressure chars was due to the resolidified tars, adding to the reduced total volatile yields at 600 ºC and 800 ºC. Based on a novel X-Ray CT application, chars produced at high pressures have a higher porosity than their atmospheric pressure counterparts and are characterised by thin walls with large voidages.

The combustion reactivity of Morupule coal chars decreased due to the loss of O-containing functional groups, and consequently active sites, when temperature was increased. High pressure chars from 0 s experiments were more reactive due to a higher volatile matter content. By contrast, the combustion reactivities of low- and high-pressure chars held at 1000 ºC for prolonged periods were similar as these chars underwent graphitisation to the same extent. The gasification reactivity in a CO_2 atmosphere revealed that the apparent reaction rates are independent of pyrolysis pressure. Although pressure affects the total volatile yields of Morupule coal during the heating up period, its influence significantly diminished under prolonged holding at 1000 ºC, resulting in chars with similar gasification and combustion reactivity to those obtained at atmospheric pressure. In this context, subsequent heterogeneous gas-char gasification reactions involving Morupule coal char will not be affected by elevated pressures in a gasifier.

References

1.   Zeng, D.; Fletcher, T. H., Effects of Pressure on Coal Pyrolysis and Char Morphology. *Energy & Fuels* **2005,** *19* (5), 1828-1838.

2.   Miller, B. G., 4 - Introduction to Coal Utilization Technologies. In *Clean Coal Engineering Technology (Second Edition)*, Miller, B. G., Ed. Butterworth-Heinemann: **2017**; pp 147-229.

3.   Bell, D. A.; Towler, B. F.; Fan, M., Chapter 4 - Gasifiers. In *Coal Gasification and Its Applications*, Bell, D. A.; Towler, B. F.; Fan, M., Eds. William Andrew Publishing: Boston, **2011**; pp 73-100.

4.   Sathe, C.; Hayashi, J.-I.; Li, C.-Z., Release of volatiles from the pyrolysis of a Victorian lignite at elevated pressures. *Fuel* **2002,** *81* (9), 1171-1178.

5.   Saxena, S. C., Devolatilization and combustion characteristics of coal particles. *Progress in Energy and Combustion Science* **1990,** *16* (1), 55-94.

6.   Guell, A. J.; Kandiyoti, R., Development of a gas-sweep facility for the direct capture of pyrolysis tars in a variable heating rate high-pressure wire-mesh reactor. *Energy & Fuels* **1993,** *7* (6), 943-952.

7.   Peralta, D.; Paterson, N.; Dugwell, D.; Kandiyoti, R., Pyrolysis and CO_2 Gasification of Chinese Coals in a High-Pressure Wire-Mesh Reactor under Conditions Relevant to Entrained-Flow Gasification. *Energy & Fuels* **2005,** *19* (2), 532-537.

8.   Wall, T. F.; Liu, G.-s.; Wu, H.-w.; Roberts, D. G.; Benfell, K. E.; Gupta, S.; Lucas, J. A.; Harris, D. J., The effects of pressure on coal reactions during pulverised coal combustion and gasification. *Progress in Energy and Combustion Science* **2002,** *28* (5), 405-433.

9.   Solomon, P. R.; Fletcher, T. H., Impact of coal pyrolysis on combustion. *Symposium (International) on Combustion* **1994,** *25* (1), 463-474.

10.   Berrueco, C.; Lorente, E.; Van Niekerk, D.; Millan, M., Evolution of Tar in Coal Pyrolysis in Conditions Relevant to Moving Bed Gasification. *Energy & Fuels* **2014,** *28* (8), 4870-4876.

11.   Zhuo, Y.; Messenböck, R.; Collot, A. G.; Megaritis, A.; Paterson, N.; Dugwell, D. R.; Kandiyoti, R., Conversion of coal particles in pyrolysis and gasification: comparison of conversions in a pilot-scale gasifier and bench-scale test equipment. *Fuel* **2000,** *79* (7), 793-802.

12.   Fidalgo, B.; Berrueco, C.; Millan, M., Chars from agricultural wastes as greener fuels for electric arc furnaces. *Journal of Analytical and Applied Pyrolysis* **2015,** *113*, 274-280.

13.   Kandiyoti, R.; Herod, A.; Bartle, K. D.; Morgan, T. J., *Solid fuels and heavy hydrocarbon liquids: thermal characterization and analysis*. Elsevier: **2016**.

14.   Sathe, C.; Pang, Y.; Li, C.-Z., Effects of Heating Rate and Ion-Exchangeable Cations on the Pyrolysis Yields from a Victorian Brown Coal. *Energy & Fuels* **1999,** *13* (3), 748-755.

15.   Messenböck, R. C. Rapid Pyrolysis and Gasification of Coal in a High Pressure Wire-Mesh Reactor. PhD Thesis, University of London, **1998**.

16.   Gibbins, J. R. Investigation of Primary Coal Pyrolysis Processes using a Variable Heating Wire-Mesh Apparatus. PhD Thesis, University of London, **1988**.

17.   Hower, J. C.; Wagner, N. J.; O'Keefe, J. M. K.; Drew, J. W.; Stucker, J. D.; Richardson, A. R., Maceral types in some Permian southern African coals. *International Journal of Coal Geology* **2012,** *100*, 93-107.

18.   Messenböck, R. C.; Dugwell, D. R.; Kandiyoti, R., CO_2 and steam-gasification in a high-pressure wire-mesh reactor: the reactivity of Daw Mill coal and combustion reactivity of its chars. *Fuel* **1999,** *78* (7), 781-793.

19.   Fidalgo, B.; van Niekerk, D.; Millan, M., The effect of syngas on tar quality and quantity in pyrolysis of a typical South African inertinite-rich coal. *Fuel* **2014,** *134*, 90-96.

20.   Berrueco, C.; Venditti, S.; Morgan, T. J.; Álvarez, P.; Millan, M.; Herod, A. A.; Kandiyoti, R., Calibration of Size-Exclusion Chromatography Columns with 1-Methyl-2-pyrrolidinone (NMP)/Chloroform Mixtures as Eluent: Applications to Petroleum-Derived Samples. *Energy & Fuels* **2008,** *22* (5), 3265-3274.

21.   Lee, C. W.; Scaroni, A. W.; Jenkins, R. G., Effect of pressure on the devolatilization and swelling behaviour of a softening coal during rapid heating. *Fuel* **1991,** *70* (8), 957-965.

22.   Yu, J.; Sun, L.; Berrueco, C.; Fidalgo, B.; Paterson, N.; Millan, M., Influence of temperature and particle size on structural characteristics of chars from Beechwood pyrolysis. *Journal of Analytical and Applied Pyrolysis* **2018,** *130*, 127-134.

23.   Dong, S. Development of Analytical Methods for Characterizing Metallurgical Coke and the Injectant Coal Chars, Tars and Soots Formed during Blast Furnace Operation. Imperial College London of Science, Technology and Medicine, **2008**.

24.   Li, X.; Hayashi, J.-i.; Li, C.-Z., Volatilisation and catalytic effects of alkali and alkaline earth metallic species during the pyrolysis and gasification of Victorian brown coal. Part VII. Raman spectroscopic study on the changes in char structure during the catalytic gasification in air. *Fuel* **2006,** *85* (10), 1509-1517.

25.   Zhang, S.; Min, Z.; Tay, H.-L.; Asadullah, M.; Li, C.-Z., Effects of volatile–char interactions on the evolution of char structure during the gasification of Victorian brown coal in steam. *Fuel* **2011,** *90* (4), 1529-1535.

26.   Keown, D. M.; Li, X.; Hayashi, J.-i.; Li, C.-Z., Characterization of the Structural Features of Char from the Pyrolysis of Cane Trash Using Fourier Transform−Raman Spectroscopy. *Energy & Fuels* **2007,** *21* (3), 1816-1821.

27.	Li, X.; Hayashi, J.-i.; Li, C.-Z., FT-Raman spectroscopic study of the evolution of char structure during the pyrolysis of a Victorian brown coal. *Fuel* **2006,** *85* (12), 1700-1707.

28.	Guizani, C.; Jeguirim, M.; Valin, S.; Limousy, L.; Sylvain, S., Biomass Chars: The Effects of Pyrolysis Conditions on Their Morphology, Structure, Chemical Properties and Reactivity. *Energies* **2017,** *10*.

29.	Dong, S.; Alvarez, P.; Paterson, N.; Dugwell, D. R.; Kandiyoti, R., Study on the Effect of Heat Treatment and Gasification on the Carbon Structure of Coal Chars and Metallurgical Cokes using Fourier Transform Raman Spectroscopy. *Energy & Fuels* **2009,** *23* (3), 1651-1661.

30.	Zeng, D.; Clark, M.; Gunderson, T.; Hecker, W. C.; Fletcher, T. H., Swelling properties and intrinsic reactivities of coal chars produced at elevated pressures and high heating rates. *Proceedings of the Combustion Institute* **2005,** *30* (2), 2213-2221.

31.	Megaritis, A.; Messenböck, R. C.; Chatzakis, I. N.; Dugwell, D. R.; Kandiyoti, R., High-pressure pyrolysis and CO_2-gasification of coal maceral concentrates: conversions and char combustion reactivities. *Fuel* **1999,** *78* (8), 871-882.

32.	Cai, H. Y.; Kandiyoti, R., Effect of Changing Inertinite Concentration on Pyrolysis Yields and Char Reactivities of Two South African Coals. *Energy & Fuels* **1995,** *9* (6), 956-961.

33.	Cairncross, B., An overview of the Permian (Karoo) coal deposits of southern Africa. *Journal of African Earth Sciences* **2001,** *33* (3), 529-562.

34.	Hertzberg, M.; Zlochower, I. A.; Edwards, J. C., Coal particle pyrolysis mechanisms and temperatures. **1987**.

35.	Bailey, J. G.; Tate, A.; Diessel, C. F. K.; Wall, T. F., A char morphology system with applications to coal combustion. *Fuel* **1990,** *69* (2), 225-239.

36.	Fermoso, J.; Gil, M. V.; Borrego, A. G.; Pevida, C.; Pis, J. J.; Rubiera, F., Effect of the Pressure and Temperature of Devolatilization on the Morphology and Steam Gasification Reactivity of Coal Chars. *Energy & Fuels* **2010,** *24* (10), 5586-5595.

37.	Tremel, A.; Haselsteiner, T.; Nakonz, M.; Spliethoff, H., Coal and char properties in high temperature entrained flow gasification. *Energy* **2012,** *45* (1), 176-182.

38.	Cai, H. Y.; Güell, A. J.; Chatzakis, I. N.; Lim, J. Y.; Dugwell, D. R.; Kandiyoti, R., Combustion reactivity and morphological change in coal chars: Effect of pyrolysis temperature, heating rate and pressure. *Fuel* **1996,** *75* (1), 15-24.

39.	Feng, B.; Jensen, A.; Bhatia, S. K.; Dam-Johansen, K., Activation Energy Distribution of Thermal Annealing of a Bituminous Coal. *Energy & Fuels* **2003,** *17* (2), 399-404.

40.	Senneca, O.; Salatino, P., A semi-detailed kinetic model of char combustion with consideration of thermal annealing. *Proceedings of the Combustion Institute* **2011,** *33* (2), 1763-1770.

41.   Roberts, D. G.; Harris, D. J.; Wall, T. F., On the Effects of High Pressure and Heating Rate during Coal Pyrolysis on Char Gasification Reactivity. *Energy & Fuels* **2003,** *17* (4), 887-895.

Chapter 5

Early-Stage Char Kinetics and Structural Evolution during Atmospheric Pressure Gasification in CO$_2$

5.1 Introduction

Chapter 4 discussed the pyrolysis behaviour of Morupule coal at atmospheric and elevated pressures. In this chapter, the atmospheric pressure gasification behaviour of Morupule coal in CO$_2$ is elucidated and compared to that of pyrolysis using identical experimental conditions. Studies pertaining to the determination of the kinetics of coal gasification are typically carried out using chars that have undergone excessive heat treatment, decoupling pyrolysis and gasification [1,2,3,4,5]. However, prolonged holding under extreme thermal histories is associated with aromatic ring condensation and loss of microporosity, reducing char reactivity [6,7,8]. This

work presents a novel alternative experimental approach, using a wire-mesh reactor (WMR), which limits the effect of char preparation on determining the kinetics of gasification. It also assesses the chemical structure and morphological development of the char, taking Morupule coal from Botswana as a case study. The findings presented in this chapter highlight a considerable scope for extensive lab-scale investigations of early-stage gasification of biomass and coals under conditions which simultaneously preserve the structural properties of the parent coal and mimic gasifier thermal histories. The results and discussion presented in this chapter are adapted from a manuscript submitted for publication [**].

5.2 Materials and Methods

5.2.1 Feedstock and WMR

Morupule raw coal used in this work, sourced from Morupule Coal Mine (Botswana), was crushed and sieved to a particle size fraction of 125 – 150 µm. The sample was dried for 12 h at 105 ºC in a vacuum oven and subsequently kept in a desiccator prior to experiments. The proximate and elemental analyses of this feedstock are provided in Sections 3.3.1.1 and 3.3.2, respectively. Pyrolysis and gasification experiments were carried out using the WMR, as detailed in Section 3.2.3.2.

5.2.2 WMR Experimental Conditions

Identical experimental conditions were used for pyrolysis and gasification experiments. These experiments were carried out in a temperature range of 900 – 1050 ºC, at a heating rate of 1000 ºC s^{-1}, for various holding times that enabled a gasification conversion of up to ~ 15 % in CO$_2$ at atmospheric pressure. Three repeats at each experimental condition were carried

---

[**] Bikane, K.; Yu, J.; Shankar, R.; Long, X.; Paterson, N.; Millan, M., Early-Stage Kinetics and Char Structural Evolution during Atmospheric Pressure Gasification of Morupule Coal in CO$_2$. Submitted, under review.

out and averaged to obtain each data point. A 95 % confidence interval was used as a statistical measure of the error. The mass loss under pyrolysis conditions was subtracted from mass loss under gasification conditions to estimate the extent of gasification (Equation 4.1) [9, 10]. Gasification conversion (Equation 4.2) was estimated as a ratio of the extent of gasification to the pyrolysis char yield obtained under identical experimental conditions.

The char – CO_2 gasification reaction rate, k, calculated using Equation 5.1, was estimated as the rate of change of conversion, X[11]. Equation 5.1 assumes that the gasification reaction rate is independent of char structural and morphological evolution in the studied conversion range. The nth order overall reaction, based on the Arrhenius representation, was used for kinetic analyses (Equation 2.9). The activation energy, E_a, and pre-exponential factor, A, were estimated from experiments carried out in 100 vol.% CO_2 at temperatures between 900 – 1050 ºC. To determine the reaction order, n, the CO_2 concentration in the feed gas was changed from 100 vol.% to 50 vol.% and 25 vol.%, with helium used to maintain the feed gas velocity, at temperatures of 900 ºC and 1000 ºC.

$$k = \frac{dX}{dt} \tag{5.1}$$

5.2.3 Char Structure and Reactivity Characterisation

The bulk chemical properties of the recovered pyrolysis and gasification chars were investigated using Raman spectroscopy. The surface chemistry of Morupule coal chars was studied using a Thermo Scientific K-Alpha[+] X-Ray photoelectron spectrometer (XPS). A scanning electron microscope (SEM) with an acceleration voltage of 20 kV was used to study the morphological evolution of the residual chars. Residual char combustion reactivity, $R_{50\%}$, was investigated in a PerkinElmer Pyris 1 thermogravimetric analyser using the isothermal method at 500 ºC and evaluated at time taken to combust 50 % of the organic material (Equation 3.6) [12].

5.3 Results and Discussion

5.3.1 Total Volatile Yields

Figures 5.1a and b show the total volatile yields from pyrolysis, in helium, and CO$_2$-gasification experiments at atmospheric pressure for different holding times at 900 ºC and 1000 ºC, respectively. Consistent with previous literature where an estimated 1 – 4 % conversion due to gasification in CO$_2$ was observed [9, 13], the total volatile yields at 0 s under both atmospheres are identical and well within experimental error. This indicates that minimal, if any, gasification took place during the heating up period. This observation is valid for the initial 30 s at 900 ºC, with the first statistically significant difference between the two total volatile yields occurring at 60 s. In contrast, differences between pyrolysis and gasification total volatile yields were observed as early as 10 s at 1000 ºC owing to increased chemisorption and reaction rates. Nonetheless, an initial lag in the heterogeneous gas – char reaction is revealed. It must be noted that experiments carried out in this work use Morupule raw coal, with little to no internal porosity. The internal porous structure develops during the rapid devolatilisation. Consequently, the reactive media (CO$_2$ in this case) can only access the intraparticle porous network once pyrolysis is advanced. As such, gasification may be initially limited to the external particle surface, due to the delayed intraparticle pore diffusion, adding to the observed initial lag. The Boudouard reaction follows a mechanistic pathway in which CO$_2$ or its radicals are initially adsorbed onto surface active sites, followed by reactions with active carbon atoms, and, lastly, the desorption of CO molecules [14]. Furthermore, it is presumed that both adsorption and desorption control the overall gasification rate [15]. Consequently, initial gasification mechanistic steps must proceed in a sequential manner, and in abundance, before significant weight losses are recorded in the quasi-batch WMR setup.

Prolonged holding to 60 s under gasification conditions at 1000 ºC increased the total volatile yields, reaching 44 wt.%, daf, compared to 35 wt.%, daf obtained from pyrolysis under identical conditions. While other WMR studies have reported a virtual halt of the gasification reaction in the 30 – 60 s hold time range for a peak temperature of 1000 ºC, possibly due to

char deactivation [13], a continued increase of the extent of gasification is observed for Morupule coal in the present work (Figure 5.2). Previous investigations on the thermochemical behaviour of Morupule coal indicated that the prolonged exposure, up to 60 s (beyond 10 s), at 1000 ºC has a negligible impact on the char chemical structure (Chapter 4), rendering the influence of heat treatment on char deactivation insignificant under the conditions studied. The negative extents of gasification at 0 s highlight the near identical total volatile yields obtained during pyrolysis and gasification.
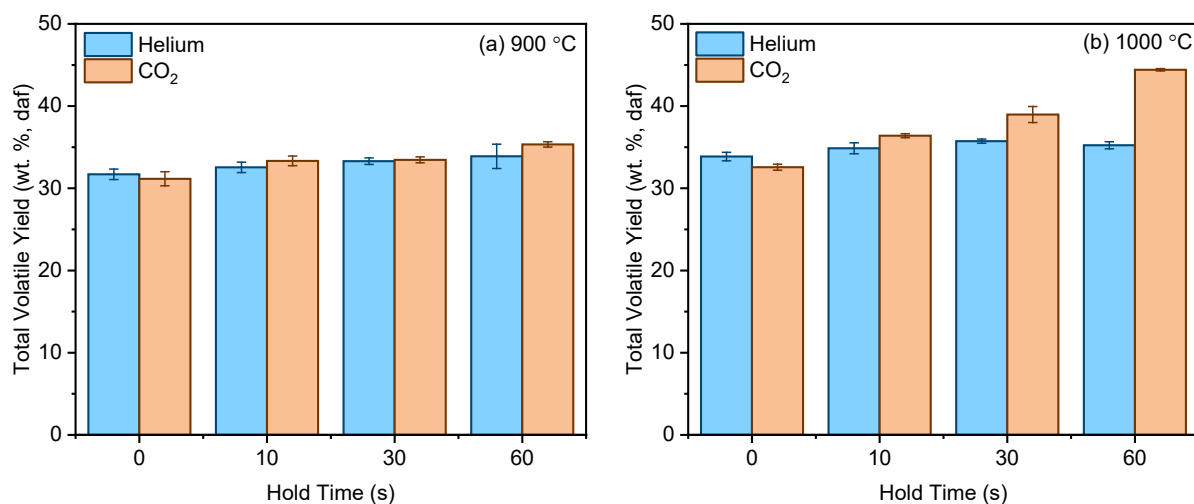
Figure 5. 1 Total volatile yields from the pyrolysis and CO$_2$ gasification of Morupule coal at (a) 900 ºC and (b) 1000 ºC, at a heating rate of 1000 ºC s^{-1} and 0 – 60 s holding times at atmospheric pressure.
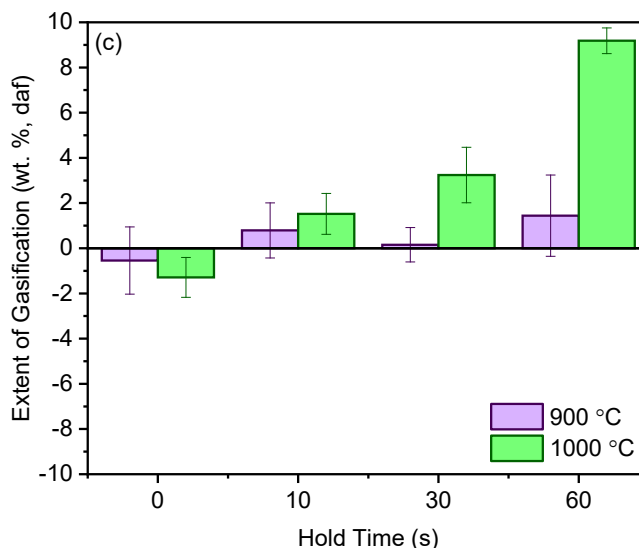
Figure 5. 2 Extents of gasification of Morupule coal in CO$_2$ at peak temperatures of 900 ºC and 1000 ºC and holding for 0 – 60 s at atmospheric pressure.

5.3.2 Intrinsic Reaction Kinetics

5.3.2.1 Conversions

To determine the gasification reaction kinetics, Morupule raw coal was gasified using CO$_2$ at atmospheric pressure in a 900 – 1050 ºC temperature range (isothermal) at various holding times (Figure 5.3a). In line with standard methodology, conversions of up to ~15 % were considered to minimise the effects of char deactivation and morphological changes [16, 17]. For all isothermal temperature experiments, a linear relationship between gasification conversion and holding time was observed, indicating an invariable apparent reaction rate in this conversion range (after the aforementioned initial lag shown in Figures 5.1a and b). The linear relationship validates the underlying assumption of a constant reaction rate (Equation 5.1). Conversions higher than 20 % deviate from this linear relationship (Figure 5.3b), with the reaction slowing down possibly due to the onset of process-induced char structural changes and deactivation as the char is exposed to high temperatures for longer periods. Considerable increases in the reaction rate with temperature are observed between 900 ºC and 950 ºC.

Further increases in the reaction rate, albeit slightly, are observed in the 975 – 1050 ºC temperature range.
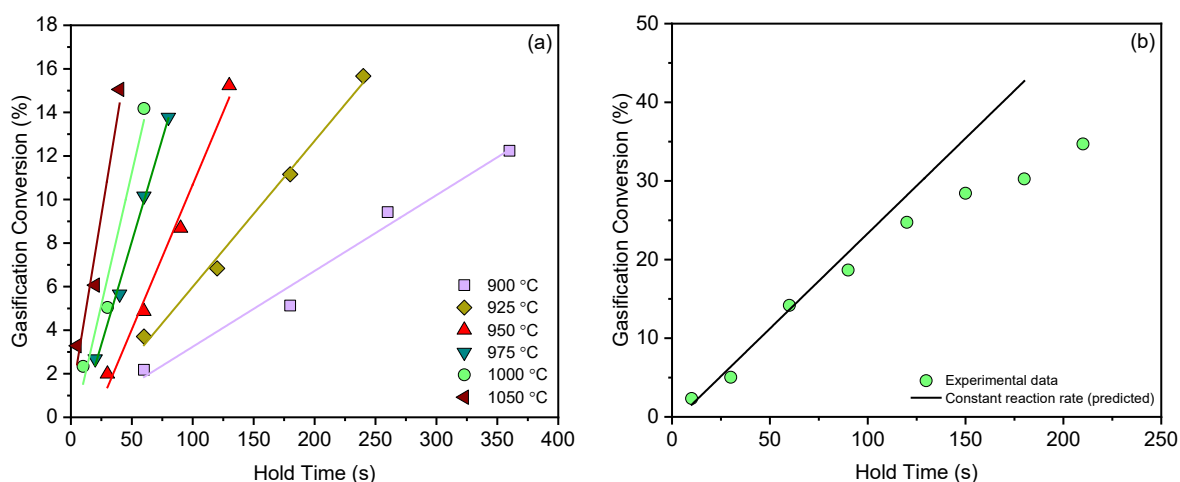
Figure 5. 3 Morupule coal CO_2 gasification conversions (a) in a 900 – 1050 ºC temperature range at atmospheric pressure, as a function hold time in the WMR (summary of the reaction rates and coefficient of determination are provided in Table 5.1) (b) at 1000 ºC under prolonged holding times to attain higher conversions.

Table 5. 1 The estimated reaction rates at different temperatures and their corresponding coefficients of determination, R^2.

Temperature (ºC)	Reaction rate (s^{-1})	R^2
900	0.00035	0.98
925	0.00067	0.99
950	0.00133	0.99
975	0.00189	0.99
1000	0.00242	0.96
1050	0.00342	0.96

5.3.2.2 Activation Energy and Pre-Exponential Factor

Figure 5.4 shows a significant change in the Arrhenius plot gradient between 950 ºC and 1000 ºC, indicating a transition between the chemical reaction controlled and mass transport

plus chemical reaction controlled kinetic regimes. This transition occurs at a lower temperature than that reported for the gasification of bituminous coal chars using CO$_2$ (1100 ºC) [18,19]. Furthermore, E_a and A values, presented in Table 5.2, from the gasification of Morupule coal in CO$_2$ are significantly higher (E_a is higher by at least 50 kJ mol^{-1} whilst A is larger by at least two orders of magnitude as shown in Table 2.4) than those from other studies investigating the gasification of coal chars of similar parent coal rank in a chemical reaction controlled kinetic regime [4,15,17]. Kinetic parameters estimated by fitting the shrinking core, random pore and volumetric models (Table 7.3) are similar to those presented in Table 5.2. A fundamental interpretation of E_a from the Arrhenius plot is based on the sensitivity of the reaction rate to changes in temperature. It is highly probable that the higher reactivity and kinetic parameters obtained for the gasification of Morupule coal are due to the reactor setup and experimental approach used in this contribution. The methodology presented in literature may therefore influence the estimated E_a as most of the kinetic studies are carried out using "well-cooked" chars that have spent extended periods at high temperatures. Excessive heat treatment induces ring condensation, loss of carbon edges and microporosity, reducing the intrinsic reactivity of the char [6]. Moreover, it has previously been shown that higher reaction rates are obtained using the direct gasification approach [20]. Consequently, the sensitivity of the char to temperature may be lessened (smaller E_a) and the reactivity decreased (smaller A) in comparison to the direct gasification kinetic analysis of Morupule raw coal presented in this work. Reactor specific effects, including mass transport limitations particularly in TGA applications, may also influence the kinetic parameters obtained from experimentation. It is well known that CO inhibits the char – CO$_2$ reaction, particularly in reactor systems such as TGAs with slow CO transport from the reaction zone [21, 22], therefore lowering the overall reaction rate. Such limitations are minimised in the present work by ensuring a monolayer distribution of the particles and utilising a continuous stream of the sweep gas, carrying volatiles away from the reaction zone.
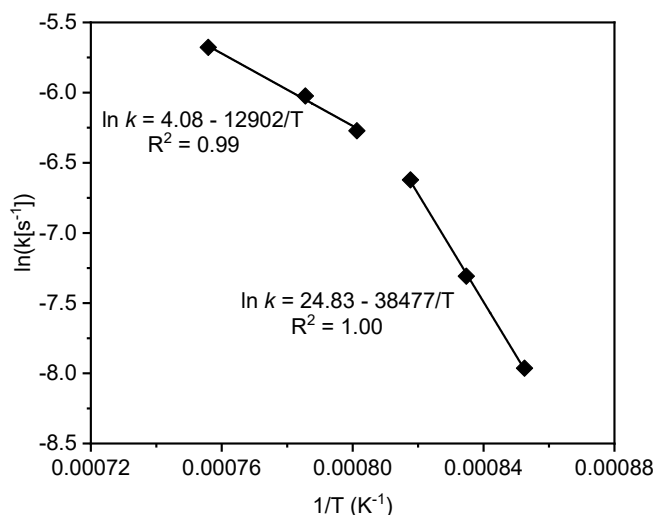
Figure 5. 4 Arrhenius plot obtained using atmospheric pressure apparent gasification reaction rates.

Table 5. 2 Activation energies and pre-exponential factors from different kinetic regimes of Morupule coal gasification in CO$_2$ at atmospheric pressure.

Temperature Range (ºC)	Activation Energy (kJ mol $^{-1}$)	Pre-exponential factor (s^{-1})
900 – 950	320	6.1×10^{10}
975 – 1050	107	5.9×10^1

Activation energy from the 975 – 1050 °C temperature range is lower than the one estimated from the 900 – 950 °C range. This is typical of pore diffusional limitations at high temperatures [18, 23], possibly restricting most of the gasification to the external surface of the particles and pores closer to the surface. Interestingly, the E_a value of the mixed pore diffusion plus chemical reaction controlled regime is a third of the E_a value obtained in the chemical reaction controlled regime. This observation compares well with a combustion theoretical prediction of an activation energy half of one obtained in the chemical reaction controlled regime [15]. The WMR mimics the thermal histories of coals in industrial gasifiers, preserving the chemical structure of the parent coal with minimal influence from the reactor or preparation effects [9]. The results presented above may therefore serve as a benchmark for appropriate

temperature and lab-scale methodology considerations when studying intrinsic gasification kinetics.

5.3.2.3 Reaction Order

The influence of CO_2 concentration on the reaction rate was studied to determine the reaction order at 900 ºC and 1000 ºC (Figures 5.5a and b, respectively). A constant reaction rate at lower CO_2 concentrations is observed in the studied conversion range. Lower CO_2 concentrations led to an increased lag in the commencement of gasification due to the reduced accessibility of the active sites by the reactive gas. At 900 ºC, changing the concentration between 50 – 100 vol.% did not affect the reaction rate as shown by the parallel lines in Figure 5.5a. The longer holding times for in Figure 5.5b are due to the slower reaction rates when the gas concentration is reduced. However, further decrease to a concentration of 25 vol.% resulted in negligible gasification, if any, and therefore is not shown in Figure 5.5a. In contrast, there are discernible changes in the reaction rate as a function of CO_2 concentration at 1000 ºC, with lower concentrations resulting in slower reaction rates. These findings further highlight the possible different kinetic regimes that are occurring at these temperatures. The presence of helium gas (used to maintain the gas velocity as the input CO_2 was reduced) may inhibit the availability of CO_2, thereby reducing the reaction rate at 1000 ºC, where the overall reaction is controlled by both mass transport and the chemical reaction.

Changes in the reaction rate at 1000 ºC translate to a reaction order of 0.6 with respect to CO_2 concentration (Figure 5.6). For experiments at 900 ºC, an approximation was made using the two reaction rates obtained at 50 vol.% and 100 vol.% CO_2 concentrations, resulting in an estimated reaction order of 0 within this concentration range. This implies that the accessibility of CO_2 to the char surface does not influence the gasification rate at 900 ºC. This is in agreement with the suggestion that the chemical reaction is the rate limiting step at lower temperatures while internal pore diffusion plays a significant role at higher temperatures, increasing the reaction order [24]. The reaction order at 900 ºC is outside the typical range

presented in literature of about 0.4 – 0.8 [15]. Temperatures at which the intrinsic kinetics have been determined may be excessively high as the kinetic regime transitional temperature may be lower than expected as shown in this work. Additionally, an inconsistent degree of gasification burn-off, between different studies, may affect the reaction order, as it is dependent on the char chemistry and pore diffusion related to the development of the internal porosity.
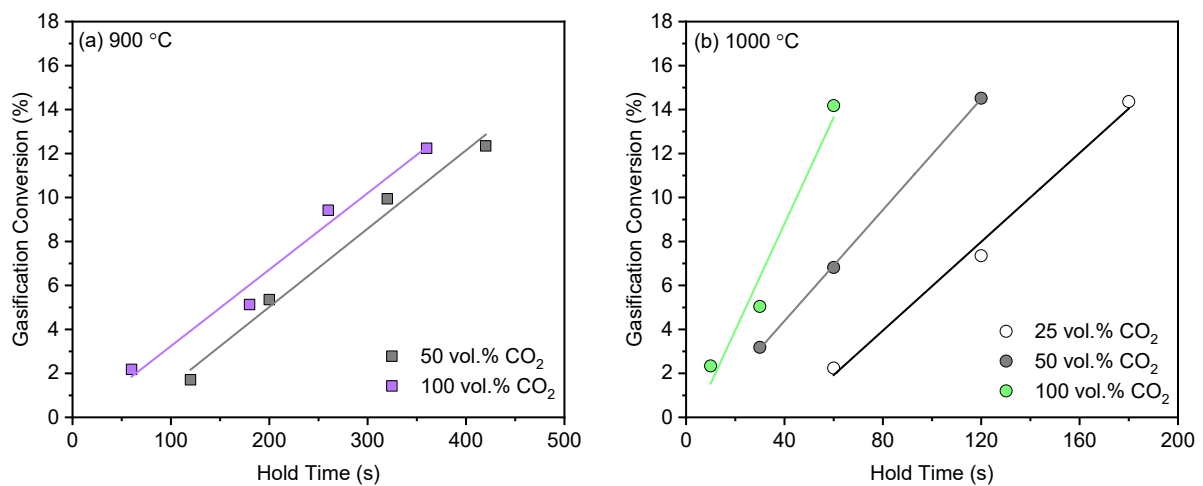
Figure 5. 5 Influence of CO_2 concentration on Morupule coal gasification conversions at (a) 900 ºC and (b) 1000 ºC.
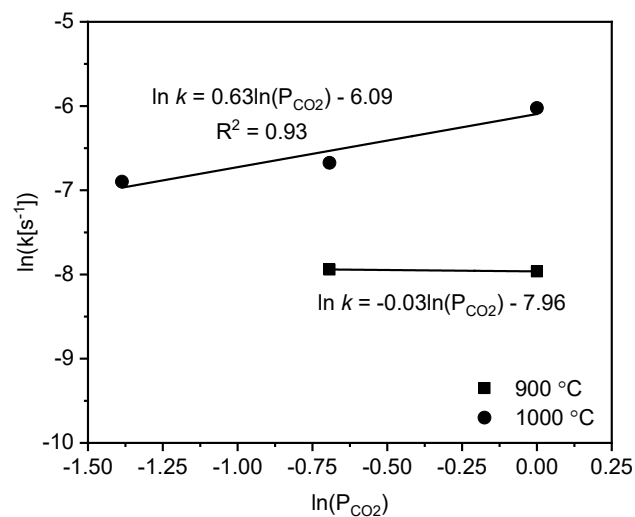
Figure 5. 6 Influence of CO_2 concentration on the rate constant from Morupule coal gasification at 900 ºC and 1000 ºC.

5.3.3 Char Structural Evolution

5.3.3.1 Raman Spectroscopy

5.3.3.1.1 Total Raman Peak Area

Raman spectra of chars produced under pyrolysis and gasification conditions at 900 ºC and 1000 ºC are presented in Figures 5.7 and 5.8, respectively. The corresponding total Raman peak areas, quantified from the Raman spectra, are shown in Figures 5.9a and b. Raman intensity is governed by various factors, among them the light absorptivity and Raman scattering ability of the char [25, 26]. The presence of the electron-rich O-containing functional groups increases the Raman intensity, and subsequently the total Raman peak area, while a higher char light absorptivity reduces Raman intensity [27]. A decrease in the Raman intensity with increasing holding time is observed for both pyrolysis and gasification chars produced at 900 ºC due to the loss of O-containing species and increased char light absorptivity. Insignificant bulk structural differences are deduced as observed that there are minimal differences between the total Raman peak areas of pyrolysis and gasification chars from 900 ºC experiments. This indicates that gasification is insignificant in the early stages at this temperature, consistent with the statistically indistinguishable total volatile yields from pyrolysis and gasification (Figure 5.1a).
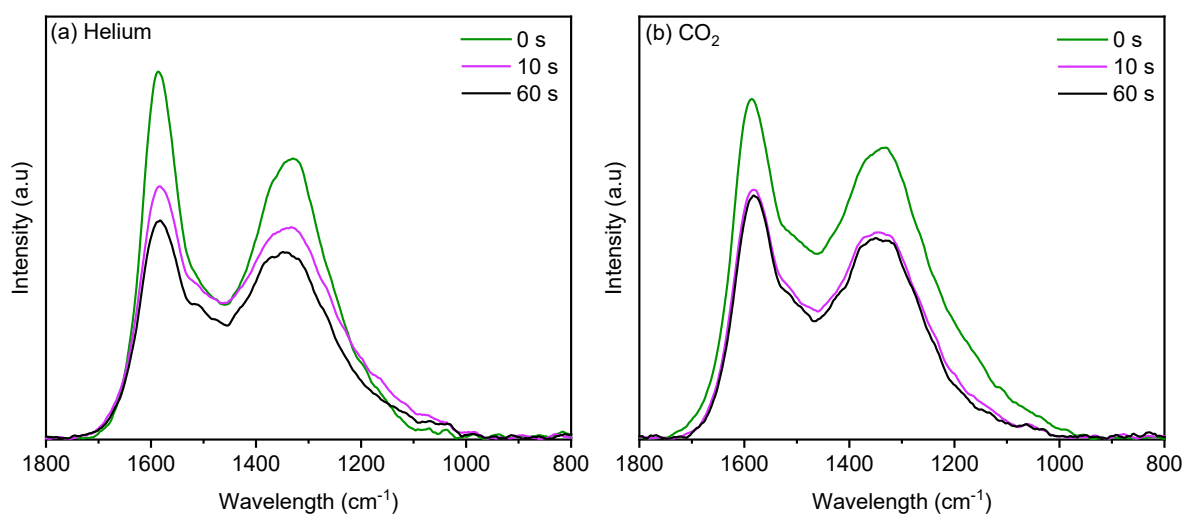
Figure 5. 7 Raman spectra of Morupule coal chars obtained from (a) pyrolysis in helium and (b) gasification in CO_2 gasification at 900 ºC.
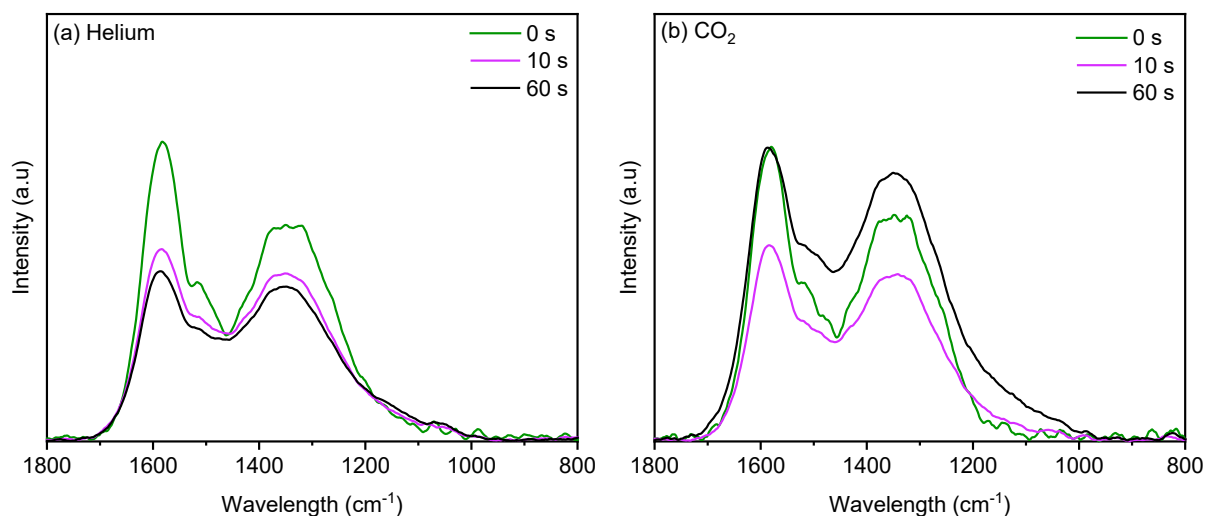
Figure 5. 8 Raman spectra of Morupule coal chars obtained from (a) pyrolysis in helium and (b) gasification in CO_2 gasification at 1000 ºC.
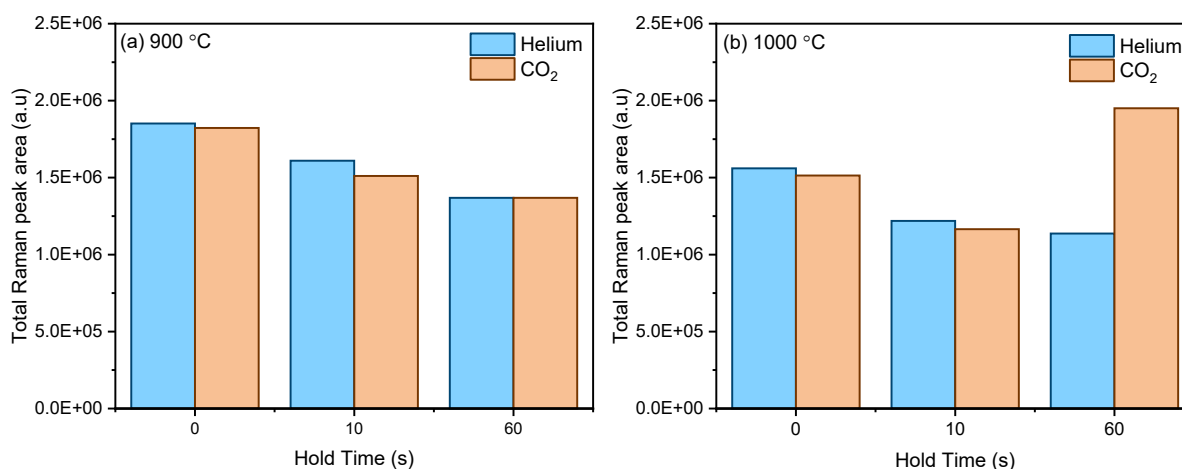
Figure 5. 9 Total Raman peak areas of pyrolysis and gasification chars produced at (a) 900 ºC and (b) 1000 ºC as a function of hold time.

Although similarities are observed for chars produced at up to 10 s holding time at 1000 ºC, a significant increase in the total Raman peak area is observed for chars produced at 60 s in CO_2 compared to their pyrolysis counterparts. This increase may be due to the presence of the newly formed O-containing species which froze on the surface of the char

when the reaction is quenched. Additionally, increased conversions may reduce the prominence of the aromatic ring systems, allowing for greater concentrations of the pre-existing O-containing groups. These findings are consistent with those in literature as Wang, *et al.* [28] observed a linear increase in the total Raman peak areas of CO$_2$-reacted chars with conversion, owing to an increase in the electron-rich functional groups.

5.3.3.1.2 Intensity Ratios

Further investigations on the bulk chemical structure differences between pyrolysis and gasification chars were carried out using the I_D/I_G and I_D/I_V intensity ratios shown in Figures 5.10 and 5.11, respectively. The I_D/I_G intensity ratio reflects the extent of graphitisation during pyrolysis or gasification. For carbon structures in the nanocrystalline graphite to amorphous carbon range, relevant for Morupule coal chars in this study, an increase in the I_D/I_G ratio is commensurate with increased char ordering [29], in contrast with more graphitic samples where this ratio decreases with increasing graphitisation. The I_D/I_V intensity ratio characterises the proportion of aromatic ring systems with six or more benzene rings relative to amorphous carbon structures with three to five fused benzene rings [28].

The I_D/I_G ratio increased as a function of hold time for chars produced in He and CO$_2$ atmospheres at both 900 ºC and 1000 ºC. This increase was more pronounced within the first 10 s of holding at peak temperature due to thermal annealing and the release of permanent gases, resulting in the formation of more ordered aromatic ring systems, enhancing crystallite growth [30]. The I_D/I_G ratio remained stable thereafter, indicating that the bulk of thermal annealing reactions and structural changes took place in the first 10 s at peak temperature. In contrast, the I_D/I_V intensity ratio decreased as a function of hold time. Similarly, a considerable reduction was observed within the first 10 s at peak temperature. This decrease is attributed to the ring condensation of the aromatic ring systems with six or more fused benzene rings that give rise to the D band, increasing the light absorptivity of the char and lowering the D band intensity. The raw spectra show that the intensity of the D and G bands underwent the greatest changes while the amorphous region, V band, had minimal changes during pyrolysis

and gasification evolution. In agreement with the I_D/I_G intensity ratio, the I_D/I_V intensity ratio was constant beyond the initial 10 s of holding at peak temperature, indicating that the relative proportions of structures represented by the intensity ratios remained fairly unchanged during the early-stage conversion.

The similarities between pyrolysis and gasification chars in terms of their I_D/I_G and I_D/I_V intensity ratios indicate that early-stage char structural changes are minimal during gasification at atmospheric pressure under the conditions presented. While this may be expected for chars produced at 900 ºC where gasification had barely commenced even after 60 s, it is an interesting observation for chars produced at 1000 ºC where gasification conversions of about 14 % were reached at 60 s holding time. The near identical I_D/I_V ratios at 60 s for pyrolysis and gasification chars therefore suggest an absence of preferential consumption of smaller aromatic ring systems in the amorphous band region. This is in contrast with previous work by Wang, *et al.* [28] who suggest a preferential polyaromatic gasification pathway, especially for conversions lower than 10 %. Alternatively, it can be argued that Morupule coal atmospheric pressure gasification reactions may be restricted to the outermost surface at 1000 ºC, leaving the bulk material relatively unchanged hence the similarity in the I_D/I_V intensity ratios. This suggestion is consistent with the pore diffusion plus chemical reaction controlled kinetic regime observed at this temperature in Figure 5.4, where pore diffusional limitations can restrict the accessibility of the reactive gas to the inner internal active surface area. Furthermore, a less developed surface porosity was observed using SEM on the external surface of Morupule coal chars, showing enclosed bubbles and localised blowholes (Figure 5.14). Consequently, the limited surface porosity may physically restrict the entrance of CO_2 into the internal porous network, limiting the gasification reactions and the bulk char chemical structure changes. This is consistent with the work by Guizani, *et al.* [31], who observed minimal volumetric gasification of biomass, and structural changes, due to limited CO_2 internal diffusivity.
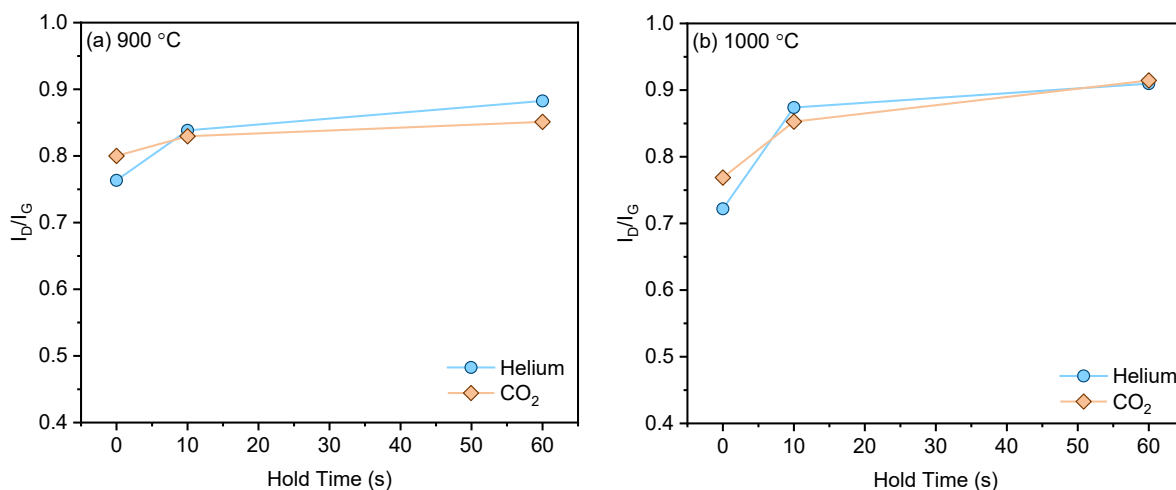
Figure 5. 10 I_D/I_G intensity ratios of Morupule coal chars from pyrolysis and gasification experiments at (a) 900 ºC and (b) 1000 ºC as a function of hold time.
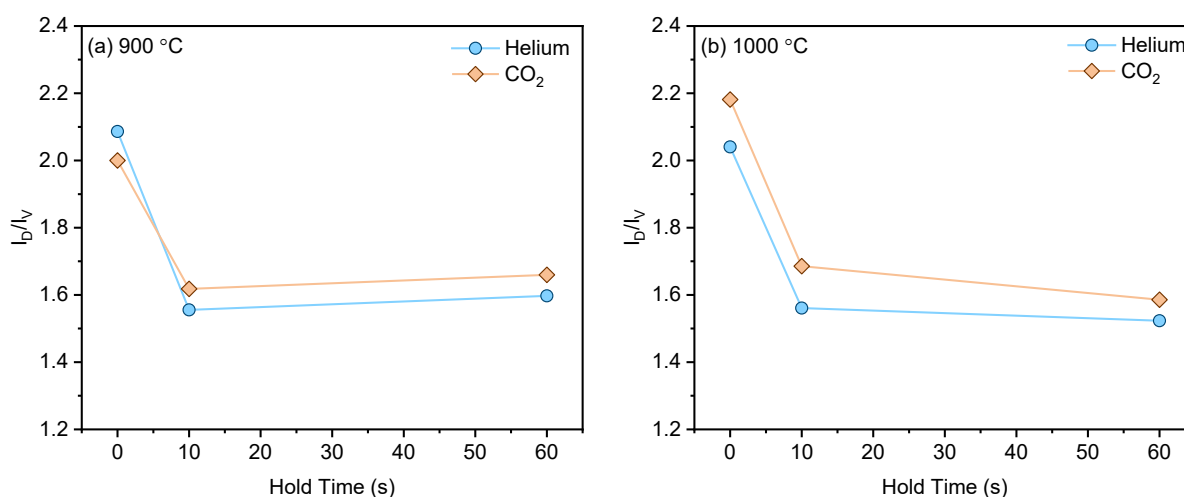
Figure 5. 11 I_D/I_V intensity ratios of Morupule coal chars from pyrolysis and gasification experiments at (a) 900 ºC and (b) 1000 ºC as a function of hold time.

5.3.3.2 X-Ray Photoelectron Spectroscopy (XPS)

Raman analyses and kinetics data established that the gasification reactions at 1000 ºC may be prominent on the external char surface. To gain further insights on the char structural evolution, the surface chemistry, based on high-resolution C 1*s* core level spectra, of Morupule coal chars from 1000 ºC pyrolysis and gasification experiments was studied using XPS (Tables 5.3 and 5.4). The deconvoluted spectra are provided in Figures 5.12 and 5.13. The peaks associated with the functional groups on the char surface were assigned as follows

149

during spectral deconvolution; C-C/C=C (aliphatic or aromatic) at 284.4 eV, C-O-R or C-OH (ether or hydroxyl) at 286.0 eV, C=O (carbonyl) at 287.4 eV, C(=O)OR (carboxyl) at 289.0 eV and carbon in carbonate groups at 290.7 eV [32, 33]. Pyrolysis and gasification chars from 0 s holding time at 1000 ºC exhibit similar atomic concentrations for all the functional groups. This provides further evidence that gasification reactions are limited in the heating up period to 1000 ºC. While the atomic concentrations of the assigned functional groups remain fairly constant under pyrolysis conditions after prolonged holding to 60 s, a decrease in the C-C/C=C bonds atomic concentration is observed for chars produced from gasification under identical experimental conditions. Therefore, the CO$_2$ gasification of Morupule coal, under these conditions and within the studied conversion range, propagates through the consumption of C-C/C=C bonds possibly from edge carbon atoms, previously identified as possible surface active sites [6]. Density functional molecular orbital calculations suggest that breaking the C-C bond to produce CO via semiquinones using CO$_2$ has an activation energy of 333.6 kJ mol^{-1} [34], a value comparable to the 320 kJ mol^{-1} obtained experimentally in the chemical reaction controlled regime free from diffusional limitations (Table 5.2).

The C 1*s* O-containing functional groups exhibit an increase in their respective atomic concentrations. While the possibility of this increase corresponding to the frozen O-containing intermediates from CO$_2$ is conceivable, it is highly possible that the consumption of C-C/C=C groups allows for an increase in the surface concentrations of other functional groups. SEM images presented in Figure 5.15b show that gasification results in a porous external surface. Therefore, the XPS measured surface chemistry at 60 s is characterised by less C-C/C=C bonds, which were consumed and developed into the surface porosity, increasing the atomic concentrations of the relatively inert groups. Literature suggests that O-containing functional groups can also act as active surface sites during gasification [6]. However, carbon defects appear to extensively participate in the early-stage CO$_2$ gasification of Morupule coal. The thermal and chemical stability of O-containing groups during both pyrolysis and gasification suggest that they may be terminating groups and/or aromatic ring system linkages.
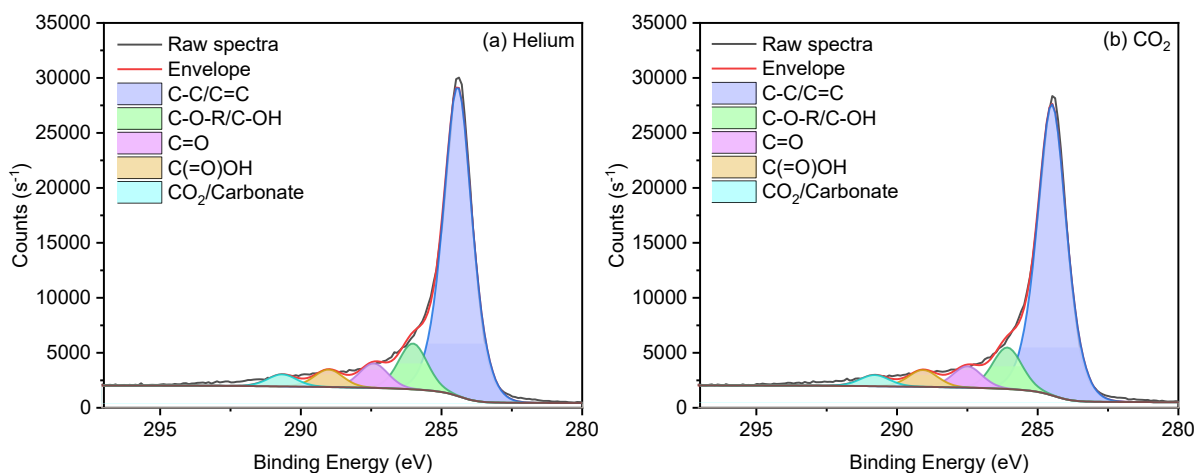
Figure 5. 12 Deconvoluted XPS spectra of Morupule coal chars obtained from (a) pyrolysis in helium and (b) gasification in CO$_2$ at 1000 ºC and 0 s holding time.
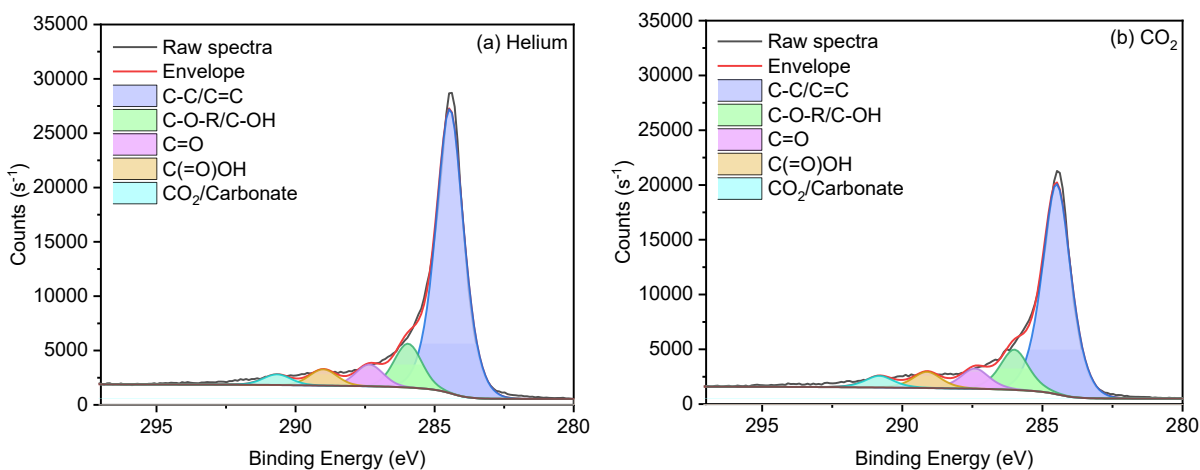
Figure 5. 13 Deconvoluted XPS spectra of Morupule coal chars obtained from (a) pyrolysis in helium and (b) gasification in CO$_2$ at 1000 ºC and 60 s holding time.

Table 5. 3 Atomic concentrations corresponding to the deconvoluted C 1*s* peaks of Morupule coal chars produced under pyrolysis and gasification conditions at 1000 ºC and a hold time of 0 s.

Atmosphere	C 1*s* Peaks (Atomic %)				
	C-C/C=C	C-OR/OH	C=O	C(=O)-OR	CO$_3^{2-}$
He	76.3	10.9	5.8	4.1	2.8
CO$_2$	76.9	10.5	5.4	4.3	2.8

Table 5. 4 Atomic concentrations corresponding to the deconvoluted C 1*s* peaks of Morupule coal chars produced under pyrolysis and gasification conditions at 1000 ºC and a hold time of 60 s.

Atmosphere	C 1*s* Peaks (Atomic %)				
	C-C/C=C	C-OR/OH	C=O	C(=O)-OR	CO$_3^{2-}$
He	76.1	11.3	5.6	4.2	2.8
CO$_2$	70.4	13.5	6.8	5.4	3.9

5.3.3.3 Scanning Electron Microscopy (SEM)

The morphological evolution of chars produced under gasification conditions was investigated using SEM (Figures 5.14 and 5.15). Chars produced at 0 s holding time and 1000 ºC in a CO$_2$ atmosphere (Figure 5.14b) retain the particle size of the parent sample (Figure 4.12), suggesting that Morupule coal is non-swelling during the rapid temperature ramp-up. Figure 5.14 exhibits localised blowholes, characteristic of the explosive volatile release typical of high heating rates [13]. Additionally, the char morphology reveals intact surface bubbles from liquid bitumen that condensed when the reaction was quenched [35]. The textural properties shown for gasification chars (Figure 5.14b) are similar to those from chars produced from pyrolysis under identical conditions (Figure 5.14a). Figure 5.1a indicated that the total volatile yields obtained in He and CO$_2$ atmospheres at 1000 ºC and 0 s holding time are statistically the same, hence the minimal influence of atmosphere on the physical evolution of char at such short holding times. The reaction is largely driven by devolatilisation during the heating up period under these conditions and gasification is insignificant, hence the indistinguishable char textural properties. In agreement with the present work, Messenböck [13] obtained near identical total volatile yields at 0 s hold time during the pyrolysis and gasification of Daw Mill coal in He and CO$_2$ at 1000 ºC using the WMR, prompting a suggestion that these yields are largely a result of pyrolysis.
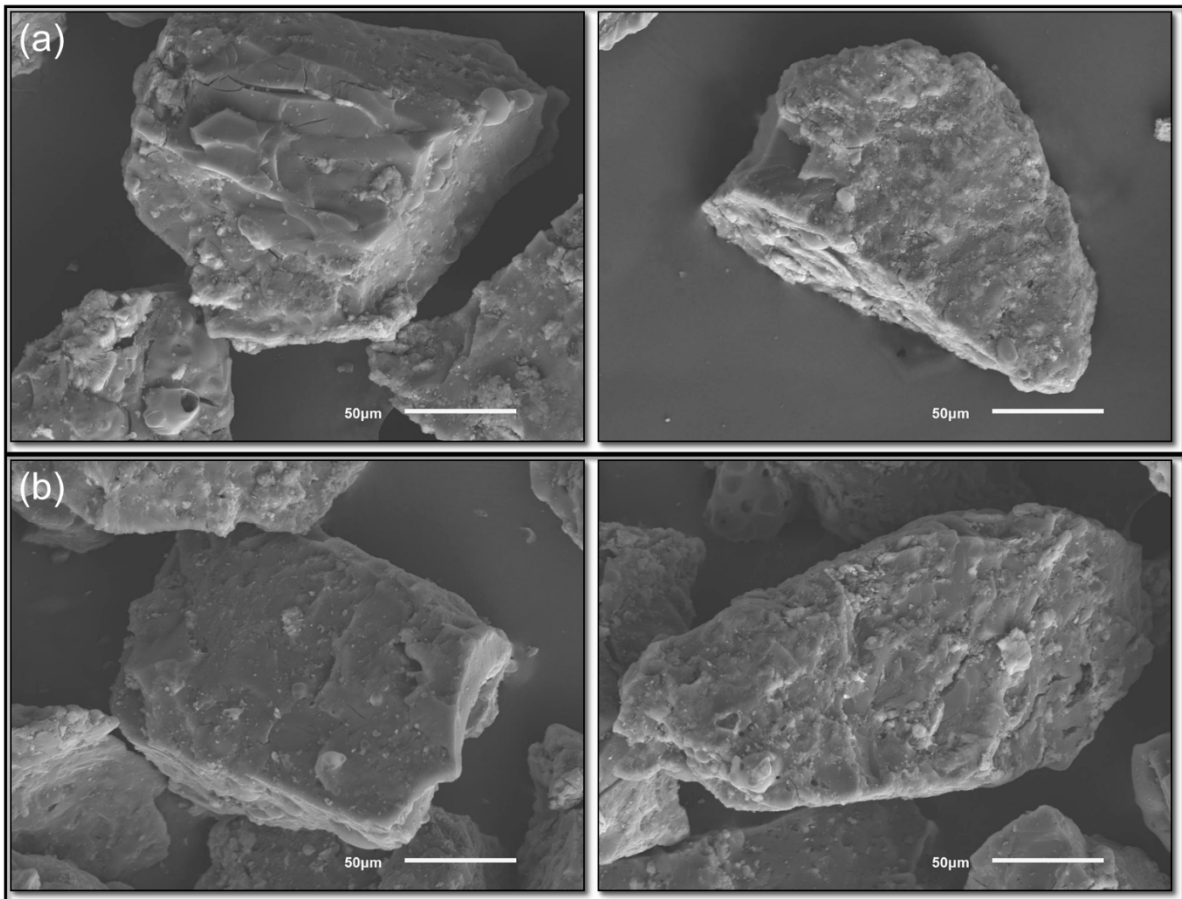
Figure 5. 14 SEM images of Morupule coal chars produced under atmospheric pressure (a) pyrolysis and (b) CO$_2$ gasification conditions at 1000 ºC, 0 s hold time and a heating rate of 1000 ºC s^{-1}.
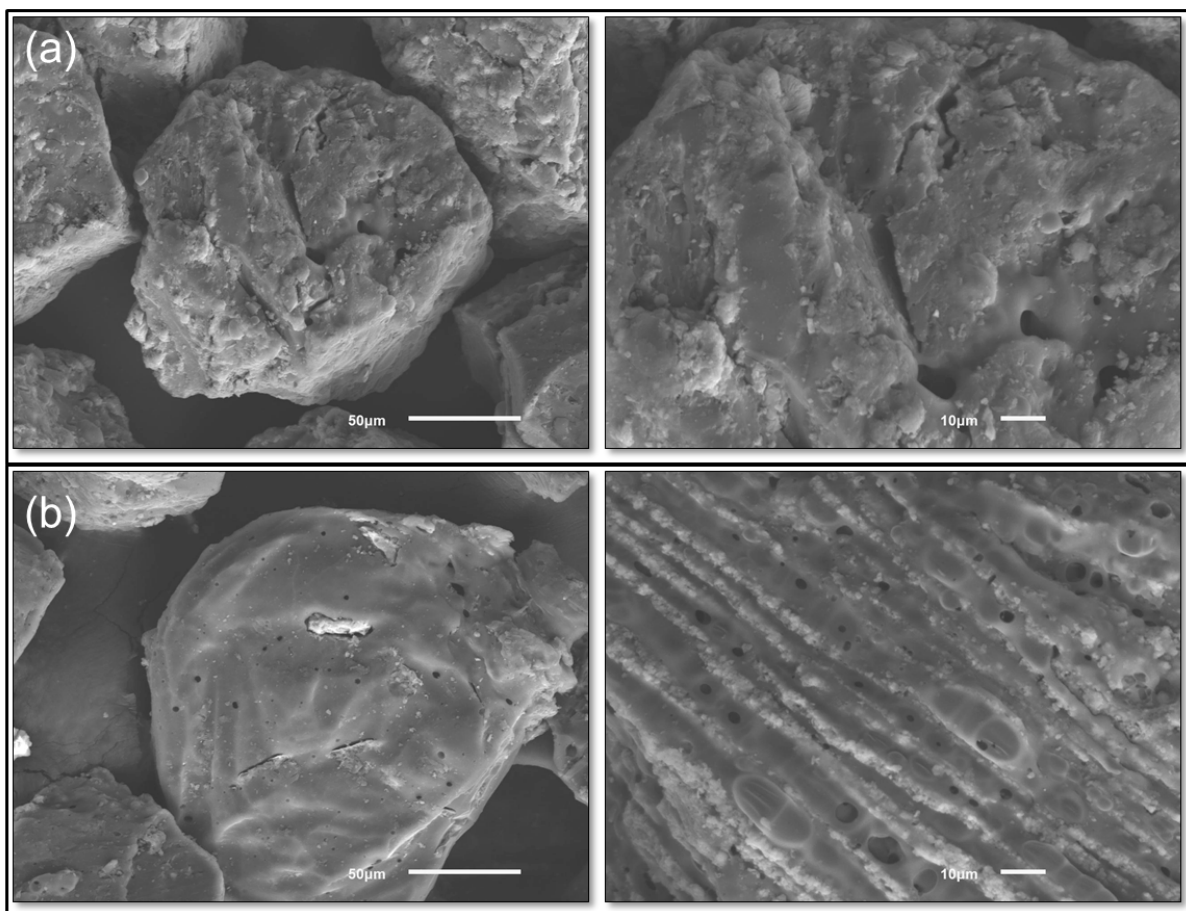
Figure 5. 15 Representative SEM images of Morupule coal chars produced under atmospheric pressure CO$_2$ gasification conditions at (a) 900 ºC and (b) 1000 ºC and a holding time of 60 s.

Figures 5.15a and b show captured SEM images of chars produced from holding Morupule coal in CO$_2$ for 60 s at 900 ºC and 1000 ºC, respectively. Under these conditions, gasification has a minimum impact on the particle size of the chars as the original particle size was preserved. Chars produced at 900 ºC do not show any developing surface porosity. This is hardly surprising given that the total volatile yield obtained during gasification is only marginally higher than that obtained under pyrolysis conditions at 60 s hold time (Figure 5.1a). As such, any changes that might have occurred are not sufficiently distinguishable. In contrast, a more developed surface porosity due to higher gasification rates and reduced initial lag is observed for chars produced at 60 s holding time at 1000 ºC. Figure 5.15b shows that the char is characterised by surface pores of different sizes, with some of the order of a micron and

some far smaller than that. Given the smooth textural surface without any developing surface porosity as shown in Figure 5.14b where gasification conversion is negligible at 0 s hold time (Figure 5.1b), it is postulated that subsequent gasification reactions take place in the proximity of where the initial char – CO_2 reaction took place, promoting pore growth. This observation is in agreement with a study by Chen and Yang [34], consistent with investigations by Zhu, *et al.* [36], suggesting that the presence of a chemisorbed oxygen radical on the char surface weakens the neighbouring C-C bonds, predisposing them for further consumption by gasification. The observed surface gasification reaction is therefore characterised by pore growth in the early stages of gasification and possible merging at high conversions, akin to a random pore model representation [37].

5.3.3.4 Char Combustion Reactivity

The relative combustion reactivities of pyrolysis and gasification chars produced at 900 ºC and 1000 ºC are presented in Figure 5.16. Generally, the combustion reactivity decreases as a function of hold time at peak temperature due to thermal annealing, consistent with the increase in the I_D/I_G intensity ratio indicating the prevalence of ring condensation (Figure 5.10). Similarly, a considerable change is observed in the first 10 s of holding at peak temperature while further holding to 60 s does not yield significant differences. Chars produced at 900 ºC are more reactive than those from 1000 ºC experiments. This corroborates the less steep I_D/I_G intensity ratio, presented in Figure 5.10a, at 900 ºC owing to a lesser extent of graphitisation and thermal annealing reactions at lower temperatures. Chars produced in CO_2 are slightly less reactive than those from He atmosphere under identical conditions for both isothermal temperatures. Although an explanation was not provided, a similar phenomenon was observed by Messenböck [13] during the pyrolysis and CO_2 gasification of Daw Mill coal. This suggests an influence of CO_2 on the char chemical structure. Based on the evidence for dissociative chemisorption of radicals, instead of molecules, on the char surface for gas-solid reactions, O radicals from O_2 (during combustion) and CO_2 react on the same active sites [6]. It

is therefore postulated that O radicals from CO_2 had already chemisorbed on the more reactive active sites before gasification was quenched, rendering O radicals from O_2 during subsequent combustion to the less reactive active sites, resulting in a lower combustion reactivity for chars obtained under gasification conditions. Despite a 14 % gasification conversion at 1000 ºC and 60 s hold time in CO_2, and the development of a porous external surface as shown by SEM images (Figure 5.15b), the residual char combustion reactivity is similar to that of a lower conversion obtained at a holding time of 10 s. This further supports the hypothesis that, within the conversion range studied, the bulk char structure and morphology are largely preserved and therefore the gasification and combustion reaction rates remain fairly unchanged.
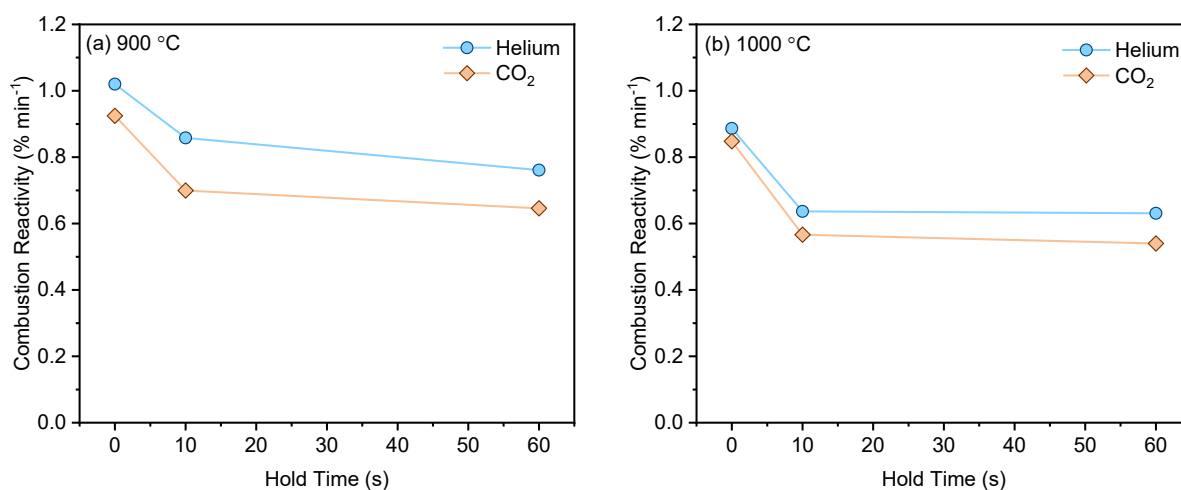
Figure 5. 16 TGA combustion reactivities of Morupule coal chars produced under pyrolysis and gasification conditions at (a) 900 ºC and (b) 1000 ºC as a function of hold time in the WMR.

5.4 Conclusions

Direct CO_2 gasification reaction kinetics of Morupule coal were measured, at atmospheric pressure, between 900 – 1050 ºC in a WMR and the char physicochemical evolution was evaluated to identify links with char reactivity and gasification kinetics. Early-stage gasification is characterised by an initial lag, dependent on temperature, and subsequent constant reaction

rates in the conversion range suitable for intrinsic kinetic determinations. A significantly higher chemical reaction controlled regime activation energy of 320 kJ mol^{-1} and lower kinetic regime transitional temperature of 975 ºC, relative to existing literature, were obtained owing to the direct gasification approach used in this work and minimised reactor design effects. A near zero reaction order was obtained at 900 ºC with CO$_2$ concentrations of 25 vol.% showing negligible gasification while increases in temperature to 1000 ºC were accompanied by an increase in the reaction order to 0.6, due to the onset of diffusional limitations.

Raman spectroscopy revealed a fairly unaltered bulk chemical structure of Morupule coal chars, indicating the absence of the preferential consumption of smaller aromatic ring systems. Surface chemistry analyses established a decrease in the C-C/C=C bonds, suggesting a gasification mechanism that propagates through the consumption of edge carbon atoms and defects. A developing surface porosity, characterised by pore growth, was observed as gasification proceeded. Chars produced under gasification conditions are less reactive than those produced in an inert atmosphere. This study highlights a considerable scope for direct gasification experiments, with minimal influence of heat treatment on chars and reactor design effects, combined with extensive structural characterisation of the char.

References

1.	Roberts, D. G.; Harris, D. J., Char Gasification with O$_2$, CO$_2$, and H$_2$O: Effects of Pressure on Intrinsic Reaction Kinetics. *Energy & Fuels* **2000,** *14* (2), 483-489.

2.	Tanner, J.; Bhattacharya, S., Kinetics of CO$_2$ and steam gasification of Victorian brown coal chars. *Chemical Engineering Journal* **2016,** *285*, 331-340.

3.	Jayaraman, K.; Gokalp, I.; Bonifaci, E.; Merlo, N., Kinetics of steam and CO$_2$ gasification of high ash coal–char produced under various heating rates. *Fuel* **2015,** *154*, 370-379.

4.	Everson, R. C.; Neomagus, H. W. J. P.; Kaitano, R.; Falcon, R.; du Cann, V. M., Properties of high ash coal-char particles derived from inertinite-rich coal: II. Gasification kinetics with carbon dioxide. *Fuel* **2008,** *87* (15), 3403-3408.

5.   Chen, J.; Chen, W.; Ji, R.; Jiao, Y.; Wang, X., Kinetic studies on bituminous coal char gasification using CO$_2$ and H$_2$O mixtures. *International Journal of Green Energy* **2019,** *16* (14), 1144-1151.

6.   Laurendeau, N. M., Heterogeneous kinetics of coal char gasification and combustion. *Progress in Energy and Combustion Science* **1978,** *4* (4), 221-270.

7.   Cai, H. Y.; Güell, A. J.; Chatzakis, I. N.; Lim, J. Y.; Dugwell, D. R.; Kandiyoti, R., Combustion reactivity and morphological change in coal chars: Effect of pyrolysis temperature, heating rate and pressure. *Fuel* **1996,** *75* (1), 15-24.

8.   Senneca, O.; Russo, P.; Salatino, P.; Masi, S., The relevance of thermal annealing to the evolution of coal char gasification reactivity. *Carbon* **1997,** *35* (1), 141-151.

9.   Kandiyoti, R.; Herod, A.; Bartle, K. D.; Morgan, T. J., *Solid fuels and heavy hydrocarbon liquids: thermal characterization and analysis*. Elsevier: **2016**.

10.   Fidalgo, B.; Berrueco, C.; Millan, M., Chars from agricultural wastes as greener fuels for electric arc furnaces. *Journal of Analytical and Applied Pyrolysis* **2015,** *113*, 274-280.

11.   Gomez, A.; Mahinpey, N., Kinetic study of coal steam and CO$_2$ gasification: A new method to reduce interparticle diffusion. *Fuel* **2015,** *148*, 160-167.

12.   Tsai, C.-Y.; Scaroni, A. W., Reactivity of bituminous coal chars during the initial stage of pulverized-coal combustion. *Fuel* **1987,** *66* (10), 1400-1406.

13.   Messenböck, R. C. Rapid Pyrolysis and Gasification of Coal in a High Pressure Wire-Mesh Reactor. PhD Thesis, University of London, **1998**.

14.   Ergun, S., Kinetics of the Reaction of Carbon with Carbon Dioxide. *The Journal of Physical Chemistry* **1956,** *60* (4), 480-485.

15.   Irfan, M. F.; Usman, M. R.; Kusakabe, K., Coal gasification in CO$_2$ atmosphere and its kinetics since 1948: A brief review. *Energy* **2011,** *36* (1), 12-40.

16.   Liu, L.; Cao, Y.; Liu, Q.; Yang, J., Experimental and kinetic studies of coal–CO$_2$ gasification in isothermal and pressurized conditions. *RSC Advances* **2017,** *7* (4), 2193-2201.

17.   Roberts, D. G.; Harris, D. J., A Kinetic Analysis of Coal Char Gasification Reactions at High Pressures. *Energy & Fuels* **2006,** *20* (6), 2314-2320.

18.   Ahn, D. H.; Gibbs, B. M.; Ko, K. H.; Kim, J. J., Gasification kinetics of an Indonesian sub-bituminous coal-char with CO$_2$ at elevated pressure. *Fuel* **2001,** *80* (11), 1651-1658.

19.   Roberts, D. G.; Hodge, E. M.; Harris, D. J.; Stubington, J. F., Kinetics of Char Gasification with CO$_2$ under Regime II Conditions: Effects of Temperature, Reactant, and Total Pressure. *Energy & Fuels* **2010,** *24* (10), 5300-5308.

20.   Gomez, A.; Silbermann, R.; Mahinpey, N., A comprehensive experimental procedure for CO$_2$ coal gasification: Is there really a maximum reaction rate? *Applied Energy* **2014,** *124*, 73-81.

21.   Moilanen, A.; Mühlen, H.-J., Characterization of gasification reactivity of peat char in pressurized conditions: Effect of product gas inhibition and inorganic material. *Fuel* **1996,** *75* (11), 1279-1285.

22.   Huang, Z.; Zhang, J.; Zhao, Y.; Zhang, H.; Yue, G.; Suda, T.; Narukawa, M., Kinetic studies of char gasification by steam and CO_2 in the presence of H_2 and CO. *Fuel Processing Technology* **2010,** *91* (8), 843-847.

23.   Liu, G.-s.; Tate, A. G.; Bryant, G. W.; Wall, T. F., Mathematical modeling of coal char reactivity with CO_2 at high pressures and temperatures. *Fuel* **2000,** *79* (10), 1145-1154.

24.   Essenhigh, R. H.; Froberg, R.; Howard, J. B., COMBUSTION BEHAVIOR OF SMALL PARTICLES. *Industrial & Engineering Chemistry* **1965,** *57* (9), 32-43.

25.   Li, X.; Hayashi, J.-i.; Li, C.-Z., FT-Raman spectroscopic study of the evolution of char structure during the pyrolysis of a Victorian brown coal. *Fuel* **2006,** *85* (12), 1700-1707.

26.   Zhang, S.; Min, Z.; Tay, H.-L.; Asadullah, M.; Li, C.-Z., Effects of volatile–char interactions on the evolution of char structure during the gasification of Victorian brown coal in steam. *Fuel* **2011,** *90* (4), 1529-1535.

27.   Keown, D. M.; Li, X.; Hayashi, J.-i.; Li, C.-Z., Characterization of the Structural Features of Char from the Pyrolysis of Cane Trash Using Fourier Transform−Raman Spectroscopy. *Energy & Fuels* **2007,** *21* (3), 1816-1821.

28.   Wang, M.; Roberts, D. G.; Kochanek, M. A.; Harris, D. J.; Chang, L.; Li, C.-Z., Raman Spectroscopic Investigations into Links between Intrinsic Reactivity and Char Chemical Structure. *Energy & Fuels* **2014,** *28* (1), 285-290.

29.   Dong, S.; Alvarez, P.; Paterson, N.; Dugwell, D. R.; Kandiyoti, R., Study on the Effect of Heat Treatment and Gasification on the Carbon Structure of Coal Chars and Metallurgical Cokes using Fourier Transform Raman Spectroscopy. *Energy & Fuels* **2009,** *23* (3), 1651-1661.

30.   Dillon, R. O.; Woollam, J. A.; Katkanant, V., Use of Raman scattering to investigate disorder and crystallite formation in as-deposited and annealed carbon films. *Physical Review B* **1984,** *29* (6), 3482-3489.

31.   Guizani, C.; Jeguirim, M.; Gadiou, R.; Escudero Sanz, F. J.; Salvador, S., Biomass char gasification by H_2O, CO_2 and their mixture: Evolution of chemical, textural and structural properties of the chars. *Energy* **2016,** *112*, 133-145.

32.   Perry, D. L.; Grint, A., Application of XPS to coal characterization. *Fuel* **1983,** *62* (9), 1024-1033.

33.   Zhou, J.-H.; Sui, Z.-J.; Zhu, J.; Li, P.; Chen, D.; Dai, Y.-C.; Yuan, W.-K., Characterization of surface oxygen complexes on carbon nanofibers by TPD, XPS and FT-IR. *Carbon* **2007,** *45* (4), 785-796.

34.   Chen, N.; Yang, R. T., Ab Initio Molecular Orbital Study of the Unified Mechanism and Pathways for Gas−Carbon Reactions. *The Journal of Physical Chemistry A* **1998,** *102* (31), 6348-6356.

35.   Hertzberg, M.; Zlochower, I. A.; Edwards, J. C., Coal particle pyrolysis mechanisms and temperatures. **1987**.

36.   Zhu, Z. H.; Finnerty, J.; Lu, G. Q.; Yang, R. T., A Comparative Study of Carbon Gasification with O$_2$ and CO$_2$ by Density Functional Theory Calculations. *Energy & Fuels* **2002,** *16* (6), 1359-1368.

37.   Bell, D. A.; Towler, B. F.; Fan, M., Chapter 3 - Gasification Fundamentals. In *Coal Gasification and Its Applications*, Bell, D. A.; Towler, B. F.; Fan, M., Eds. William Andrew Publishing: Boston, 2011; pp 35-71.

Chapter 6

Early-Stage Kinetics and Char Structural Evolution during High Pressure CO$_2$ Gasification

6.1 Introduction

Chapter 5 extensively discussed the kinetics of Morupule coal gasification in CO$_2$ and the early-stage structural evolution of the char under atmospheric pressure conditions. Whilst atmospheric pressure gasification provides useful fundamental research data, commercial gasifiers are typically operated at high pressures to increase feedstock throughput and ensure suitable pressures for downstream processes such as Fischer-Tropsch synthesis [1]. As such, the applicability of pyrolysis and gasification data is significantly dependent on the laboratory conditions at which they are produced. It is therefore essential to accurately represent commercial gasifier conditions in bench-scale studies, *i.e.* high heating rates (fluidised bed

and entrained flow gasifiers) and pressures [2]. The influence of elevated pressures on pyrolysis was demonstrated in Chapter 4. However, most research aimed at providing fundamental gasification kinetic data are carried out at atmospheric pressure, with only few studies investigating high-pressure performance.

Similar to published literature on atmospheric pressure gasification, high-pressure CO$_2$ gasification studies have largely focused on the conversion of chars in a two-step process, with pyrolysis and gasification carried out *ex-situ* [3,4,5]. However, it is important to study the combined effects of pressure on pyrolysis and gasification with aim to mimic behaviour representative of commercial gasifiers and to suppress the influence of experimental methods on the overall findings. Furthermore, there are no studies investigating the structural evolution of chars produced under high pressure gasification conditions. This chapter therefore investigates the influence of pressure on the single particle early-stage direct gasification of Morupule coal in a CO$_2$ atmosphere using a high-pressure wire-mesh reactor (HPWMR). The study also seeks to present a comprehensive characterisation of the char structural and morphological properties.

6.2 Materials and Methods

6.2.1 Feedstock and HPWMR

Morupule raw coal, characterised in Chapter 3, with a particle size fraction of 125 – 150 µm was dried for 12 h at 105 ºC in a vacuum oven and used as feedstock for high pressure gasification and pyrolysis experiments. These experiments were carried out using the HPWMR, detailed in Chapter 3, with a continuous sweep flow gas (flow velocity of 0.1 m s^{-1}), of helium, during pyrolysis, and CO$_2$, during gasification.

6.2.2 HPWMR Experimental Conditions

Both pyrolysis and gasification were carried out under identical experimental conditions at 900 ºC and 1000 ºC and pressures of 1, 10 and 20 bar$_a$. Pressures above 20 bar$_a$ in CO$_2$ resulted in an unreliable temperature measurement, with temperature variations of over ± 10 ºC (maximum allowed was ± 5 ºC). Chapter 5 has shown that gasification proceeds in different kinetic regimes at 900 ºC and 1000 ºC. The chemical reaction controlled regime occurs at 900 ºC while gasification at 1000 ºC is dominated by pore diffusion plus the chemical reaction. A heating rate of 1000 ºC s^{-1} to peak temperature was used for all experiments. The sample was held at peak temperature for 0, 10, 30 and 60 s at 900 ºC and 0, 10, 20 and 30 s at 1000 ºC. Prolonged holding beyond 30 s at 1000 ºC and 20 bar$_a$ in CO$_2$ led to some of the particles falling through the aperture of the wire-mesh (106 μm) as the particles reduced in size due to gasification. Each experimental condition was repeated three times and averaged to obtain the data point. Error bars were calculated using a 95 % confidence interval statistical measure.

The extent of gasification was estimated by subtracting the mass loss under pyrolysis conditions from that obtained under gasification conditions as shown in Equation 4.1 [2,6]. Gasification conversion was estimated as the ratio of the extent of gasification to the char yield generated under pyrolysis conditions (Equation 4.2). The gasification reaction rate was calculated for conversions below 20 % using Equation 5.1.

6.2.3 Char Characterisation

The bulk structural and surface chemistry properties of Morupule coal residual chars were assessed using Raman and X-Ray photoelectron (XPS) spectroscopy, respectively. The morphological evolution of the chars was studied using a scanning electron microscope (SEM). The relative combustion reactivities of the chars were investigated using

thermogravimetric analysis (TGA). These analytical techniques are comprehensively presented in Chapter 3.

6.3 Results and Discussion

6.3.1 Yields and Kinetics

6.3.1.1 Total Volatile Yields

In the previous chapters, it was demonstrated that pyrolysis was nearly complete upon reaching peak temperature. Chapter 5 has shown that gasification rates are much slower at 900 °C than 1000 °C, highlighting a significant dependence on temperature. A gasification lag of up to 60 s, before measurable char weight losses were recorded, was observed at 900 °C. The influence of pressure on pyrolysis and CO_2 gasification total volatile yields at 900 °C and 1000 °C under various holding times is presented in Figures 6.1a and b, respectively. 0 s experiments at 900 °C and a given pressure are characterised by similar pyrolysis and gasification yields, which shows that negligible gasification occurred during the heating up period. However, high CO_2 pressures led to slightly lower total volatile yields in comparison to identical pyrolysis experiments at 1000 °C and 0 s. This phenomenon is likely due to the enhanced char surface coverage by CO_2 in the internal porous network due to the pressure gradient and faster chemisorption rates at elevated pressures and temperatures, increasing the measured weight of the residual char. High pressures are known to intensify chemisorption of CO_2 on coals, with possible diffusion through the coal matrix even at temperatures as low as 200 °C [7]. The temperature dependence of the differences in the pyrolysis and gasification total volatile yields is possibly linked to the enthalpy of reaction as the char – CO_2 reaction is endothermic (Equation 2.1), with slower chemisorption rates occurring at low temperatures (900 °C) hence the near identical total volatile yields. While further holding to 10 s at 900 °C did not show discernible changes in both the pyrolysis and gasification total volatile yields, increases in the gasification total volatile yields were observed at 1000 °C, indicating that CO desorption is presumably underway.

For coals that undergo significant tar repolymerisation under high pyrolysis pressures, there tends to be an observed minimum total volatile yield as a function of pressure at 1000 °C and for relatively short holding times (10 s) [8,9]. This is reportedly due to a trade-off between the presence of a relatively unreactive secondary char layer which coats the main residual char and faster gasification reaction rates at high pressures. While this phenomenon is absent at 1000 °C in the case of Morupule coal (Figure 6.1b), a similar observation is made at 900 °C and 10 – 30 s holding times (Figure 6.1a). Figure 4.3a showed that pressure tends to suppress volatile release during the pyrolysis of Morupule coal at temperatures lower than 1000 °C. Volatile suppression under elevated pressures was negligible at 1000 °C, possibly due to the thermal cracking of the repolymerisation structures at this temperature and thus the absence of a total volatile yield minimum as a function of pressure for constant holding times.
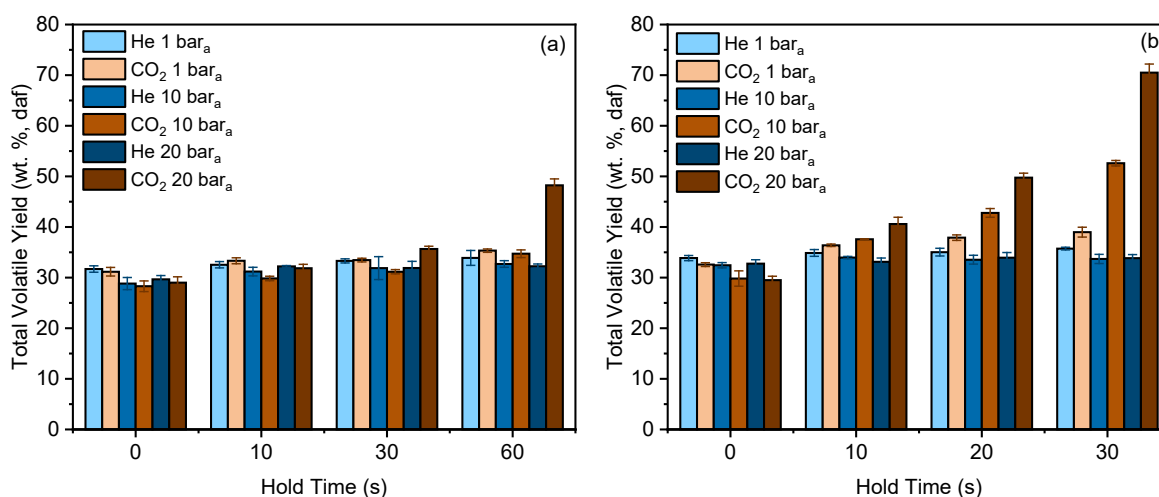
Figure 6. 1 Total volatile yields from the helium pyrolysis and CO$_2$ gasification of Morupule coal at a heating rate of 1000 °C s^{-1} to (a) 900 °C and 0 – 60 s holding times and (b) 1000 °C and 0 – 30 s holding times at pressures of 1, 10 and 20 bar$_a$.

6.3.1.2 Extents of Gasification

CO$_2$ pressures at 10 bar$_a$ resulted in negligible extents of gasification at 900 °C during the early stages of gasification up to 60 s (Figure 6.2a). However, a 20 bar$_a$ CO$_2$ pressure led to statistically significant extents of gasification from 30 s onwards (based on the error bars). This

suggests a similar reaction progression at pressures of 1 bar$_a$ and 10 bar$_a$. The gasification reaction at 900 ºC and CO$_2$ pressures of up to 10 bar$_a$ is therefore possibly characterised by slow initial CO$_2$ chemisorption kinetics (an in-depth discussion of this behaviour is presented in Section 6.3.1.3). This suggestion is further substantiated by an observed decrease in the gasification lag at 20 bar$_a$, suggesting a promotion of CO$_2$ adsorption under such pressures. The collision rate of CO$_2$ molecules with the active sites is enhanced under high pressure, resulting in enhanced chemisorption [10]. The gasification lag prominent at 900 ºC is not observed at 1000 ºC, where there are apparent increases in the extents of gasification for all holding times studied at both 10 bar$_a$ and 20 bar$_a$ in CO$_2$ (Figure 6.2b).

20 bar$_a$ experiments in CO$_2$ at 1000 ºC show higher extents of gasification than those conducted at 10 bar$_a$ for holding times of 10 s or longer (Figure 6.2b). While the extents of gasification between the 10 bar$_a$ and 20 bar$_a$ experiments were fairly comparable in the initial 10 s of holding at peak temperature, notable differences in the extent of gasification were attained at 20 s and 30 s. Therefore, pressure has a significant role in the overall gasification reaction rate under the conditions studied, especially at higher conversions. In agreement with this contribution, Messenböck [9] found that high CO$_2$ pressures significantly increased the extent of gasification, with near complete gasification of Daw Mill coal at 60 s holding time.
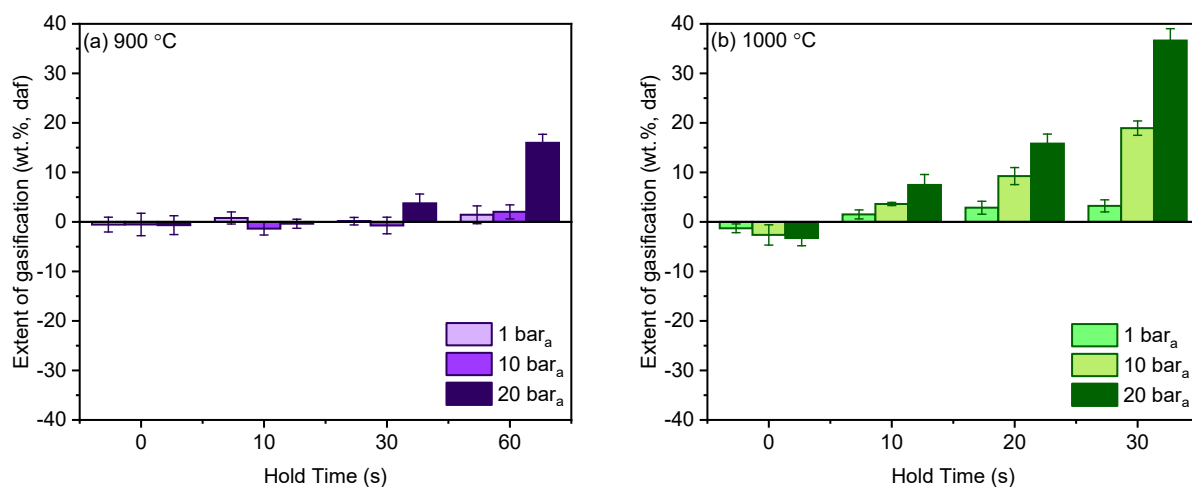
Figure 6. 2 Extents of gasification of Morupule coal in CO$_2$ at (a) 900 ºC and (b) 1000 ºC at pressures of 1, 10 and 20 bar$_a$.

6.3.1.3 Gasification Conversions

Figures 6.3a and b show the gasification conversions of Morupule coal in CO$_2$ as a function of hold time at 900 ºC and 1000 ºC, respectively. As previously discussed, a gasification lag at 900 ºC, identical to that observed during atmospheric pressure gasification, is observed for a CO$_2$ pressure of 10 bar$_a$ (Figure 6.3a). This result suggests that an increase in pressure to 10 bar$_a$ does not influence the rate of CO$_2$ chemisorption under these conditions. Prolonged holding at 900 ºC under 10 bar$_a$ led to increased conversions, and by extension, the apparent gasification reaction rate. Chapter 4 has shown that Morupule coal chars tend to have a poorly developed external surface porosity, with only localised blowholes. The smaller number of feeder pores can physically restrict the access of CO$_2$ to the well-developed inner porous network observed using X-Ray CT measurements (Figures 4.15 and 4.16) [11]. Since the CO$_2$ adsorption rate remains unchanged in the 1 – 10 bar$_a$ range, the increase in the apparent reaction rate is likely due to the enhanced surface coverage of CO$_2$ in the internal porous network, through the feeder pores, under a high external pressure. This would result in the formation of more surface complexes than at atmospheric pressure, leading to higher CO yields. Roberts and Harris [3] similarly observed increases in the apparent reaction rate at higher pressures, owing to the unsaturation of the char surface at atmospheric pressure.

Interestingly, a CO$_2$ pressure of 20 bar$_a$ shortened the delay in gasification by about 30 s (Figure 6.3a). However, a modest increase in the reaction rate, in comparison to data produced at 10 bar$_a$, was observed (Figure 6.4), suggesting a near complete saturation of the surface by CO$_2$ complexes for pressures above 10 bar$_a$ [4,12]. Such a significant reduction in the gasification lag suggests a pressure dependence of chemisorption at 900 ºC and an adsorption-limited gasification mechanism. This discussion is further expanded in Section 6.3.1.5 based on the Langmuir – Hinshelwood rate model application.

At 1000 ºC, the gasification lag was largely minimised due to increased chemisorption and overall reaction rates. The faster reaction rates made it difficult to discern any changes that might have been taking place before significant weight losses were recorded. Increases in CO$_2$ pressure led to higher reaction rates, with significantly higher conversions attained at higher pressures by 10 s. Unlike at 900 ºC, prolonged holding at 1000 ºC under high pressures was characterised by precipitous increases in conversions (Figure 6.3b). This phenomenon appears to be intensified in the 20 – 30 s hold time range. These steep increases are likely due to the enhanced porosity development (Figure 6.13d), commensurate with higher levels of char burn-off, increasing the accessible active surface area for further gasification. In contrast, Messenböck [9] found that the CO$_2$ gasification reactivity of Daw Mill in the WMR decreased at longer holding times. High conversions, between 65 – 85 % (24 % conversion was attained under identical conditions in this study), were obtained at 20 s, possibly reducing the amount of char available for reaction when approaching gasification completion.
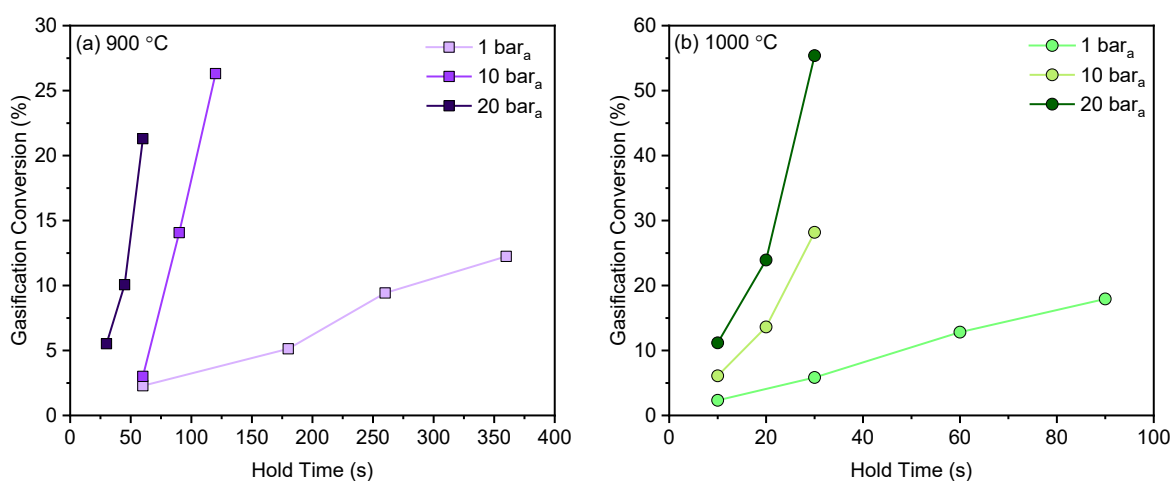
Figure 6. 3 Early-stage gasification conversions of Morupule coal in CO$_2$ under pressures of 1, 10 and 20 bar$_a$ at (a) 900 ºC and (b) 1000 ºC.

6.3.1.4 Gasification Reaction Rates

The effect of pressure on the apparent gasification reaction rates of Morupule coal in CO_2 at 900 ºC and 1000 ºC is presented in Figure 6.4. For the 900 ºC data, the reaction rates were estimated in the conversion ranges shown in Figure 6.3a. A linear relationship between conversion and holding time is deduced at 900 ºC under the conditions presented. This suggests an unchanged gasification reaction at this level of char burn-off and temperature. However, Figure 6.3b shows a slight change in the conversion – hold time relationship at 1000 ºC, particularly at higher conversions. Although fitting a linear relationship yields a satisfactory coefficient of determination, $R^2 > 0.94$ (Appendix D), the reaction rates at 10 bar_a and 20 bar_a were approximated using the two lowest conversions [9]. This allows for a direct comparison of the reaction rates in an identical conversion range. While significant increases in the reaction rate were observed when increasing the pressure to 10 bar_a at 900 ºC, further increases to 20 bar_a resulted in limited increases owing to the previously alluded near approach to char surface saturation. This suggests that the influence of pressure on the reaction rate at this temperature is dependent on the surface saturation. Under such occurrences, the pressure order with respect to CO_2 is close to 0 [3].

Hüttinger and Nill [12] suggest that the gasification reaction rate is commensurate with the formation of char surface CO_2 complexes. In this context, assuming complete surface saturation at 20 bar_a, an approximated 7 % and 74 % of surface complexes were formed at 1 bar_a and 10 bar_a, respectively, based on the ratios of the reaction rates. This highlights the low active surface coverage during atmospheric pressure gasification and demonstrates the limitations of the data processing methodology, largely utilised in literature [3,13,14], where intrinsic reactivity is defined as the apparent reaction rate normalised by the total specific surface area instead of the active specific surface area [15]. Such a procedure underestimates the gasification kinetics and the influence of other factors on gasification, such as the accessibility of the reactive gas to the internal porous network. High pressure studies, carried

out under conditions relevant for intrinsic kinetics, can be used to approximate the active surface area to overcome the underestimation of the kinetics of coal gasification.

A positive linear relationship between pressure and the apparent reaction rate is observed at 1000 ºC. Atmospheric pressure gasification studies of Morupule coal have indicated that the overall reaction rate is limited by the chemical reaction plus pore diffusion at this temperature (Chapter 5). Increases in pressure are known to lower the temperature threshold for kinetic regime transitions due to lower gas diffusivities [16]. As such, the faster reaction rates at 10 bar$_a$ and 20 bar$_a$ were a result of the larger surface area coverages and enhanced chemisorption. While the reaction rate became less sensitive to increases in pressure beyond 10 bar$_a$ at 900 ºC, in agreement with literature [3], a pressure of 20 bar$_a$ was observed to have a continued significant effect on the reaction rate at 1000 ºC. It is possible that 10 bar$_a$ is insufficient to completely offset the mass transport limitations in the chemical plus pore diffusion controlled kinetic regime on the account of rapid chemical reaction kinetics.
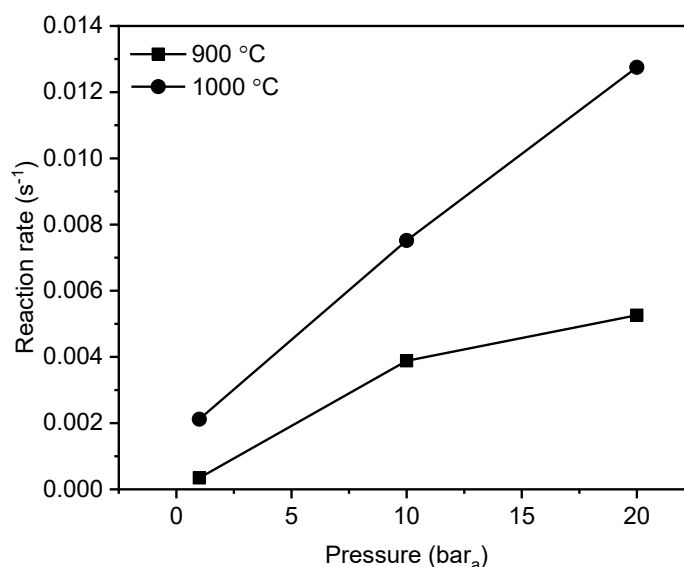
Figure 6. 4 Morupule coal CO$_2$ gasification reaction rates as a function of pressure at temperatures of 900 ºC and 1000 ºC.

6.3.1.5 Langmuir – Hinshelwood Rate Model Approximation

Low temperature gasification studies, appropriate for intrinsic kinetic determinations, have found a negligible influence of pressure on char – O$_2$ and char – CO$_2$ reaction activation energies [3,17]. On this basis, an activation energy of 320 kJ mol^{-1}, obtained in the 900 – 950 ºC temperature range in Chapter 5, is valid for high pressure gasification modelling using the nth power global rate equation. However, pressure influences are known to change the apparent activation energy at relatively high temperatures, where such data was produced without complete isolation of pore diffusional contributions [3,18]. This highlights the limited validity of the nth power global reaction model across a range of experimental conditions. The Langmuir-Hinshelwood (L – H) reaction rate model, based on the Ergun mechanism (Equations 2.6 and 2.7) [19,20], is typically used in high-pressure gasification kinetic analyses (Equation 2.8). For the L – H rate equation to be applicable, there must be a linear relationship between the inverse reaction rate, $1/R_{in}$, and the inverse pressure, $1/P_{CO_2}$ [4,5,21]. In the context of the present work, $(k_2/k_3)P_{CO}$, a term representing the CO inhibition of the gasification reaction, is assumed to be negligible, reducing Equation 2.8 to Equation 6.1. This assumption is reasonably given by the use of a continuous sweep flow gas in the HPWMR, carrying the product gases away from the reaction zone and therefore keeping P_{CO} low.

$$\frac{1}{R_{in}} = \frac{1}{k_1[C_t]P_{CO_2}} + \frac{1}{k_3[C_t]} \tag{6.1}$$

Albeit with a limited set of data, Figure 6.5 shows a strong linear correlation, based on the coefficient of determination ($R^2 > 0.99$), indicating that the Ergun mechanism is sufficient to characterise the WMR high-pressure CO$_2$ gasification behaviour of Morupule coal both in the chemical reaction and pore diffusion plus chemical reaction controlled kinetic regimes, without the need to introduce complex auxiliary adsorption and kinetic parameters, as is the case in other studies [21,22,23,24]. Similarly, Roberts and Harris [4], using the TGA, found that the L – H rate equation was suitable for high pressure gasification in CO$_2$, and in other oxidising

atmospheres such as steam. Table 6.1 summarises the k_1/k_3 ratio and $k_1[C_t]$ values from Morupule coal high pressure CO_2 gasification. A k_1/k_3 ratio of less than 1 is obtained for both temperatures, suggesting a CO_2 chemisorption limited reaction mechanism. This finding is consistent with the discussion provided for the reduced gasification lag when increasing pressure from 10 bar$_a$ to 20 bar$_a$ at 900 °C as observed in Figure 6.3a. The k_1/k_3 value at 900 °C is smaller than that obtained at 1000 °C by two orders of magnitude, suggesting a possible increase in the rate of CO_2 chemisorption on the char surface with temperature. The higher $k_1[C_t]$ value for gasification at 1000 °C further supports the discussion that the rate of chemisorption is enhanced at higher temperatures, hence the absence of the gasification lag as shown in Figure 6.3b.
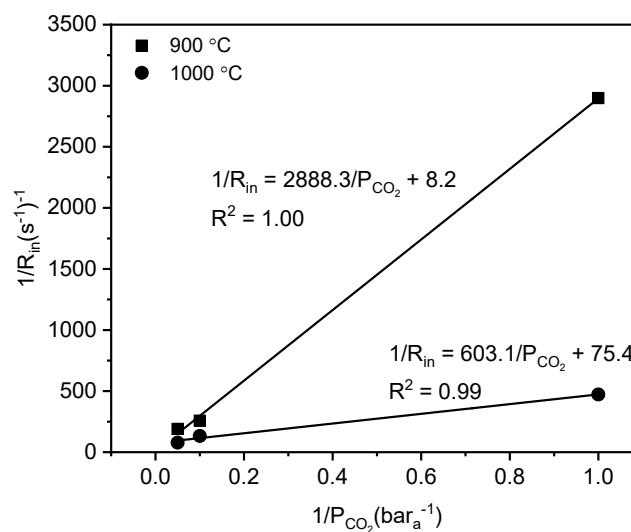
Figure 6. 5 Inverse gasification rate of Morupule coal as a function of inverse CO_2 pressure at 900 °C and 1000 °C.

Table 6. 1 k_1/k_3 ratio and $k_1[C_t]$ values for the modified Langmuir – Hinshelwood rate model.

Temperature (°C)	$k_1[C_t]$ (bar$_a^{-1}$ s^{-1})	k_1/k_3 (bar$_a^{-1}$)
900	0.00035	0.0028
1000	0.0025	0.19

6.3.2 Raman Spectroscopy

6.3.2.1 Total Raman Peak Areas

Raman spectral measurements, shown in Figures 6.6 and 6.7, were made on Morupule coal chars from atmospheric and high-pressure CO_2 gasification experiments. As a quantitative measure of Raman peak intensity, the total Raman peak area was calculated (Figures 6.8a and b). The Raman scattering ability of the char, dependent on the concentration of oxygen-containing species, and its light absorptivity affect the intensity of spectral measurements, and subsequently the total Raman peak areas [25]. Slower overall CO_2 gasification kinetics led to comparatively similar total Raman peak areas observed for chars obtained under low- and high-pressure gasification conditions at 900 ºC and 1000 ºC for 0 s holding time. This is consistent with observations made in Figure 6.1 which showed indistinguishable total volatile yields between pyrolysis and gasification conditions. A notable decrease in the total Raman peak areas, owing to thermal annealing processes and the increased char light absorptivity [11], is apparent in the first 10 s of holding at peak temperature. Further holding to 30 s allows for the commencement of CO desorption from the char, reducing the concentration of aromatic ring systems, and the light absorptivity of the char by extension. Chapter 5 indicated that gasification propagates through the consumption of C-C/C=C bonds. It is also possible that the presence of frozen reaction intermediates, when the reaction was quenched, translate to a stronger Raman scattering ability hence the higher total Raman peak area at a holding time of 30 s at 900 ºC. This effect is greatly pronounced under identical conditions at 1000 ºC where a substantial increase in the total Raman peak area is largely promoted by the synergy between high levels of carbon burn-off, reducing the proclivity of the char to light absorptivity, and a higher concentration of O-containing species. The total Raman peak area is therefore dependent on the extent of thermal annealing in the early stages while carbon conversion and the concentration of O-containing species is principal in the latter stages.
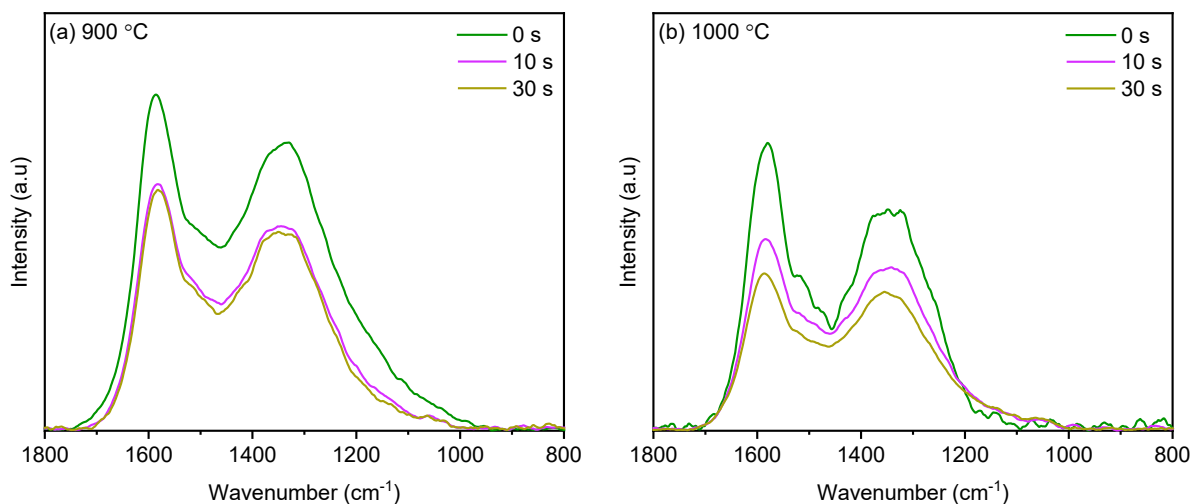
Figure 6. 6 Raman spectra of Morupule coal chars obtained from atmospheric pressure CO$_2$ gasification at (a) 900 ºC and (b) 1000 ºC for 0, 10 and 30 s holding times.
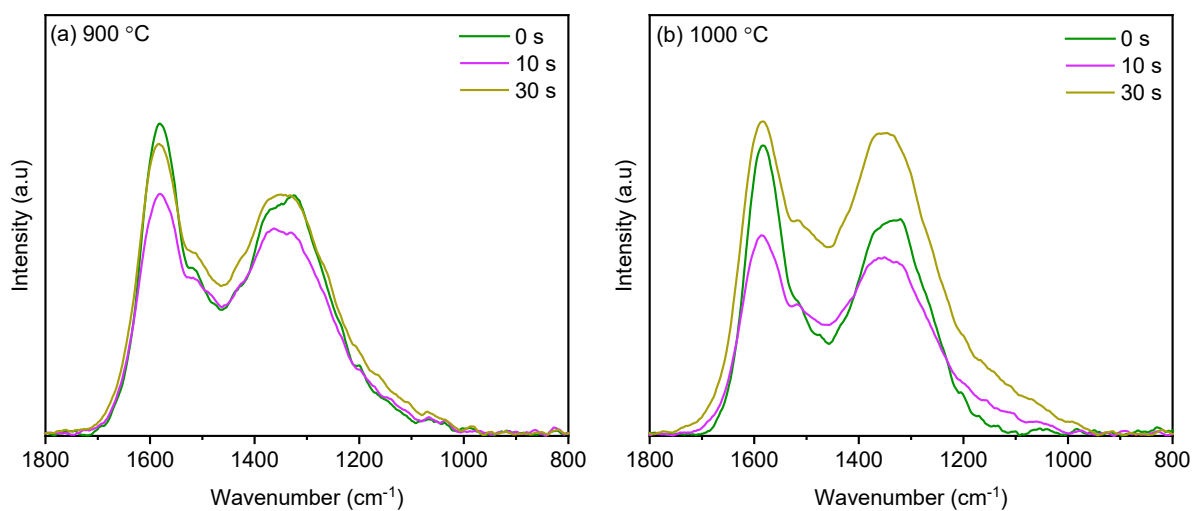
Figure 6. 7 Raman spectra of Morupule coal chars obtained from high pressure CO$_2$ gasification at (a) 900 ºC and (b) 1000 ºC for 0, 10 and 30 s holding times.
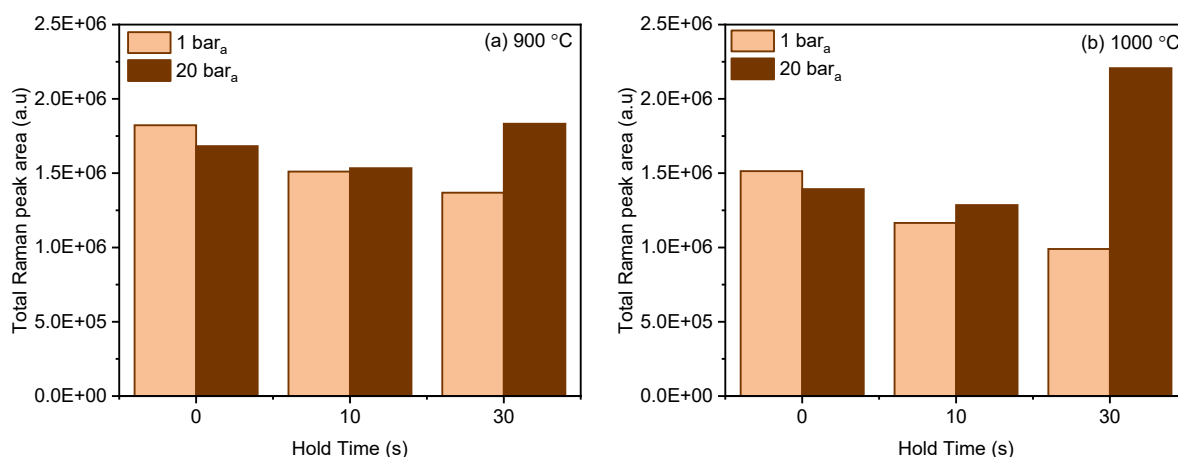
Figure 6. 8 Total Raman peak areas of chars obtained from 1 bar$_a$ and 20 bar$_a$ gasification of Morupule coal as a function of hold time at (a) 900 ºC and (b) 1000 ºC.

6.3.2.2 Intensity Ratios

Further insights on the influence of pressure on the structural evolution of Morupule coal chars from CO$_2$ gasification are gained using the I$_D$/I$_G$ band intensity ratios presented in Figures 6.9a and b, corresponding to experiments undertaken at 900 ºC and 1000 ºC, respectively. An increase in the I$_D$/I$_G$ intensity ratio denotes the formation of larger and more ordered aromatic ring systems [26], typical under conditions that promote ring condensation. Figure 6.9a shows a slight increase in the I$_D$/I$_G$ ratio in the first 10 s at 900 ºC, in comparison to a clear and steep increase at 1000 ºC. This is likely due to a more extreme heat treatment at 1000 ºC, favourable for thermal annealing processes. While there are further increases in the I$_D$/I$_G$ intensity ratio beyond 10 s, they are much gentler, indicating that the bulk of char structural changes take place in the early stages. This agrees with observations made in Chapters 4 and 5 where a stable I$_D$/I$_G$ ratio was obtained between 10 s and 60 s at 1000 ºC under pyrolysis conditions. Although they have similar profiles, Figure 6.9b shows that chars produced under high pressures have a slightly higher I$_D$/I$_G$ intensity ratio than their low-pressure counterparts at longer holding times. This is possibly linked to the disparity in the conversions studied for these chars. 1 bar$_a$ experiments were studied at a maximum conversion of 6 % while 20 bar$_a$ chars

are from a maximum conversion of 55 %. The dependence of the I_D/I_G intensity ratio on conversion at 1000 °C shows a slightly steep positive correlation at high conversions (Figure 6.10), suggesting a more ordered residual char at 30 s [26] as the less graphitic structures are consumed. However, this effect is relatively modest given the wide conversion range presented. It must be noted that the initial steep increase, below 10 % conversion has previously been attributed to thermal annealing under prolonged holding at peak temperature rather than influences of CO_2 on char structure (see Chapter 5).
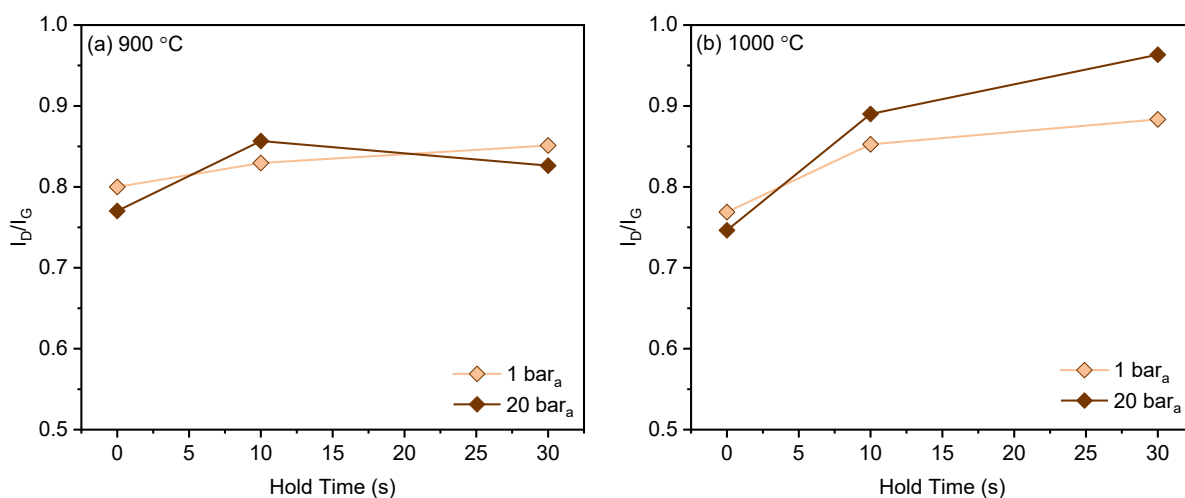
Figure 6. 9 I_D/I_G intensity ratios of Morupule coal chars obtained after 1 bar$_a$ and 20 bar$_a$ CO_2 gasification at (a) 900 °C and (b) 1000 °C as a function of hold time.
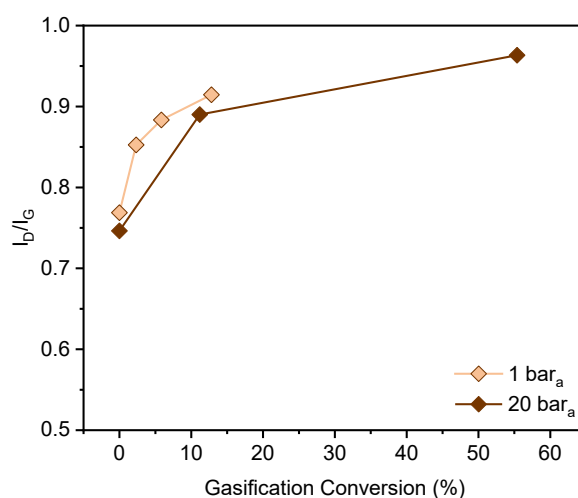
Figure 6. 10 I_D/I_G intensity ratios as a function of gasification conversion at 1000 °C and pressures of 1 bar$_a$ and 20 bar$_a$.

Figures 6.11a and b present I_D/I_V intensity ratios of 1 bar_a and 20 bar_a CO_2 gasification chars as a function of hold time at peak temperatures of 900 ºC and 1000 ºC, respectively. The I_D/I_V intensity ratio represents the relative proportions of aromatic rings with six or more fused benzene rings and amorphous carbon [25,26]. Consistent with previous observations in Chapters 4 and 5, remarkable changes in the I_D/I_V intensity ratio take place in the initial 10 s of holding at peak temperature when the structures previously unaltered during the heating up period are rearranged. The decrease in the I_D/I_V intensity ratio signifies a net decrease in the D band intensity as the aromatic ring systems that give rise to the D band undergo ring condensation during prolonged holding at high temperatures, increasing light absorptivity of the char. Interestingly, identical I_D/I_V intensity ratio values are observed for chars generated from both low- and high-pressure gasification experiments at 1000 ºC and longer holding times despite the substantially higher conversions attained in high pressure investigations. This suggests that amorphous structures of three to five fused benzene rings in the V band and structures with more than six fused benzene rings are equally likely to be consumed. This is perhaps testament to the direct gasification method used in the present work which minimises the prominence of thermal annealing reactions and allows for preservation of char properties that closely resemble those of the parent coal. Contrastingly, Wang, *et al.* [27] observed a preferential consumption of smaller aromatic ring systems during coal char gasification at atmospheric pressure. This could be an artefact of the experimental methodology where coals are subjected to harsh heat pre-treatment procedures [3,27]. This methodology potentially enhances the ordering of larger aromatic ring systems and significantly lowers their reactivity, creating an artificial hierarchy of ring consumption.
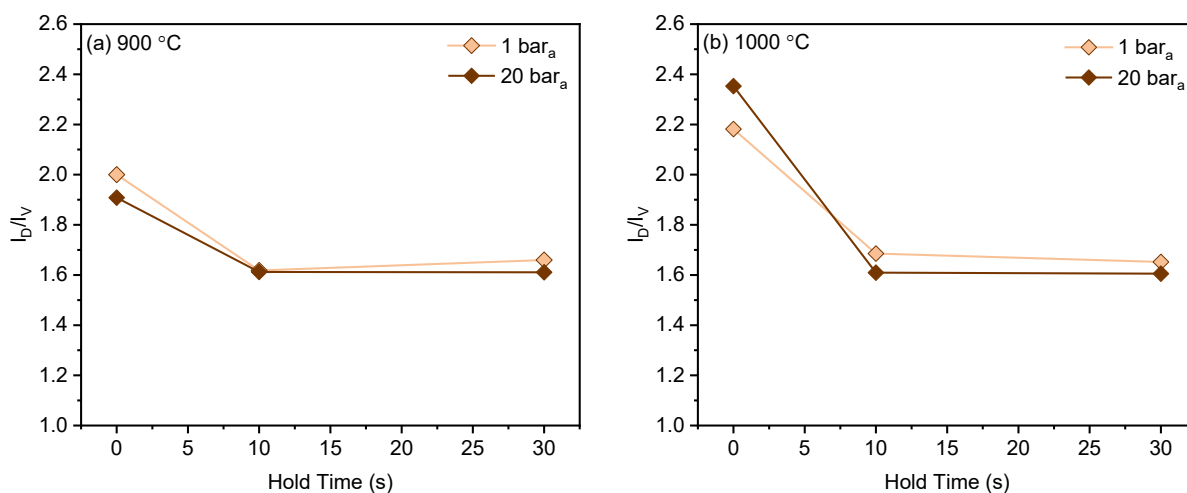
Figure 6. 11 I_D/I_G intensity ratios of Morupule coal chars obtained after 1 bar$_a$ and 20 bar$_a$ CO$_2$ gasification at (a) 900 ºC and (b) 1000 ºC as a function of hold time.

6.3.3 X-Ray Photoelectron Spectroscopy (XPS)

Changes in the surface chemistry of Morupule coal chars produced under high CO$_2$ pressures were assessed using XPS (Figures 6.12a and b) and the resulting functionalities derived from the C 1*s* peaks are summarised in Table 6.3. XPS C 1*s* data of chars produced from atmospheric pressure gasification is given Section 5.3.3.2. The peaks are assigned to the functional groups as follows: C-C/C=C (aliphatic or aromatic) at 284.4 eV, C-O-R or C-OH (ether or hydroxyl) at 286.0 eV, C=O (carbonyl) at 287.4 eV, C(=O)OR (carboxyl) at 289.0 eV and carbon in carbonate groups at 290.7 eV [28,29] as specified in Chapter 5. Consistent with the total volatile yields data (Figure 6.1b) and total Raman peak areas (Figure 6.8b) which showed that negligible, if any, gasification took place during the heating up period to 1000 ºC, similar surface chemistry characterisation is deduced at 0 s holding time for residual chars from atmospheric and high-pressure gasification experiments (Table 6.2). A decrease in the C-C/C=C bonds atomic concentration is observed under extended holding at 1000 ºC and a pressure of 20 bar$_a$ while O-containing functional groups all show a slight increase (Table 6.3). The increase in the relative concentration of O-containing species, known to promote the Raman scattering ability of the char, is consistent with the higher total Raman peak area shown in Figure 6.8b. This suggests that Morupule coal gasification adheres to a similar reaction mechanism, propagating through the consumption of the aliphatic and/or aromatic

edge carbons [11], in the pressure range studied, as similar surface chemistry properties were reported for atmospheric pressure gasification. In assessing the surface chemistry evolution in relation to the level of burn-off, it is interesting to point out that the 70.4 % C-C/C=C atomic concentration for chars produced at 1000 ºC and 60 s holding time at atmospheric pressure corresponds to a gasification conversion of 14 % while 67.5 % C-C/C=C atomic concentration shown in Table 6.3 corresponds to a conversion of 55 %. It must be highlighted that XPS is a surface chemistry characterisation technique. Therefore, the relatively close C-C/C=C atomic concentrations, despite the significant differences in char conversion, are likely due to the rapid consumption of the outer surface occurring under high pressures, exposing the relatively unreacted surfaces. SEM images in Figure 6.13d, for chars obtained after a holding time of 30 s at 1000 ºC (20 bar$_a$ CO$_2$ gasification) reveal a decimated external char surface.
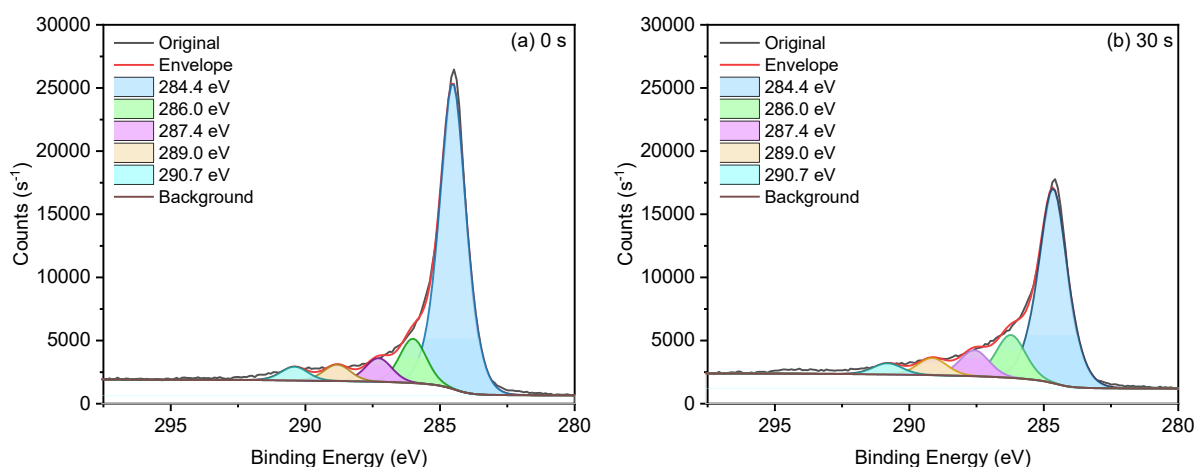
Figure 6. 12 Deconvoluted XPS C 1*s* spectra of Morupule coal chars obtained from 20 bar$_a$ CO$_2$ gasification at 1000 ºC for holding times of (a) 0 s and (b) 30 s.

Table 6. 2 Estimated atomic concentrations of the C 1*s* deconvoluted XPS peaks for chars obtained from the CO$_2$ gasification of Morupule coal at 1000 ºC and pressures of 1 bar$_a$ and 20 bar$_a$ for a holding time of 0 s.

Pressure (bar$_a$)	C 1*s* Peaks (Atomic %)				
	C-C/C=C	C-OR/OH	C=O	C(=O)-OR	CO$_3^{2-}$
1	76.9	10.5	5.4	4.3	2.8
20	76.4	10.7	5.7	3.9	3.3

Table 6. 3 Estimated atomic concentrations of the C 1*s* deconvoluted XPS peaks for chars obtained from the 20 bar$_a$ CO$_2$ gasification of Morupule coal at 1000 ºC and holding times of 0 s and 30 s.

Hold Time (s)	C 1*s* Peaks (Atomic %)				
	C-C/C=C	C-OR/OH	C=O	C(=O)-OR	CO$_3^{2-}$
0	76.4	10.7	5.7	3.9	3.3
30	67.5	14.3	8.7	5.7	3.7

6.3.4 Scanning Electron Microscopy

SEM images for residual chars produced at various holding times of 0, 10, 20 and 30 s at 1000 ºC and 20 bar$_a$ were captured (Figures 6.13a - d). The char particle size was preserved in the initial 20 s of holding at peak temperature, while a significant reduction in particle size was observed at 30 s (Figure 6.13d). Similar to observations made in Chapter 4 for chars produced under pyrolysis conditions and 0 s holding time, localised blowholes are also observed on the char surface. The physical properties of residual chars from 0 s experiments are therefore largely influenced by temperature and not reactant atmosphere during the heating up period. Despite an 11 % gasification conversion at 10 s, the char surface morphology is not dissimilar to that of chars from 0 s holding time. An isoconversional comparison of the morphology of atmospheric pressure gasification chars from 60 s holding time at 1000 ºC (total volatile yield of 43.9 wt.%, daf, Figure 5.1b) and 20 bar$_a$ gasification chars at 10 s holding time, with a similar total volatile yield of 40.5 wt.%, daf (Figure 6.1b), exhibits significant differences in the surface textural properties. Chars produced during gasification at atmospheric pressure demonstrated a more developed surface porosity, characterised by pores of varying sizes (Figure 5.15b). External char surface porosity appears to develop at higher gasification conversions under high pressures as shown that chars produced at 20 s and 20 bar$_a$ (total volatile yield of 49.7 wt.%, daf) have a comparable surface porosity to those from 60 s holding time at 1000 ºC. This suggests that, at identical conversions, gasification under high pressures takes place over a larger surface area,

approaching surface saturation. These observations further substantiate the suggestion that atmospheric pressure gasification at 1000 °C may largely be restricted to the external surface area due to pore diffusional limitations while the pressure gradient at 20 bar$_a$ promotes the accessibility of the reactive gas to the internal porous structure of the particle, utilising most of the available surface area. These findings agree with those made by Gouws, *et al.* [30] who reported an increase in char surface coverage at high CO$_2$ partial pressures during the gasification of a South African coal.

As gasification proceeds to higher conversions of 24 % at 20 s holding time, a number of pores less than 5 µm in size are revealed (Figure 6.13c). It is reported that coal char gasification in CO$_2$ is characterised by the development of micro and transitional pores [31]. These pores are not observed in chars produced at a holding time of 0 s (Figure 6.13a), where cracks of sizes greater than 10 µm largely dominate the surface of the char. These surface cracks still appear for char produced at 20 s (Figure 6.13c). The consumption of the external surface was intensified at 30 s holding time, with Figure 6.13d showing the internal char porous structure. The near complete outer surface consumption provides a direct access of the reactive gas to the inner surface area of the char, unlike during the early stages where the reactive gas was transported through the small surface feeder pores. The enhanced porosity allows for an increased number of available active sites on the char surface. It is therefore hardly surprising that Figure 6.3b exhibits a steep increase in conversion between 20 and 30 s holding time for 20 bar$_a$ experiments. Intraparticle surfaces are observed to have wide pore sizes in the order of 10 microns, possibly produced during the explosive devolatilisation driven by the high heating rate of 1000 °C s^{-1} used in this work. In some cases, the chars are characterised by flaky textural surfaces owing to high burn-off levels. This is consistent with previous studies which have shown that high pressure gasification residual chars obtained at high conversion levels tend to have an extensively porous and sponge-like structure [9].
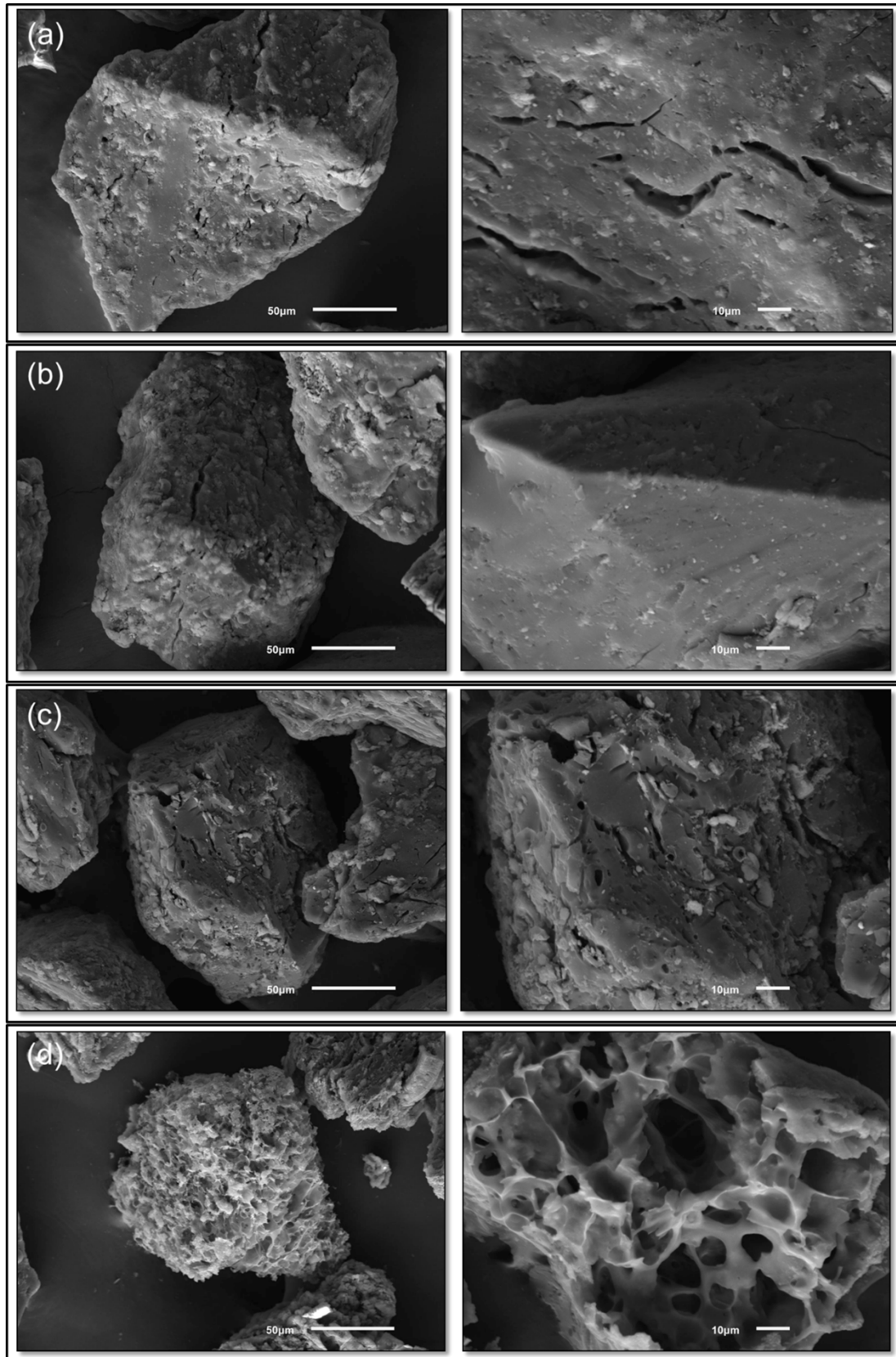
Figure 6. 13 Representative SEM images of Morupule coal chars from 20 bar$_a$ CO$_2$ gasification at 1000 ºC and holding times of (a) 0 s, (b) 10 s, (c) 20 s and (d) 30 s.

6.3.5 Char Combustion Reactivity

The combustion reactivities of residual chars from the initial 30 s of gasification in CO$_2$ at different pressures and isothermal temperatures of 900 ºC and 1000 ºC are shown in Figures 6.14a and b, respectively. Chapter 4 demonstrated that the combustion reactivity of Morupule coal chars produced under pyrolysis conditions at 1000 ºC is independent of pyrolysis pressure. As such, any differences presented in Figures 6.14a and b are influenced by the level of burn-off and/or physicochemical changes induced by high pressure CO$_2$ gasification. Similar combustion reactivity profiles are observed for chars produced at 900 ºC, with those obtained from high pressure gasification showing a slightly lower reactivity. The initial decrease within the first 10 s of holding at peak temperature, consistent with previous observations (Chapters 4 and 5), is largely driven by thermal annealing processes and a subsequent loss of active sites [11]. Figure 6.1a showed that within the gasification holding time studied, CO desorption had not commenced. Therefore, any possible changes in reactivity are restricted to the adsorption of CO$_2$ or its radicals on the reactive surface. These results possibly suggest that high external pressures promote accessibility of CO$_2$ to the more reactive active sites, forming stable intermediates when the reaction is quenched. With the more reactive active sites occupied, O$_2$ may be restricted to the less reactive active sites during combustion, hence lower reactivities for chars produced under high pressure conditions.

Chars produced at high pressure at 1000 ºC and 30 s holding time are shown to be more reactive than their atmospheric pressure counterparts. SEM studies, shown in Figure 6.13d, reveal a more developed porosity at 30 s holding time, presenting a larger surface area for combustion hence the faster burn-off rates due to an increase in the number of emerging active sites. Contrastingly, Messenböck [9] observed a continued decrease of the combustion reactivity of Daw Mill coal chars from high pressure CO$_2$ gasification experiments as a function of hold time owing to char deactivation. In the context of Morupule coal, thermal annealing processes were largely confined to the early stages of holding at peak temperature under both pyrolysis and gasification conditions, with minimal influence in the 10 – 60 s range as indicated

by the stable I_D/I_G Raman intensity ratios in this period. The variation in influential factors affecting reactivity highlights the need for an extensive characterisation of both the chemical structure and morphological development of chars to support reactivity studies, as is done in this work.
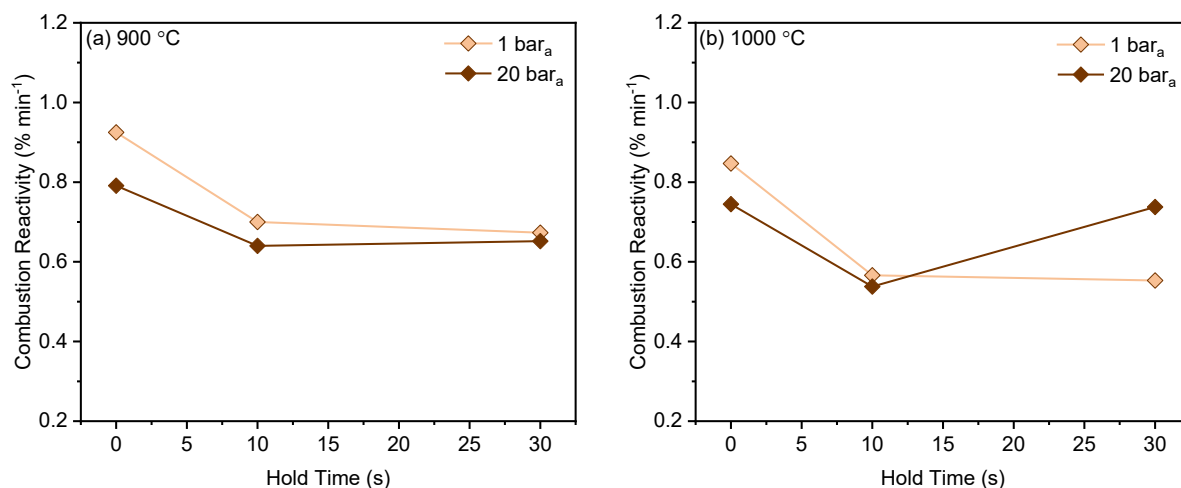
Figure 6. 14 A comparison of the TGA combustion reactivities of Morupule coal chars from 1 bar$_a$ and 20 bar$_a$ CO_2 gasification as a function of hold time at (a) 900 ºC and (b) 1000 ºC.

6.4 Conclusions

The influence of pressure on the early-stage gasification of Morupule coal in CO_2 is presented in this study. High pressure measurements exhibit higher reaction rates owing to enhanced CO_2 surface complex formation due to higher surface coverages. The sensitivity of the gasification reaction rate under high pressures is dependent on temperature, with relatively low temperatures (900 ºC) approaching an insensitive dependence on pressures above 10 bar$_a$ while a continued increase in the reaction rate is observed at 1000 ºC. The Langmuir – Hinshelwood rate model, based on the Ergun mechanism, was found to be applicable in the pressure range studied and demonstrated a chemisorption limited reaction, particularly in a chemical reaction controlled regime. As a first in the field, an extensive characterisation of char structural evolution under high CO_2 pressures is presented. The effect of pressure on early-stage structural changes of Morupule coal char is insignificant, even at high conversions,

184

demonstrating a mechanistic pathway equally favourable for the consumption of both amorphous carbon structures and aromatic ring systems with more than six fused benzene rings. While isoconversional porosity studies do not show any surface porosity development on gasification chars obtained under high pressures compared to those obtained at atmospheric pressure, which have discernible surface pores, high pressures intensified char surface consumption at high conversions. The increased porosity yielded precipitous increases in both gasification and combustion reactivities. This study highlights the general scope of a simultaneous deconvolution of the char structural evolution and reactivity to provide a comprehensive understanding of the overall gasification process at high pressures.

References

1.   Schubert, P. F.; Bayens, C. A.; Weick, L.; Haid, M. O., Expanding Markets for GTL Fuels and Specialty Products. In *Studies in Surface Science and Catalysis*, Iglesia, E.; Spivey, J. J.; Fleisch, T. H., Eds. Elsevier: **2001**; Vol. 136, pp 459-464.

2.   Kandiyoti, R.; Herod, A.; Bartle, K. D.; Morgan, T. J., *Solid fuels and heavy hydrocarbon liquids: thermal characterization and analysis*. Elsevier: **2016**.

3.   Roberts, D. G.; Harris, D. J., Char Gasification with O$_2$, CO$_2$, and H$_2$O: Effects of Pressure on Intrinsic Reaction Kinetics. *Energy & Fuels* **2000,** *14* (2), 483-489.

4.   Roberts, D. G.; Harris, D. J., A Kinetic Analysis of Coal Char Gasification Reactions at High Pressures. *Energy & Fuels* **2006,** *20* (6), 2314-2320.

5.   Liu, L.; Cao, Y.; Liu, Q.; Yang, J., Experimental and kinetic studies of coal–CO$_2$ gasification in isothermal and pressurized conditions. *RSC Advances* **2017,** *7* (4), 2193-2201.

6.   Fidalgo, B.; Berrueco, C.; Millan, M., Chars from agricultural wastes as greener fuels for electric arc furnaces. *Journal of Analytical and Applied Pyrolysis* **2015,** *113*, 274-280.

7.   Mirzaeian, M.; Hall, P. J., The Interactions of Coal with CO$_2$ and Its Effects on Coal Structure. *Energy & Fuels* **2006,** *20* (5), 2022-2027.

8.   Messenböck, R. C.; Dugwell, D. R.; Kandiyoti, R., CO$_2$ and steam-gasification in a high-pressure wire-mesh reactor: the reactivity of Daw Mill coal and combustion reactivity of its chars. *Fuel* **1999,** *78* (7), 781-793.

9.   Messenböck, R. C. Rapid Pyrolysis and Gasification of Coal in a High Pressure Wire-Mesh Reactor. PhD Thesis, University of London, **1998**.

10.   Molina, A.; Montoya, A.; Mondragón, F., CO$_2$ strong chemisorption as an estimate of coal char gasification reactivity. *Fuel* **1999,** *78* (8), 971-977.

11.   Laurendeau, N. M., Heterogeneous kinetics of coal char gasification and combustion. *Progress in Energy and Combustion Science* **1978,** *4* (4), 221-270.

12.   Hüttinger, K. J.; Nill, J. S., A method for the determination of active sites and true activation energies in carbon gasification: (II) Experimental results. *Carbon* **1990,** *28* (4), 457-465.

13.   Ahn, D. H.; Gibbs, B. M.; Ko, K. H.; Kim, J. J., Gasification kinetics of an Indonesian sub-bituminous coal-char with CO$_2$ at elevated pressure. *Fuel* **2001,** *80* (11), 1651-1658.

14.   Everson, R. C.; Neomagus, H. W. J. P.; Kaitano, R.; Falcon, R.; du Cann, V. M., Properties of high ash coal-char particles derived from inertinite-rich coal: II. Gasification kinetics with carbon dioxide. *Fuel* **2008,** *87* (15), 3403-3408.

15.   Basu, P., Chapter 5 - Gasification Theory and Modeling of Gasifiers. In *Biomass Gasification and Pyrolysis*, Basu, P., Ed. Academic Press: Boston, **2010**; pp 117-165.

16.   Tremel, A. Reaction Kinetics of Solid Fuels during Entrained Flow Gasification. PhD Thesis, Technical University of Munich, **2012**.

17.   Ranish, J. M.; Walker, P. L., High pressure studies of the carbon-oxygen reaction. *Carbon* **1993,** *31* (1), 135-141.

18.   MacNeil, S.; Basu, P., Effect of pressure on char combustion in a pressurized circulating fluidized bed boiler. *Fuel* **1998,** *77* (4), 269-275.

19.   Ergun, S., Kinetics of the Reaction of Carbon with Carbon Dioxide. *The Journal of Physical Chemistry* **1956,** *60* (4), 480-485.

20.   Irfan, M. F.; Usman, M. R.; Kusakabe, K., Coal gasification in CO$_2$ atmosphere and its kinetics since 1948: A brief review. *Energy* **2011,** *36* (1), 12-40.

21.   Nozaki, T.; Adschiri, T.; Fujimoto, K., Coal char gasification under pressurized CO$_2$ atmosphere. *Fuel* **1992,** *71* (3), 349-350.

22.   Kajitani, S.; Suzuki, N.; Ashizawa, M.; Hara, S., CO$_2$ gasification rate analysis of coal char in entrained flow coal gasifier. *Fuel* **2006,** *85* (2), 163-169.

23.   Liu, G.-s.; Tate, A. G.; Bryant, G. W.; Wall, T. F., Mathematical modeling of coal char reactivity with CO$_2$ at high pressures and temperatures. *Fuel* **2000,** *79* (10), 1145-1154.

24.   Blackwood, J. D.; Ingeme, A. J., The Reaction of Carbon with Carbon Dioxide at High Pressure. *Australian Journal of Chemistry* **1960,** *13* (2), 194-209.

25.   Li, X.; Hayashi, J.-i.; Li, C.-Z., FT-Raman spectroscopic study of the evolution of char structure during the pyrolysis of a Victorian brown coal. *Fuel* **2006,** *85* (12), 1700-1707.

26.   Dong, S.; Alvarez, P.; Paterson, N.; Dugwell, D. R.; Kandiyoti, R., Study on the Effect of Heat Treatment and Gasification on the Carbon Structure of Coal Chars and Metallurgical

Cokes using Fourier Transform Raman Spectroscopy. *Energy & Fuels* **2009,** *23* (3), 1651-1661.

27.   Wang, M.; Roberts, D. G.; Kochanek, M. A.; Harris, D. J.; Chang, L.; Li, C.-Z., Raman Spectroscopic Investigations into Links between Intrinsic Reactivity and Char Chemical Structure. *Energy & Fuels* **2014,** *28* (1), 285-290.

28.   Perry, D. L.; Grint, A., Application of XPS to coal characterization. *Fuel* **1983,** *62* (9), 1024-1033.

29.   Zhou, J.-H.; Sui, Z.-J.; Zhu, J.; Li, P.; Chen, D.; Dai, Y.-C.; Yuan, W.-K., Characterization of surface oxygen complexes on carbon nanofibers by TPD, XPS and FT-IR. *Carbon* **2007,** *45* (4), 785-796.

30.   Gouws, S. M.; Neomagus, H. W. J. P.; Roberts, D. G.; Bunt, J. R.; Everson, R. C., The effect of carbon dioxide partial pressure on the gasification rate and pore development of Highveld coal chars at elevated pressures. *Fuel Processing Technology* **2018,** *179*, 1-9.

31.   Salatino, P.; Senneca, O.; Masi, S., Gasification of a coal char by oxygen and carbon dioxide. *Carbon* **1998,** *36* (4), 443-452.

Chapter 7

Modelling of Single Particle Behaviour during Pyrolysis and Gasification

7.1 Introduction

The previous chapters investigated the thermochemical conversion of Morupule coal under pyrolysis and gasification conditions using a wire-mesh reactor (WMR). This reactor configuration allows a study of the independent particle behaviour, with minimal interparticle interactions and transport phenomena influences, during the primary pyrolysis and gasification of the feedstock. In this chapter, the single particle behaviour in the WMR is predicted using widely recognised pyrolysis and gasification conversion models. Capability of predicting conversion trajectories using models is particularly useful for WMRs as this would provide a continuous temporal resolution of the weight-loss. Furthermore, modelling single particle behaviour allows for prediction of higher gasification conversions as the WMR is limited by

particles falling through the wire-mesh (sample holder) under gravity as the particle size decreases (Figure 6.13d). The capability of representing pyrolysis and gasification is useful in computational fluid dynamics (CFD) simulations applied in describing performance in a gasifier. This chapter focuses on modelling the intrinsic thermochemical behaviour of 125 – 150 μm particles only, without considering mass and heat transfer limitations.

The applicability of the distributed activation energy (DAE) model in representing the pyrolysis of Morupule coal under various operating conditions *i.e.* heating rate and pressure, is investigated in this study. Section 2.6.1.2.1 of Chapter 2 presented the potential limitations of model-free methods, widely used in kinetic analyses of coal pyrolysis [1,2], in application to data obtained from the WMR. These limitations are verified in this chapter. The volumetric, shrinking core and random pore models are fitted to the WMR experimental gasification data to estimate the kinetic parameters, and compare the findings to the non-model fitting presented in Chapter 5. Modelling of high-pressure gasification using the Langmuir – Hinshelwood rate expression is also discussed.

7.2 Materials and Methods

7.2.1 Distributed Activation Energy (DAE) Pyrolysis Model

The DAE model was selected to predict the total volatile yields in pyrolysis as a function of temperature. It is a first-order kinetic model, of a simple form presented in Equation 7.1, based on an Arrhenius representation and assumes an infinite number of parallel reactions [3,4]. V is the volatile yield, V^* is the ultimate volatile yield, E_a is the activation energy, A is the pre-exponential factor, R is the universal gas constant and T represents temperature. Separating the variables in Equation 7.1 yields Equation 7.2.

$$\frac{dV}{dt} = Ae^{-\frac{E_a}{RT}}(V^* - V) \tag{7.1}$$

$$\int_0^V \frac{dV}{V^* - V} = \int_0^t A e^{-\frac{E_a}{RT}} dt \tag{7.2}$$

Given that the non-isothermal pyrolysis experiments in this work were carried out at a constant heating rate, β, temperature is determined as shown in Equation 7.3, where T_0 is the initial temperature and t is the time taken to reach temperature T.

$$T = T_0 + \beta t \tag{7.3}$$

Therefore, Equation 7.2 can be represented using Equation 7.4.

$$\int_0^V \frac{dV}{V^* - V} = \int_0^T \frac{A}{\beta} e^{-\frac{E_a}{RT}} dT \tag{7.4}$$

Integrating the left-hand side of Equation 7.4 leads to Equation 7.5.

$$\frac{V}{V^*} = 1 - exp\left[\int_0^T \frac{A}{\beta} e^{-\frac{E_a}{RT}} dT\right] \tag{7.5}$$

As previously discussed, the DAE model assumes an infinite number of parallel first-order reactions with a distribution of activation energies. As such, compounding the yields of the infinite reactions results in Equation 7.6. In this thesis, a Gaussian distribution, $f(E_a)$, Equation 7.7, was assumed to describe the distribution of activation energies, where E_0 is the mean activation energy and σ is the standard deviation.

$$\frac{V}{V^*} = 1 - \int_0^\infty exp\left[\int_0^T \frac{A}{\beta} e^{-\frac{E_a}{RT}} dT\right] f(E_a) \, dE_a \tag{7.6}$$

$$f(E_a) = \frac{1}{\sigma\sqrt{2\pi}} e^{-\frac{(E_a - E_0)}{2\sigma}} \tag{7.7}$$

7.2.2 Gasification Kinetic Models

The volumetric, shrinking core and random pore models, described in Section 2.6.2.1, were fitted to the WMR experimental data using linear regression to estimate the intrinsic kinetic parameters of the atmospheric pressure gasification of Morupule coal in CO_2. The linear forms of these models are presented in Equations 7.8 (volumetric model), 7.9 (shrinking core model) and 7.10 (random pore model) [5]. k_{VM}, k_{SCM} and k_{RPM} represent the intrinsic reaction rate constants for the volumetric, shrinking core and random pore models, respectively. X is the gasification conversion while Ψ is the dimensionless structural property parameter used in the random pore model.

$$k_{VM}t = -\ln(1 - X) \tag{7.8}$$

$$k_{SCM}t = 3\left[1 - (1 - X)^{\frac{1}{3}}\right] \tag{7.9}$$

$$k_{RPM}t = \frac{2}{\Psi}\left[\sqrt{1 - \Psi ln(1 - X)} - 1\right] \tag{7.10}$$

7.2.3 gPROMS

A gPROMS ModelBuilder 6.0.2 software was used to solve the DAE model equations. An inbuilt parameter estimation function was used to estimate the mean activation energy and standard deviation to provide an optimised description of the Gaussian distribution (Equation 7.7) representative of accurately reproducing the non-isothermal pyrolysis of Morupule coal using the DAE model. The goodness of fit test was evaluated by comparing the weighted residual value to the χ^2 value, which defines the degree at which a predicted value compares with the empirical value. A smaller weighted residual value than the χ^2 value indicates a good fitting of the DAE model to the WMR experimental data.

7.3 Results and Discussion

7.3.1 Pyrolysis

7.3.1.1 Effect of Pyrolysis Temperature

The written gPROMS code was verified by fitting literature data using the corresponding published DAE model kinetic parameters (Appendix E). This code accurately reproduced the experimental data. As discussed previously, the pre-exponential factor, A, must be fixed (typically in a range of $10^{10} - 10^{22}$ s^{-1} [6, 7]) and is shared by all parallel reactions. In the present work, an A of 6×10^{12} s^{-1}, obtained from the literature that used the DAE model for the pyrolysis of a coal of similar elemental composition and proximate analysis [8], was selected as an input to the model. Figure 7.1 shows that the DAE model fits the atmospheric pressure pyrolysis experimental data well. The fitting has a smaller weighted residual value (0.90) than the χ^2 value (9.49), indicating that there is a good agreement between the derived model and the experimental data. The mean activation energy and standard deviation, obtained from the parameter estimation function, are 183.3 kJ mol^{-1} and 36.3 kJ mol^{-1}, respectively. The gPROMS model also confirms a high linearity between the pre-exponential factor and the mean activation energy, yielding a value of 0.998 from the correlation matrix. This means that the two kinetic parameters vary proportionally, a phenomenon known as the kinetic compensation effect [9]. Appendix E shows the relationship between A and E_0 while having a negligible impact on the goodness of fit. The good representation of the data by the DAE model also suggests that the assumed Gaussian distribution can adequately describe the distribution of Morupule coal pyrolysis activation energies without the need for additional terms or modification as is often the case in literature.
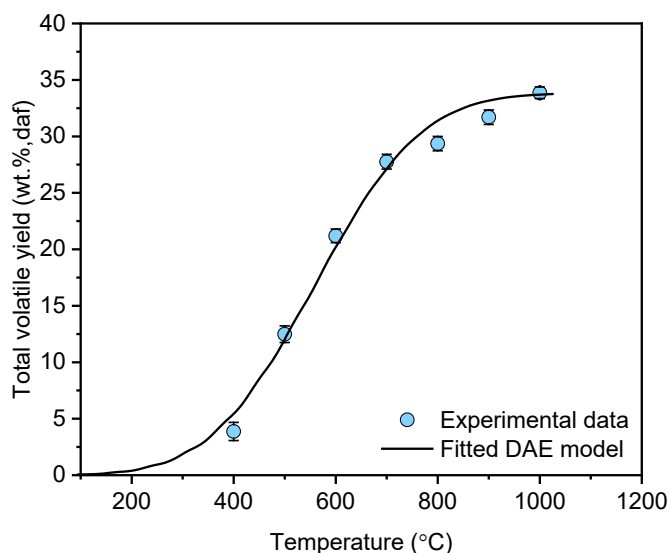
Figure 7. 1 An optimum fitting of the DAE model to the atmospheric pressure Morupule coal pyrolysis data. Heating rate of 1000 °C s^{-1} and 0 s holding time for various peak temperatures.

The approximated mean activation energy is in the typical range of those presented in literature using the DAE model (150 – 500 kJ mol^{-1} [2,6]). Compared with coals that used the same pre-exponential factor value [8], or an order of magnitude lower [7], the mean activation energy obtained for Morupule coal is slightly lower. Mean activation energies of 197 kJ mol^{-1} and 246 kJ mol^{-1} were obtained in the kinetic modelling of a Hunter Valley coal [8] and a Russian coal [7], respectively, using a DAE model. Lower mean activation energies are attributed to feedstocks characterised by aliphatic bridges which are much easier to break, releasing lighter components [7,10]. This discussion is in accordance with the previously observed size exclusion chromatogram of Morupule coal tar which illustrated a liquid product dominated by compounds in the low molecular weight end, typical of smaller-sized aromatic hydrocarbon molecules (Figure 4.2). However, it must also be noted that the differences in the reactor configuration used to experimentally determine the weight-loss profile during pyrolysis may influence the observed thermal breakdown behaviour of coal. Most researchers use TGAs, which are affected by both particle stacking and larger sample mass, inducing heat and mass transport limitations [11,12]. The review presented in Chapter 2 has highlighted that the TGA promotes

secondary reactions between evolving tars and heated char surfaces due to the stacking of the particles, adding further reactions to the kinetic model. This is perhaps highlighted by the larger standard deviations of 50 – 60 kJ mol^{-1} obtained using DAE model fittings in coal pyrolysis literature using the TGA [7,13,14], compared to the 36.3 kJ mol^{-1} obtained in the present work that uses the WMR, indicating a narrower set of chemical reactions. Furthermore, Niksa and Lau [8] obtained a standard deviation value 21.4 kJ mol^{-1} for the pyrolysis of a Pittsburgh No. 8 coal studied by Gibbins-Matham and Kandiyoti [15] using a WMR. This potentially reflects the minimised intraparticle and interparticle interactions in the WMR, limiting the occurrence of secondary reactions.

7.3.1.2 Effect of Heating Rate on Pyrolysis

Figure 7.2a illustrates the effect of heating rate on the pyrolysis of Morupule coal as a function of temperature. While the heating rate plays a negligible role in the release of volatile yields at temperatures lower than 500 ºC, a clear reduction in the total volatile yield is discerned for temperatures at 600 ºC and higher. This behaviour is attributed to the rearrangement reactions, involving tar precursors, that take place in the coal as it spends extended periods at high temperatures [16]. It is therefore unsurprising that the reduction in the volatile yield takes place in the 500 – 600 ºC temperature range where the majority of the tar compounds are normally released (Figure 4.1a). The difference in the total volatile yields remains fairly constant at temperatures above 600 ºC, indicating that the effect of heating rate on Morupule coal pyrolysis is mainly restricted to tar evolution. Quantifying tar yields to substantiate the above discussion was a challenge at low heating rates as the experimental test incurred heat radiation from the wire-mesh to the tar trap, evaporating all the liquid nitrogen (used to rapidly condense the liquid products).

A simple change of the heating rate from 1000 ºC s^{-1} to 1 ºC s^{-1} in the gPROMS DAE model using the kinetic parameters obtained in Section 7.3.1.1 produces the total volatile yield prediction shown in Figure 7.2b. In comparison to the experimental data, the DAE model

significantly overpredicts the Morupule coal volatile release. An interpretation of the DAE model prediction is that prolonged exposure to lower temperatures (low heating rate) allows for higher conversions as high heating rates perhaps induce heat transfer limitations or a possibility that the pyrolysis reactions have slower kinetics, leading to lower total volatile yields [17]. It is suggested that temperature gradients, due to localised heating at points in contact with the wire-mesh, can delay the attainment of a homogeneous temperature distribution within the particle, thus the lower pyrolysis conversions at high heating rates [17]. However, Figure 7.2a shows that, despite the 375 – 1000 s time difference, the heating rate does not influence pyrolysis in the WMR at low temperatures (with the main effect taking place at high temperatures due to thermal annealing). Moreover, pyrolysis is virtually completed during the heating up period (Figure 4.1b), highlighting the extremely fast kinetics of this process and the minimal heat transfer limitations in the WMR. Similar findings have been observed during the pyrolysis of other coals using the WMR [18, 19].

The DAE model prediction behaviour at low heating rates discussed above is rather reminiscent of most studies investigating the non-isothermal pyrolysis of solid fuels and polymers using TGAs [20,21]. The behaviour suggests that the temperature dependence of the individual devolatilisation reactions plays a smaller role with the time dependence being the major driving force for pyrolysis reactions. This is perhaps a fundamental flaw in the kinetic analyses widely presented in literature where the kinetics are treated as exclusively controlled by the chemical reactions all the while having significant influences of heat transfer limitations due to the reactor design [22]. In fact, some kinetic analyses methods, such as the Friedman, KAS and Ozawa-Flynn-Wall, are predicated on differences in the heating rate dependence of volatile release (see Section 7.3.1.4 of this chapter). A comprehensive study by Richter and Rein [22] has shown that interparticle heat transfer limitations are significantly affected by mass used in TGAs, with a conservative 0.15 mg suitable for heating rates of 50 K min^{-1}. In contrast, most TGA-based studies use a constant mass, typically larger than 5 mg [20, 21], for all heating rates without any basis for whether heat transfer limitations are prominent or negligible.

In the context of the present work, it is proposed that for fast pyrolysis kinetics and in the absence of heat transfer limitations, the A/β term in Equation 7.5 should be fixed even when changing the heating rate as such conditions approximate a significant dependence of pyrolysis on temperature (Figure 4.1b) rather than time spent at peak temperature. For non-isothermal processes, both time and temperature are changing. For the pre-exponential factor to truly be constant over the temperature range of interest, considerations must be made with regard to the time taken to reach temperature. A general understanding of the pre-exponential factor is that it defines the frequency of collisions (self-collisions in the case of thermal decomposition). Therefore, fixing the pre-exponential factor while reducing the heating rate by a factor of 1000 results in an increase in the number of collisions by a factor of 1000 within a constant temperature range. This overestimates the number of possible collisions, hence the faster kinetics approximated in Figure 7.2b. As such, the proposed solution serves to ensure that the number of collisions remains unchanged in a constant temperature range even when changing the heating rate. Based on this discussion, a reduction in the heating rate to 1 ℃ s^{-1} is proposed to be accompanied by a commensurate decrease in A to 6×10^9 s^{-1}. Using these values, the DAE model was used to predict the total volatile yields at a lower heating rate (Figure 7.2c). It is demonstrated that the model reproduces the experimental data fairly well. However, it slightly overpredicts the total volatile yields for temperatures above 500 ℃ as it fails to account for the auxiliary reactions that occur under extended exposure to high temperatures as discussed above (Figure 7.2a). It has been noted by other researchers that the use of the ultimate volatile yield in the DAE model does not consider the influence of heating rate on pyrolysis reactions [4].

An optimised fitting of the DAE model to the 1 ℃ s^{-1} experimental data (Figure 7.2d) yields a similar mean activation energy of 185.3 kJ mol^{-1} to that obtained at a heating rate of 1000 ℃ s^{-1} (183.3 kJ mol^{-1}). This suggests that average Morupule coal pyrolysis reactions taking place under different heating rates are largely similar and less susceptible to changes in heating rate as the difference in the total volatile yields is well within 5 wt.%, daf. However,

a larger standard deviation of 44.1 kJ mol^{-1} was obtained, indicating a wider Gaussian distribution possibly stemming from a slight variation in pyrolysis reactions due to additional reactions involving tar precursors which would otherwise be released under rapid heating.
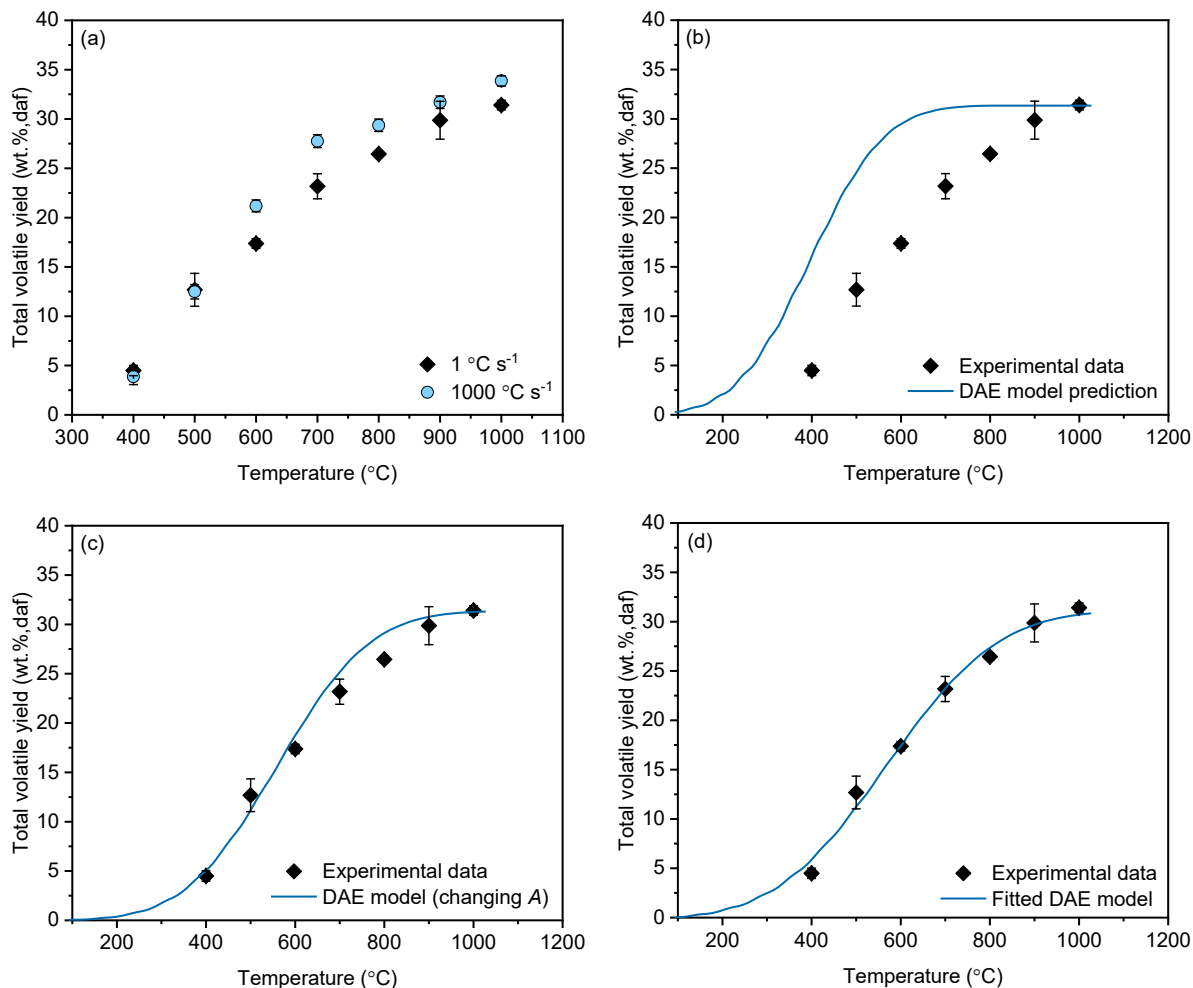
Figure 7. 2 (a) Atmospheric pressure pyrolysis of Morupule coal using heating rates of 1 ºC s^{-1} and 1000 ºC s^{-1} at various temperatures and 0 s holding time. (b) A comparison of the WMR experimental data and DAE model prediction of Morupule coal total volatile yields at a heating rate of 1 ºC s^{-1} using a pre-exponential factor of 6×10^{12} s^{-1}, mean activation of 183.3 kJ mol^{-1} and standard deviation of 36.3 kJ mol^{-1}. (c) DAE model prediction of Morupule coal total volatile yields at a heating rate of 1 ºC s^{-1} using a pre-exponential factor of 6×10^{9} s^{-1}, mean activation of 183.3 kJ mol^{-1} and standard deviation of 36.3 kJ mol^{-1}. (d) An optimum fitting of the DAE model to the WMR experimental data obtained from the atmospheric pressure pyrolysis of Morupule coal using a heating rate of 1 ºC s^{-1}.

7.3.1.3 High Pressure Pyrolysis

Figure 7.3a shows a comparison of the DAE model derived for atmospheric pressure pyrolysis (mean activation of 183.3 kJ mol^{-1} and standard deviation of 36.3 kJ mol^{-1}) compared to the WMR experimental data obtained from the high-pressure pyrolysis of Morupule coal (30 bar$_a$). The ultimate volatile yield was adjusted for the value obtained from the experimental pyrolysis at 30 bar$_a$. The model predicts the low temperature (< 500 °C) total volatile yields accurately. However, the total volatile yields are overestimated at temperatures higher than 600 °C. Chapter 4 has shown that elevated pressures tend to suppress the volatile release. This phenomenon is widely accepted to be a result of tar repolymerisation under increased residence times in the particle due to the external pressure [18,23,24]. An optimised fitting of the DAE model (Figure 7.3b) yields a mean activation energy of 191.3 kJ mol^{-1} and a standard deviation of 45.6 kJ mol^{-1} for the Gaussian distribution, and accurately reproduces the total volatile yields as a function of temperature. The increase in the activation energy suggests a possible increased difficulty in breaking the repolymerised chemical bonds. High pressure pyrolysis of Morupule coal is characterised by a broader Gaussian distribution, suggesting an increased variation in the bond breaking as additional reactions and products are introduced through intraparticle tar repolymerisation under elevated pressures and possible thermal cracking after further increases in pyrolysis temperature (Chapter 4).
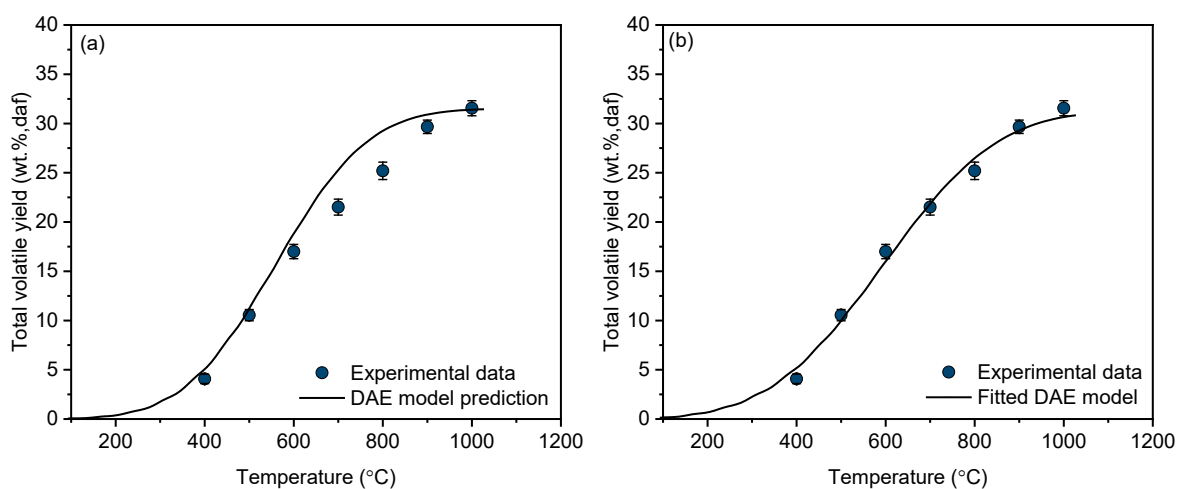
Figure 7. 3 (a) A comparison of the WMR experimental data obtained from the pyrolysis of Morupule coal at 30 bar$_a$ and a heating rate of 1000 °C s^{-1} as a function of temperature

compared to the DAE model prediction with a pre-exponential factor of 6×10^{12} s^{-1}, mean activation of 183.3 kJ mol^{-1} and standard deviation of 36.3 kJ mol^{-1}. (b) An optimum fitting of the DAE model to the WMR experimental data obtained from the pyrolysis of Morupule coal at 30 bar$_a$ using a heating rate of 1000 ºC s^{-1}.

7.3.1.4 Analysis of Model-Free Methods

The previous sections showcased the applicability of the model-based DAE method in describing the pyrolysis behaviour of Morupule coal under various operating conditions. Model-free methods were previously introduced in Section 2.6.1.2.1. When using these methods, kinetic parameters are estimated from data sets obtained for at least three different heating rates and analysed at constant conversion [25,26]. These methods are widely favoured due to their reduced complexity and ability to process data from the TGA [2,27]. However, as the review presented in Chapter 2 suggested, when using data obtained from the WMR, a dependence of coal pyrolysis conversion on heating rate is likely to only be confined to the influence of thermal annealing reactions as extremely fast pyrolysis kinetics and minimal heat transfer limitations are obtained in this reactor configuration. This may limit the applicability of the model-free methods, especially at low temperatures where thermal annealing reactions are minimal, as significantly large activation energies would be obtained.

Due to the inability of the WMR to provide a continuous weight-loss measurement, an estimate of the continuous pyrolysis profile trajectory was provided using the optimised fitting of the DAE model to the WMR data. Figures 7.1 and 7.2d present the DAE model estimates of the pyrolysis of Morupule coal carried out under atmospheric pressure conditions at heating rates of 1000 ºC s^{-1} and 1 ºC s^{-1}, respectively. An optimised fit of the DAE model to data obtained at a heating rate of 10 ºC s^{-1} is given in Appendix E. Using the optimised DAE model data, iso-conversion Arrhenius plots were obtained using the Friedman method (Figure 7.4a), KAS method (Figure 7.4b) and the Ozawa-Flynn-Wall method (Figure 7.4c). These methods

are detailed in Section 2.6.1.2.1. A summary of the coefficients of determination (R^2) and activation energies at various conversions for the different methods is given in Table 7.1.

The R^2 values show a good correlation of the data except at a conversion of 30 % where an R^2 value of 0.33 was obtained for all the three methods (the linear regression plot fails to join all the points due to the poor linearity of the data). It is likely that this was due to the narrow temperature range of the data and a rather steep inclination of the curve as the Arrhenius plot transitions from an inverse correlation to a positive correlation. Therefore, a minuscule variation in the total volatile yield has a profound impact on the correlation of the data. The activation energy values presented in Table 7.1 are significantly outside the range of those typically presented in literature (150 – 500 kJ mol^{-1} [2,6,21]). For conversions lower than 30 %, positive activation energy values were obtained (750 – 4000 kJ mol^{-1}). Beyond a conversion of 30 %, negative activation energy values were deduced (-3500 kJ mol^{-1} to -1000 kJ mol^{-1}). The positive values suggest a slightly higher pyrolysis conversion at lower heating rates. Previous studies using the WMR suggested that this reactor configuration could suffer from heat transfer limitations at high heating rates for temperatures below 500 °C as extensively discussed in Section 7.3.1.2 [11,17]. However, data obtained from the pyrolysis of Morupule coal at different heating rates is within the same experimental error limits at such temperatures as shown in Figure 7.2a. The rather large activation energy values presented in this work highlight the increased steepness of the Arrhenius plots, compared to less than 250 kJ mol^{-1} obtained for coal pyrolysis as reported by Yan, *et al*. [2], suggesting that there is little variation between conversions at different heating rates. This speaks to the fast kinetics of Morupule coal pyrolysis obtained in the WMR and the ability of this reactor to sufficiently minimise both intraparticle (small particle size fraction of 125 – 150 µm) and interparticle (monolayer segregation, allowing direct contact of each particle with the wire-mesh) heat transfer limitations during the primary thermal breakdown of this coal. The negative activation energy values obtained at higher conversions are due to the lower pyrolysis conversions when using slower heating rates as the coal undergoes thermal rearrangement involving tar precursors as

discussed in Section 7.3.1.2. Rapid heating rates (1000 ºC s^{-1}) limit the prolonged exposure of the coal to high temperatures, as opposed to low heating rates, minimising the impact of thermal annealing reactions on pyrolysis conversion. It must be highlighted that this is the first time that negative activation energies are reported using model-free kinetic methods. It is highly likely that the effect of low heating rates on thermal annealing is not effectively elucidated in most studies given the narrow heating rate range in the TGA, a reported 0.15 – 1.7 ºC s^{-1} [2,3,28], compared to the 1 – 1000 ºC s^{-1} used in the present work. These findings may find relevance in the research community given the vast amount of published literature that employs these methods on data obtained from TGAs.

The findings and discussion presented above significantly deviate from those widely presented in literature, where changes in heating rate are observed to shift pyrolysis to lower temperatures. While it is possible that such a behaviour may be due to the slower pyrolysis kinetics under rapid heating rates, it is most likely that TGAs incur interparticle heat transfer limitations due to larger sample masses as extensively discussed by Richter and Rein [22]. If this is the case, then the vast literature using these methods therefore analyses the effect of the reactor design instead of the true intrinsic pyrolysis behaviour. Efforts must be made in ensuring that the reported TGA data is free from heat transfer limitations. Basing on experimental tests carried out in the WMR, for extremely fast reaction kinetics and in the absence of heat transfer limitations (assuming negligible thermal annealing), pyrolysis approaches a near complete temperature dependence (with little dependence on time spent at peak temperature as shown in Figures 4.1b and 7.2a). For such a process, the effect of heating rate on pyrolysis would be negligible. This yields model-free methods Arrhenius plots that approach an infinite gradient as highlighted by the steep curves shown in Figure 7.4. Therefore, model-free methods would prove to be redundant in this case. The rather large differences in kinetic parameters obtained using these methods, compared to literature, suggest a significant dependence on the reactor design. This highlights a significant limitation in the application of these methods if the main objective is to determine intrinsic kinetics of

single particle solid fuels such as coal and biomass (and in other applications such as plastic and polymer pyrolysis).
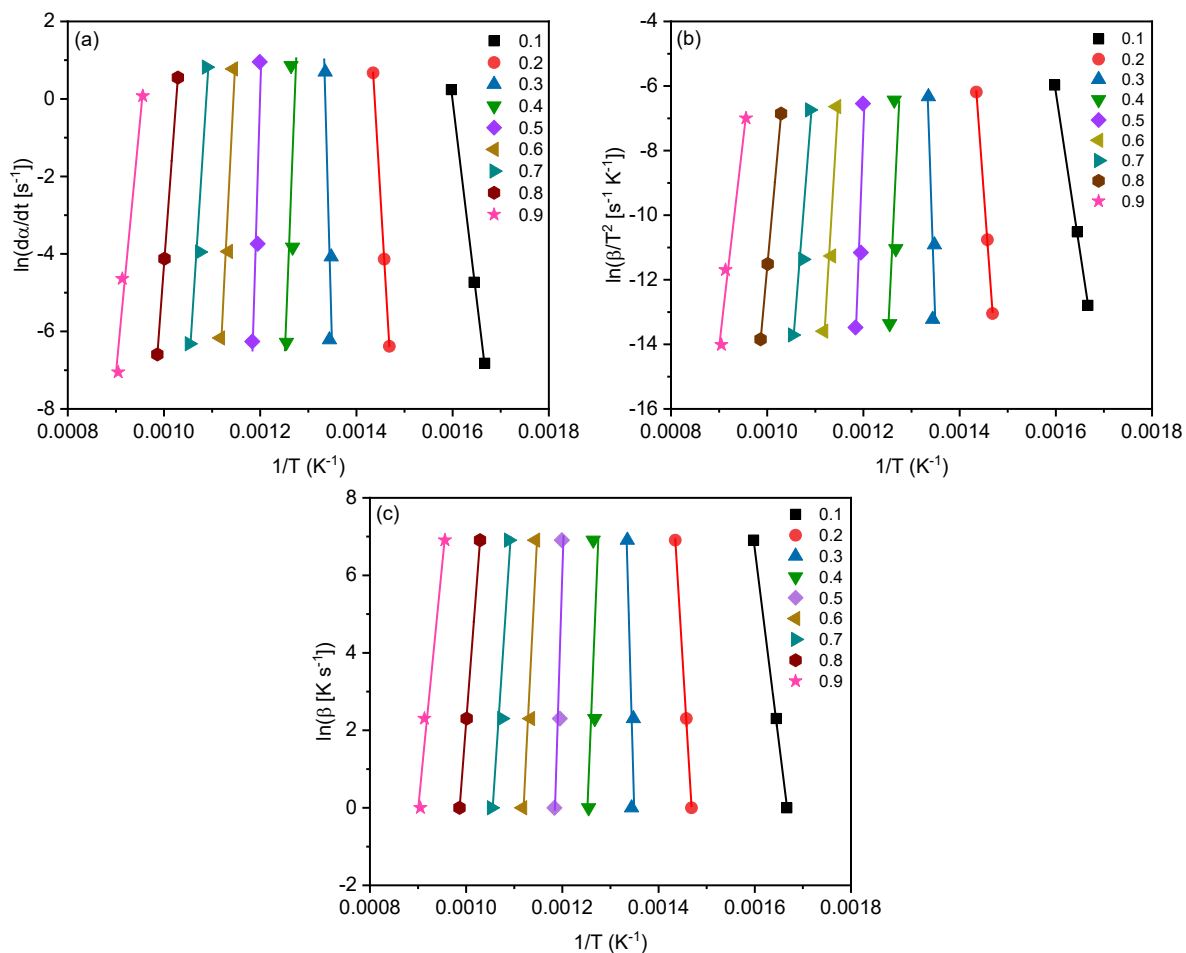
Figure 7. 4 Arrhenius plots obtained for the pyrolysis of Morupule coal at various conversions using model-free methods (a) Friedman (b) KAS and (c) Ozawa-Flynn-Wall.

Table 7. 1 Coefficients of determination (R^2) and activation energies (E_a) estimated using the Friedman, KAS and Ozawa-Flynn-Wall methods to describe the kinetics of Morupule coal pyrolysis at heating rates of 1, 10 and 1000 ºC s^{-1}.

Conversion	Friedman		KAS		Ozawa-Flynn-Wall	
	E_a (kJ mol^{-1})	R^2	E_a (kJ mol^{-1})	R^2	E_a (kJ mol^{-1})	R^2
0.1	852	1.00	816	1.00	786	1.00
0.2	1740	1.00	1686	1.00	1614	1.00
0.3	3753	0.69	3667	0.66	3497	0.67
0.4	-2665	0.34	-2554	0.33	-2528	0.33
0.5	-3439	0.83	-3289	0.82	-3113	0.82
0.6	-2058	0.89	-2065	0.90	-1949	0.90
0.7	-1609	0.91	-1572	0.91	-1480	0.91
0.8	-1395	1.00	-1368	1.00	-1285	1.00
0.9	-1081	0.97	-1067	0.97	-998	0.97

7.3.2 Gasification

7.3.2.1 Atmospheric Pressure Gasification

7.3.2.1.1 Kinetic Parameter Estimation

The volumetric, shrinking core and random pore models, described in Section 2.6.2.1, have been used to describe the atmospheric pressure coal gasification behaviour in CO_2. The early stage kinetic data presented in Chapter 5 was fitted with these models, to estimate the respective reaction rate constants at various temperatures and produce the corresponding Arrhenius plots of Morupule coal gasification in CO_2. Figures 7.5, 7.6 and 7.7 show the linear form model fittings (Equations 7.7 – 7.9) and the Arrhenius plots derived from using the shrinking core, volumetric and random pore models, respectively. Typically, the structural parameter, used in the random pore model, is approximated using micropore surface area and image analyses (such as those presented in Appendix B) [29]. However, given the sample mass limitations associated with the use of the WMR, it was impossible to determine the structural parameter experimentally. Alternatively, this parameter can be estimated by fitting

the random pore model to the data [5]. Although higher values have been reported [30], typical values of the structural parameter range from 1 to 10 [5,29,31]. Differences in the use of values in this range are not sufficiently clear in the present work (Appendix E), perhaps showing the limited influence of char porosity development on early-stage gasification. A structural parameter value of 4, based on literature of a coal char of similar porosity (0.3 [31]), 0.4 – 0.48 obtained for Morupule coal chars from atmospheric pressure pyrolysis using X-Ray CT measurements (Table 4.3), was selected for the random pore model calculations in this work.

Table 7.2 provides a summary of the reaction rate constants estimated by the respective models and a comparison of the coefficients of determination (R^2). All the three models accurately represent the early-stage WMR gasification data well without any distinguishable differences in the degree of correlation, with the lowest R^2 being 0.95. This suggests that the main assumptions for which each model is based do not have an impact on the early-stage conversions used in this work. This further supports the assumption given in Chapter 5 that the effects of char structure and morphology on the early-stage intrinsic gasification reaction rates are negligible when studying unadulterated gasification conversions of up to 15 % using a direct gasification approach. From the Arrhenius plots, the activation energies and pre-exponential factors associated with the three models can be estimated (Table 7.3). The models confirm a kinetic regime transition temperature between 950 ºC and 975 ºC as pore diffusional limitations start to influence the gasification reaction. The activation energy values presented, 323 – 326 kJ mol^{-1}, are near identical to the 320 kJ mol^{-1} obtained for the chemical reaction controlled regime without fitting a model in Chapter 5. Similarly, the activation energies in the pore diffusion plus chemical reaction controlled regime obtained using the models and without the model are similar.
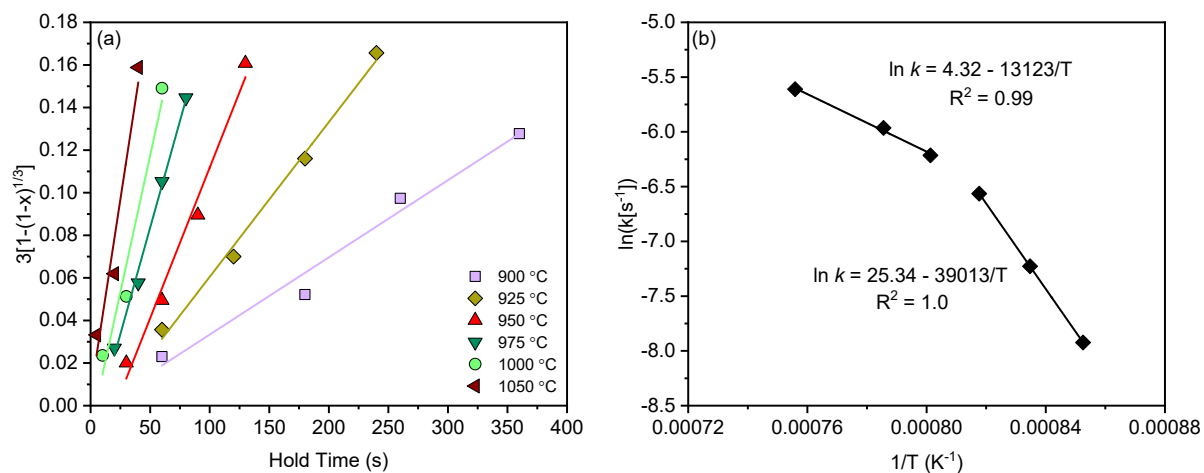
Figure 7. 5 Shrinking core model (a) fitting and (b) resulting Arrhenius plot.
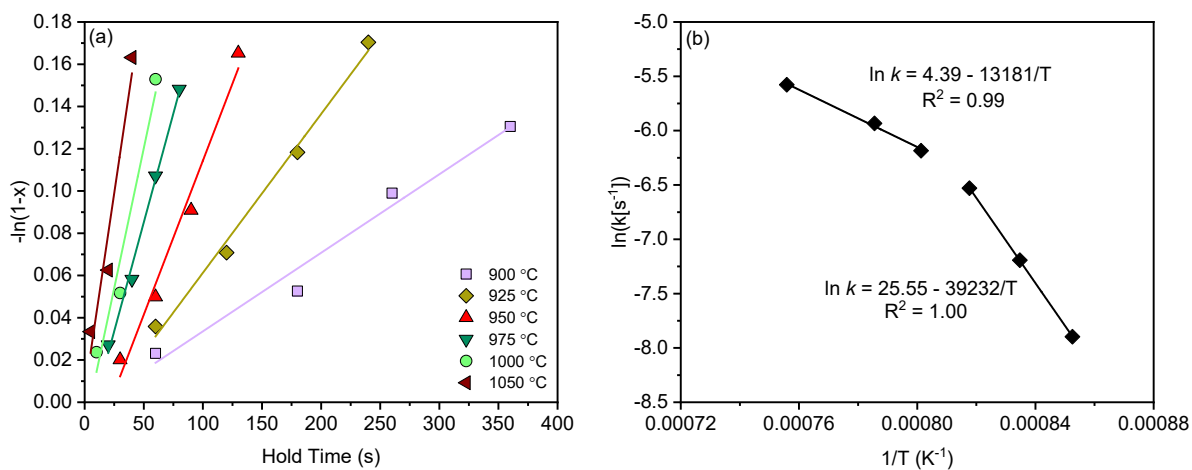
Figure 7. 6 Volumetric model (a) fitting and (b) resulting Arrhenius plot.
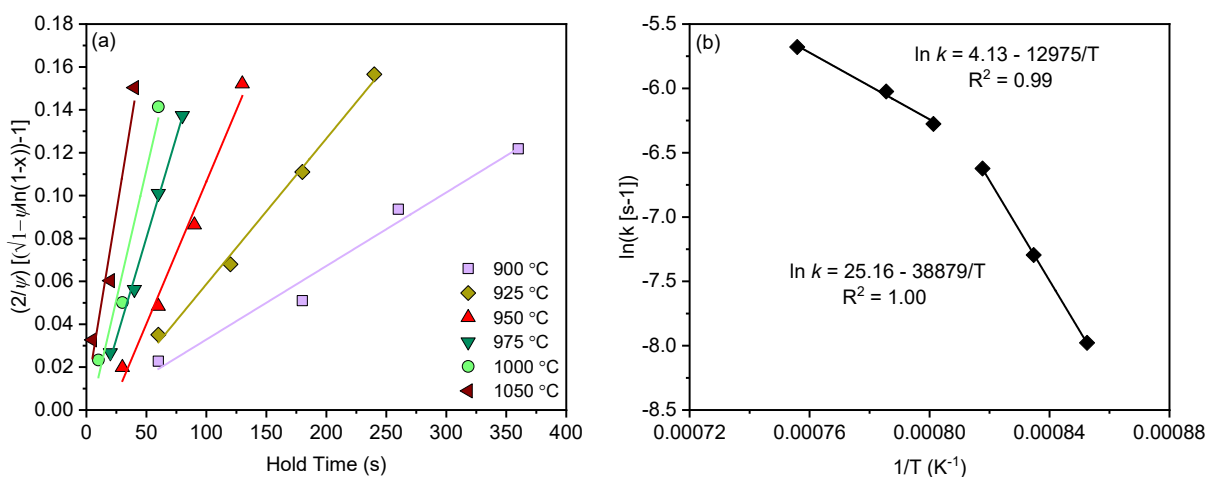
Figure 7. 7 Random pore model (a) fitting and (b) resulting Arrhenius plot.

Table 7. 2 The model estimated reaction rate constants at different temperatures and their corresponding coefficients of determination, R^2.

Temperature (°C)	Shrinking core		Volumetric		Random pore	
	Rate constant (s^{-1})	R^2	Rate constant (s^{-1})	R^2	Rate constant (s^{-1})	R^2
900	0.00036	0.98	0.00037	0.98	0.00034	0.98
925	0.00073	1.00	0.00075	0.99	0.00068	0.99
950	0.00141	0.98	0.00146	0.98	0.00133	0.99
975	0.00200	1.00	0.00206	0.99	0.00188	0.99
1000	0.00257	0.96	0.00265	0.96	0.00242	0.96
1050	0.00366	0.95	0.00378	0.95	0.00342	0.95

Table 7. 3 Kinetics parameters estimated by fitting the shrinking core, volumetric and random pore models.

Temperature range	Shrinking core		Volumetric		Random pore	
	E_a (kJ mol^{-1})	A (s^{-1})	E_a (kJ mol^{-1})	A (s^{-1})	E_a (kJ mol^{-1})	A (s^{-1})
900 - 950	324	1.0×10^{11}	326	1.2×10^{11}	323	8.5×10^{10}
975 - 1050	109	75	110	81	108	62

7.3.2.1.2 High Conversion Prediction

WMRs are designed to provide informative early-stage primary gasification behaviour in the absence of the effects of char deactivation. Higher conversions were limited when using this reactor setup as the char particle size reduced with further consumption during gasification. This leads to the char falling through the mesh under gravity, compromising the subsequent char weight measurements. The data presented in this thesis was obtained before the sample was observed to fall through the aperture of the mesh. Using the previously estimated early-stage kinetic parameters, the gasification conversion can be extrapolated with the aid of the different kinetic models accounting for changes in char structure and porosity. The optimum kinetic parameters obtained for each model, given in Table 7.3, were used to predict

conversions at extended holding times to obtain high gasification conversion data at 1000 ºC (Figure 7.8). These models can predict the early-stage CO_2 gasification conversions well. However, the model predictions slightly deviate from the experimental data for conversions higher than 25 %. The WMR experimental data exhibits a slight decrease in the reaction rate, possibly due to the onset of char deactivation after prolonged holding at 1000 ºC [18]. It has also been reported that as the conversion increases, pore coalescence takes place, reducing the surface area available for gasification [5]. However, this might not be applicable in the present work given the rather low conversions illustrated in Figure 7.8. The observed decrease in the reaction rate validates the conversion range (up to 15 %) used to estimate the intrinsic kinetic parameters in Chapter 5 to ensure that they are free from the influences of char deactivation and other structural changes that may result in the underestimation of the reaction rate. In a commercial process setting, the coal char can be held at peak temperature for periods as low as 100 s in entrained flow gasifiers [32], and in the presence of steam and O_2, limiting the influence of char deactivation.
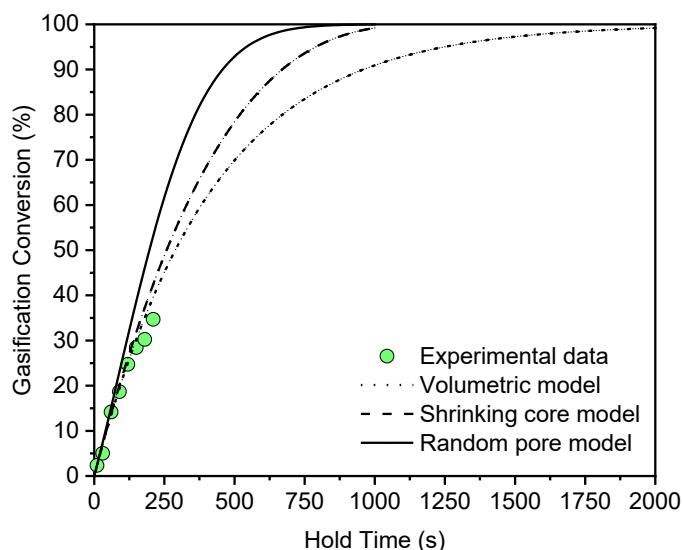
Figure 7. 8 Morupule coal CO_2 gasification conversions at 1000 ºC and atmospheric pressure as a function of hold time in the WMR compared to the shrinking core, volumetric and random pore model predictions using the estimated kinetic parameters.

7.3.2.2 High Pressure Gasification

Chapter 6 showed that high-pressure gasification of Morupule coal can be described using the modified L – H rate expression where the inhibition of the CO_2 gasification reaction by CO is assumed to be negligible on the basis that the WMR employs a continuous sweep flow gas that carries the product gases away from the reaction zone. The applicability of the nth power global equation on data produced under elevated pressures is limited due to changes in the pre-exponential factor and reaction order with pressure, necessitating the use of the L – H rate expression [33]. Using the kinetic parameters obtained from the modified L – H rate expression (Equation 6.1), the conversion – time relationship during gasification at 900 ºC and 1000 ºC was predicted as shown in Figures 7.9a and b, respectively. The modified L – H rate expression predicts the 1 bar_a CO_2 gasification at 900 ºC accurately. However, the model overestimates the conversions at gasification pressures of 10 bar_a and 20 bar_a as it fails to account for the lag in gasification during the early periods of holding at 900 ºC. As previously discussed in Chapters 5 and 6, the initial gasification delay is a result of the slow chemisorption kinetics and the need for a substantial build-up of surface CO_2 complexes as the WMR essentially operates as a semi-batch system. Furthermore, the extent of chemisorption may initially be limited by the smaller available surface area. Unlike the many studies presented in literature which investigate gasification using the already prepared char [5,29,30,33], the present work studied the combined processes of pyrolysis and gasification from raw coal. Consequently, pyrolysis had to take place before the intraparticle diffusion of the reactive gas took place. Nevertheless, the reaction rates predicted by the model (0.0034 s^{-1} at 10 bar_a and 0.0066 s^{-1} at 20 bar_a) are close to those estimated by a linear fit without a model (0.0039 s^{-1} at 10 bar_a and 0.0053 s^{-1} at 20 bar_a), indicating that the inability of the model to accurately map out the conversion – time relationship is mainly due to the failure of accounting for the initial delay in gasification. Perhaps future reaction kinetics models should account for this limitation in the L – H rate model by equipping it with a term that describes the extent of surface saturation as a function of time.

At 1000 ºC, the L – H model accurately predicts early-stage conversions for different gasification pressures (Figure 7.9b), showing capability to adapt to changes in pressure. At this temperature, the previously observed gasification lag is reduced due to the faster chemisorption and chemical reaction rates. Therefore its influence on the predicted conversion – time relationship is rather minimal. However, the model significantly underestimates high gasification conversions at 20 bar_a as the experimental gasification reaction rate increases due to increased surface area and ease of access to the internal pore network. Scanning electron microscopy imaging revealed a well-developed porosity and severely consumed external surface for chars produced at 30 s holding time and 1000 ºC (Figure 6.13d). Increases in the surface area as porosity develops affects the extent of surface complex formation, further highlighting the need for a term that tracks the evolution of surface saturation during gasification. It must be reinforced that the discussion presented in this section, and a constant theme throughout this thesis, refers to the early-stage unadulterated kinetics. In commercial gasifiers, as well as at high conversions, considerations have to be made for the influence of reaction rate inhibition by the product gas, changes in char structure and morphology, interparticle interactions and the impact of longer residence times (applicable to fluidised and fixed bed gasifiers) on char deactivation.
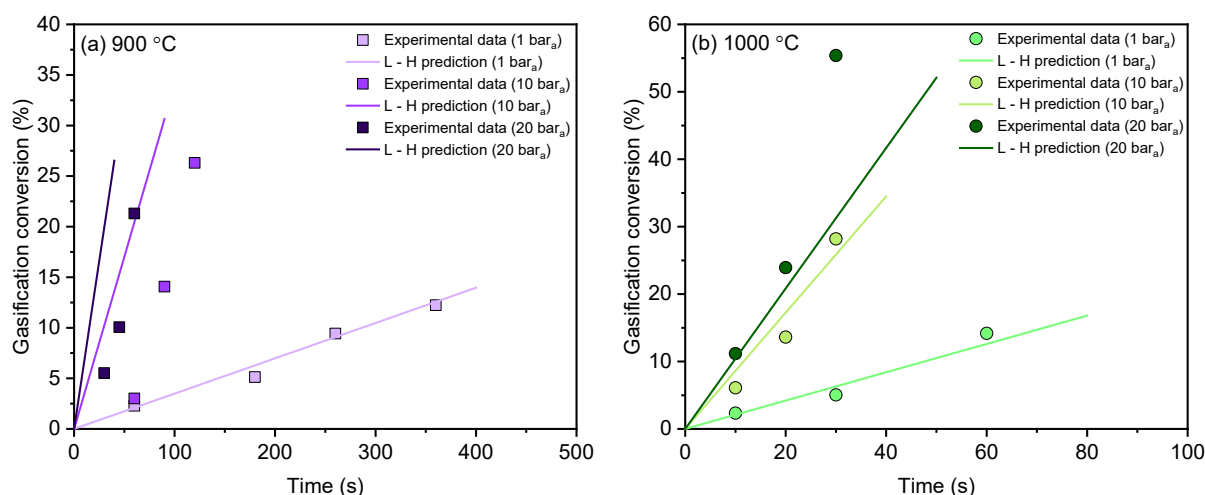
Figure 7. 9 Prediction of the high pressure Morupule coal CO_2 gasification early-stage conversions using the Langmuir – Hinshelwood rate expression at (a) 900 ºC and (b) 1000 ºC.

7.4 Conclusions

This chapter investigated the applicability of widely known empirical models in describing the experimental data obtained from the WMR for the thermochemical conversion of Morupule coal. The ability to predict both pyrolysis and gasification also enables a suppression of the reactor design limitations, such as the intermittent data collection and low gasification conversion ranges. The DAE model demonstrated an excellent capability of accurately representing the pyrolysis data using a Gaussian distribution. However, it was found that, all things equal, a decrease in the heating rate overestimated the conversion as the model fails to account for the extremely fast pyrolysis kinetics of Morupule coal in the WMR. With a commensurate decrease in the pre-exponential factor, the DAE model adequately predicted low heating rate data from the WMR. Similarly, the derived kinetic parameters showed good ability to adapt to changes in pyrolysis pressure. In reactor configurations where transport phenomena limitations are sufficiently suppressed, such as the WMR, coupled with feedstocks with fast pyrolysis kinetics, model-free kinetic methods yield rather large activation energies due to little dependence of pyrolysis on heating rates. Negative activation energies are reported for the first time when using model-free methods due to thermal annealing reactions prevalent when using low heating rates.

The shrinking core, volumetric and random pore models were demonstrated to fit the experimental atmospheric pressure gasification data well, resulting in kinetic parameters that are near identical to those obtained without fitting a model. The volumetric model was found to best represent high conversion gasification data. However, it failed to account for the slight decrease in the reaction rate due to the onset of char deactivation after the char was held at peak temperature for prolonged periods. The Langmuir – Hinshelwood rate model accurately predicted the high-pressure gasification reaction rates at both 900 ºC and 1000 ºC. However, the conversion – time profile showed an overestimation of the data at 900 ºC as the model could not capture the gasification lag resulting from poor surface saturation and slower chemisorption kinetics in the early stages of gasification. This model must be modified to

encompass the extent of surface saturation and chemisorption as a function time to allow for an accurate description of surface complex formation.

References

1.   Liu, H., Combustion of Coal Chars in O_2/CO_2 and O_2/N_2 Mixtures: A Comparative Study with Non-isothermal Thermogravimetric Analyzer (TGA) Tests. *Energy & Fuels* **2009,** *23* (9), 4278-4285.

2.   Yan, J.; Jiao, H.; Li, Z.; Lei, Z.; Wang, Z.; Ren, S.; Shui, H.; Kang, S.; Yan, H.; Pan, C., Kinetic analysis and modeling of coal pyrolysis with model-free methods. *Fuel* **2019,** *241*, 382-391.

3.   Miura, K.; Maki, T., A Simple Method for Estimating f(E) and k_0(E) in the Distributed Activation Energy Model. *Energy & Fuels* **1998,** *12* (5), 864-869.

4.   Richards, A. P.; Fletcher, T. H., A comparison of simple global kinetic models for coal devolatilization with the CPD model. *Fuel* **2016,** *185*, 171-180.

5.   Tanner, J.; Bhattacharya, S., Kinetics of CO_2 and steam gasification of Victorian brown coal chars. *Chemical Engineering Journal* **2016,** *285*, 331-340.

6.   Maki, T.; Takatsuno, A.; Miura, K., Analysis of Pyrolysis Reactions of Various Coals Including Argonne Premium Coals Using a New Distributed Activation Energy Model. *Energy & Fuels* **1997,** *11* (5), 972-977.

7.   de Caprariis, B.; De Filippis, P.; Herce, C.; Verdone, N., Double-Gaussian Distributed Activation Energy Model for Coal Devolatilization. *Energy & Fuels* **2012,** *26* (10), 6153-6159.

8.   Niksa, S.; Lau, C.-W., Global rates of devolatilization for various coal types. *Combustion and Flame* **1993,** *94* (3), 293-307.

9.   Vyazovkin, S., Modification of the integral isoconversional method to account for variation in the activation energy. *Journal of Computational Chemistry* **2001,** *22* (2), 178-183.

10.   Solomon, P. R.; Hamblen, D. G.; Carangelo, R. M.; Serio, M. A.; Deshpande, G. V., General model of coal devolatilization. *Energy & Fuels* **1988,** *2* (4), 405-422.

11.   Kandiyoti, R.; Herod, A.; Bartle, K. D.; Morgan, T. J., *Solid fuels and heavy hydrocarbon liquids: thermal characterization and analysis*. Elsevier: **2016**.

12.   Messenböck, R. C.; Dugwell, D. R.; Kandiyoti, R., CO_2 and steam-gasification in a high-pressure wire-mesh reactor: the reactivity of Daw Mill coal and combustion reactivity of its chars. *Fuel* **1999,** *78* (7), 781-793.

13.   Wang, J.; Lian, W.; Li, P.; Zhang, Z.; Yang, J.; Hao, X.; Huang, W.; Guan, G., Simulation of pyrolysis in low rank coal particle by using DAEM kinetics model: Reaction behavior and heat transfer. *Fuel* **2017,** *207*, 126-135.

14.   Liu, J.-Z.; Yang, Y.-M.; Wang, Z.; Cen, K., Pyrolysis characteristics of low-rank coals based on double-gaussian distributed activation energy model. *The Canadian Journal of Chemical Engineering* **2019,** *97* (10), 2642-2652.

15.   Gibbins-Matham, J.; Kandiyoti, R., Coal pyrolysis yields from fast and slow heating in a wire-mesh apparatus with a gas sweep. *Energy & Fuels* **1988,** *2* (4), 505-511.

16.   Cai, H. Y.; Güell, A. J.; Chatzakis, I. N.; Lim, J. Y.; Dugwell, D. R.; Kandiyoti, R., Combustion reactivity and morphological change in coal chars: Effect of pyrolysis temperature, heating rate and pressure. *Fuel* **1996,** *75* (1), 15-24.

17.   Barr, M. R.; Volpe, R.; Kandiyoti, R., Influence of Reactor Design on Product Distributions from Biomass Pyrolysis. *ACS Sustainable Chemistry & Engineering* **2019,** *7* (16), 13734-13745.

18.   Messenböck, R. C. Rapid Pyrolysis and Gasification of Coal in a High Pressure Wire-Mesh Reactor. PhD Thesis, University of London, **1998**.

19.   Gibbins, J. R. Investigation of Primary Coal Pyrolysis Processes using a Variable Heating Wire-Mesh Apparatus. PhD Thesis, University of London, **1988**.

20.   Bhagavatula, A.; Shah, N.; Honaker, R., Estimating the Pyrolysis Kinetic Parameters of Coal, Biomass, and Their Blends: A Comparative Study. *Energy & Fuels* **2016,** *30* (12), 10045-10054.

21.   Zhang, Q.; Luo, M.; Yan, L.; Yang, A.; Hui, X., Kinetic Analysis of Low-Rank Coal Pyrolysis by Model-Free and Model-Fitting Methods. *Journal of Chemistry* **2019,** *2019*, 9075862.

22.   Richter, F.; Rein, G., The Role of Heat Transfer Limitations in Polymer Pyrolysis at the Microscale. *Frontiers in Mechanical Engineering* **2018,** *4*, 18.

23.   Zhuo, Y.; Messenböck, R.; Collot, A. G.; Megaritis, A.; Paterson, N.; Dugwell, D. R.; Kandiyoti, R., Conversion of coal particles in pyrolysis and gasification: comparison of conversions in a pilot-scale gasifier and bench-scale test equipment. *Fuel* **2000,** *79* (7), 793-802.

24.   Wall, T. F.; Liu, G.-s.; Wu, H.-w.; Roberts, D. G.; Benfell, K. E.; Gupta, S.; Lucas, J. A.; Harris, D. J., The effects of pressure on coal reactions during pulverised coal combustion and gasification. *Progress in Energy and Combustion Science* **2002,** *28* (5), 405-433.

25.   Mishra, A.; Gautam, S.; Sharma, T., Effect of operating parameters on coal gasification. *International Journal of Coal Science & Technology* **2018,** *5* (2), 113-125.

26.   Liu, S.; Yu, J.; Bikane, K.; Chen, T.; Ma, C.; Wang, B.; Sun, L., Rubber pyrolysis: Kinetic modeling and vulcanization effects. *Energy* **2018,** *155*, 215-225.

27.   Opfermann, J. R.; Kaisersberger, E.; Flammersheim, H. J., Model-free analysis of thermoanalytical data-advantages and limitations. *Thermochimica Acta* **2002,** *391* (1), 119-127.

28.   Hattingh, B. B.; Everson, R. C.; Neomagus, H. W. J. P.; Bunt, J. R.; van Niekerk, D.; Ashton, B. P., Modeling the Nonisothermal Devolatilization Kinetics of Typical South African Coals. *Energy & Fuels* **2014,** *28* (2), 920-933.

29.   Everson, R. C.; Neomagus, H. W. J. P.; Kaitano, R.; Falcon, R.; du Cann, V. M., Properties of high ash coal-char particles derived from inertinite-rich coal: II. Gasification kinetics with carbon dioxide. *Fuel* **2008,** *87* (15), 3403-3408.

30.   Kajitani, S.; Suzuki, N.; Ashizawa, M.; Hara, S., CO_2 gasification rate analysis of coal char in entrained flow coal gasifier. *Fuel* **2006,** *85* (2), 163-169.

31.   Kim, R.-G.; Hwang, C.-W.; Jeon, C.-H., Kinetics of coal char gasification with CO_2: Impact of internal/external diffusion at high temperature and elevated pressure. *Applied Energy* **2014,** *129*, 299-307.

32.   Wagner, N. J.; Coertzen, M.; Matjie, R. H.; van Dyk, J. C., Chapter 5 - Coal Gasification. In *Applied Coal Petrology*, Suárez-Ruiz, I.; Crelling, J. C., Eds. Elsevier: Burlington, 2008; pp 119-144.

33.   Roberts, D. G.; Harris, D. J., A Kinetic Analysis of Coal Char Gasification Reactions at High Pressures. *Energy & Fuels* **2006,** *20* (6), 2314-2320.

Chapter 8

Effect of Particle Size on the Pyrolysis and Gasification of Morupule Coal

8.1 Introduction

Amongst several factors affecting the pyrolysis and gasification of coal, such as heating rate, temperature and pressure, *etc.,* the influence of particle size is particularly influential in understanding the impact of transport phenomena limitations on thermochemical conversion [1]. Chapters 4, 5 and 6 have extensively discussed the intrinsic pyrolysis and gasification behaviour of Morupule coal sample of a 125 – 150 μm particle size fraction. While the aforementioned particle size is suitable for intrinsic kinetic measurements and applications in entrained flow reactors, which typically use feedstock of up to 200 μm in size [2], fluidised bed gasifiers use particle sizes of 0.5 – 8 mm [2,3,4]. Temperatures at which studies in Chapters 4, 5

and 6 were conducted, up to 1050 ºC, are suitable for fluidised bed applications (800 – 1000 ºC [5]) whereas entrained flow gasifiers operate at 1500 – 1800 ºC [2]. Therefore, for the direct application of data accrued in this work, an in depth understanding of the role of heat and mass transfer limitations on the pyrolysis and gasification of Morupule coal is warranted. In addition, particle size plays an important role in the pyrolysis product distribution and affects the modelling of fluid bed stability [6], as well as the fragmentation and swelling of larger particles due to an intraparticle pressure build-up [7].

As discussed in Chapter 2, intraparticle secondary charring reactions are reportedly prominent in larger-sized particles due to longer residence times, affecting the char and tar product distributions and subsequent char reactivity [6,8,9,10]. In this chapter, the influence of particle size on pyrolysis and gasification is investigated, both at atmospheric and high pressures, to gain further insights into the thermochemical behaviour of Morupule coal. Furthermore, the morphology of residual chars from pyrolysis and gasification is studied using scanning electron microscopy (SEM). A thermogravimetric analyser was used to study the combustion reactivity of the residual chars.

8.2 Materials and Methods

8.2.1 Feedstock and Experimental Setup

Morupule coal, of proximate and elemental analyses given in Section 3.3, was used in this investigation. The effect of particle size on pyrolysis and gasification was evaluated using the 125 – 150 µm and 425 – 500 µm size fractions (suitable for the lower end particle size used in fluidised bed gasifiers). The coal samples were dried at 105 ºC for 12 h in a vacuum oven and stored in a desiccator. The wire-mesh reactor (WMR), described in Chapter 3, was used to perform the experiments. 5 – 6 mg of sample was used for each experimental run. At least three experimental tests were carried out and averaged to obtain each data point presented in this chapter. The errors bars correspond to a statistical measure of 95 % confidence interval.

8.2.2 Pyrolysis

Atmospheric pressure pyrolysis experiments were carried out in a 400 – 1000 ºC temperature range, at intervals of 100 ºC, and 0 s holding time at peak temperature, using a heating rate of 1000 ºC s^{-1} in helium gas flowing at a velocity of 0.1 m s^{-1}. The effect of holding time at 1000 ºC was studied by extending the time at temperature to 10, 30 and 60 s. The tar was collected and quantified as described in Section 3.2.3.3.2. The effect of pressure on pyrolysis was investigated at pressures of 1 bar$_a$ and 30 bar$_a$. Experiments were carried out at 400 – 1000 ºC and 0 s holding time at a heating rate of 1000 ºC s^{-1}. The effect of prolonged holding at 1000 ºC was studied at 10, 30 and 60 s.

8.2.3 Gasification

Gasification was studied at 1000 ºC for various holding times, identical to those used during pyrolysis (0, 10, 30 and 60 s), in a CO_2 atmosphere, fed to the reactor at a velocity of 0.1 m s^{-1}. In some cases, holding time was extended beyond 60 s to obtain comparable gasification conversions and determine the influence of particle size on early-stage gasification reaction rates. A heating rate of 1000 ºC s^{-1} was used for all the gasification experiments. The effect of pressure on the gasification of larger-sized particles was compared for pressures of 1 bar$_a$ and 20 bar$_a$. CO_2 gasification at 30 bar$_a$ resulted in an unreliable temperature control and weakening of the molybdenum wire-mesh.

8.2.4 Char Characterisation

The morphological development of the residual chars obtained from pyrolysis and gasification was studied using SEM to gain insights on the volatile transport mechanism and gasification progression. This analytical technique is described in Section 3.3.7. The combustion reactivity of residual chars was investigated using a Pyris 1 TGA, detailed in Section 3.3.1.2.

8.3 Results and Discussion

8.3.1 Atmospheric Pressure Pyrolysis

8.3.1.1 Product Yields

The effect of particle size on the total volatile, tar and gas yields from the pyrolysis of Morupule coal between 400 ºC and 1000 ºC at atmospheric pressure is summarised in Table 8.1. As extensively discussed in literature [11,12], temperature is observed to have a significant influence on the thermal breakdown of coal despite the short holding time of 0 s at peak temperature and a rapid heating rate of 1000 ºC s^{-1}, highlighting the fast kinetics of the pyrolysis step. The larger particle size fraction exhibits lower total volatile yields at all temperatures. This effect can be due to heat transfer limitations, inducing a temperature gradient in the particle, intraparticle reactions leading to secondary charring and/or diffusional limitations incurred by the volatile products [6]. The differences in the total volatile yields are particularly pronounced at 600 ºC and converge at higher temperatures. This is hardly surprising as Table 8.1 shows that the maximum tar yield obtained from the pyrolysis of the 125 – 150 µm particle size fraction is attained at 600 ºC, in agreement with other researchers [13], whilst the maximum tar yield from the 425 – 500 µm particle size was reached at 800 ºC, suggesting a delay in the release of tars.

Interestingly, near identical tar yields, within experimental error, are obtained at temperatures higher than 800 ºC for both particle size fractions. Other researchers have observed a decrease in the tar yield commensurate with an increase in the gas yield for larger particle sizes [6,9,14]. It is suggested that tars undergo both intraparticle and interparticle thermal degradation reactions, resulting in higher gas yields. However, in the case of Morupule coal, gas yields from the 425 – 500 µm size fraction are lower than those from the 125 – 150 µm size fraction, suggesting a possible incomplete devolatilisation. The near identical tar yields presented in Table 8.1 for temperatures higher than 700 ºC suggest that there are minimal intraparticle reactions involving tars in larger particle sizes of Morupule coal during pyrolysis. In the present work, interparticle secondary reactions are minimised by the continuous sweep

flow gas which carries the volatiles away from the reaction zone as they evolve. The potential effects of thermal lagging and diffusional limitations on the reduced total volatile yields in larger particles during the heating up period are discussed below.

Table 8. 1 Total volatile, tar and gas yields of the atmospheric pressure Morupule coal pyrolysis for the 125 – 150 μm and 425 – 500 μm particle size fractions (Heating rate: 1000 ºC s^{-1}, Hold time: 0 s, Gas: Helium). a – by difference.

Temperature (ºC)	Total Volatile Yield (wt.%, daf)		Tar Yields (wt.%, daf)		Gas Yields (wt.%, daf) [a]	
	125 - 150 μm	425 - 500 μm	125 - 150 μm	425 - 500 μm	125 - 150 μm	425 - 500 μm
400	3.9	0.0	0.0	0.0	3.9	0.0
500	12.5	2.4	6.2	0.4	6.3	2.0
600	21.2	9.6	10.8	2.5	10.4	7.0
700	27.8	19.4	11.9	9.4	15.9	10.0
800	29.5	25.4	11.9	11.2	17.6	14.2
900	31.7	27.7	11.4	10.7	20.3	17.0
1000	33.1	29.4	11.8	11.0	21.2	19.4

While Table 8.1 shows slightly lower total volatile yields at 1000 ºC, it should be noted that these experimental tests were carried out at 0 s and a rapid heating rate of 1000 ºC s^{-1}. Longer holding time experiments were carried out at 1000 ºC to investigate the product distribution evolution in larger particle sizes (Table 8.2). Although the maximum product yields from the pyrolysis of the 125 – 150 μm particle size fraction were virtually attained at 0 s of holding at 1000 ºC, near identical products yields were obtained at 10 s for the 425 – 500 μm particle size fraction. This further supplements the discussion of a possible incomplete devolatilisation in larger particles at 0 s holding time. Unlike in other coals for which charring reactions were reported, Morupule coal is characterised by identical total volatile yields, given sufficient holding at peak temperature, in the particle size range studied. Perhaps the particle size range investigated is too narrow to observe any charring reactions between tars and heated internal surfaces. However, Chapter 4 has shown that Morupule coal is also less

susceptible to the influence of pressure, well known to promote tar repolymerisation and produce relatively stable residues in some coals [11,15]. In addition, a critical review of the petrographic properties of Morupule coal in Chapter 2 indicated that it is inertinite-rich [16,17] and has a low hydrogen/carbon ratio (Table 3.2). These properties are associated with relatively low total volatile and tar yields [18,19], as shown in Table 8.1 that the maximum tar yield is 11.9 wt.%, daf. This limits the potential secondary charring reactions between the char internal surface and evolving tars. Therefore, the discussions presented on the limited secondary charring of Morupule coal tars sufficiently characterise the thermochemical behaviour of larger-sized Morupule coal particles.

Table 8. 2 Total volatile yields from the atmospheric pressure pyrolysis of 125 – 150 μm and 425 – 500 μm Morupule coal particle size fractions in helium as a function of hold time (0 – 60 s) at 1000 ºC.

Hold Time (s)	Total Volatile Yield (wt.%, daf)		Tar Yields (wt.%, daf)		Gas Yields (wt.%, daf) [a]	
	125 - 150 μm	425 - 500 μm	125 - 150 μm	425 - 500 μm	125 - 150 μm	425 - 500 μm
0	33.1	29.4	11.8	11.0	21.2	19.4
10	34.9	32.9	11.8	10.8	22.1	23.1
30	35.7	35.2	12.0	11.5	23.7	23.7
60	35.2	35.0	11.7	11.3	23.7	22.5

The above discussion highlights the limited influence of intraparticle secondary reactions on the liberation of volatile products from Morupule coal. Other factors that can control the release of volatiles are mass and heat transport limitations. Based on data obtained from the pyrolysis of different sized Morupule coal particles at 700 ºC shown in Table 8.1, it is clear that the tar yields are close, with a difference of only 2.5 wt.%, daf. In contrast, there is a larger difference of 5.9 wt.% in gas yields. Given their lower molecular weights, higher average molecular velocities would be expected for gases, yielding a larger diffusion coefficient. Therefore, gases would be the least affected by diffusional limitations. However, from the data,

there a greater disparity in gas yields than the higher molecular weight tars (heavier compounds are being released while lighter compounds are retained in the char). With this discussion, it is postulated that the actual thermal breakdown of uncracked structures takes precedence over the influence of mass transport limitations in the delay of volatile release.

A rather simplistic approach was used to estimate the time taken to achieve a uniform temperature between the particle surface and the centre of the particle (Table 8.3). This approach was based on the unsteady-state thermal conduction method of a spherical particle outlined in Appendix F. For a particle with a maximum diameter of 150 μm, estimated times are well within the time taken to reach peak temperature given a heating rate of 1000 ºC s^{-1} (0.975 s at 1000 ºC). However, in larger particles and particularly at temperatures below 600 ºC, times taken to reach a homogeneous intraparticle temperature are of the order equal to those taken during the heating up period. This potentially highlights a significant heat transfer limitation at relatively low temperatures (less than 600 ºC) as previously indicated that larger particle sizes had a lower total volatile yield than their smaller particle size counterparts by 10 wt.%, daf. The estimated time for thermal conduction reduces with increasing temperature due to increases in the thermal conductivity of the coal. The relatively short period at 1000 ºC is consistent with the experimental data presented in Table 8.2, showing near identical pyrolysis product yields at 10 s for both particle size fractions. It must be highlighted that the effect of heat transfer limitations during experimental tests might be initially exacerbated by the possible localised heating of the particles at points directly in contact with the wire-mesh sample holder, with other areas remaining at lower temperatures, creating 'hot' and 'cold' spots on the particle.

Table 8. 3 Estimated time taken for the centre of an assumed solid spherical coal to reach a temperature equivalent to the surface temperature under thermal conduction.

Temperature (ºC)	Time (s)	
	150 μm	500 μm
400	0.089	0.985
600	0.026	0.289
800	0.006	0.072
1000	0.001	0.010

8.3.1.2 Char Morphology

Further insights on the effect of particle size on the volatile transport mechanism during atmospheric pressure pyrolysis were obtained by studying the surface morphology of the 425 – 500 μm particle size fraction residual chars using SEM (Figures 8.1a and b). Chapter 4 established a bubble transport phenomenon, for a particle size fraction of 125 – 150 μm, characterised by an explosive volatile release both at 600 ºC and 1000 ºC, leading to the formation of blowholes and condensed bubbles of liquid bitumen on the surface of the char (see Figures 4.13 and 4.14). Figure 8.1a exhibits limited blowholes on the surface of the chars obtained from pyrolysis at 600 ºC for the 425 – 500 μm size fraction. It can be argued that this could be due to a lower tar yield of 2.5 wt.% compared to 9.6 wt.% attained from the 125 – 150 μm particle size under identical experimental conditions. However, Figure 8.1b shows that further increases in temperature to 1000 ºC, where a tar yield of 10.7 wt.% was obtained, do not yield substantive morphological differences, showing the absence of blowholes. Instead, SEM images of both chars from 600 ºC and 1000 ºC show apparent condensed and intact bubbles from liquid bitumen [20] of sizes in the order of 10 μm. The bubble formation is suggestive of a pyrolytic behaviour characterised by gluey viscous intermediate products rather than the more violent release of lighter material as vapour. Pyrolysis in larger particles avoids an extreme internal pressure build-up and subsequent explosive volatile release which would otherwise occur during a rapidly attained homogenous temperature distribution in the particle, as is the case for the 125 – 150 μm particles. In agreement with the

present work, Cousins, *et al.* [10] attributed the relatively smaller pores on larger particles to the inherently difficult volatile transport due to a lower internal pressure build-up.
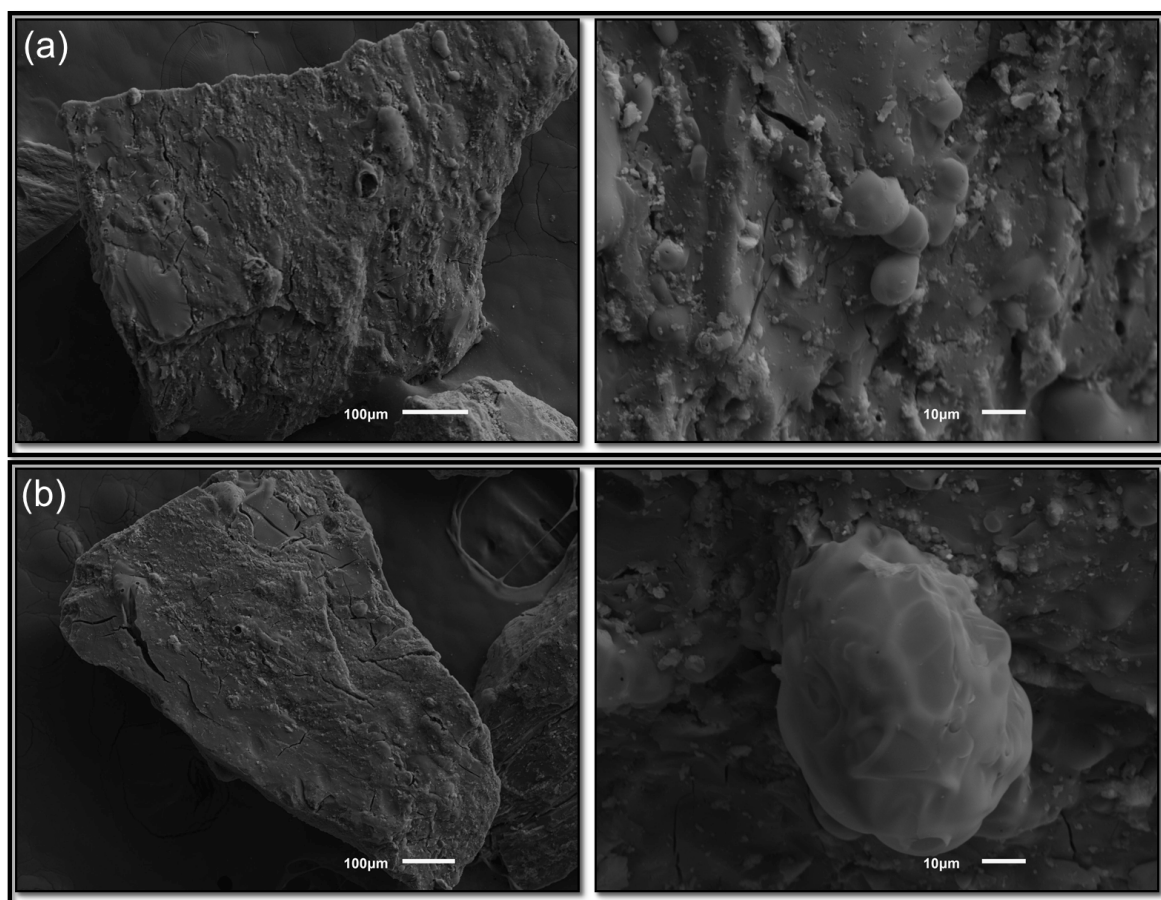
Figure 8. 1 SEM images of the 425 – 500 μm size fraction Morupule coal chars from atmospheric pressure pyrolysis at (a) 600 ℃ and (b) 1000 ℃. 0 s hold time in a helium atmosphere.

8.3.1.3 Char Combustion Reactivity

The effect of particle size on the relative TGA combustion reactivity of residual chars was studied for both the heating up and holding periods (Figures 8.2a and b respectively). A decrease in the combustion reactivity as a function of pyrolysis temperature is observed in Figure 8.2a. The higher volatile matter content in chars obtained at lower pyrolysis temperatures, constituting more oxygen-containing species and smaller aromatic ring systems, is known to promote higher char reactivity [9]. An increase in pyrolysis temperature is

associated with significant active site losses and thermal annealing reactions [11,21]. Interestingly, despite a lesser volatile release (Table 8.1), residual chars from the 425 – 500 µm size fraction have a comparable combustion reactivity with their 125 – 150 µm counterparts pyrolysed under identical conditions at 600 ºC and 800 ºC. The particle size independence of char reactivity, despite a higher volatile matter content, suggests the presence of an opposing effect in larger particle sizes, yielding similar char reactivities for the two particle size fractions. In consideration of the lower total volatile yields obtained at 600 ºC and 800 ºC for larger particles (Table 8.1), the char porosity may be less developed, resulting in a lower surface area available for combustion. Yi, *et al.* [22] states that the effect of particle size on combustion is particularly pronounced in coal than its char due to significant differences in the surface area. Therefore, for larger-sized chars obtained at lower pyrolysis temperatures, the effect of residual volatiles (higher reactivity) is counteracted by the possible low available surface areas, decreasing the number of active sites on the char surface perimeter (lower reactivity). Figure 8.2a also shows that the 425 – 500 µm size fraction chars obtained at 1000 ºC and 0 s holding time, however, appear to be more reactive than their smaller particle size fraction counterparts. It is likely that the two chars are at different stages of thermal annealing, and subsequent structural ordering. Devolatilisation is virtually completed within 0 s of holding at 1000 ºC for the 125 – 150 µm size fraction whilst further exposure to temperature is necessary for the larger particles to ensure the thermal breakdown of previously uncracked structures due to the temperature gradient. Although the experimental temperature is 1000 ºC, bulk structures of the larger particle may have only 'seen' a temperature lower than 1000 ºC. The effect of surface area development may be limited seeing as over 85 % of volatiles had been released at this stage, with subsequent volatile release constituting lighter gases produced during rearrangement reactions. Therefore, the extent of thermal annealing may be predominant over surface area development at 1000 ºC.

A steeper decrease in reactivity is observed for chars produced under prolonged holding at 10 s, resulting in similar combustion reactivities for both particle size fractions (including at

60 s holding time) (Figure 8.2b). Chapter 4 established a substantial extent of graphitisation during the first 10 s of holding at 1000 ºC. However, identical combustion reactivities are demonstrated for the two chars studied. Given the temperature at which the combustion reactivity was studied (500 ºC, known to be in the chemical reaction controlled regime [8]), char reactivity is typically independent of particle size under conditions isolated from diffusional limitations [7,23]. The findings presented in this work are in contrast with those presented in the literature, where an increase in particle size is associated with a decrease in reactivity due to secondary charring reactions [6]. In their study, char yield increased by almost 10 wt.% in larger particle sizes. Table 8.2 shows similar product yields for different sized Morupule coal particles, suggesting that secondary reactions between evolving tars and the heated coal char surfaces are negligible.
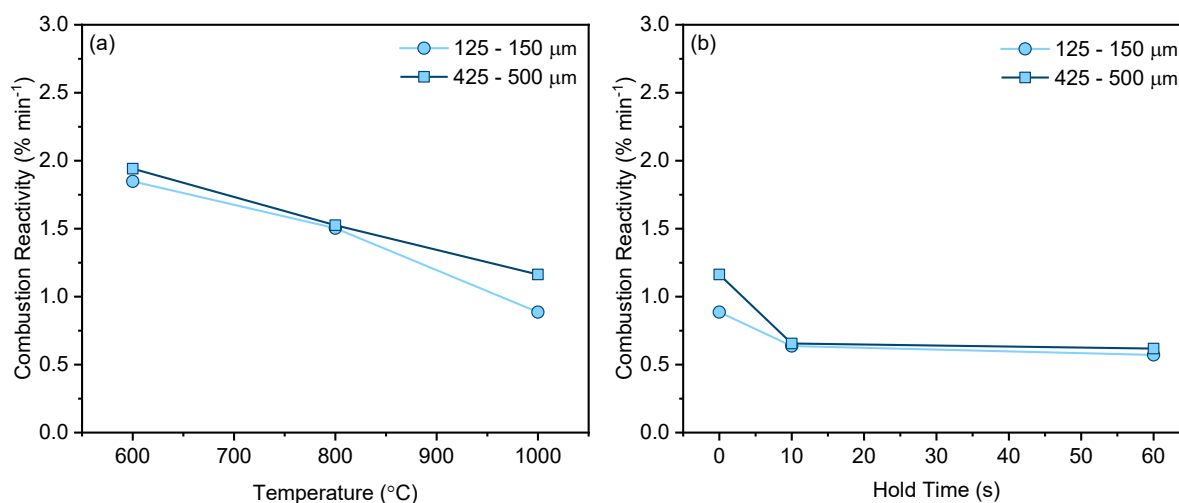
Figure 8. 2 Combustion reactivities of 125 – 150 µm and 425 – 500 µm char size fractions as a function of (a) pyrolysis temperature (0 s hold time experiments) and (b) hold time at 1000 ºC.

8.3.2 High Pressure Pyrolysis

8.3.2.1 Total Volatile Yields

Chapter 4 extensively discussed the effect of pressure on the pyrolysis of Morupule coal in the absence of transport phenomena limitations. This section extends the discussion by introducing heat and mass transport limitations incurred in larger particle sizes. Total volatile yields of a 425 – 500 μm Morupule coal particle size fraction obtained at pressures of 1 bar$_a$ and 30 bar$_a$ during the heating up period to 1000 ºC (Figure 8.3a) and holding at peak temperature for up to 60 s (Figure 8.3b) are presented. A clear decrease in the total volatile yields, attributed to the suppression of volatile release under high external pressures [24], is observed during the heating up period. Table 8.4 summarises the influence of pressure on the extents of volatile suppression for both particle size fractions studied. Higher external pressures appear to have a more profound effect on the inhibition of volatile release in larger particles, particularly at temperatures higher than 600 ºC. This is likely due to the lower internal pressure build up in larger particles, due to the induced temperature gradient, limiting the explosive release of volatiles. It was previously suggested that elevated pressures promote the formation of tar repolymerisation structures at low temperatures, which possibly undergo further cracking at 1000 ºC (Chapter 4). Figure 8.3b shows that despite the possible tar repolymerisation reactions and delays in volatile product diffusion, the ultimate total volatile yield obtained under prolonged holding at peak temperature is insensitive to changes in particle size. These findings are particularly important in defining the bed stability of fluidised bed gasifiers. Their relevance is also predicated on the reduced complexity of the development of kinetic models predicting pyrolysis behaviour without additional complex secondary charring reactions, with main considerations only made for the transport phenomena limitations.
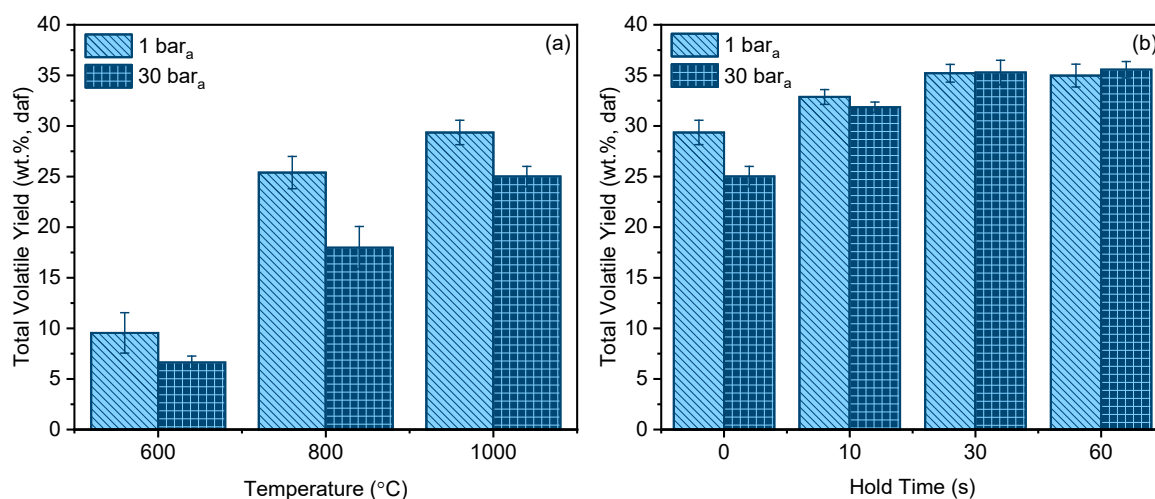
Figure 8. 3 Total volatile yields from the pyrolysis of the 425 – 500 μm Morupule coal size fraction in a helium pressure of 1 bar_a and 30 bar_a as a function of (a) pyrolysis temperature (0 s hold time) and (b) hold time at 1000 ºC.

Table 8. 4 Comparison of the extent of pressure induced volatile release suppression during pyrolysis at different temperatures in different particle size fractions.

Temperature (ºC)	Volatile Release Suppression (wt.%, daf)	
	125 - 150 μm	425 - 500 μm
600	4.2	2.9
800	4.3	7.4
1000	1.5	4.4

8.3.2.2 Char Morphology

SEM characterisation of the surface morphology of the 425 – 500 μm residual chars from 30 bar_a pyrolysis at 600 ºC and 1000 ºC is presented in Figures 8.4a and b, respectively. The chars are characterised by large surface crack lines, with some about 200 μm in size, and pores of sizes less than 10 μm. While some condensed bubbles are observed on the char surface, their prevalence is significantly lower than for chars of similar size obtained from pyrolysis at atmospheric pressure. In stark contrast, Figures 8.1a and b do not show any crack

lines on the surface of chars produced from atmospheric pressure pyrolysis, suggesting a possible different volatile release transport mechanism. Char surface cracks may therefore stem from the forceful release of volatiles as the internal pressure increases with temperature [25,26]. Other researchers associate the fragmentation of coals with increases in particle size [27]. However, the absence of cracking in chars produced at atmospheric pressure suggests that pressure plays a prominent role in the propagation of Morupule coal particle cracking during pyrolysis. Residual chars produced at 600 ºC have surface cracks which appear to be widened at 1000 ºC following a further release of about 20 wt.%, daf volatiles. The presence of these crack lines at low temperatures therefore presents a gateway for the release of the remaining volatiles, without the need for further surface pore development which is observed for chars pyrolysed at atmospheric pressure. The surface morphology presented in Figure 8.4 deviates from the general expectation of enhanced bubble formation in larger particles at elevated pressures as the coal undergoes a fluid stage [10]. Such variations may be rooted in the petrographic properties of the parent coal. It was previously deduced (in Chapter 4) that the limited susceptibility of Morupule coal to the fluid stage is linked to the dominant inertinite maceral, accounting for over 75 % of the total maceral concentration [16]. In accordance with findings presented in this work, it is suggested that low-rank inertinite-rich coals, such as Morupule coal, tend to fragment during pyrolysis at temperatures as low as 700 ºC due to thermal stresses [28,29].
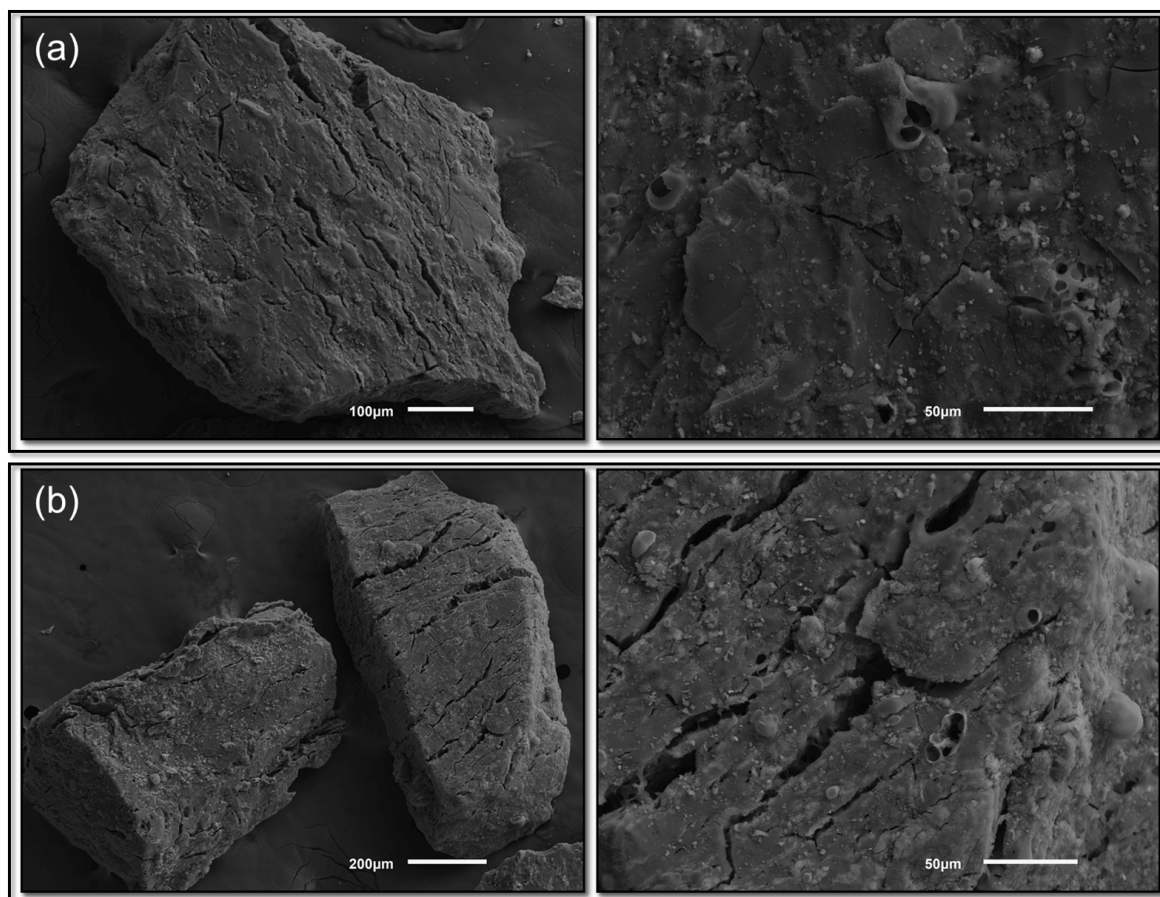
Figure 8. 4 SEM images of the 425 – 500 µm particle size fraction of Morupule coal chars from pyrolysis at (a) 600 ºC and (b) 1000 ºC. 0 s hold time in a helium atmosphere at a pressure of 30 bar$_a$.

8.3.2.3 Char Combustion Reactivity

Figure 8.5a compares the relative combustion reactivities of the 425 – 500 µm size fraction char particles obtained from pyrolysis at 1 bar$_a$ and 30 bar$_a$ as a function of temperature. A decrease in the combustion reactivity with an increase in temperature, attributed to volatile matter release resulting in more ordered chars [11,21], is observed. Consistent with observations made in Chapter 4, chars produced at 30 bar$_a$ display a higher reactivity than their 1 bar$_a$ counterparts for all pyrolysis temperatures. Figure 8.3a showed that high pressure suppresses the release of volatile matter during the heating up period. The suppression of volatiles

produces relatively stable structures, presumably from repolymerised tars (see Chapter 4). As such, chars produced under high pressure have a higher volatile matter content, and by extension, oxygen-containing functional and aliphatic groups, associated with higher char reactivity [9,30]. Previous studies on the influence of pressure on the pyrolysis of other coals, albeit for smaller particle sizes, have shown that pressure induces the formation of a relatively unreactive secondary char layer, reducing char reactivity [11,24]. As such, the result obtained in Figure 8.5a further substantiates the discussion that Morupule coal does not appear to be susceptible to secondary charring reactions even under high pressures. In this context, the absence of the unreactive secondary char layer ensures an unrestricted subsequent gasification of the main residual char during heterogeneous gas-solid reactions.

Extended holding of the coal at 1000 ºC yields chars of identical combustion reactivity irrespective of the pyrolysis pressure (Figure 8.5b). The steep decrease in reactivity in the initial 10 s is attributed to the combined effects of the release of previously uncracked volatile matter and thermal annealing processes, inducing char ring condensation. Extensive heat treatment is well known to reduce char microporosity, leading to loss of active sites and lower reactivity [21,31]. Similar to observations made in Chapter 4, further holding to 60 s does not a show an apparent change in reactivity. This suggests that bulk chemical structural changes take place in the initial 10 s of holding at peak temperature.
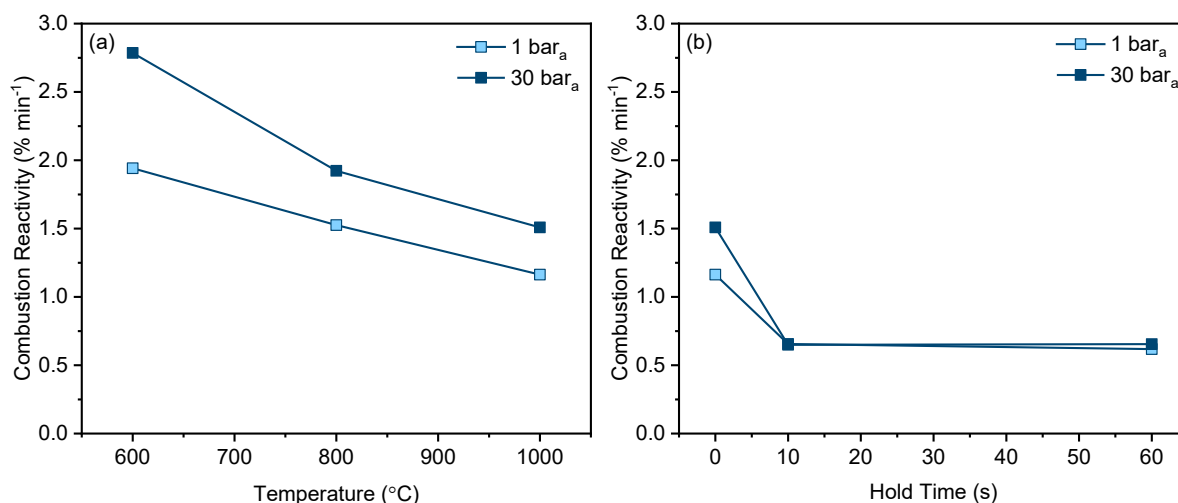
Figure 8. 5 Combustion reactivities of the 425 – 500 μm particle size fraction chars produced at 1 bar$_a$ and 30 bar$_a$ as a function of (a) pyrolysis temperature (0 s hold time) and (b) hold time at 1000 ºC.

8.3.3 Atmospheric Pressure Gasification

8.3.3.1 Total Volatile Yields and Extents of Gasification

The effect of particle size on the total volatile yields and extents of gasification of Morupule coal gasification in CO_2 at 1000 ºC and atmospheric pressure has been studied (Figures 8.6a and b, respectively). The slightly negative extents of gasification observed at 0 s and 30 s are because of the proximity of pyrolysis and gasification yields due to limited gasification, as accounted for by the relatively large error bars. At all holding times shown, the total volatile yields from particles of the 125 – 150 μm size fraction exceed those of the 425 – 500 μm size fraction. The 425 – 500 μm particle size fraction exhibits limited gasification in the first 60 s of holding at 1000 ºC as evidenced by extents of gasification below 2 wt.%, daf (Figure 8.6a). Chapter 5 has shown that gasification at 1000 ºC is dominated by both the chemical reaction and pore diffusion. Moreover, increases in particle size are known to reduce the transitional temperature between the chemical reaction controlled kinetic regime and the mixed chemical reaction plus pore diffusion kinetic regime [32]. Furthermore, Table 8.2 revealed the existence of thermal lagging in the initial 10 s at 1000 ºC in larger particles. The amalgamation of

diffusional limitations and thermal lagging yields the extensive gasification lag in larger particles as shown in Figure 8.6b.
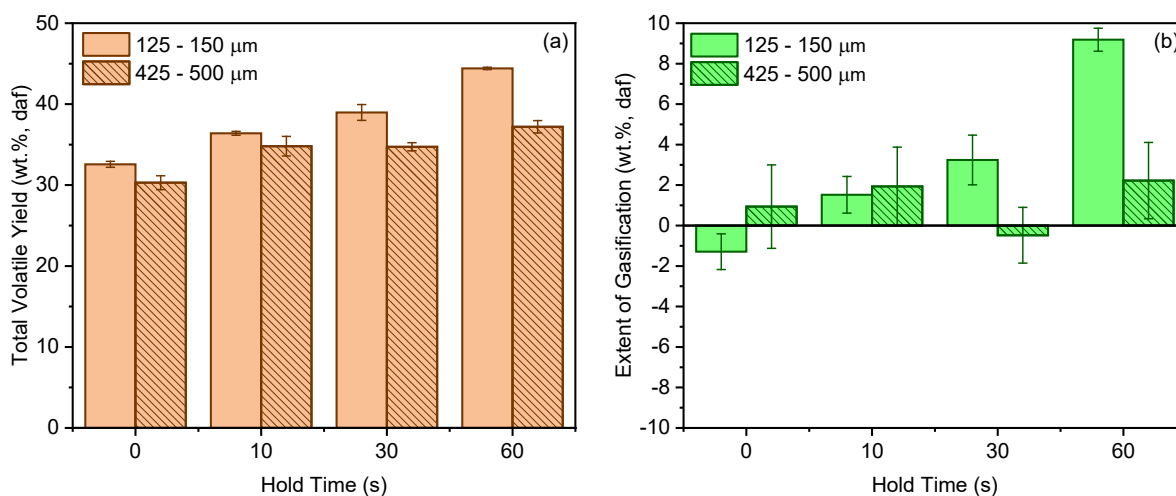
Figure 8. 6 (a) Total volatile yields and (b) extents of gasification from the atmospheric pressure gasification of 125 – 150 μm and 425 – 500 μm Morupule coal particle size fractions in CO_2 as a function of hold time at 1000 ºC.

8.3.3.2 Reaction Rates

The early-stage conversions of the 125 – 150 μm and 425 – 500 μm particle size fractions gasified in CO_2 at 1000 ºC and atmospheric pressure are presented in Figure 8.7. A linear relation ($R^2 > 0.96$) between the gasification conversion and hold time is observed, validating the use of the reaction rate equation presented in Equation 5.1, based on the assumption that the reaction rate is independent of structural and morphological changes. An increase in particle size reduces the gasification reaction rate by half as indicated that the approximated reaction rate is 0.0024 s^{-1} and 0.0012 s^{-1} for the 125 – 150 μm and 425 – 500 μm particle size fractions, respectively. This is in stark contrast with the earlier data (Figure 8.2b) which showed a combustion reactivity independent of particle size for chars produced under extended holding at peak temperature. This is perhaps indicative of the different reaction mechanisms in combustion and CO_2 gasification. However, it must also be noted that combustion reactivity was studied at 500 ºC, well known to be in the chemical reaction controlled kinetic regime for

combustion [8], whereas the current gasification temperature of 1000 ºC was shown to have contributions of both chemical reaction and pore diffusional limitations (Chapter 5). Therefore, gasification may largely be restricted to the pores close to the outer surface and external particle surface, significantly reducing the reaction rate due to the lower accessible surface area for the same sample weight on the wire-mesh. Kim, *et al.* [33] observed a decrease in char reactivity when the particle size was increased during gasification in CO_2 at temperatures similar to those used here (1050 – 1400 ºC). It is comprehensively argued that in the chemical reaction dominated kinetic regime, the effect of particle size is negligible [7,23,34], akin to observations made in combustion reactivity studies in Figure 8.2b. These observations, in conjunction with literature, suggest a mass transport controlled overall gasification rate in larger particles under conditions which are not completely isolated from diffusional effects.
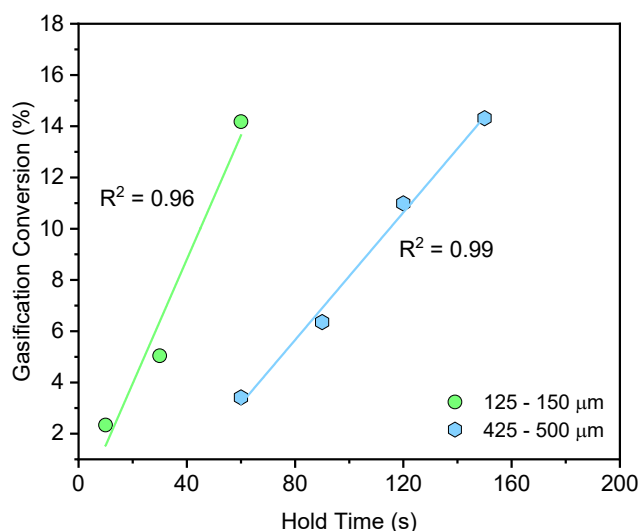
Figure 8. 7 Early-stage atmospheric pressure CO_2 gasification conversions at 1000 ºC for the 125 – 150 µm and 425 – 500 µm particle size fractions as a function of hold time.

8.3.3.3 Char Morphology

The surface morphology of the 425 – 500 µm size fraction chars from gasification in CO_2 at a temperature of 1000 ºC and a holding time of 60 s was studied using SEM (Figure 8.8). The chars are characterised by the presence of enclosed bubbles, most likely stemming from the condensed liquid bitumen released in bubble volatile transport as discussed in Section 8.3.1.2.

Unlike their smaller particle size counterparts, obtained under identical experimental conditions, which show a developing surface porosity (Figure 5.15b), the 425 – 500 μm char particles generally have limited surface porosity. This observation agrees with Figure 8.6b which shows negligible gasification, characterised by low extents of gasification in the initial 60 s of holding at 1000 ºC. It is likely that if gasification took place, enclosed bubbles would display significant surface porosity since they constitute less ordered and more reactive structures as they are made of tars [20] (Figure 8.12), and provide a gateway into the internal porous structure. Therefore, the absence of substantive surface porosity may also physically restrict CO_2 access to the internal porous network developed during devolatilisation [21]. This further adds to the diffusional limitations and thermal lagging factors which influence the previously observed extended gasification lag in larger particles.
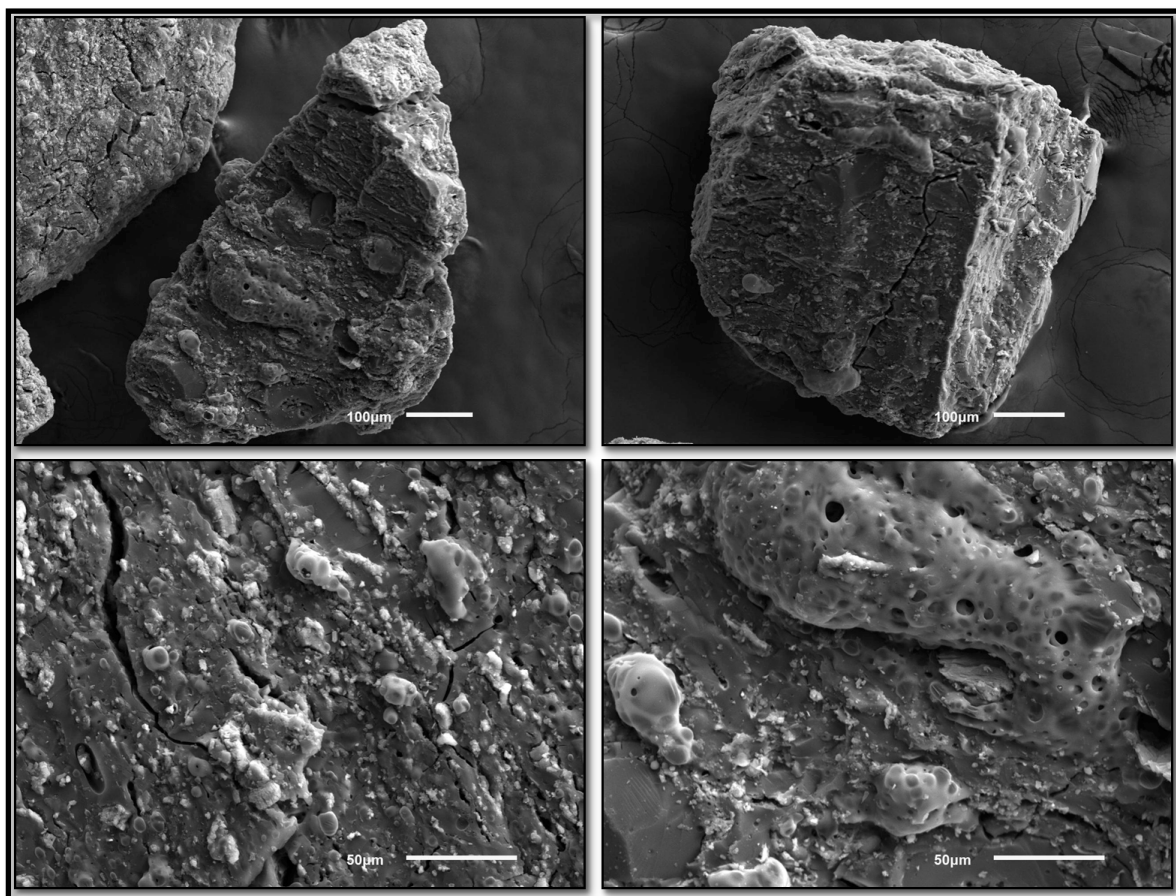
Figure 8. 8 SEM images of the 425 – 500 μm size fraction residual chars obtained from atmospheric pressure CO_2 gasification at 1000 ºC and 60 s hold time.

8.3.3.4 Char Combustion Reactivity

Figure 8.9 presents the relative combustion reactivity of 425 – 500 µm char particles obtained under identical atmospheric pressure pyrolysis and gasification conditions at 1000 ºC. Both pyrolysis and gasification chars have a similar combustion reactivity in the 0 – 60 s holding time range. This is hardly surprising given the substantial gasification lag observed in Figure 8.6b, where CO desorption is presumed to have commenced at around 60 s. However, this is in contrast with observations made in Chapter 5 where the 125 – 150 µm particle size fraction chars produced in a CO_2 atmosphere were noticeably less reactive than their pyrolysis counterparts, possibly due to the occupation of the more reactive sites by CO_2. O_2, during combustion, therefore, likely adsorbs on the less reactive sites. In larger particle sizes, the gasification lag is linked to the lower accessible char surface area, reducing the number of potential CO_2 complexes that could be formed. Balsamo, *et al*. [35] reported faster adsorption kinetics of CO_2 on activated carbons in smaller particles when investigating the particle size screening. In the context of the present study, the observed indistinguishable combustion reactivities are therefore due to the limited gasification taking place in the first 60 s of holding at 1000 ºC. Consequently, chars produced under CO_2 gasification conditions in the initial 60 s at 1000 ºC retain similar structural properties to those from pyrolysis.
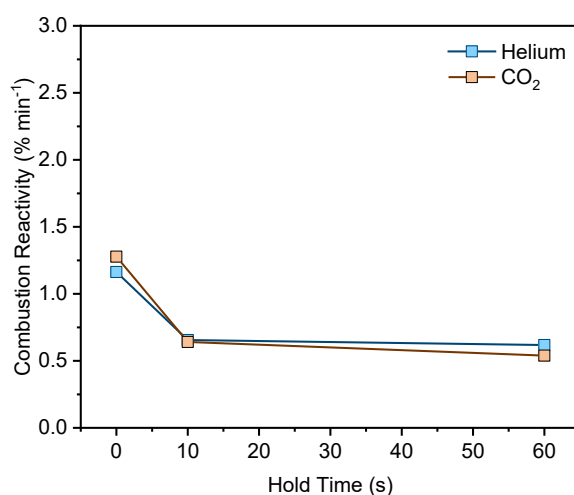
Figure 8. 9 Combustion reactivities of the 425 – 500 µm size fraction chars produced under atmospheric pressure pyrolysis (helium) and gasification (CO_2) conditions as a function of hold time at 1000 ºC.

8.3.4 High Pressure Gasification

8.3.4.1 Total Volatile Yields and Extents of Gasification

The effect of particle size on the 20 bar$_a$ CO_2 gasification of Morupule coal at 1000 ºC and 0 – 30 s hold time was investigated. Figures 8.10a and b present the total volatile yields and extents of gasification, respectively. At all holding times, the total volatile yields from the 125 – 150 µm particles substantially exceed those from the 425 – 500 µm size fraction (Figure 8.10a). This effect becomes more pronounced at longer holding times when the two particle size fractions are at different levels of char burn-off. The gasification lag previously alluded to during atmospheric pressure gasification (Figure 8.6b), appears to be present in the initial 20 s of gasification at 20 bar$_a$, as indicated by a low extent of gasification (Figure 8.10b). This is a fascinating observation as a high pressure gradient would promote the transport of the reactive gas to the unsaturated internal porous structure, forming more surface CO_2 complexes [36], therein overcoming diffusional limitations to an extent. However, it was previously shown that there is a further release of about 10 wt.%, daf volatiles between 0 s and 30 s of holding at 1000 ºC during pyrolysis (Figure 8.3b). This was attributed to overcoming the thermal lagging, resulting in a homogenous temperature distribution being attained throughout the particle. Therefore, although the pressure gradient may allow for CO_2 to access the internal char porous network, the intraparticle temperature is likely to be lower than essential for substantial CO_2 gasification in the early stages, resulting in lower chemisorption rates. This further substantiates the discussion presented in Section 8.3.1.1 that volatile release is mainly limited by thermal lagging rather than diffusional transport. A notable extent of gasification for the 425 – 500 µm particle size fraction occurs at 30 s of holding at 1000 ºC, whilst the 125 – 150 µm showed significant gasification at 10 s.
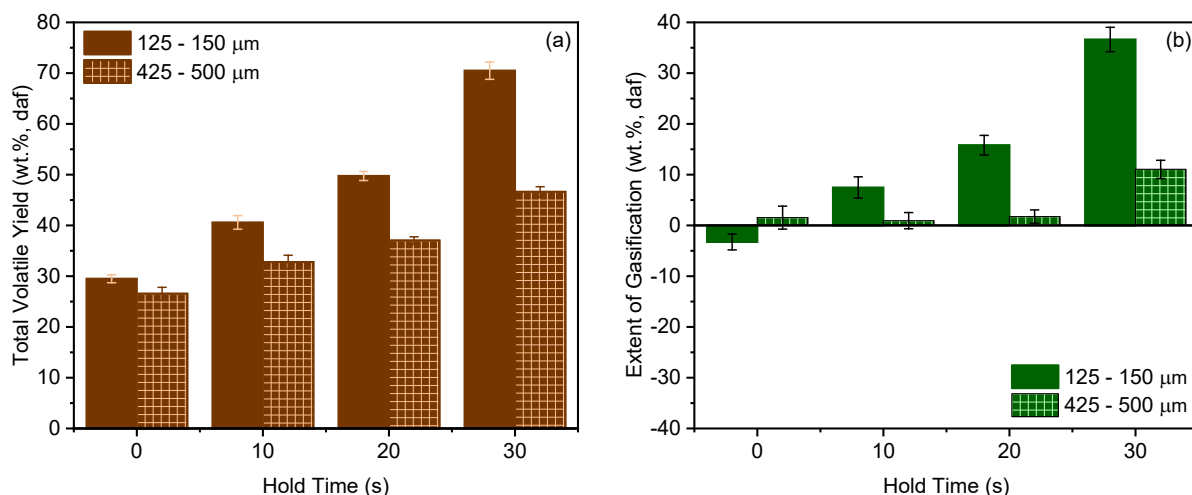
Figure 8. 10 (a) Total volatile yields and (b) extents of gasification of the 125 – 150 µm and 425 – 500 µm Morupule coal particle size fractions during gasification in CO_2 at 20 bar_a as a function of hold time at 1000 ºC.

8.3.4.2 Reaction Rates

The gasification reaction rates were estimated using the hold time dependence of conversion shown in Figure 8.11. It is apparent that in an identical hold time range at 1000 ºC, the 425 – 500 µm particle size fraction has a substantially lower conversion than the 125 – 150 µm size fraction. This is due to the combined effects of the gasification lag, described in Section 8.3.4.1, and mass transport diffusional limitations in larger particles. A linear relation between conversion and hold time is deduced for 425 – 500 µm particle size fraction (R^2 = 1.00), with an estimated reaction rate of 0.0081 s^{-1}. Smaller particles are characterised by a clear inflection at 30 s owing to the significant char morphological changes under fast gasification reaction rates (Chapter 6). Therefore, a fairer comparison estimates the reaction rate in the 10 – 20 s hold time as 0.013 s^{-1}. The lower gasification reaction rate when using the 425 – 500 µm particles is unsurprising given the vast literature that suggest a particle size dependence of the gasification reaction rate under conditions where diffusional limitations are dominant [1, 23]. In addition, larger particles tend to have a lower specific surface area [37]. Although the pressure gradient may promote the transport of CO_2 to the internal particle porosity, the observed lower gasification rates may be due to the reduced solid-gas contact

owing to a smaller total surface area available in larger particles (for the same sample amount of 5 – 6 mg) [38]. On this basis, heat transfer limitations play a crucial role in the initial gasification lag, significantly delaying CO_2 chemisorption given the endothermic nature of the Boudouard reaction [39], while diffusional limitations and available surface area control the overall gasification reaction rate in the latter stages.
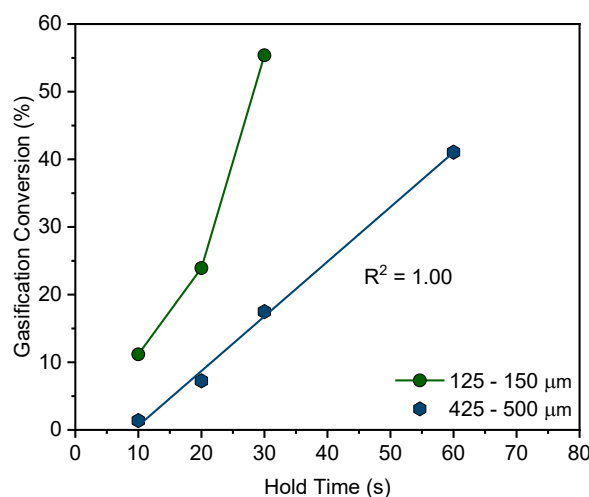
Figure 8. 11 Early-stage gasification conversions of Morupule coal at 1000 °C for the 125 – 150 µm and 425 – 500 µm particle size fractions in CO_2 at 20 bar$_a$ as a function of hold time.

8.3.4.3 Char Morphology

SEM images of the 425 – 500 µm particle size fraction of Morupule coal chars from 20 bar$_a$ CO_2 gasification at 1000 °C and 30 s holding time are illustrated in Figure 8.12. The surface morphology reveals a developing porosity, with pore sizes in the order of microns. Interestingly, the previously evident surface cracks on 30 bar$_a$ pyrolysis chars are not as apparent for chars obtained from gasification in CO_2 at 20 bar$_a$. This further supports the suggestion, made in Section 8.3.2.2, that experimental pressure appears to play a significant role in the propagation of particle cracking. Therefore, pressures of 20 bar$_a$ and below may not provide enough external resistance capable of compromising the tensile strength of the particle. The images also demonstrate an intense consumption of the previously condensed

intact bubbles, in comparison to the main char skeleton. The above observation further supports the discussion that the majority Morupule coal tars are predominated by compounds in the low molecular weight end (Figure 4.2a) which are highly reactive, and less susceptible to secondary charring reactions which typically produce fairly unreactive residues [24]. Under identical experimental conditions, SEM images of the 125 – 150 µm char size fraction revealed a severely consumed char surface with a reduction in the particle size (Figure 6.13d). This shows the contrasting levels of char burn-off during the gasification of the two particle size fractions. As shown in Figure 8.11, chars from the 425 – 500 µm size fraction have a significantly lower conversion (by an absolute value of 38 %) than those from the 125 – 150 µm size fraction at 30 s holding time. These findings support the slower gasification rate deduced in Section 8.3.4.2. and the gasification lag incurred in the initial 10 s on the account of intraparticle heat transfer limitations in larger particles.
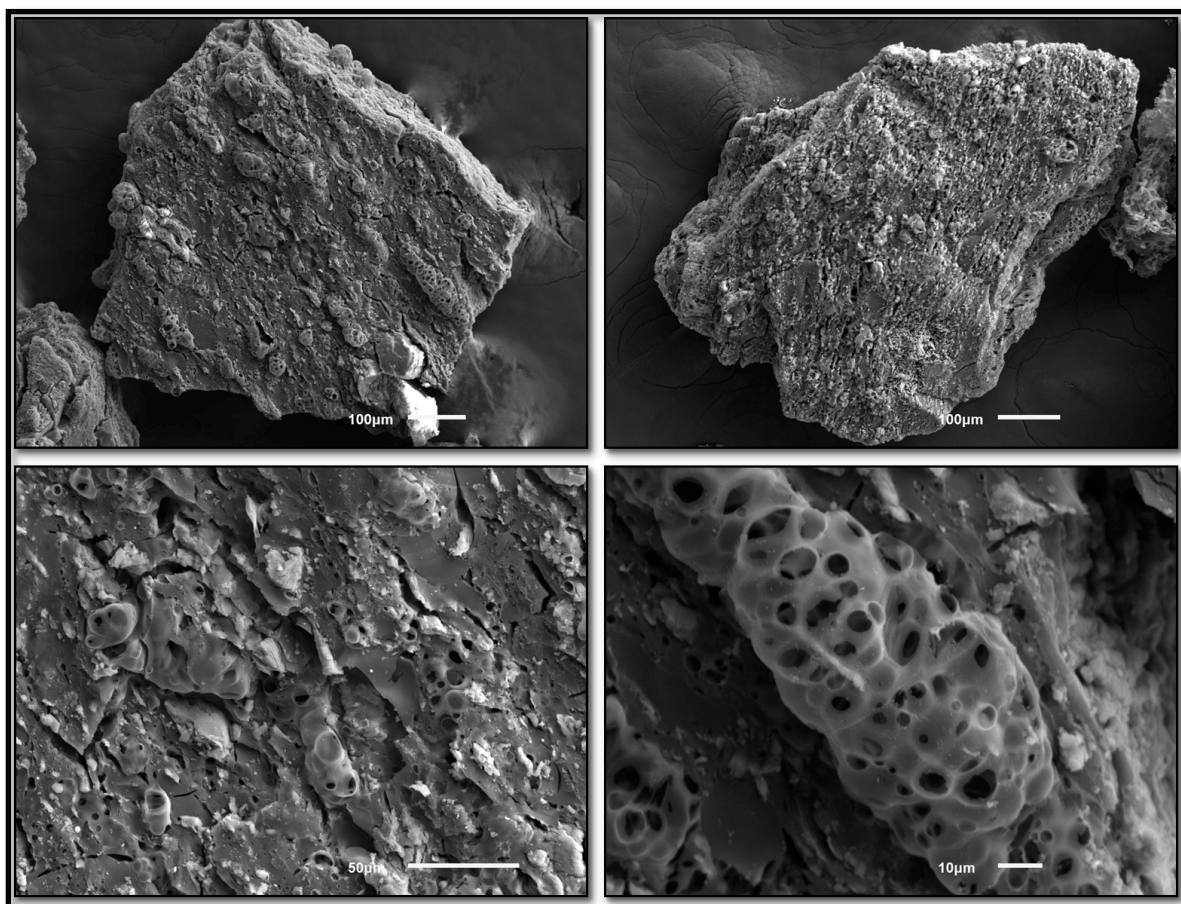
Figure 8. 12 SEM images of the 425 – 500 µm size fraction Morupule coal chars obtained from 20 bar_a CO_2 gasification at 1000 ºC and 60 s hold time.

8.3.4.4 Char Combustion Reactivity

Structural and morphological changes of chars from the 425 – 500 µm size fraction obtained from both high-pressure pyrolysis and gasification at 1000 ºC were evaluated by studying their relative combustion reactivities (Figure 8.13). Both pyrolysis and gasification chars show comparable combustion reactivities in the initial 10 s of holding at peak temperature. This is expected given the similarity in the total volatile yields from both sets of experiments. Moreover, the influence of CO_2 on char structural changes is limited by intraparticle heat transfer which induces the gasification lag as the internal particle temperature is insufficient to promote the Boudouard reaction. However, prolonged holding to 30 s in CO_2 produces chars that are slightly less reactive than their pyrolysis counterparts. This is consistent with the general observation made for the 125 – 150 µm particle size fraction in Chapter 5 that showed lower relative reactivities for chars produced under gasification conditions. Given a conversion of about 8 %, it is possible that the most reactive sites were already consumed by CO_2 and occupied *via* chemisorption when the reaction was quenched at 30 s, limiting combustion to the less reactive sites. Conversely, the 125 – 150 µm char size fraction from high pressure CO_2 gasification at 1000 ºC and 30 s holding time had a higher reactivity than the pyrolysis char obtained under identical conditions. This was due to the enhanced porosity at high conversions, allowing for the emergence of substantial active sites in a larger surface area, thereby increasing char – O_2 interactions and leading to faster burn-off rates.
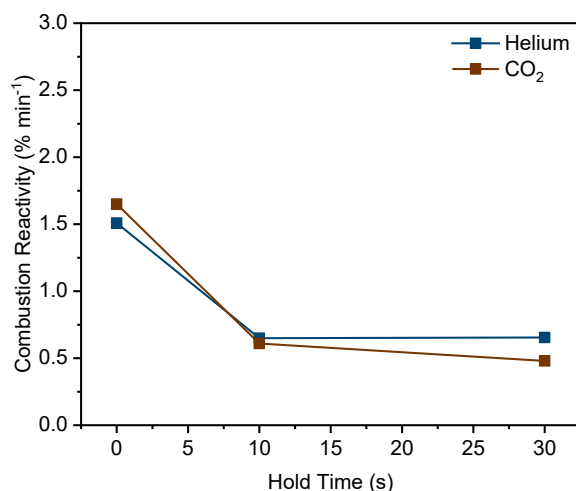
Figure 8. 13 Combustion reactivities of the 425 – 500 µm size fraction chars produced under high pressure pyrolysis (helium) and gasification (CO_2) conditions as a function of hold time at 1000 ºC.

8.4 Conclusions

This chapter presented the effect of particle size on the pyrolysis and gasification of Morupule coal, coupled with the characterisation of surface morphology and combustion reactivity of residual chars. Heat transfer limitations influence the pyrolysis product yields of larger-sized particles during the rapid temperature ramp up. Prolonged holding at peak temperature yields product distributions independent of particle size, indicating that secondary intraparticle reactions are minimal. High pressure induces further suppression of evolving volatiles during the heating up period. However, the ultimate total volatile yields are insensitive to pressure upon overcoming transport phenomena limitations. Morupule coal tends to crack at a pressure of 30 bar$_a$ due to the competing effects of intraparticle pressure-build up and external pressure, compromising the tensile strength of the coal. The negligible impact of particle size on pyrolysis product distributions as presented in this work can aid in reducing the complexity of accounting for secondary charring reactions in predictive model development.

The combustion reactivity, in a chemical reaction controlled kinetic regime, of chars produced under extended heat treatment is unaffected by particle size. Combined effects of

thermal lagging, CO_2 mass transport limitations and lower surface area for solid – gas contact render larger particles less reactive during both low and high pressure gasification in CO_2 at 1000 ºC. Atmosphere has little influence on the combustion reactivity of larger particle chars obtained from holding for up to 10 s at peak temperature. However, further exposure to CO_2 produces chars of lower reactivity than their pyrolysis counterparts obtained under identical experimental conditions.

References

1.   Irfan, M. F.; Usman, M. R.; Kusakabe, K., Coal gasification in CO_2 atmosphere and its kinetics since 1948: A brief review. *Energy* **2011,** *36* (1), 12-40.

2.   Harris, D. J.; Roberts, D. G., Chapter 16 - Coal gasification and conversion. In *The Coal Handbook: Towards Cleaner Production*, Osborne, D., Ed. Woodhead Publishing: **2013**; Vol. 2, pp 427-454.

3.   Mishra, A.; Gautam, S.; Sharma, T., Effect of operating parameters on coal gasification. *International Journal of Coal Science & Technology* **2018,** *5* (2), 113-125.

4.   Everson, R. C.; Neomagus, H. W. J. P.; van der Merwe, G. W.; Koekemoer, A.; Bunt, J. R., The properties of large coal particles and reaction kinetics of corresponding chars. *Fuel* **2015,** *140*, 17-26.

5.   Zhu, Y.; Frey, H. C., 3 - Integrated gasification combined cycle (IGCC) power plant design and technology. In *Advanced Power Plant Materials, Design and Technology*, Roddy, D., Ed. Woodhead Publishing: **2010**; pp 54-88.

6.   Zhu, W.; Song, W.; Lin, W., Effect of the Coal Particle Size on Pyrolysis and Char Reactivity for Two Types of Coal and Demineralized Coal. *Energy & Fuels* **2008,** *22* (4), 2482-2487.

7.   Hanson, S.; Patrick, J. W.; Walker, A., The effect of coal particle size on pyrolysis and steam gasification. *Fuel* **2002,** *81* (5), 531-537.

8.   Zhuo, Y.; Messenböck, R.; Collot, A. G.; Megaritis, A.; Paterson, N.; Dugwell, D. R.; Kandiyoti, R., Conversion of coal particles in pyrolysis and gasification: comparison of conversions in a pilot-scale gasifier and bench-scale test equipment. *Fuel* **2000,** *79* (7), 793-802.

9.   Yu, J.; Sun, L.; Berrueco, C.; Fidalgo, B.; Paterson, N.; Millan, M., Influence of temperature and particle size on structural characteristics of chars from Beechwood pyrolysis. *Journal of Analytical and Applied Pyrolysis* **2018,** *130*, 127-134.

10.   Cousins, A.; Paterson, N.; Dugwell, D. R.; Kandiyoti, R., An Investigation of the Reactivity of Chars Formed in Fluidized Bed Gasifiers: The Effect of Reaction Conditions and Particle Size on Coal Char Reactivity. *Energy & Fuels* **2006,** *20* (6), 2489-2497.

11.   Cai, H. Y.; Güell, A. J.; Chatzakis, I. N.; Lim, J. Y.; Dugwell, D. R.; Kandiyoti, R., Combustion reactivity and morphological change in coal chars: Effect of pyrolysis temperature, heating rate and pressure. *Fuel* **1996,** *75* (1), 15-24.

12.   Wall, T. F.; Liu, G.-s.; Wu, H.-w.; Roberts, D. G.; Benfell, K. E.; Gupta, S.; Lucas, J. A.; Harris, D. J., The effects of pressure on coal reactions during pulverised coal combustion and gasification. *Progress in Energy and Combustion Science* **2002,** *28* (5), 405-433.

13.   Sathe, C.; Hayashi, J.-I.; Li, C.-Z., Release of volatiles from the pyrolysis of a Victorian lignite at elevated pressures. *Fuel* **2002,** *81* (9), 1171-1178.

14.   Cui, L.-j.; Lin, W.-g.; Yao, J.-z., Influences of Temperature and Coal Particle Size on the Flash Pyrolysis of Coal in a Fast-entrained Bed1. *Chemical Research in Chinese Universities* **2006,** *22* (1), 103-110.

15.   Messenböck, R. C.; Dugwell, D. R.; Kandiyoti, R., CO_2 and steam-gasification in a high-pressure wire-mesh reactor: the reactivity of Daw Mill coal and combustion reactivity of its chars. *Fuel* **1999,** *78* (7), 781-793.

16.   Hower, J. C.; Wagner, N. J.; O'Keefe, J. M. K.; Drew, J. W.; Stucker, J. D.; Richardson, A. R., Maceral types in some Permian southern African coals. *International Journal of Coal Geology* **2012,** *100*, 93-107.

17.   Cairncross, B., An overview of the Permian (Karoo) coal deposits of southern Africa. *Journal of African Earth Sciences* **2001,** *33* (3), 529-562.

18.   Kandiyoti, R.; Herod, A.; Bartle, K. D.; Morgan, T. J., *Solid fuels and heavy hydrocarbon liquids: thermal characterization and analysis*. Elsevier: **2016**.

19.   Xu, W.-C.; Tomita, A., Effect of coal type on the flash pyrolysis of various coals. *Fuel* **1987,** *66* (5), 627-631.

20.   Hertzberg, M.; Zlochower, I. A.; Edwards, J. C., Coal particle pyrolysis mechanisms and temperatures. **1987**.

21.   Laurendeau, N. M., Heterogeneous kinetics of coal char gasification and combustion. *Progress in Energy and Combustion Science* **1978,** *4* (4), 221-270.

22.   Yi, B.; Zhang, L.; Mao, Z.; Huang, F.; Zheng, C., Effect of the particle size on combustion characteristics of pulverized coal in an O_2/CO_2 atmosphere. *Fuel Processing Technology* **2014,** *128*, 17-27.

23.   Kajitani, S.; Suzuki, N.; Ashizawa, M.; Hara, S., CO_2 gasification rate analysis of coal char in entrained flow coal gasifier. *Fuel* **2006,** *85* (2), 163-169.

24.   Messenböck, R. C. Rapid Pyrolysis and Gasification of Coal in a High Pressure Wire-Mesh Reactor. PhD Thesis, University of London, **1998**.

25.   Chirone, R.; Massimilla, L., Primary fragmentation of a coal in fluidized bed combustion. *Symposium (International) on Combustion* **1989,** *22* (1), 267-277.

26.   Wu, X.; Lin, X.; Yao, L.; Wu, Y.; Wu, C.; Chen, L.; Cen, K., Primary Fragmentation Behavior Investigation in Pulverized Coal Combustion with High-Speed Digital Inline Holography. *Energy & Fuels* **2019,** *33* (9), 8126-8134.

27.   Zhang, H.; Cen, K.; Yan, J.; Ni, M., The fragmentation of coal particles during the coal combustion in a fluidized bed. *Fuel* **2002,** *81* (14), 1835-1840.

28.   van Dyk, J. C., Development of an alternative laboratory method to determine thermal fragmentation of coal sources during pyrolysis in the gasification process. *Fuel* **2001,** *80* (2), 245-249.

29.   Everson, R. C.; Neomagus, H. W. J. P.; Kaitano, R.; Falcon, R.; Alphen, C. v.; du Cann, V. M., Properties of high ash char particles derived from inertinite-rich coal: 1. Chemical, structural and petrographic characteristics. *Fuel* **2008,** *87* (13), 3082-3090.

30.   Lu, L.; Sahajwalla, V.; Harris, D., Coal char reactivity and structural evolution during combustion—Factors influencing blast furnace pulverized coal injection operation. *Metallurgical and Materials Transactions B* **2001,** *32* (5), 811-820.

31.   Feng, B.; Bhatia, S. K.; Barry, J. C., Structural ordering of coal char during heat treatment and its impact on reactivity. *Carbon* **2002,** *40* (4), 481-496.

32.   Tremel, A. Reaction Kinetics of Solid Fuels during Entrained Flow Gasification. PhD Thesis, Technical University of Munich, **2012.**

33.   Kim, Y. T.; Seo, D. K.; Hwang, J., Study of the Effect of Coal Type and Particle Size on Char–CO_2 Gasification via Gas Analysis. *Energy & Fuels* **2011,** *25* (11), 5044-5054.

34.   Matsui, I.; Kunii, D.; Furusawa, T., Study of char gasification by carbon dioxide. 1. Kinetic study by thermogravimetric analysis. *Industrial & Engineering Chemistry Research* **1987,** *26* (1), 91-95.

35.   Balsamo, M.; Rodríguez-Reinoso, F.; Montagnaro, F.; Lancia, A.; Erto, A., Highlighting the Role of Activated Carbon Particle Size on CO_2 Capture from Model Flue Gas. *Industrial & Engineering Chemistry Research* **2013,** *52* (34), 12183-12191.

36.   Roberts, D. G.; Harris, D. J., A Kinetic Analysis of Coal Char Gasification Reactions at High Pressures. *Energy & Fuels* **2006,** *20* (6), 2314-2320.

37.   Zou, J.; Rezaee, R., Effect of particle size on high-pressure methane adsorption of coal. *Petroleum Research* **2016,** *1* (1), 53-58.

38.   Speight, J. G., 2 - Types of gasifier for synthetic liquid fuel production: design and technology. In *Gasification for Synthetic Fuel Production*, Luque, R.; Speight, J. G., Eds. Woodhead Publishing: **2015**; pp 29-55.

39.   Speight, J. G., Chapter 13 - Upgrading by Gasification. In *Heavy Oil Recovery and Upgrading*, Speight, J. G., Ed. Gulf Professional Publishing: **2019**; pp 559-614.

Chapter 9

Conclusions, Recommendations for Future Work and Implications of Study

9.1 Conclusions

A novel direct gasification approach, coupling pyrolysis and gasification as representative of the thermal history of coals in a gasifier, was investigated in this work using a wire-mesh reactor (WMR) and taking as a case study Morupule coal from Botswana. This approach minimises the excessive heat treatment of coals which typically lead to reduced char reactivity as this heat treatment is known to result in loss of microporosity and active sites. Structural and morphological properties of the residual chars were also characterised. The WMR allows for a study of single particle pyrolysis and early-stage gasification behaviour, free from char deactivation and reactor specific effects.

There is currently no empirical literature that characterises the primary thermochemical conversion of Botswana coals. Morupule coal, used in this work, has lower total and tar yields than other coals studied using the WMR due to its high inertinite content. Volatile matter release was virtually completed during the rapid heating up period, highlighting the relatively fast kinetics of coal pyrolysis. Characterisation of the liquid product demonstrated a domination of compounds at the low molecular weight end, indicating that the tar is mainly composed of smaller aromatic hydrocarbon molecules.

Investigating the effect of pressure on pyrolysis is particularly important as gasifiers operate at pressures of up to 35 bar_a. However, few studies have investigated the effect of pressure on coal char structural evolution especially during the rapid temperature ramp up. Elevated pressures suppress the volatile release of Morupule coal at 600 ºC *via* tar repolymerisation wherein tar precursors undergo secondary reactions to produce larger hydrocarbon structures. The repolymerisation structures were found to be stable at temperatures below 800 ºC. However, further increases in temperature to 1000 ºC led to near identical total volatile yields irrespective of pressure, suggesting a possible occurrence of the thermal cracking of the repolymerisation structures. The extent of graphitisation of Morupule coal chars was limited during the heating up period due to the minimised thermal annealing reactions, owing to a rapid heating rate of 1000 ºC s^{-1} used in this work. Extended holding at peak temperature promoted the ordering of the char matrix, with the bulk thermal annealing reactions taking place in the early stages of holding. The graphitisation of Morupule coal chars was observed to be insensitive to changes in pressure. For coal chars held at peak temperature for prolonged periods, both the combustion and gasification reactivities were shown to be independent of pyrolysis pressure.

One of the challenges facing the WMR is the use of small sample amounts, limiting char morphological characterisations. A novel X-Ray computed tomography (CT) technique was shown to be capable of characterising chars produced in the WMR as a first of its kind in the field. This imaging technique showed that chars produced at elevated pressures were

characterised by thin walls and high porosities possibly due to enhanced coal fluidity and plasticity at high pressures.

An initial gasification lag, with an inverse dependence on temperature, was observed during the direct CO_2 gasification of Morupule coal. This was likely due to the slower chemisorption rates at low temperatures combined with the limited initial internal porosity as raw coal was used. A higher activation energy, compared to published literature, was obtained in the chemical reaction controlled kinetic regime, likely due to the limited char deactivation during *in-situ* gasification. The characterisation of the chemical structure of the char did not reveal a preferential consumption of smaller aromatic ring systems, as often reported in literature. Morupule coal gasification proceeds through the consumption of C-C/C=C chemical bonds, resulting in a developing external surface porosity, while oxygen-containing functional groups are relatively inert.

There is a research gap pertaining to the investigation of *in-situ* high pressure gasification of coal, with no studies characterising the structural evolution of chars produced under high pressure conditions. The previously observed initial gasification lag is reduced at high pressures, suggesting enhanced CO_2 chemisorption kinetics. Increases in CO_2 pressure led to higher gasification reaction rates due to increased char surface coverages. Akin to gasification at atmospheric pressure, structural properties of the char did not exhibit any preferential consumption of smaller aromatic ring systems. Owing to faster char burn-off rates at high pressures, significant porosity developments were observed in conjunction with reduced particle sizes.

Model development is crucial in the description of intrinsic pyrolysis and gasification chemical interactions for computational fluid dynamics applications. A first order kinetic model, based on a distribution of activation energies (DAE model) combined with a Gaussian distribution, was demonstrated to provide a good fit to the pyrolysis experimental data. Slight increases in both the mean activation energy and standard deviation (describing the Gaussian distribution) were observed for high pressure and low heating rate pyrolysis investigations.

This suggested that more complex and a broader range of chemical bonds were broken during devolatilisation due to tar repolymerisation and cracking under high pressure conditions and rearrangement reactions at high temperatures in a low heating rate operation. Model-free kinetic methods were shown to yield higher activation energies, than those presented in literature, indicating the little dependence of the pyrolysis of Morupule coal on heating rate. As a first, negative activation energies were obtained using these methods due to the thermal annealing reactions prevalent when using low heating rates compared to the explosive release of volatiles at high heating rates. The shrinking core, volumetric and random pore models were found to represent early-stage WMR gasification data fairly well. Similarly, the modified Langmuir – Hinshelwood rate model was found to predict the high-pressure gasification reaction rates well. However, the model failed to account for the observed initial delay in the commencement of gasification at low temperatures.

The effect of particle size on the thermochemical behaviour of Morupule coal was examined in this study. It was demonstrated that larger-sized particles tend to have lower total volatile yields during the heating up period under both atmospheric and high pressure pyrolysis conditions due to transport phenomena limitations. However, extended holding at peak temperature allowed the previously unreleased structures to be liberated from the coal, with the ultimate product yields (total volatiles, tars and gases) reaching identical final values to those obtained when using smaller particle size fractions. Larger-sized chars from pyrolysis at high pressure exhibited surface cracks, a phenomenon previously not observed at atmospheric pressure, due to the intraparticle pressure build-up which compromised the tensile strength of the coal. Combustion reactivities, carried out in a chemical reaction controlled kinetic regime, of chars obtained from extended holding at peak temperature under pyrolysis conditions were independent of particle size. Gasification reaction rates were observed to decrease with increases in particle size due to the reduced surface area available for reaction and increased diffusional limitations.

9.2 Recommendations for Future Work

This work has extensively studied the pyrolysis and gasification behaviour of Morupule coal using the wire-mesh reactor. An in-depth characterisation of the structural and morphological evolution of both pyrolysis and gasification chars was demonstrated. However, char morphological studies were investigated using X-Ray CT and scanning electron microscopy analytical techniques only, suitable for characterising macropore properties. With the limited amount of sample used in the WMR (5 – 6 mg), micropore surface area analyses were not performed in this work. Understanding the development of micropore textural properties is crucial in assessing the extent of intraparticle mass transport limitations and the dependence of gasification reaction rates on char surface area development. Further works on the pyrolysis and gasification of Morupule coal should focus on elucidating the evolution of micropore properties. These are crucial in the prediction of high temperature gasification kinetics necessary for the design of entrained flow gasifiers.

Although unadulterated intrinsic gasification kinetics were determined in the present work, an additional limitation of the WMR is its inability to produce high conversion data, approaching complete char consumption, as this would require extended holding times at peak temperature (for atmospheric pressure gasification) which may result in the overheating of the reactor. Furthermore, the particles tend to fall through the aperture of the mesh as the particle size decreases at high conversions. Consequently, both the determination of the complete gasification profile and the structural evolution of the char at high conversions are limited. Given the comparative operation conditions used in this work to applications in fluidised bed gasifiers, a bench-scale fluidised bed gasification system is recommended to investigate higher gasification conversions and the structural evolution of the char while providing a direct comparison to findings presented in this thesis. However, a comprehensive isolation of the effect of pyrolysis gases and tars on char structure would also be necessary since, unlike in the WMR, pyrolysis products circulate in the reaction zone in fluidised bed systems.

Future works using the WMR should incorporate the use of a highly sensitive on-line gas detection (given the high flowrates of the continuous sweep flow gas necessary for minimising secondary interactions between evolving products and the heated char) and measurement system to characterise product gases during both pyrolysis and gasification. A laser-based gas detection approach may prove useful given its high sensitivity, necessary for identifying trace amounts of gas within the continuous sweep flow gas, and ability to detect short-lived gas pulses during the rapid heating in the WMR. In addition, an exhaustive characterisation of the constituents of the tar product is essential in elucidating the pyrolysis mechanistic pathway. Analytical techniques that could be of consideration in determining the constituents of the tar are the gas chromatography – mass spectrometry and simulated distillation, with size exclusion chromatography used in conjunction to assist in accounting for the mass ceiling in these techniques. An in-depth knowledge of product evolution, in combination with char structural and morphological characterisation presented in this work could prove useful in the development of predictive models used to describe the thermal breakdown of Morupule coal.

While the present work aimed at studying the char – CO_2 heterogeneous reaction, the gaseous atmosphere in a gasifier is rather complex, allowing for interactions of the char with other gases (H_2O, CO and H_2 in particular). The thermochemical behaviour of Morupule coal in the presence of each of these gases and multi-component mixtures should be carefully investigated to gain insights on their mechanistic gasification pathways under conditions that simulate performance in commercial gasifiers. This would also provide information on the competitive or synergistic behaviour of various gases during gasification, an area that has not been adequately studied.

Due to time constraints, modelling of single particle behaviour was restricted to the kinetic data obtained under conditions where the influences of transport phenomena are minimised. It is suggested that the kinetic modelling should be extended to larger particle sizes using intrinsic kinetic parameters determined in this work. Such a model would encompass

mass and heat diffusion equations to account for the effects of transport phenomena influences. The inability of the Langmuir – Hinshelwood rate model to describe the initial gasification lag highlights a significant gap in the characterisation of the evolution of char surface saturation. Future works should investigate the extent of char surface saturation as a function of time, temperature and pressure, and incorporate the findings in a modified Langmuir – Hinshelwood rate model. Temperature programmed desorption can be used to quantify the amount of CO_2 adsorbed on the surface of the char obtained under different experimental conditions.

This thesis discussed the limitations of model-free methods in describing non-isothermal pyrolysis kinetics obtained under conditions where transport phenomena are minimised and in fast pyrolysis kinetics. However, the application of model-free methods has gained reputation in data acquired using TGAs. Further work should be carried out to disentangle the influences of reactor design induced heat transfer limitations and slower kinetics in thermogravimetric analysers (TGA) on the non-isothermal kinetics of pyrolysis to ensure the determination of '*true'* intrinsic kinetic parameters using this reactor configuration. This would allow for an accurate application of model-free methods on non-isothermal pyrolysis data obtained from TGA.

9.3 Implications of Study

This work sought to provide a thorough understanding of the coal gasification process using a novel direct gasification approach, which eliminates the influence of char preparation effects on the subsequent gasification kinetics and char structural evolution. The findings presented in this work showcase a considerable scope for undertaking bench-scale experiments under conditions (temperature, heating rate and pressure) representative of the thermal history of coals in commercial gasifiers. The experimental work presented in this thesis therefore provides accurate empirical data necessary for the design and optimisation of gasifiers, as

well as unravelling the complex chemical phenomena occurring within gasifiers. An additional implication of this contribution is predicated on the utilisation of the non-destructive X-Ray computed tomography for characterising the morphology and porosity of chars. The capability to quantitatively characterise char morphology using this analytical technique through image analysis methods opens avenues in the agricultural industry where biochar (and its pore dimensions) is increasingly gaining recognition in a bid to enhance the water holding capacity of heavy clay soils. The work presented on the analysis of model-free methods using data acquired from the WMR indicate a significant need to decouple reactor design effects from intrinsic particle behaviour when investigating the non-isothermal pyrolysis kinetics of solid feedstocks. This is particularly important since these methods are widely utilised on data from a broad range of experimental usage beyond coal conversion, which includes biomass and polymer/plastics conversion. In the context of Botswana, this contribution provides the first characterisation of Morupule coal in terms of its thermochemical conversion behaviour, directly applicable to the manifestation of a coal-based industrialisation in the country. This work is therefore timely given the advanced efforts by the Government of Botswana, through the Botswana Oil Limited, to institute a coal to liquids refinery anticipated to be in operation by 2025.

Appendices

Appendix A

Experimental Methods

Table A. 1 WMR pyrolysis training results under standardised conditions (700 ºC, 30 s hold time, 1000 ºC s^{-1}, helium gas) using Linby coal.

Experimental Number	Total Volatile Yield (wt.%, daf)
1	45.5
2	45.4
3	45.3
4	45.1
5	44.3
6	45.0
7	44.6
8	45.1
9	44.3
10	45.4
11	44.7
12	44.3
13	45.1
14	45.4
15	46.3
95 % CI	0.3

Table A. 2 Comparison of Linby coal total volatile yields obtained by various WMR users at Imperial College London.

Operator	Total Volatile Yield (wt.%, daf)
Gibbins	45.9
Guell	45.1
Li	46.6
Madrali	44.3
Cai	42.7
Pindoria	44.8
Pipatmanomai	43.1
Fukuda	43.5
Wu	42.9
Dong	43.5
Somrang	44.4
Fidalgo	46.0
Jie	45.3
Kagiso	45.1

Appendix B

Characterisation of Morupule Coal Pyrolysis Behaviour at Elevated Pressures

Table B. 1 Conditions of cycling experiments carried out at 600 ºC to illustrate the experimental methodology. Run 1 and Run 2 were completed with the sample still in place. The sample was cooled to room temperature before Run 2 commenced.

	Temperature (ºC)	Hold Time (s)	Pressure (bar$_a$)
Run 1	600	0	30
Run 2	600	0	1

Table B. 2 WMR experimental data for total volatile yields obtained from the pyrolysis of Morupule coal at different temperatures (400 – 1000 °C) and pressures (1 – 30 bar$_a$), at a heating of 1000 °C s^{-1} and 0 s holding time at peak temperature in a helium atmosphere.

Temperature (ºC)	Total Volatile Yields and Errors (wt.%, daf)					
	1 bar$_a$		10 bar$_a$		30 bar$_a$	
	Yield	Error	Yield	Error	Yield	Error
400	3.9	0.8	4.1	0.3	4.1	0.5
600	21.2	0.6	17.2	0.9	17.0	0.7
800	29.4	0.6	24.6	1.2	25.2	0.9
1000	33.9	0.5	32.4	0.5	31.6	0.8

Table B. 3 WMR experimental data for the cycling pyrolysis of Morupule coal at various temperatures and pressures (1 bar$_a$ and 30 bar$_a$), heating rate of 1000 °C s^{-1} at 0 s holding time at peak temperature in a helium atmosphere.

Temperature (°C)	Total Volatile Yields and Errors (wt%, daf)							
	1 bar$_a$		1 bar$_a$ & 1 bar$_a$		30 bar$_a$		30 bar$_a$ & 1 bar$_a$	
	Yield	Error	Yield	Error	Yield	Error	Yield	Error
600	21.2	0.6	20.8	1.6	17.0	0.7	17.7	0.4
800	29.4	0.6	30.0	0.1	25.2	0.9	26.4	1.1
1000	33.9	0.5	34.0	0.3	31.6	0.8	31.1	1.5

Table B. 4 WMR experimental data for total volatile yields obtained from the pyrolysis of Morupule coal at 1000 °C at a heating rate of 1000 °C s^{-1} in a helium atmosphere under different pressures (1 – 30 bar$_a$) and holding times (0 – 60 s).

Holding Time (s)	Total Volatile Yields and Errors (wt.%, daf)					
	1 bar$_a$		10 bar$_a$		30 bar$_a$	
	Yield	Error	Yield	Error	Yield	Error
0	33.9	0.5	32.4	0.5	31.6	0.8
10	34.9	0.7	34.0	0.2	33.3	0.2
30	35.7	0.3	33.7	0.9	34.0	0.5
60	35.2	0.4	34.8	0.7	34.1	0.4
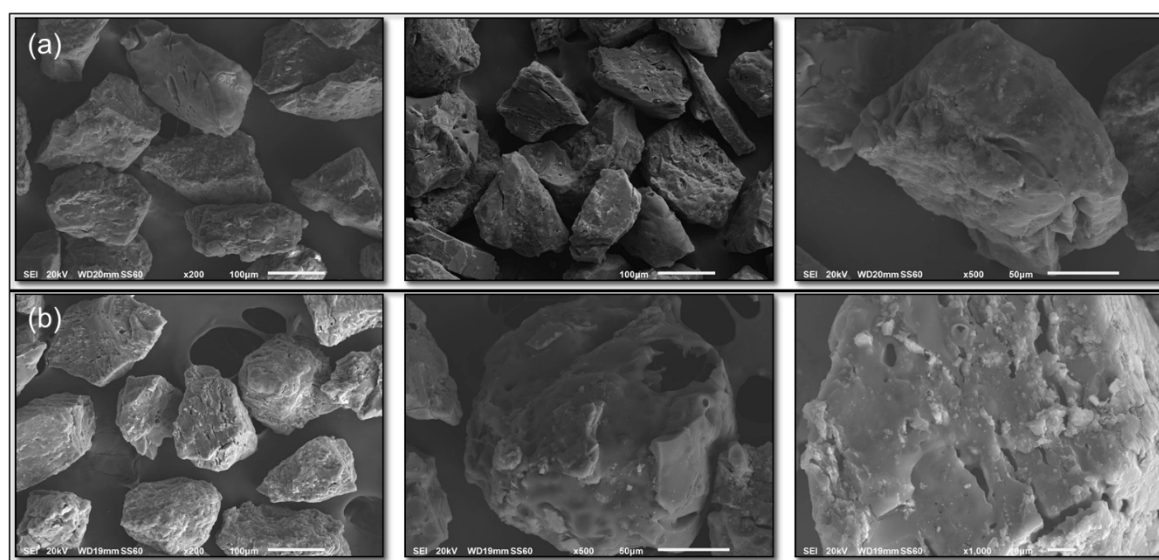
Figure B. 1 SEM images of Morupule coal chars obtained from pyrolysis at 600 ºC and holding for 0 s in a helium atmosphere. Pressures of (a) 1 bar$_a$ and (b) 30 bar$_a$.
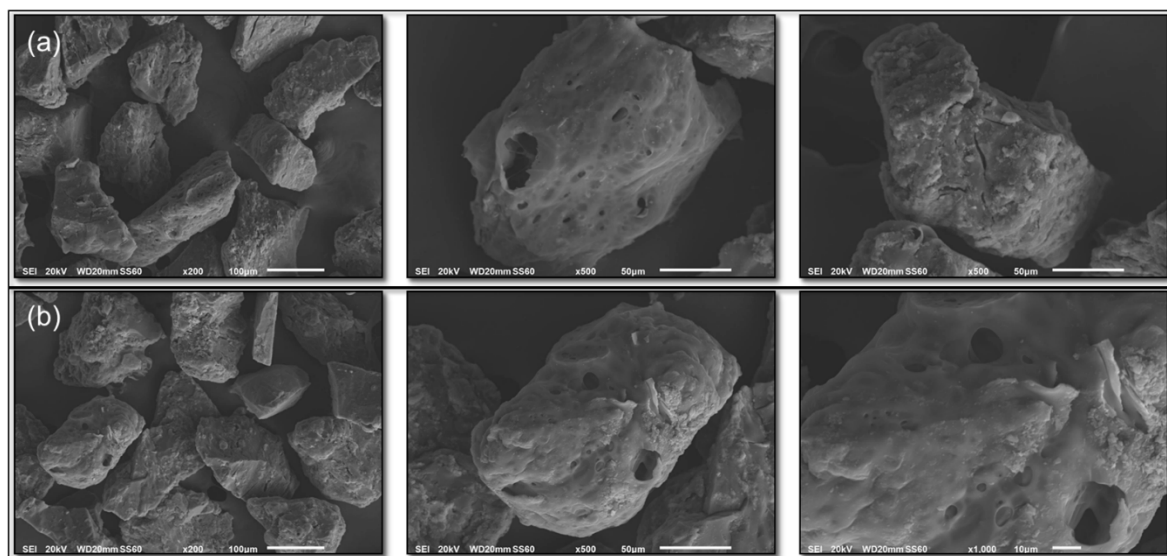
Figure B. 2 SEM images of Morupule coal chars obtained from pyrolysis at 1000 ºC and holding for 0 s in a helium atmosphere. Pressures of (a) 1 bar$_a$ and (b) 30 bar$_a$.
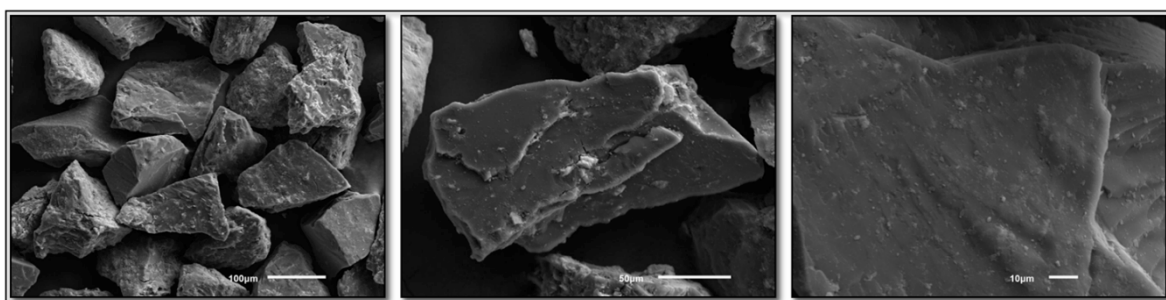
Figure B. 3 SEM images of Morupule coal chars obtained from pyrolysis at 1000 ºC and 0 s holding time in a helium atmosphere using a heating rate of 1 ºC s^{-1}. Atmospheric pressure.
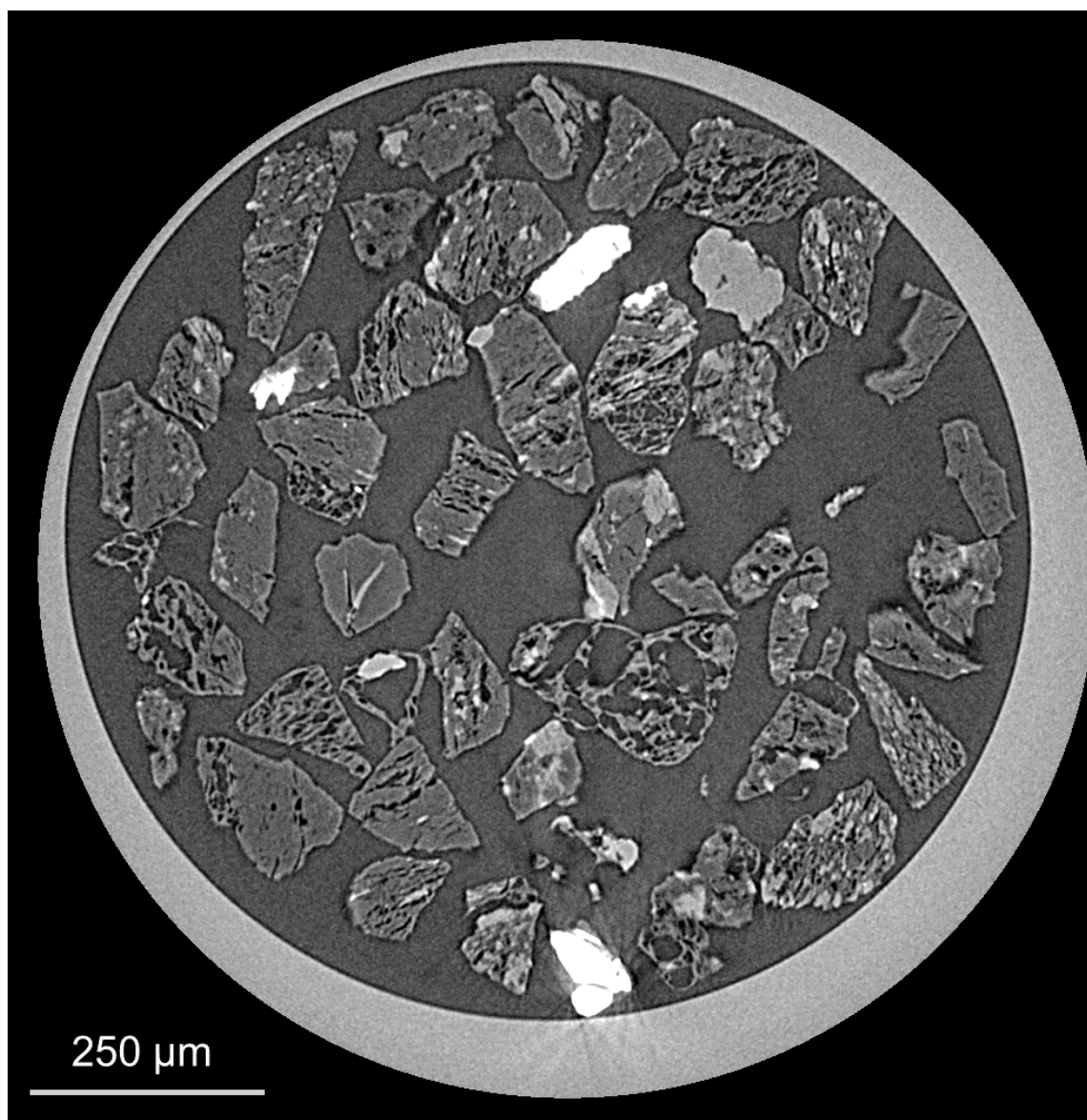
Figure B. 4 An X-Ray computed tomography (CT) image slice.
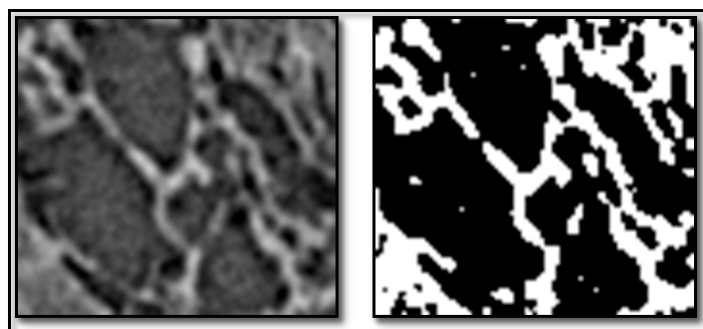
Figure B. 5 Application of an Otsu threshold on the image obtained *via* X-Ray CT used to estimate char porosity. Black – pores and white – char walls. A binary histogram was produced accounting for the voxels in black or white. Porosity is defined as the ratio of black voxels to the total number of voxels.

257

Appendix C

Early-Stage Char Kinetics and Structural Evolution during Atmospheric Pressure Gasification in CO$_2$

Table C. 1 Total volatile yields obtained from the wire-mesh reactor during atmospheric pressure pyrolysis of Morupule coal in helium and gasification in CO$_2$ at 900 °C. Heating rate of 1000 °C s^{-1}.

Hold Time (s)	He		CO$_2$	
	Total volatile yield (wt.%,daf)	**Error (wt.%, daf)**	**Total volatile yield (wt.%,daf)**	**Error (wt.%, daf)**
0	31.7	0.6	31.2	0.9
10	32.6	0.6	33.3	0.6
30	33.3	0.4	33.5	0.4
60	33.9	1.5	35.3	0.3

Table C. 2 Total volatile yields obtained from the wire-mesh reactor during atmospheric pressure pyrolysis of Morupule coal in helium and gasification in CO$_2$ at 1000 °C. Heating rate of 1000 °C s^{-1}.

Hold Time (s)	He		CO$_2$	
	Total volatile yield (wt.%,daf)	**Error (wt.%, daf)**	**Total volatile yield (wt.%,daf)**	**Error (wt.%, daf)**
0	33.9	0.5	32.6	0.4
10	34.9	0.7	36.4	0.2
30	35.7	0.3	39.0	1.0
60	35.2	0.4	44.4	0.1

Table C. 3 Atmospheric pressure Morupule coal CO_2 gasification conversions at different holding times (900 – 950 °C).

900 °C		925 °C		950 °C	
Hold Time (s)	**Conversion (%)**	**Hold Time (s)**	**Conversion (%)**	**Hold Time (s)**	**Conversion (%)**
60	2.2	60	3.7	30	2.0
180	5.1	120	6.8	60	4.9
260	9.4	180	11.2	90	8.7
360	12.2	240	15.7	130	15.2

Table C. 4 Atmospheric pressure Morupule coal CO_2 gasification conversions at different holding times (975 – 1050 °C).

975 °C		1000 °C		1050 °C	
Hold Time (s)	**Conversion (%)**	**Hold Time (s)**	**Conversion (%)**	**Hold Time (s)**	**Conversion (%)**
20	2.7	10	2.3	5	3.3
40	5.7	30	5.0	20	6.1
60	10.2	60	14.2	40	15.1
80	13.8	-	-	-	-

Table C. 5 Atmospheric pressure Morupule coal gasification conversions at 900 °C under different CO_2 concentrations.

50 vol.%		100 vol.%	
Hold Time (s)	**Conversion (%)**	**Hold Time (s)**	**Conversion (%)**
120	1.7	60	2.2
200	5.4	180	5.1
320	9.9	260	9.4
420	12.3	360	12.2

Table C. 6 Atmospheric pressure Morupule coal gasification conversions at 1000 °C under different CO_2 concentrations.

25 vol.%		50 vol.%		100 vol.%	
Hold Time (s)	**Conversion (%)**	**Hold Time (s)**	**Conversion (%)**	**Hold Time (s)**	**Conversion (%)**
60	2.2	30	3.2	10	2.3
120	7.4	60	6.8	30	5.0
180	14.4	120	14.5	60	14.2
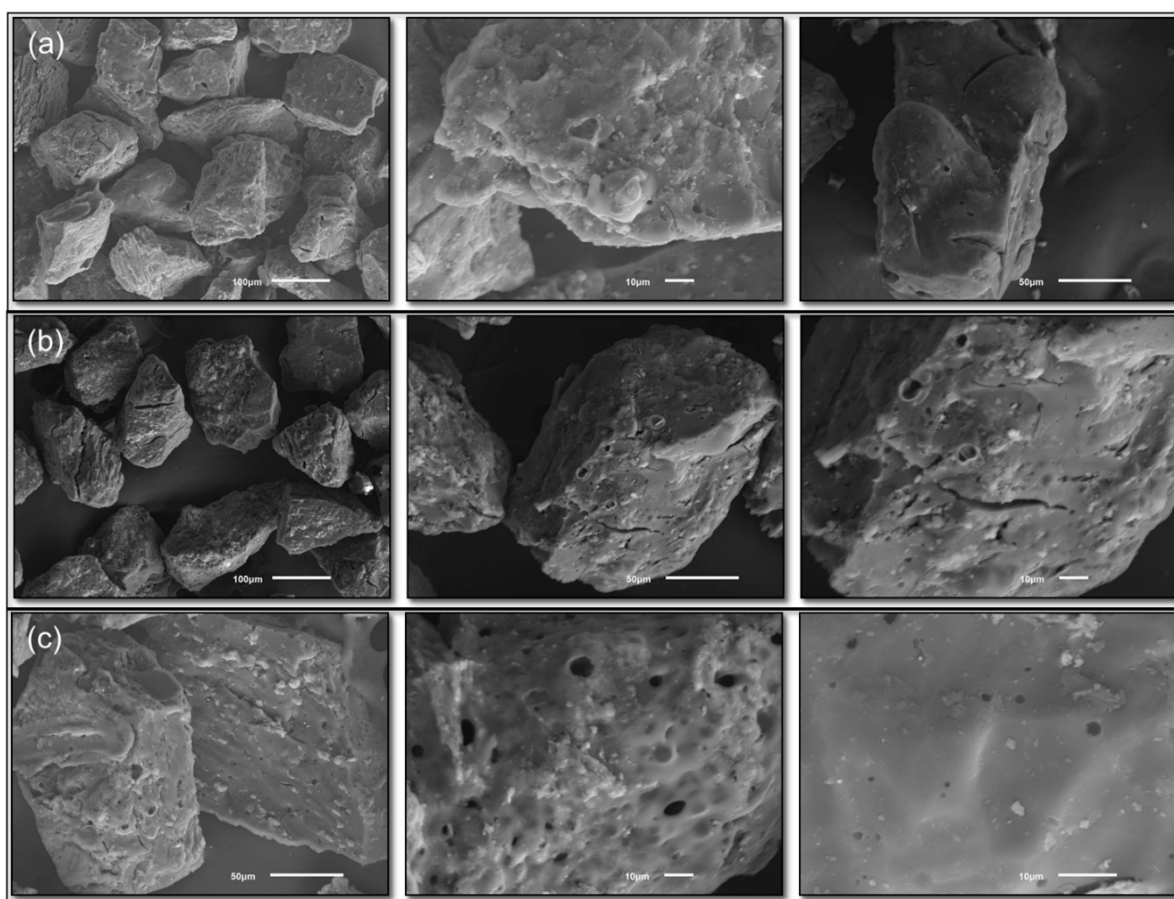
Figure C. 1 SEM images of Morupule coal chars obtained from atmospheric pressure gasification in CO_2 at 1000 °C for different holding times (a) 0 s, (b) 30 s and (c) 60 s.

Appendix D

Early-Stage Kinetics and Char Structural Evolution during High Pressure CO_2 Gasification

Table D. 1 Total volatile yields obtained from the wire-mesh reactor during pyrolysis of Morupule coal in helium and gasification in CO_2 at 900 °C and a pressure of 10 bar$_a$. Heating rate of 1000 °C s^{-1}.

Hold Time (s)	He		CO_2	
	Total volatile yield (wt.%,daf)	**Error (wt.%, daf)**	**Total volatile yield (wt.%,daf)**	**Error (wt.%, daf)**
0	28.8	1.2	28.3	1.1
10	31.2	0.8	29.8	0.4
30	31.9	2.3	31.2	0.4
60	32.7	0.7	34.7	0.8

Table D. 2 Total volatile yields obtained from the wire-mesh reactor during pyrolysis of Morupule coal in helium and gasification in CO_2 at 900 °C and a pressure of 20 bar$_a$. Heating rate of 1000 °C s^{-1}.

Hold Time (s)	He		CO_2	
	Total volatile yield (wt.%,daf)	**Error (wt.%, daf)**	**Total volatile yield (wt.%,daf)**	**Error (wt.%, daf)**
0	29.7	0.7	29.0	1.2
10	32.2	0.2	31.9	0.8
30	31.9	1.3	35.7	0.5
60	32.3	0.4	48.2	1.3

Table D. 3 Total volatile yields obtained from the wire-mesh reactor during pyrolysis of Morupule coal in helium and gasification in CO_2 at 1000 °C and a pressure of 10 bar$_a$. Heating rate of 1000 °C s^{-1}.

Hold Time (s)	He		CO_2	
	Total volatile yield (wt.%,daf)	Error (wt.%, daf)	Total volatile yield (wt.%,daf)	Error (wt.%, daf)
0	32.4	0.5	29.8	1.5
10	34.0	0.2	37.6	0.1
20	33.5	0.9	42.8	0.9
30	33.7	0.9	52.6	0.5

Table D. 4 Total volatile yields obtained from the wire-mesh reactor during pyrolysis of Morupule coal in helium and gasification in CO_2 at 1000 °C and a pressure of 20 bar$_a$. Heating rate of 1000 °C s^{-1}.

Hold Time (s)	He		CO_2	
	Total volatile yield (wt.%,daf)	Error (wt.%, daf)	Total volatile yield (wt.%,daf)	Error (wt.%, daf)
0	32.8	0.8	29.5	0.8
10	33.1	0.8	40.6	1.3
20	33.9	1.0	49.7	0.9
30	33.9	1.7	70.5	1.7

Table D. 5 Morupule coal gasification conversions at 900 °C under different CO_2 pressures (1, 10 and 20 bar$_a$).

1 bar$_a$		10 bar$_a$		20 bar$_a$	
Hold Time (s)	Conversion (%)	Hold Time (s)	Conversion (%)	Hold Time (s)	Conversion (%)
60	2.2	60	3.0	30	5.5
180	5.1	90	14.1	45	10.1
260	9.4	120	26.3	60	21.3
360	12.2	-	-	-	-

Table D. 6 Morupule coal gasification conversions at 1000 °C under different CO_2 pressures (1, 10 and 20 bar_a).

1 bar_a		10 bar_a		20 bar_a	
Hold Time (s)	Conversion (%)	Hold Time (s)	Conversion (%)	Hold Time (s)	Conversion (%)
10	2.3	10	6.1	10	11.2
30	5.0	20	13.6	20	23.9
60	14.2	30	28.2	30	55.4
90	17.9	-	-	-	-
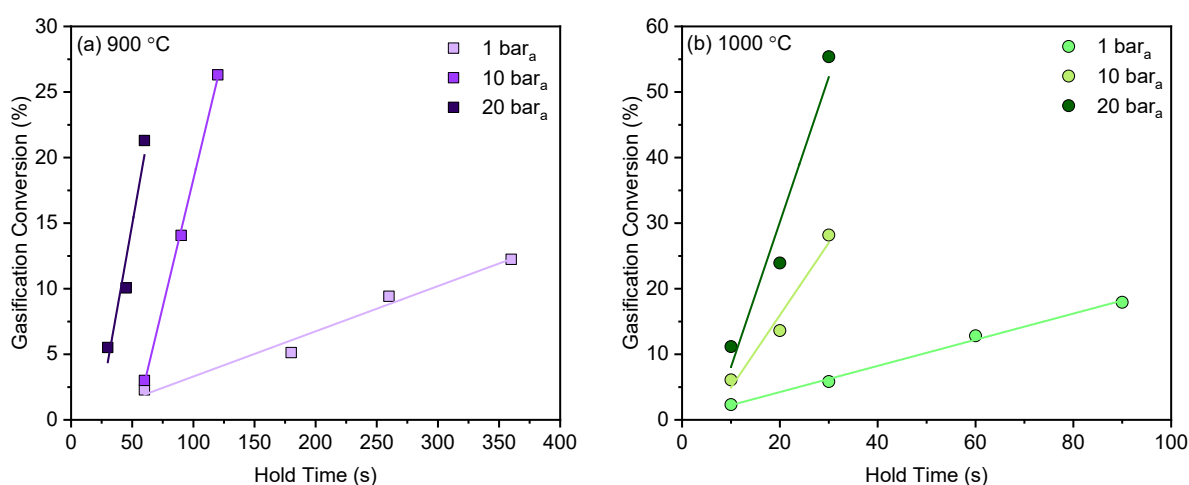
Figure D. 1 Linear fittings of early-stage gasification conversions of Morupule coal in CO_2 under pressures of 1, 10 and 20 bar_a at (a) 900 ºC and (b) 1000 ºC.

Table D. 7 Reaction rates and R^2 values obtained from the linear fitting of the high-pressure gasification data.

Temperature (ºC)	1 bar_a		10 bar_a		20 bar_a	
	Reaction rate (s^{-1})	R^2	Reaction rate (s^{-1})	R^2	Reaction rate (s^{-1})	R^2
900	0.00034	0.98	0.00388	1.00	0.00526	0.94
1000	0.00200	1.00	0.01104	0.97	0.02210	0.94
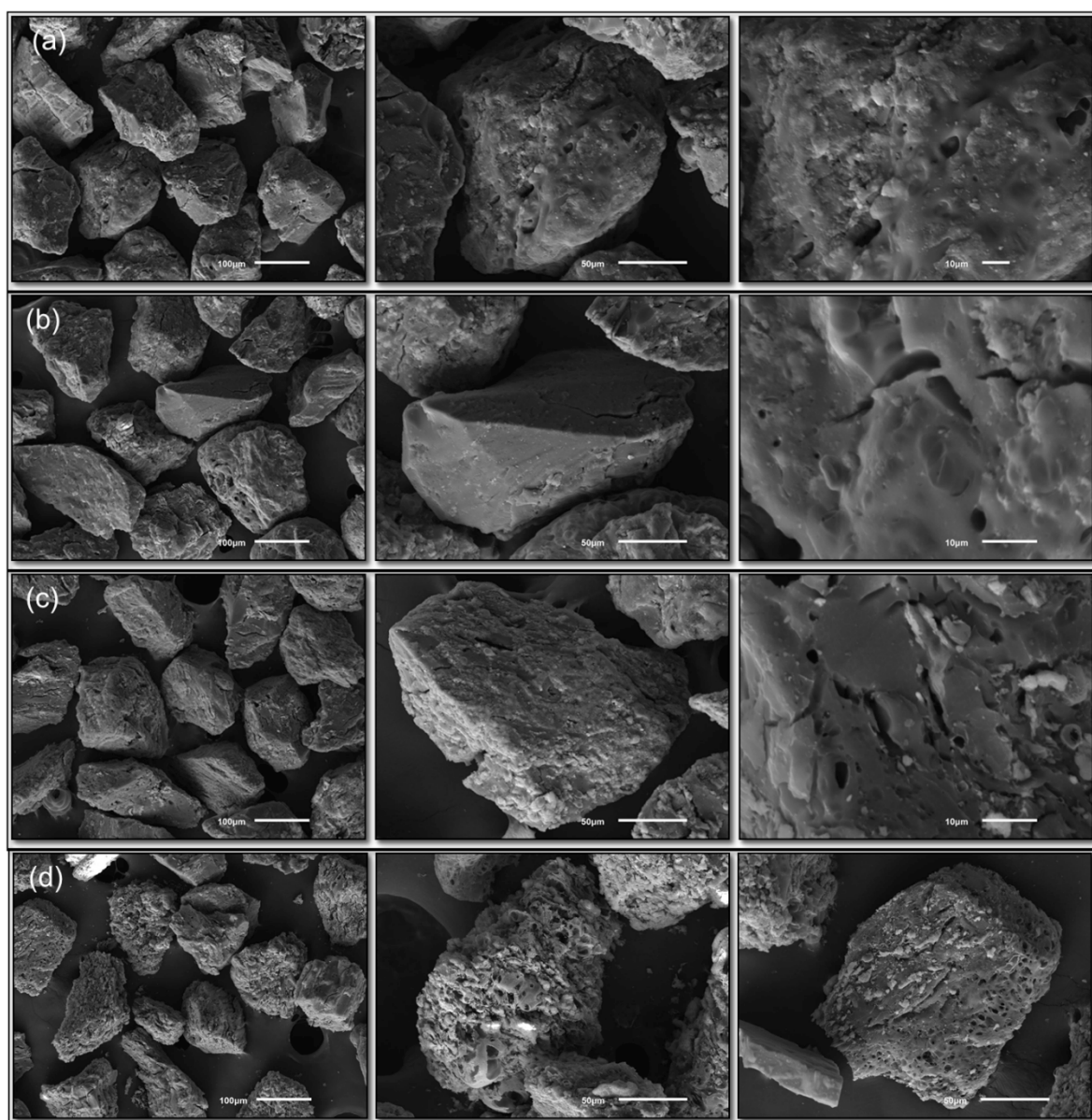
Figure D. 2 SEM images of Morupule coal chars from 20 bar$_a$ CO_2 gasification at 1000 ºC and holding times of (a) 0 s, (b) 10 s, (c) 20 s and (d) 30 s.

Appendix E

Modelling of Single Particle Behaviour during Pyrolysis and Gasification
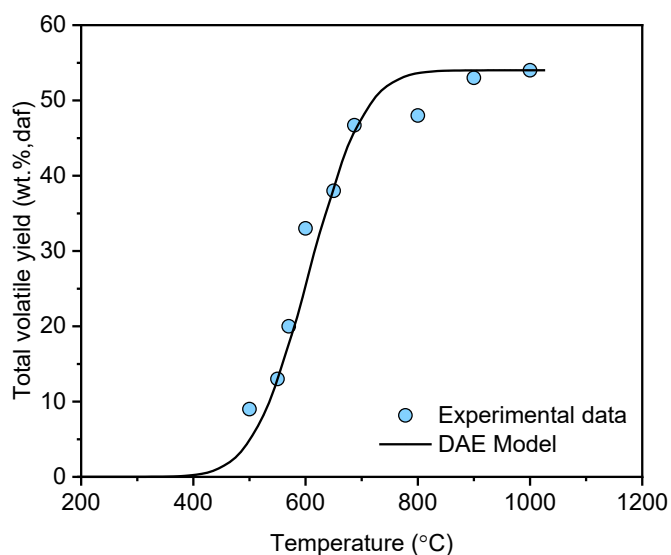
Figure E. 1 gPROMS DAE model code validation using mean activation energy and pre-exponential factor values presented by Niksa and Lau [1] for a Pittsburgh coal pyrolysis data obtained by Gibbins-Matham and Kandiyoti [2].
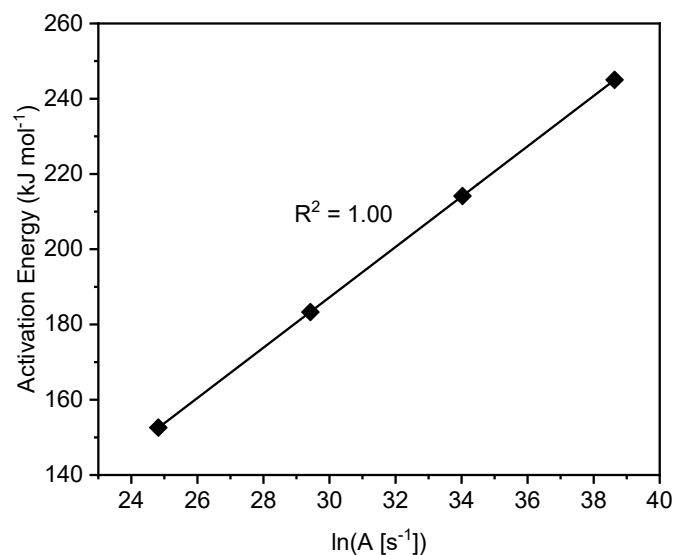
Figure E. 2 Demonstration of the kinetic compensation effect for kinetic parameters estimated by fitting the DAE pyrolysis model to Morupule coal pyrolysis data obtained using the wire-mesh reactor under atmospheric pressure conditions.
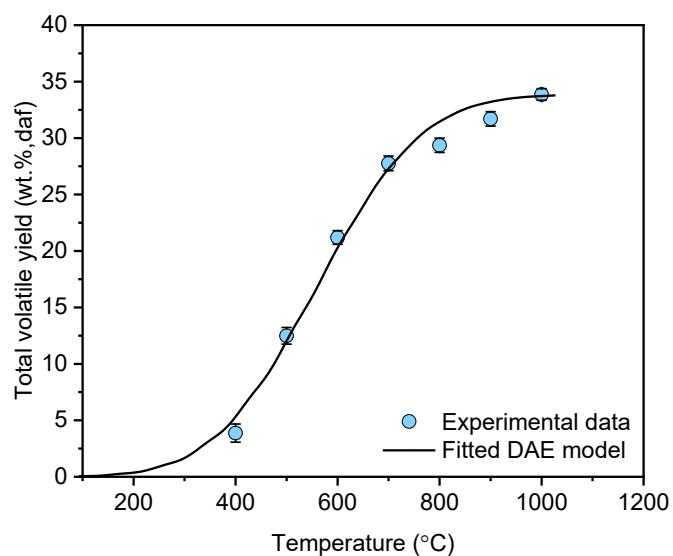
Figure E. 3 DAE model fitting to the Morupule coal pyrolysis data obtained using a heating rate of 1000 ºC s-1 under atmospheric pressure conditions using a mean activation energy of 152.6 kJ mol^{-1} and a standard deviation of 29.6 kJ mol^{-1}.

Table E. 1 Total volatile yields obtained from the atmospheric pressure pyrolysis of Morupule coal in the wire-mesh reactor using different heating rates. 0 s holding at peak temperature.

| Temperature (ºC)	Total Volatile Yields and Errors (wt.%, daf)					
	1 ºC s^{-1}		10 ºC s^{-1}		1000 ºC s^{-1}	
	Yield	Error	Yield	Error	Yield	Error
400	4.5	0.5	4.3	0.6	3.9	0.8
500	12.7	1.7	12.6	0.5	12.5	0.7
600	17.4	0.5	13.4	0.9	21.2	0.6
700	23.2	1.3	25.2	0.8	27.8	0.7
800	26.5	0.3	27.8	0.9	29.4	0.6
900	29.9	1.9	30.2	0.3	31.7	0.6
1000	31.4	0.5	32.2	0.7	33.9	0.5
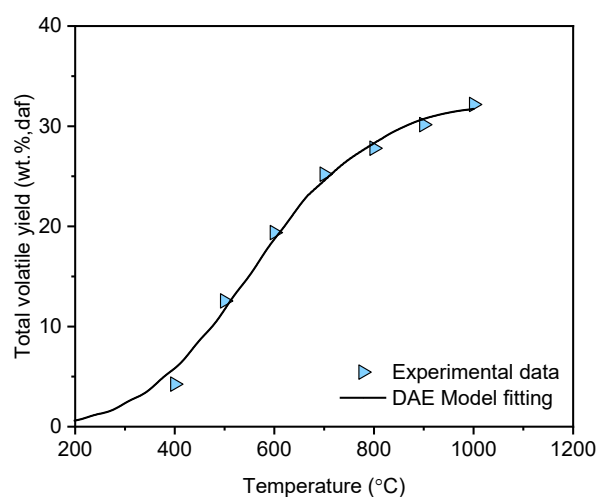
Figure E. 4 DAE model fitting to the Morupule coal pyrolysis data obtained using a heating rate of 10 ºC s^{-1} under atmospheric pressure conditions.

Table E. 2 Comparison of the random pore model fitting to the Morupule coal CO_2 gasification using different values of the structural parameter (Ψ).

Temperature (°C)	$\Psi = 2$		$\Psi = 4$		$\Psi = 8$	
	Rate constant (s^{-1})	R^2	Rate constant (s^{-1})	R^2	Rate constant (s^{-1})	R^2
900	0.00035	0.98	0.00034	0.98	0.00032	0.98
925	0.00069	0.99	0.00068	0.99	0.00062	1.00
950	0.00134	0.99	0.00133	0.99	0.00122	0.99
975	0.00190	0.99	0.00188	0.99	0.00173	0.99
1000	0.00244	0.96	0.00242	0.96	0.00222	0.97
1050	0.00346	0.95	0.00342	0.96	0.00312	0.96

Appendix F

Effect of Particle Size on the Pyrolysis and Gasification of Morupule Coal

Table F. 1 Morupule coal pyrolysis total volatile yields during the heating up period (0 s holding time) at peak temperatures of 600, 800 and 1000 ºC using a 425 – 500 µm particle size at 1 bar$_a$ and 30 bar$_a$.

Temperature (°C)	1 bar$_a$		30 bar$_a$	
	Total volatile yield (wt.%,daf)	Error (wt.%, daf)	Total volatile yield (wt.%,daf)	Error (wt.%, daf)
600	9.6	2.0	6.6	0.6
800	25.4	1.6	18.0	2.1
1000	29.4	1.2	25.0	1.0

Table F. 2 Morupule coal pyrolysis total volatile yields at 1000 ºC for different holding times of 0, 10, 30 and 60 s using a 425 – 500 µm particle size at 1 bar$_a$ and 30 bar$_a$.

Hold Time (s)	1 bar$_a$		30 bar$_a$	
	Total volatile yield (wt.%,daf)	Error (wt.%, daf)	Total volatile yield (wt.%,daf)	Error (wt.%, daf)
0	29.4	1.2	25.0	1.0
10	32.9	0.7	31.9	0.5
30	35.2	0.9	35.3	1.2
60	35.0	1.1	35.6	0.8

Table F. 3 Total volatile yields obtained from the wire-mesh reactor during the gasification of Morupule coal in CO_2 at 1000 °C and pressures of 1 bar$_a$ and 20 bar$_a$ using a 425 – 500 μm particle size fraction.

Hold Time (s)	1 bar$_a$		20 bar$_a$	
	Total volatile yield (wt.%,daf)	Error (wt.%, daf)	Total volatile yield (wt.%,daf)	Error (wt.%, daf)
0	30.3	0.9	26.5	1.3
10	34.8	1.2	32.8	1.3
30	34.7	0.5	37.0	0.8
60	37.2	0.8	46.6	1.0

Table F. 4 Morupule coal gasification conversions at 1000 °C under different CO_2 pressures (1 bar$_a$ and 20 bar$_a$) using a particle size fraction of 425 – 500 μm.

1 bar$_a$		20 bar$_a$	
Hold Time (s)	Conversion (%)	Hold Time (s)	Conversion (%)
60	3.4	10	1.4
90	6.4	20	7.2
120	11.0	30	17.5
150	14.3	60	41.0

The time taken for the temperature at the centre of the particle (for 150 μm and 500 μm particle sizes) to equal the particle surface temperature was estimated using the method outlined in Section 5 – 11 of Perry's Chemical Engineers Handbook [3]. The thermal conductivity, λ, of the coal was estimated using Equation F.1 for temperatures above 400 °C (below 400 °C, λ is 0.23 W m^{-1} K^{-1}) [4], where T is temperature in °C. The specific heat capacity of coal, c_p, was calculated using Equation F.2 for temperatures above 350 °C (below 350 °C, c_p is 1254 J kg^{-1} K^{-1}) [4].

$$\lambda = 0.23 + 2.24 \times 10^{-5}(T - 400)^{1.8} \tag{F.1}$$

$$c_p = 1254 - 1.75(T - 350)^{1.8} \tag{F.2}$$

The dimensionless factor, Y, was calculated using Equation F.3, where T' is the particle surface temperature, T_b is the initial temperature of the particle and T is the temperature of the particle at any time after the heating had commenced. $m = 2$ (Equation F.4, where r_p is the radius of the particle and h_T is the total heat convection coefficient) was assumed given the that the wire-mesh reactor employs a continuous sweep flow gas that might increase the heat convection from the particle surface. At lower values of m, the estimated time is even shorter. Using the value of Y for various temperatures and $m = 2$, the dimensionless factor θ was estimated from the heating or cooling curve for a spherical particle given in Perry's Chemical Engineers Handbook to calculate the time using Equation F.5, where ρ is the density of the coal and is the time taken for the centre of the particle to have a temperature equal to the surface temperature. A density of 850 kg m^{-3} was assumed for Morupule coal [4]. A summary of the values used in the calculations is provided in Table F.5.

$$Y = \frac{T' - T}{T' - T_b} \tag{F.3}$$

$$m = \frac{\lambda}{h_T r_p} \tag{F.4}$$

$$\theta = \frac{\lambda t}{\rho c_p r_p{}^2} \tag{F.5}$$

Table F. 5 A summary of values used in the calculation of the estimated time taken for the centre of the particle to reach a temperature equal to that at the particle surface.

T (°C)	Y (-)	λ (W m^{-1} K^{-1})	c_p (J kg^{-1} K^{-1})	θ (-)	t (s) (for 150 μm)	t (s) (for 500 μm)
400	0.013	0.23	1254.0	3.40	0.089	0.985
600	0.009	0.54	816.5	3.60	0.026	0.289
800	0.006	1.31	466.5	3.80	0.006	0.072
1000	0.005	2.47	116.5	4.00	0.001	0.001

References

1.   Niksa, S.; Lau, C.-W., Global rates of devolatilization for various coal types. *Combustion and Flame* **1993,** *94* (3), 293-307.

2.   Gibbins-Matham, J.; Kandiyoti, R., Coal pyrolysis yields from fast and slow heating in a wire-mesh apparatus with a gas sweep. *Energy & Fuels* **1988,** *2* (4), 505-511.

3.   Perry, R. H. G., D.W., *Perry's Chemical Engineers' Handbook*. McGraw-Hill: New York, **2008**.

4.   Liu, X.; Wang, G.; Pan, G.; Wen, Z., Numerical analysis of heat transfer and volatile evolution of coal particle. *Fuel* **2013,** *106*, 667-673.